FIGURES

CHAPTER 1

FIGURE 1.01 Geographical map of the study area. Based on Topographisk Kart 11171, Dale, 1:50,000.

Figure 1·01

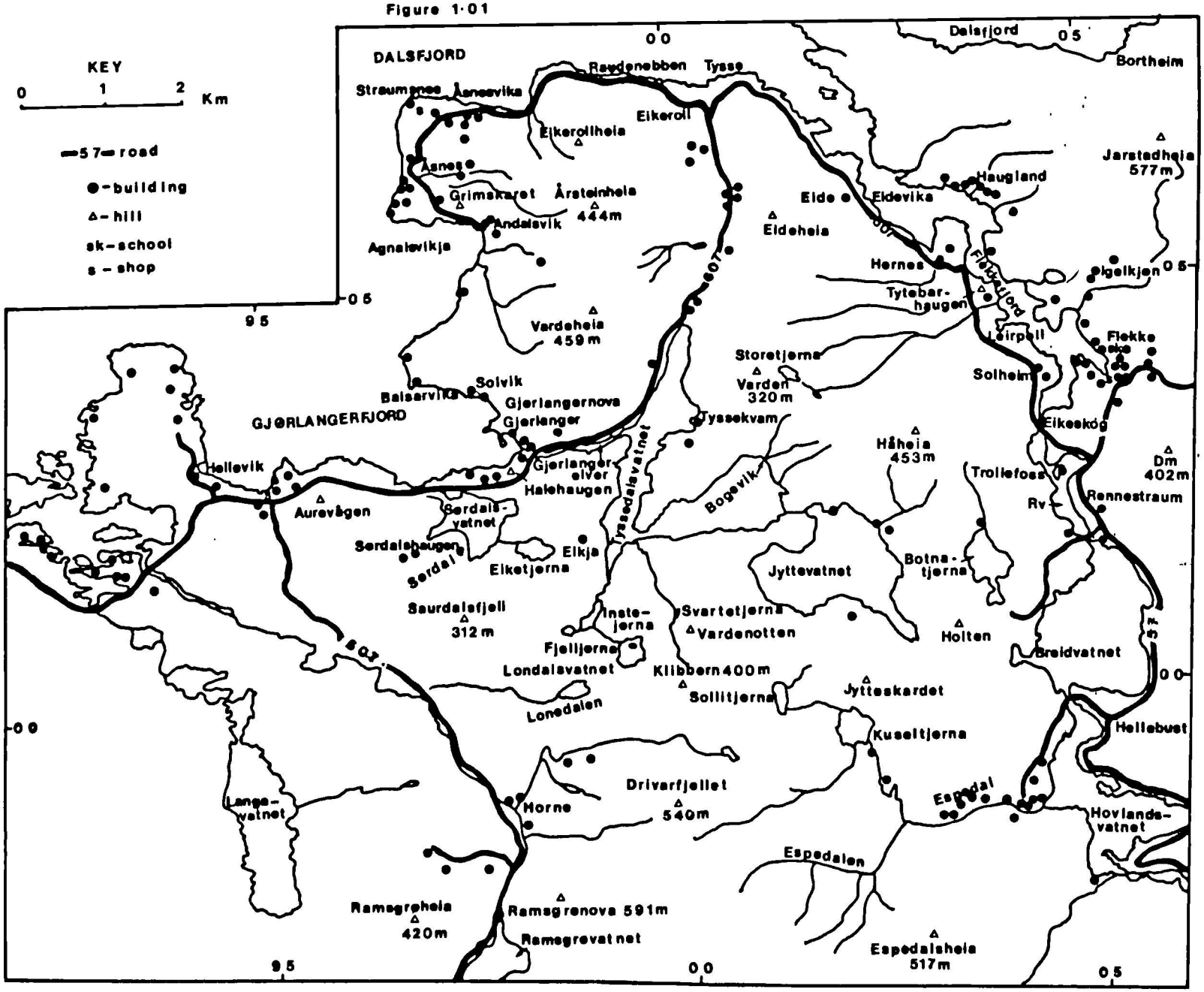
KEY
0 1 2 Km
57 road
building
hill
sk - school
s - shop
DALSFJORD
Straumnes
Åsnesvika
Raudanebben
Tysse
Eikeroll
Eikerollheia
Åsnes
Grimskaret
Årsteinheia
444m
Åndalsvik
Agnalevikja
Verdeheia
459m
Solvik
Balsarvika
Gjerlangernova
Gjerlanger
GJØRLANGERFJORD
Hellevik
Aurevågen
Gjerlanger-elver
Halehaugen
Gerdalsvatnet
Serdalshaugen
Serdalen
Elkja
Elketjerna
Saurdalsfjell
312 m
Fjelljerna
Londalsvatnet
Lonedalen
Langevatnet
Horne
Drivarfjellet
540m
Ramsgreheia
420m
Ramsgrenova 591m
Ramsgrevatnet
Espedalsheia
517m
Espedalen
Espedal
Hovlandsvatnet
Hellebust
Kuseltjerna
Jytteskardet
Sollitjerna
Klibbern 400m
Svartetjerna
Vardenotten
Instetjerna
Jyttevatnet
Botnatjerna
Holten
Breidvatnet
Tyssedalsvatnet
Bogevik
Håheia
453m
Tyssekvam
Storetjerna
Varden
320m
Eide
Eidevika
Eideheia
Haugland
Jarstadheia
577m
Hernes
Tytebarhaugen
Fitjakollen
Leirpoll
Solheim
Elkeskog
Trollefoss
Rv
Rennestraum
Dm
402m
Flekke
Sigelkjen
Dalsfjord
Bortheim
57
507

FIGURE 1.02 Tectonostratigraphic map of Central and Southern Norway, after Roberts et al, 1981.

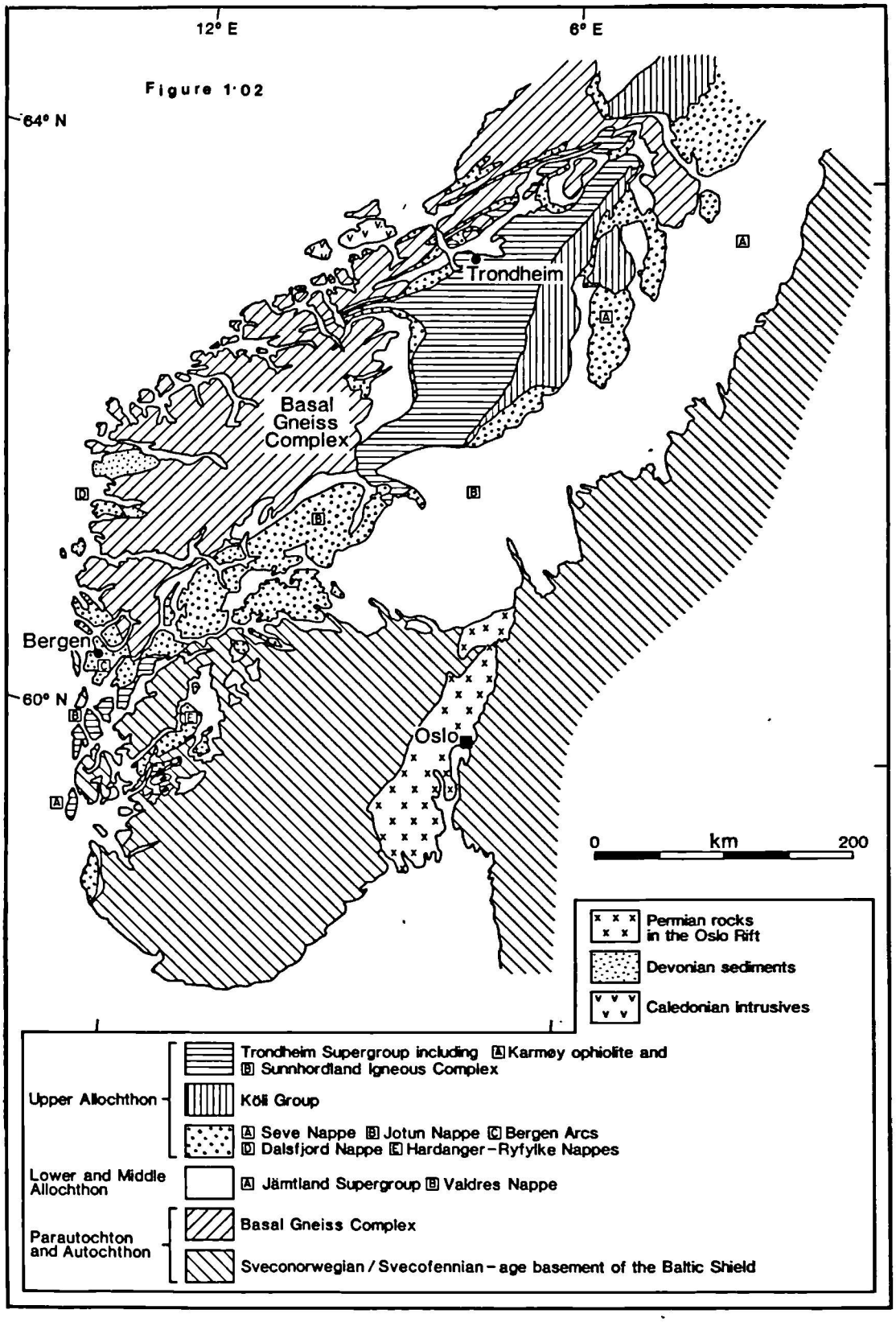
12° E
6° E
Figure 1·02
64° N
Trondheim
Basal
Gneiss
Complex
Bergen
60° N
Oslo
0
km
200
Permian rocks
in the Oslo Rift
Devonian sediments
Caledonian intrusives
Upper Allochthon
Trondheim Supergroup including A Karmøy ophiolite and
B Sunnhordland Igneous Complex
Köli Group
A Seve Nappe B Jotun Nappe C Bergen Arcs
D Dalsfjord Nappe E Hardanger–Ryfylke Nappes
Lower and Middle
Allochthon
A Jämtland Supergroup B Valdres Nappe
Parautochton
and Autochthon
Basal Gneiss Complex
Sveconorwegian / Svecofennian – age basement of the Baltic Shield

FIGURE 1.03 Locality map of the Basal Gneiss Region, showing the main areas of interest discussed in the text.

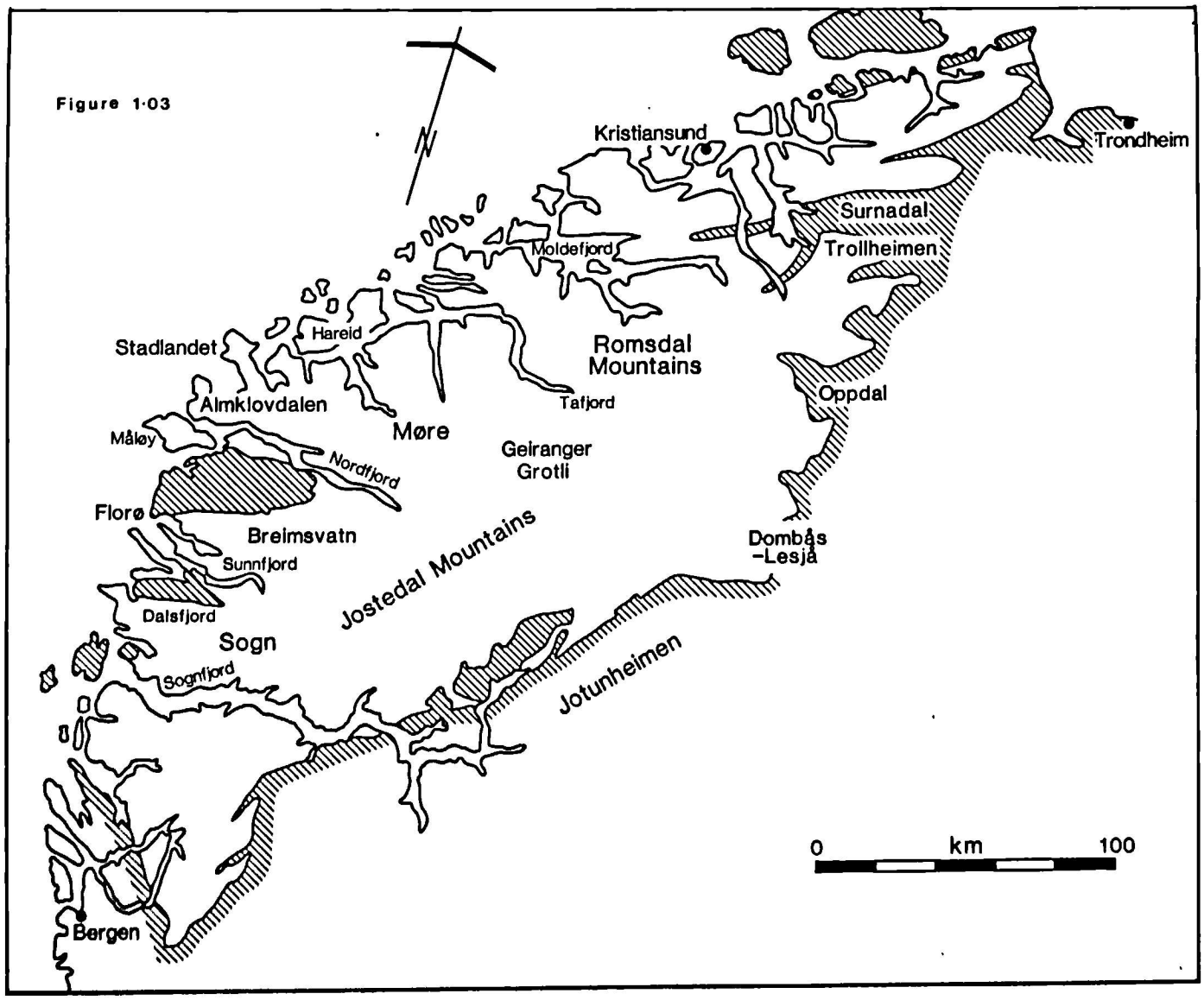
Figure 1·03
Kristiansund
Trondheim
Surnadal
Trollheimen
Moldefjord
Romsdal
Mountains
Hareid
Stadlandet
Almklovdalen
Tafjord
Møre
Oppdal
Måløy
Nordfjord
Geiranger
Grotli
Florø
Breimsvatn
Jostedal Mountains
Dombås
-Lesjå
Sunnfjord
Dalsfjord
Sogn
Sognfjord
Jotunheimen
0
km
100
Bergen

FIGURE 1.04 Geological map of the Sunnfjord area, modified after Kildal (1970).

Figure 1.04

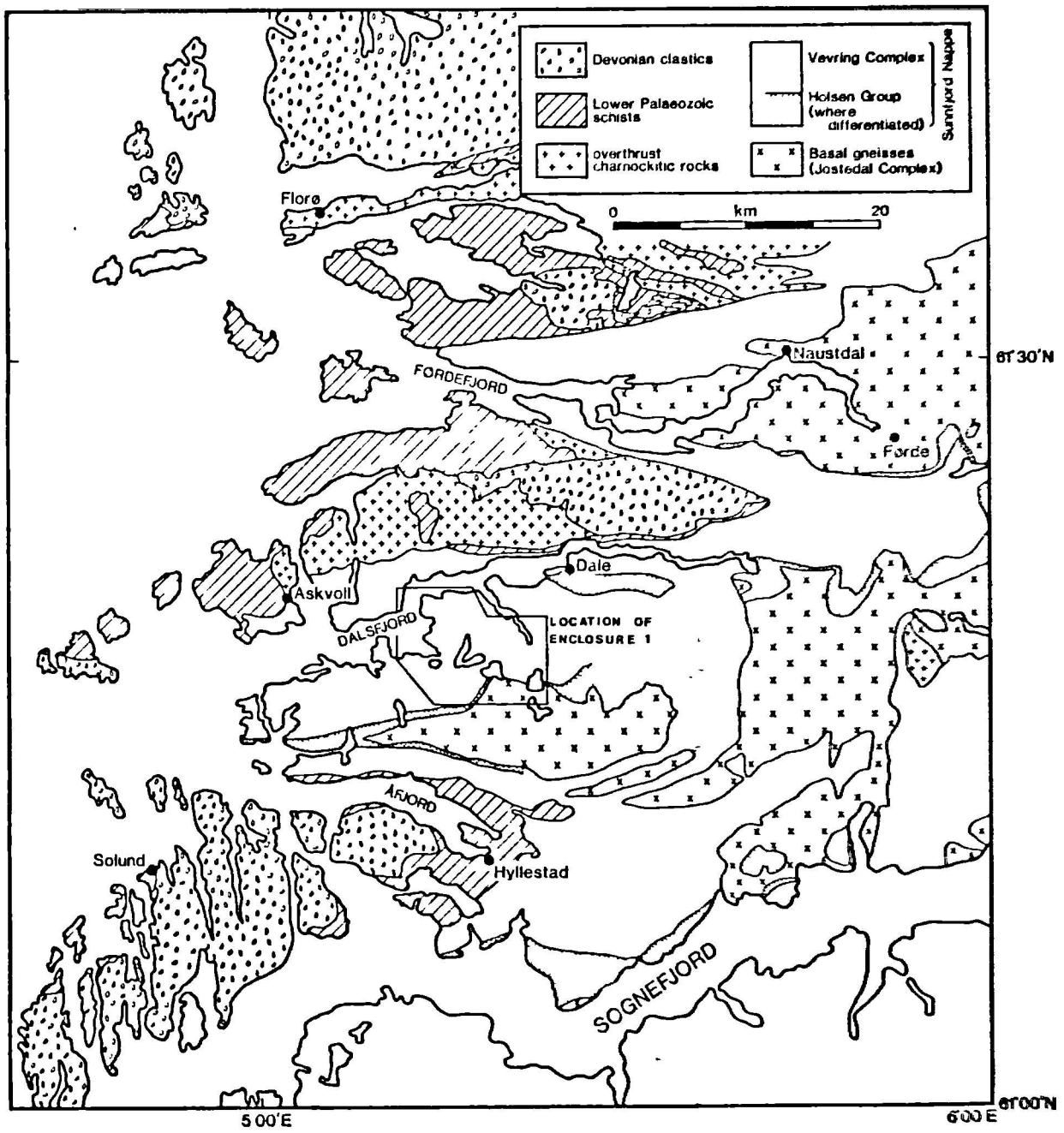
Devonian clastics
Lower Palaeozoic schists
overthrust charnockitic rocks
Vevring Complex
Holsen Group (where differentiated)
Basal gneisses (Jostedal Complex)
Sunnfjord Nappe
0 km 20
Florø
Naustdal
FØRDEFJORD
Førde
Dale
Askvoll
DALSFJORD
LOCATION OF ENCLOSURE 1
ÅRJORD
Solund
Hyllestad
SOGNEFJORD
61°30'N
61°00'N
5°00'E
6°00'E

FIGURES

CHAPTER 2

FIGURE 2.01 Typical stripey gneiss of the Vardheia Unit from near Elde, Flekkefjord. Note dark micaeous and pale quartzo-feldspathic layers. Also note disharmonic folding of more competent quartzo-feldspathic layers.

FIGURE 2.02 Large mesoperthite megablast showing strain induced extinction and marginal development of phengite and albite subgrains (top RHS). The mesoperthite sits in a matrix of granulated feldspar and quartz. Crossed polars, scale bar 1 mm. Specimen 79/19, Vardheia Unit, Elde.

FIGURE 2.03 Hinge of F_2 microfold in phengite-gneiss. Phengites lie in a matrix of sodic plagioclase (cloudy) and quartz (clear) and contain abundant sphene inclusions (dark lozenges). Plane polarised light, scale bar 1 mm. Specimen 79/21, Vardheia Unit, Eldevika.

FIGURE 2.04 Migmatitic gneiss, Raudenebben, by Dalsfjord, from the Vardheia Unit. Scale bar 30 cm.

2.01

2.02

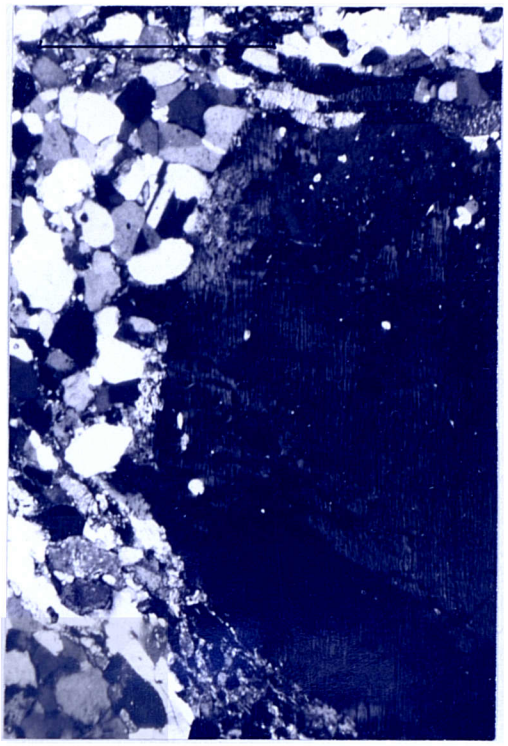

2.03

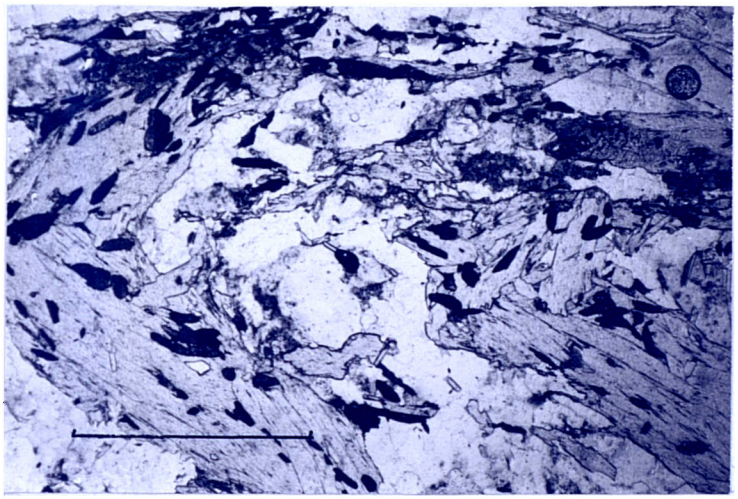

2.04

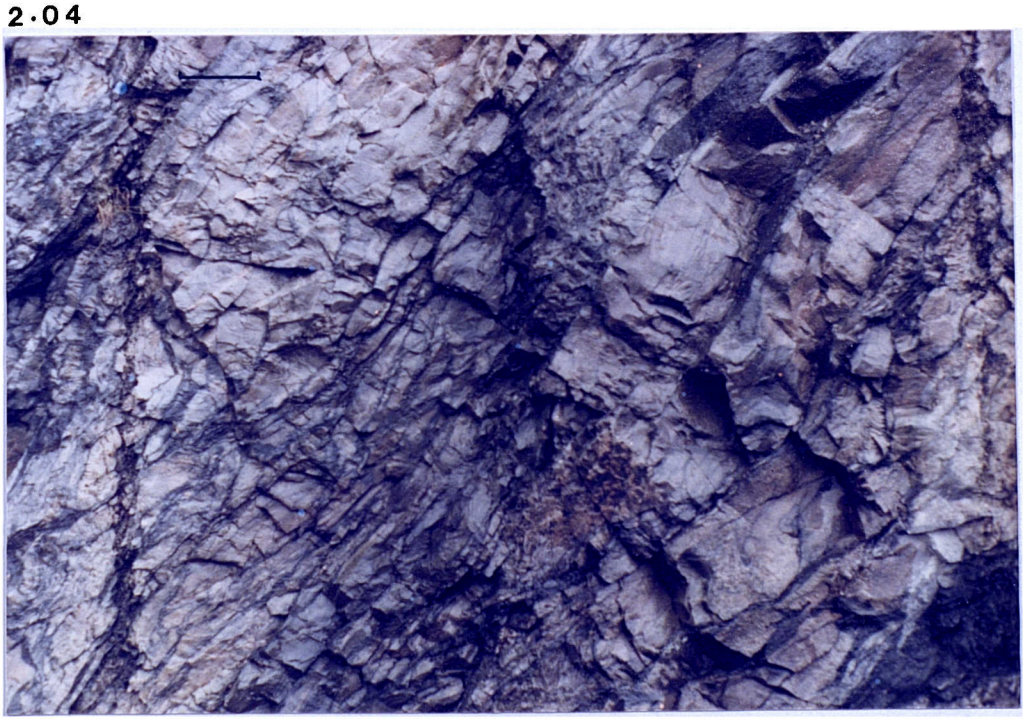

FIGURE 2.05 Boudinaged rootless recumbant isoclinal fold (F_2) in mafic pod within psammitic gneiss. Coast south of Asnes, Gjörlangerfjord.

FIGURE 2.06 Margin of felsic backvein in phengite-eclogite, coast south of Asnes. Eclogite is LHS, passing rightwards into garnet + quartz + phengite +/- omphacite. Note increasing symplectisation of omphacite into the ore quartz-rich area. Q = quartz, p = phengite, O = omphacite, G = garnet. Scale bar 1 mm.

2·05

2·06

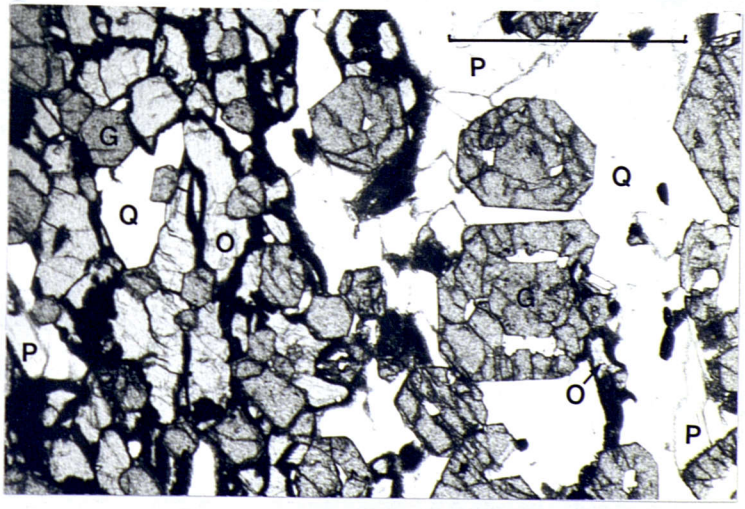

FIGURE 2.07 Section through peridotite-gneiss outcrop to the north of Varden, by Storetjörna, showing a relationship of peridotite to K-poor gneisses of the Gjörlanger Unit. See text for details.

Figure 2.07

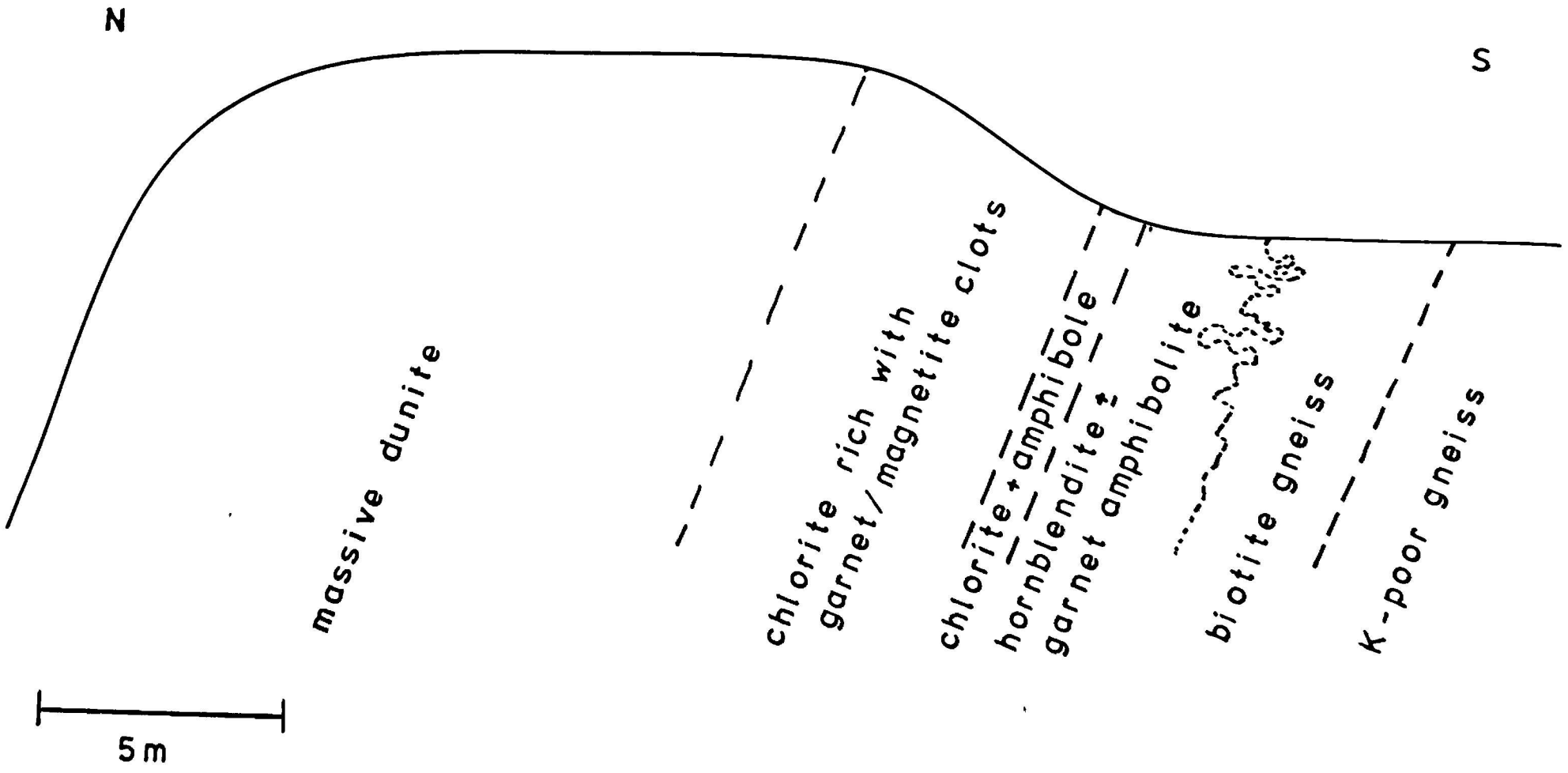
N
S
massive dunite
chlorite rich with garnet/magnetite clots
chlorite + amphibole
hornblendite ±
garnet amphibolite
biotite gneiss
K-poor gneiss
5m

FIGURE 2.08 Fresh anorthositic troctolite, Instetjörna, showing olivine and plagioclase-rich layers.

FIGURE 2.09 Photomicrograph of anorthositic troctolite (specimen D170) illustrating cumulus olivine (O) and plagioclase (p) with intercumulus augite (A) and hypersthene (H). Note cloudy nature of plagioclase and deep pigmentation of pyroxene cores.

FIGURE 2.10 Fine-grained 2-pyroxene + spinel symplectite between olivine (bottom left) and plagioclase (RHS). The dark rim between symplectite and plagioclase contains tiny garnets. The minute needles in the plagioclase are probably zoisites. Scale bar 0.1 mm.

FIGURE 2.11 Garnet-zoisite-amphibolite mimiking rhythmic graded igneous layering, north of Instetjörna. Hammer head points towards top of graded units.

2·08

2·09

2·10

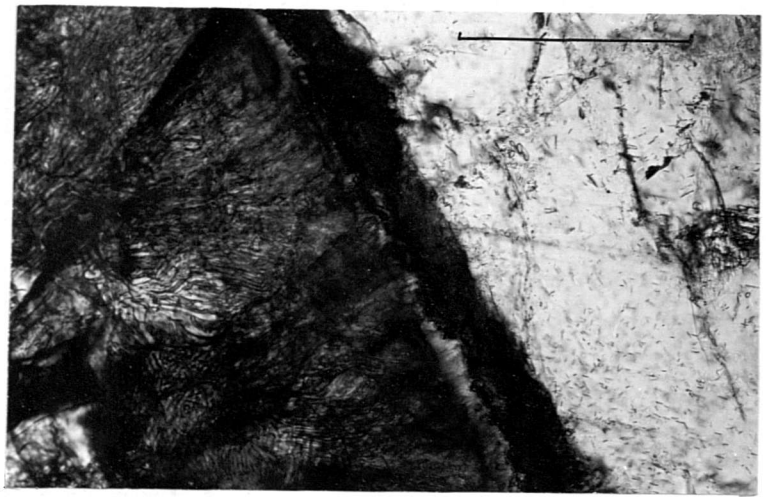

2·11

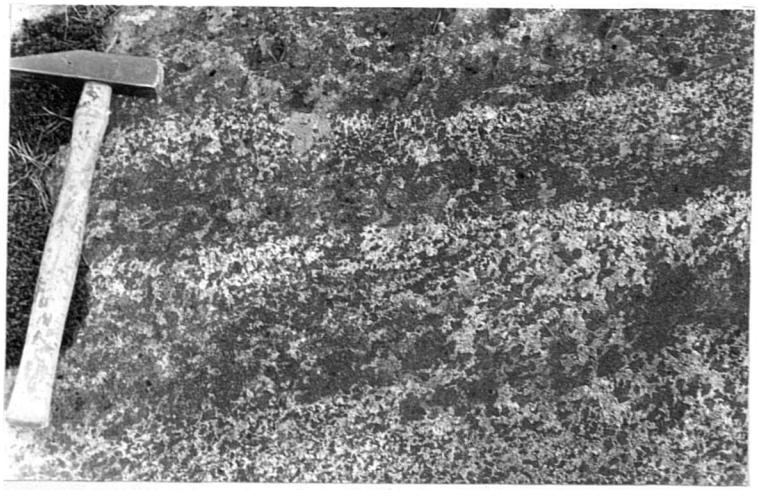

FIGURE 2.12 Displacement of light bands across a dark amphibolite streak - syn-igneous fault? North of Instetjörna.

FIGURE 2.13 Strongly attenuated metabasite with white bands forming due to streaking-out and decomposition of igneous plagioclase. Recumbant folds are F_2. West of Saurdalsfjellen.

FIGURE 2.14 Thick granular garnet corona in coronite from Aurevagen, south of Hellevik (specimen D132). Below garnet is fine-grained omphacite + kyanite +/- zoisite intergrowth (after plagioclase). Above garnet are coarser omphacites, probably replacing igneous augite. Scale bar 1 mm.

FIGURE 2.15 Omphacite + kyanite intergrowth as in Figure 2.14 overgrown by discreet euhedra of garnet, with omphacite inclusions. Scale bar 1 mm. Specimen D133, Aurevagen near Hellevik.

2·12

2·13

2·14

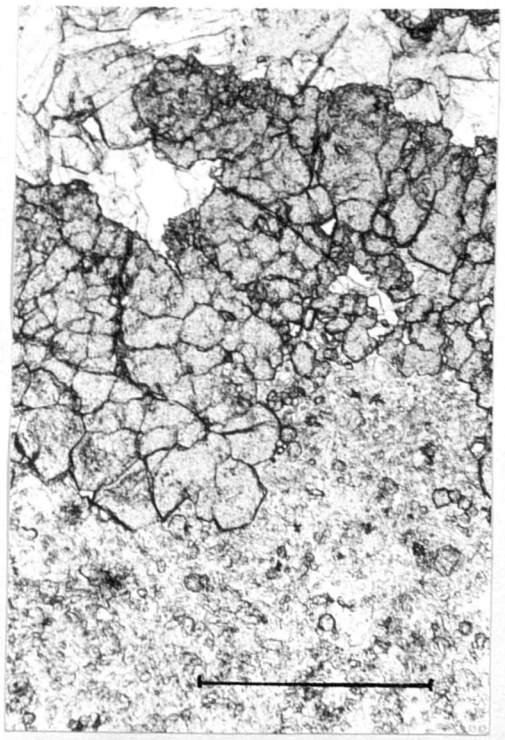

2·15

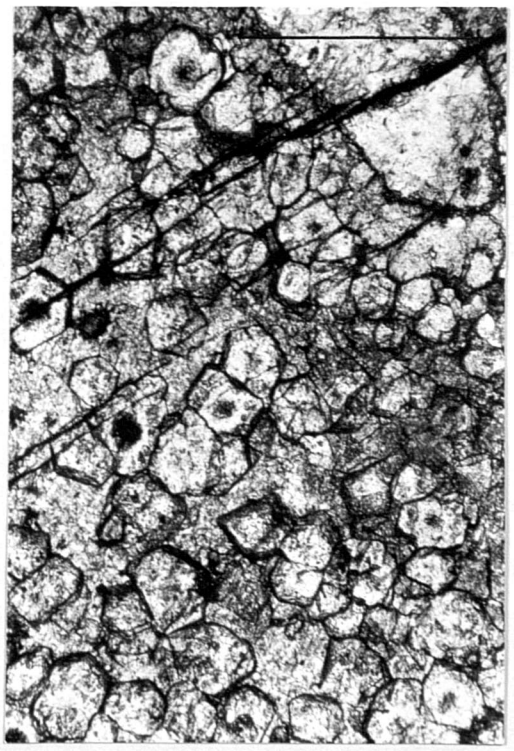

FIGURE 2.16 Extremely fine-grained sillimanite needles intergrown with plagioclase after white mica. Foliated meta-anorthosite, Gjörlangernova.

FIGURE 2.17 Typical amphibole-plagioclase-quartz symplectite after omphacite. Coarse-grained retroded eclogite, Gjörlangernova. Scale bar 1 mm.

FIGURE 2.18 Eclogite/amphibolite showing actinlitic amphibole (pale, thin dark rims) in apparent textural equilibrium with omphacite (darker, thick dark rims). Garnet in lower right-hand corner.

2·16

2·17

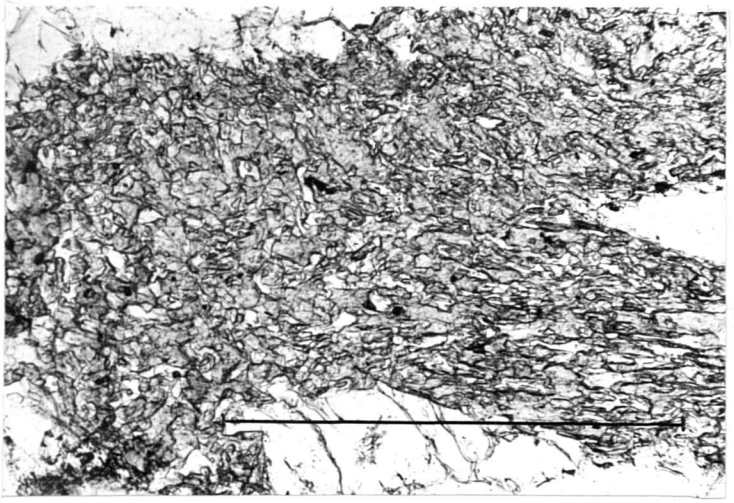

2·18

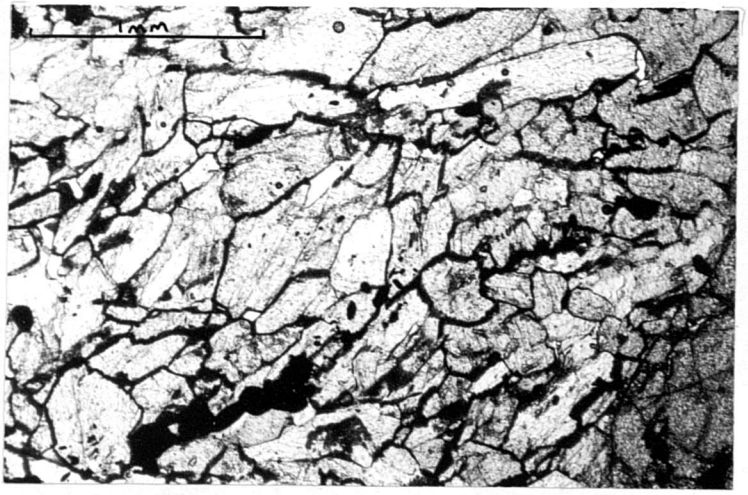

FIGURE 2.19 Garnet from bimineralic eclogite between Gjörlanger and Solvik (specimen D205). The micrograph is reproduced in figure 4.11 as a line drawing. Note colour zoning with darker red core, small hornblende (H) and ilmenite (I) inclusions in the core and rutile (R) and omphacite (O) inclusions near the paler rim.

FIGURE 2.20 Textural relationships in a chlorite harzburgite. Note parallel orientation of chlorite (C), enstatite (E) and oxide (O); also replacement of enstatite by talc (T) + olivine (F) or anthophyllite (A) + olivine, with anthophyllite overgrowing the foliation.

FIGURE 2.21 Pod of chlorite-pyroxene-garnetite in chlorite harzburgite, Solvik. Scale bar 30 cm.

2·19

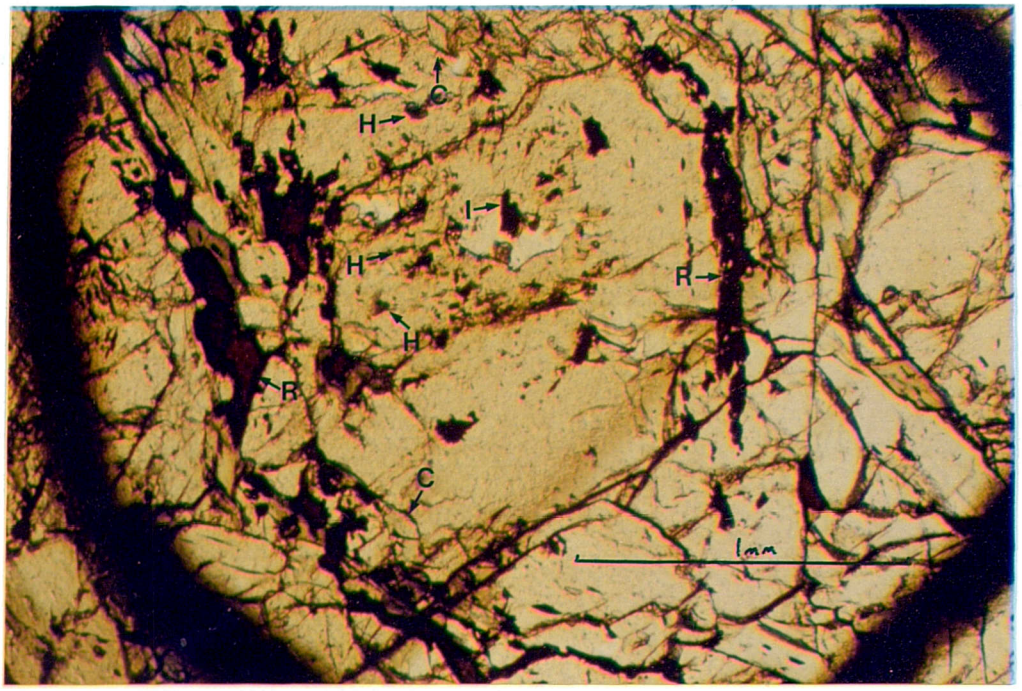

2·20

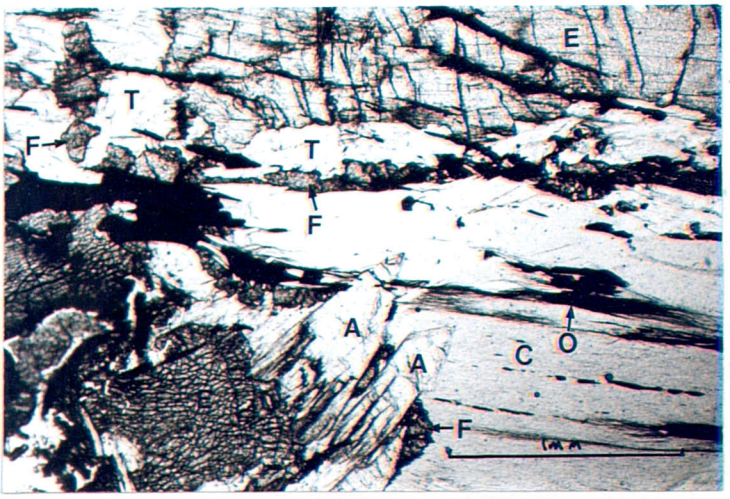

2·21

FIGURE 2.22 Jadeite-bearing coronite, Balsarvika. White patches are intergrowths of jadeite + zoisite + paragonite, green patches are omphacite, pink coronas are garnet with jadeite or omphacite inclusions. Black is lichen.

FIGURE 2.23 Coronite-eclogite with meta-anorthositic blocks, Balsarvika.

FIGURE 2.24 Bimineralic coronite-eclogite, Balsarvika. Note the omphacite-filled veins (V).

2·22

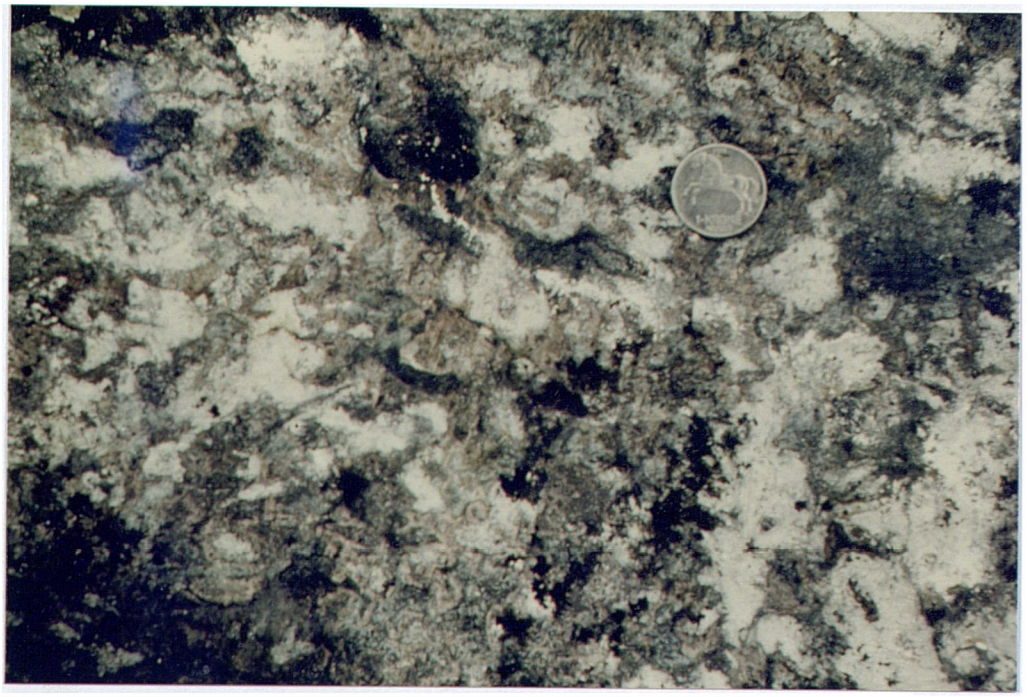

2·23

2·24

FIGURE 2.25 Photomicrograph of jadeite-zoisite intergrowth with paragonite (P) and the edge of a garnet corona at the top of the field of view with abundant jadeite inclusions. From Balsarvika, specimen D187. Scale bar 1 mm.

FIGURE 2.26 Augite heavily clouded with ilmenite, partially transformed to omphacite (O) and rutile (R) by garnet corona (G). Secondary hornblende (A) overgrows the omphacite and garnet. Scale bar 1 mm.

FIGURE 2.27 Idiomorphic Fe-Ti oxide with clear chlorite inclusions, surrounded and partly replaced by garnet. Textural relationships suggest an igneous origin. From the ilmenite-ore mine, Sördal. Scale bar 1 mm.

FIGURE 2.28 Coarse garnet-amphibole-Fe-Ti oxide rock which can locally be seen to be mimicking an igneous texture. Leirpol, Flekkefjord.

2·25

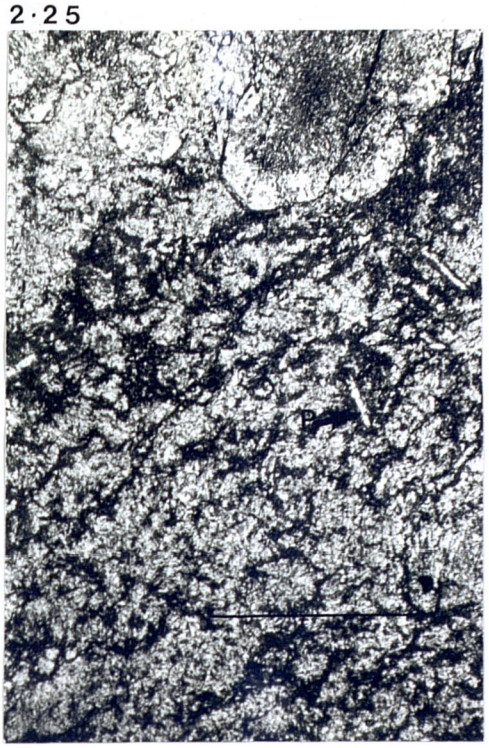

2·26

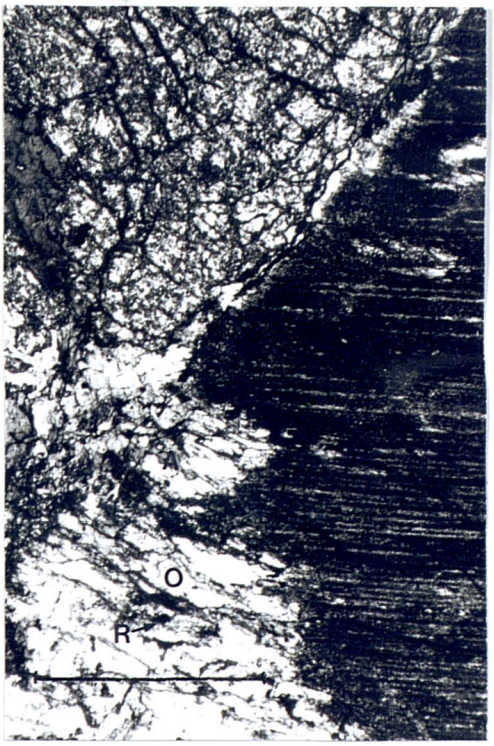

2·27

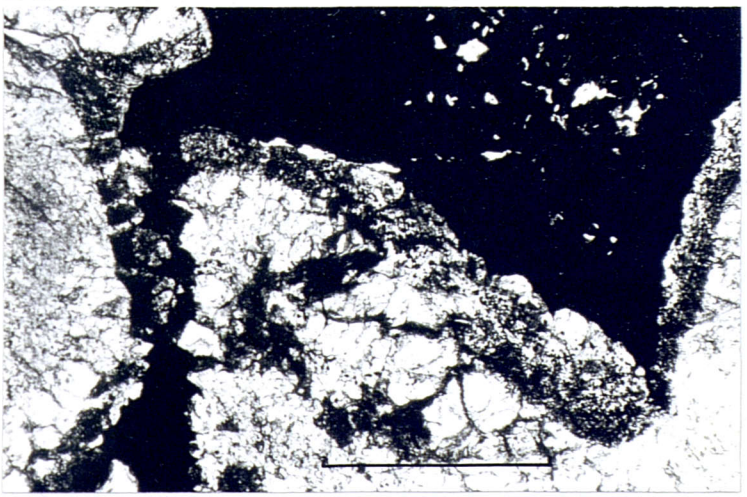

2·28

FIGURE 2.29 Pod of white zoisitite pod with blackwall reaction selvage against enclosing dunite. Successive reaction zones are garnet (pink), hornblende and chlorite (black) and anthophyllite/talc (not visible in this photograph).

2·29

FIGURE 2.30 Schematic section through the Flekke Unit as reconstructed from a number of localities. E = eclogites, squares indicate coronites or unaltered igneous assemblages. See text for details.

Figure 2.30

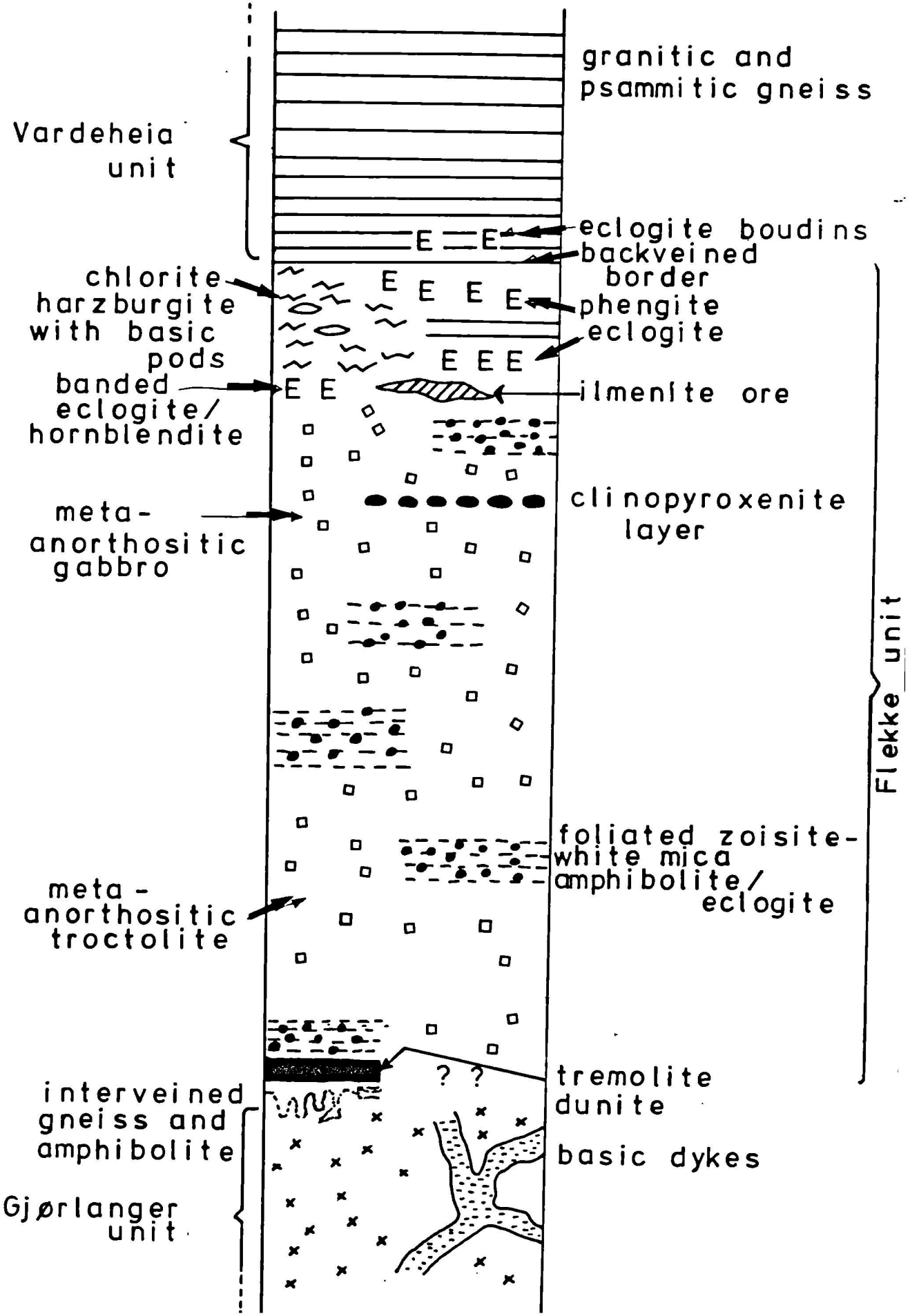
granitic and
psammitic gneiss
Vardeheia
unit
eclogite boudins
backveined
border
phengite
eclogite
chlorite
harzburgite
with basic
pods
banded
eclogite/
hornblendite
ilmenite ore
meta-
anorthositic
gabbro
clinopyroxenite
layer
Flekke unit
foliated zoisite-
white mica
amphibolite/
eclogite
meta-
anorthositic
troctolite
tremolite
dunite
basic dykes
interveined
gneiss and
amphibolite
Gjørlanger
unit

FIGURE 2.31 Typical appearance of grey, poorly deformed gneisses of the Gjörlanger Unit, Gjörlanger. Note patchy grain size variation and fine-grained aplitic lens above and left of hammer head. The gneiss at the extreme top left of the field of view has been mildly sheared to form an augen-gneiss.

FIGURE 2.32 Close-up of centre of field of view in figure 2.31, showing porphyroblastic texture and aplite lens. This is typical of the least altered charnockitic rocks.

FIGURE 2.33 Shear-zone in grey augen-gneiss of the Gjörlanger Unit, south of Flekke. Note the extreme flattening of the white feldspar augen. Pencil is 15 cm long.

2·31

2·32

2·33

FIGURE 2.34

A. Photomicrograph of charnokitic gneiss from south of Flekke in the Gjörlanger Unit. Clots of lamellar hypersthene (H), augite (A) and quartz lie in a matrix of plagioclase (P) clouded with extremely fine zoisite and white mica. Plane-polarised light, scale bar 1 mm.

B. Expanded view of hypersthene with exsolution lamellae of calcic pyroxene. Clear grains are quartz. Fine coronas of garnet (G) rim the pyroxene against the plagioclase. Scale bar 0.5 mm.

FIGURE 2.35 Hydration products in altered charnockitic grey gneiss from the Gjörlanger Unit. Slightly altered pink hypersthene lies at top right, surrounded by quartz. To its left is a corona with a core of actinolite + quartz +/- biotite (A), rimmed by fine beads of garnet, then hornblende + biotite (HB) against plagioclase (perthitic) clouded with fine zoisite (P). Note the more brown-coloured biotite replacing the ilmenite. The corona is a result of hydration of granulite-facies pyroxenes. Plane polars, scale bar 1 mm.

FIGURE 2.36 Slightly deformed grey gneiss with recrystallisation of hydrous phases. B = biotite G = garnet, Z = zoisite, H = hornblende, F granular microcline + albite intergrowth. Scale bar 1 mm.

2·34 A

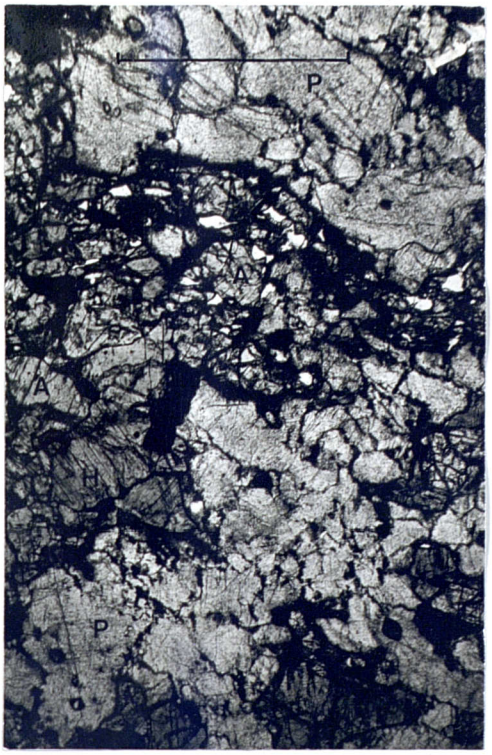

2·34 B

2·35

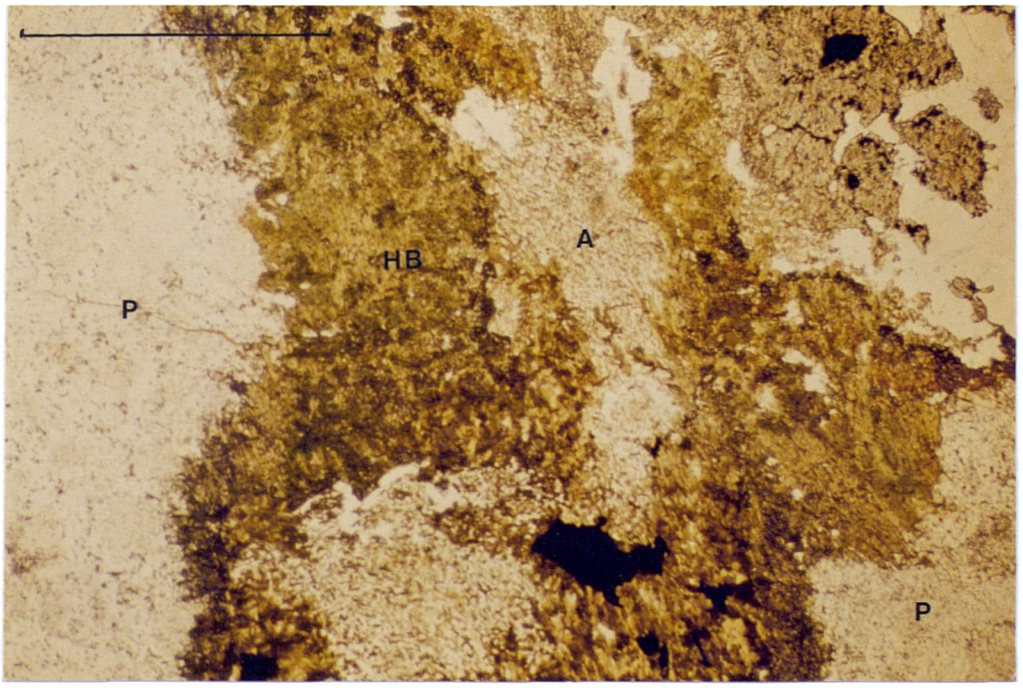

2·36

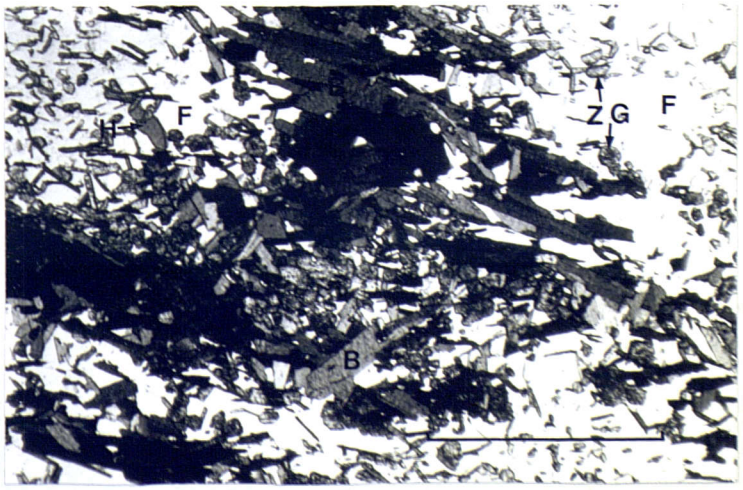

FIGURE 2.37 Sketch of metabasic dykes now consisting of eclogite, in grey orthogneisses of the Gjörlanger Unit. Solid lines - sharp margin. Hatched lines - diffuse margin. "Lobe" indicated is that shown in figure 2.39. Figures indicate locations of samples D80-83 and D83A. From cutting by road from Gjörlanger to Solvik.

Figure 2.37

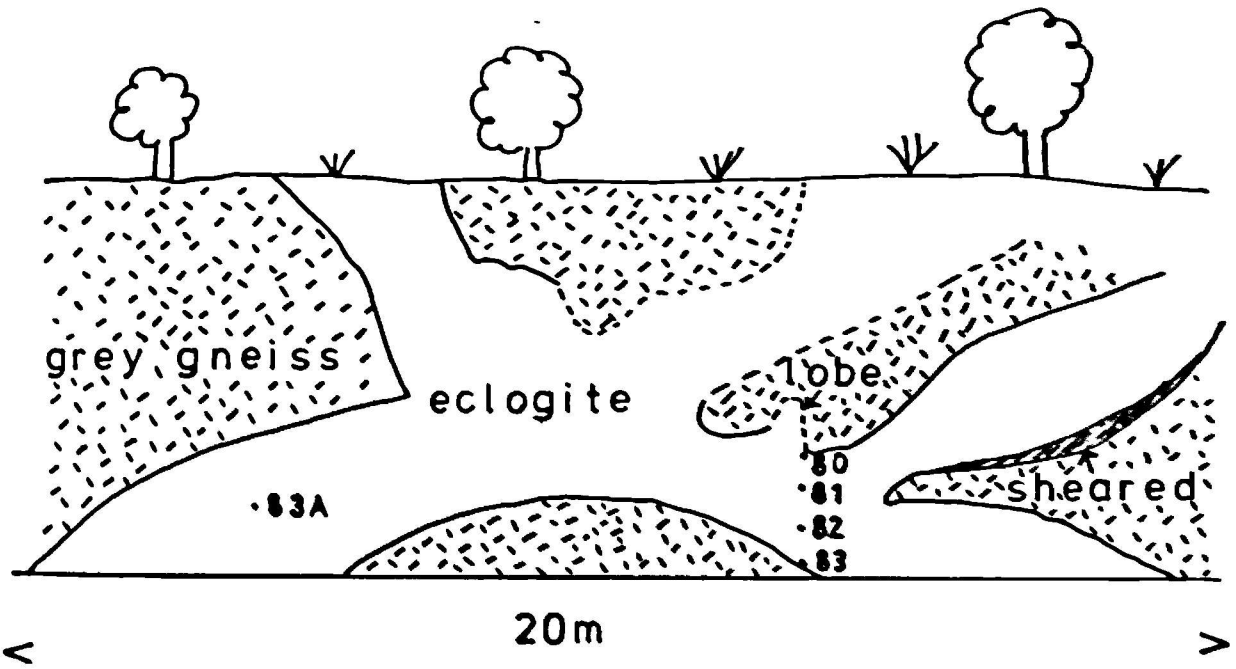

FIGURE 2.38 Basic sheet in grey gneiss, Gjörlanger Unit between Gjörlanger and Solvik. The basic sheet is an eclogite with a blocky appearance (lower half of field of view) whose upper boundary is diffuse, marked by the whiter, streaky rock, some of which extends into the eclogite sheet as back-veins. Sample D83A comes from just below the hammer head.

FIGURE 2.39 Metabasic sheet (now eclogite) in lower field of view, with a diffuse-bordered lobe of eclogite extending into the overlying gneiss - Samples D80, D81, D82 and D83 come from the area right of the hammer. Note the unfoliated nature of the gneiss and the eclogite.

FIGURE 2.40 Partly altered granulite-facies paragenesis from basic dyke by Gjörlangerfjord. Marginally amphibolitised augite (A) and hypersthene (H) lie in a matrix of heavily clouded plagioclase (P) and clear K-feldspar (K). Later beads of garnet rim the pyroxenes.

2·38

2·39

2·40

FIGURE 2.41 Basic dyke cutting charnockitic granodiorites south of Flekke. This dyke has a granulite-facies paragenesis similar to that in figure 2.40.

FIGURE 2.42 Close-up of dyke margin showing its sharp, non-tectonic nature.

FIGURE 2.43 Streaky grey gneiss with more mafic and more felsic areas, typical of the transition between grey gneiss and metabasite.

2·41

2·42

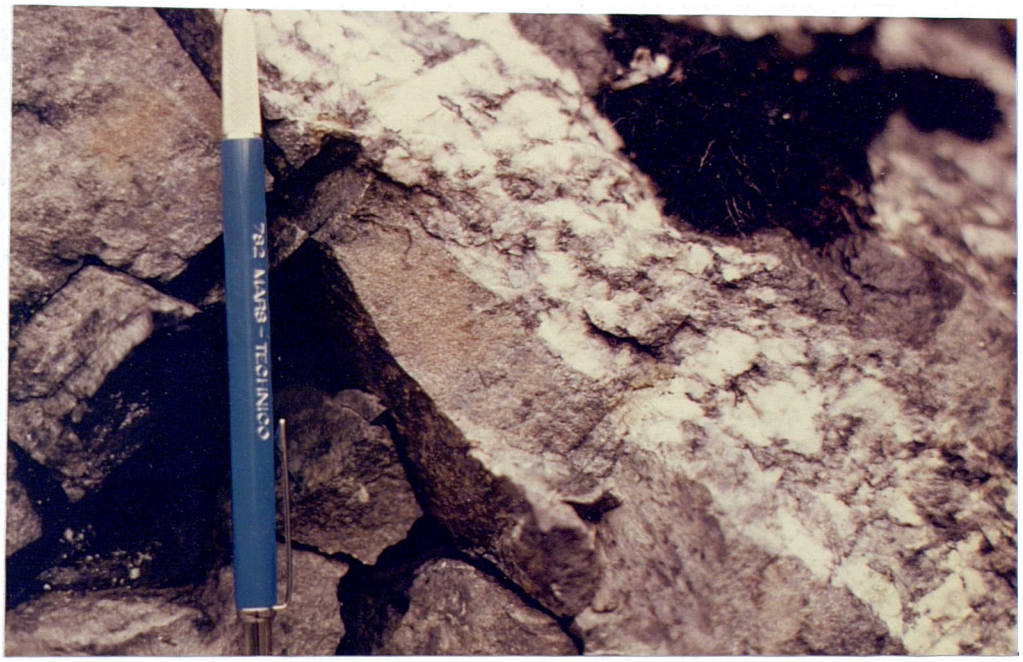

2·43

FIGURE 2.44 Diffuse bodies of metabasite (amphibolite with relics of garnet and omphacite) in grey gneisses, Gjörlanger Unit near Trollefoss, south of Flekke.

FIGURE 2.45 Garnet in kyanite eclogite from Haheia (specimen D123) with core zone full of hornblendic actinolite inclusions, along with minor quartz and zoisite. This photomicrograph is reproduced as a line drawing in figure 4.10. Scale bar 1 mm.

FIGURE 2.46 Kyanite eclogite west of Jyttevatnet (specimen D77). G = garnet, O = omphacite (with dark marginal symplectite), K = kyanite (with zoisite inclusions), P = phengite, Z = zoisite. Scale bar 1 mm.

FIGURE 2.47 Quartz-phengite-omphacite-kyanite rock with omphacite almost completely altered to a submicroscopic symplectite and kyanite (K) rimmed by fibrolitic sillimanite (S). Scale bar 1 mm.

2·44

2·45

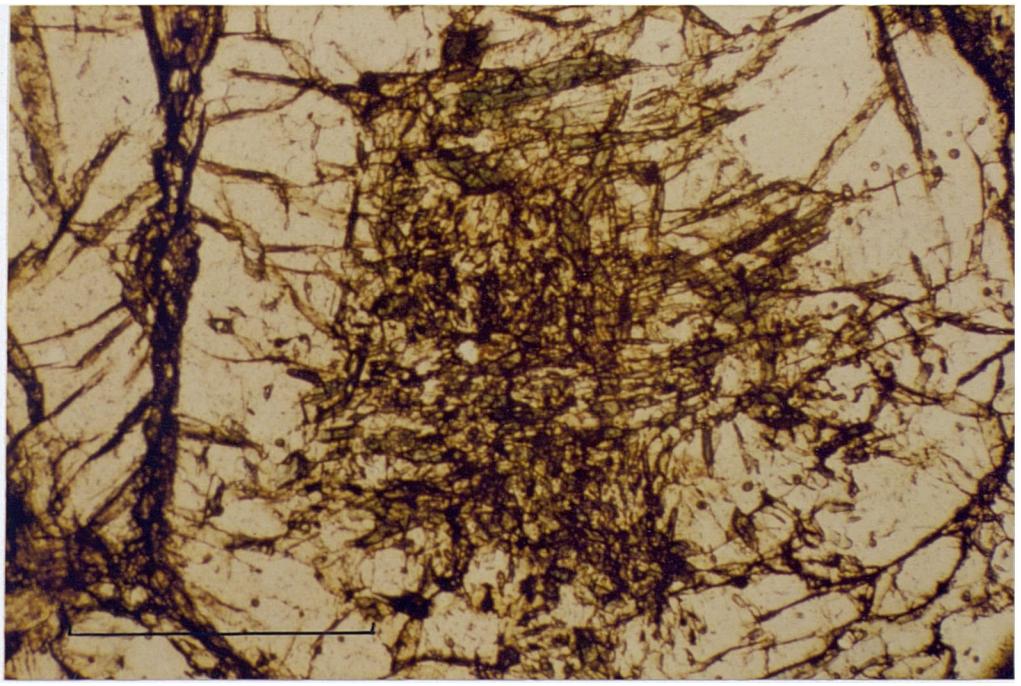

2·46

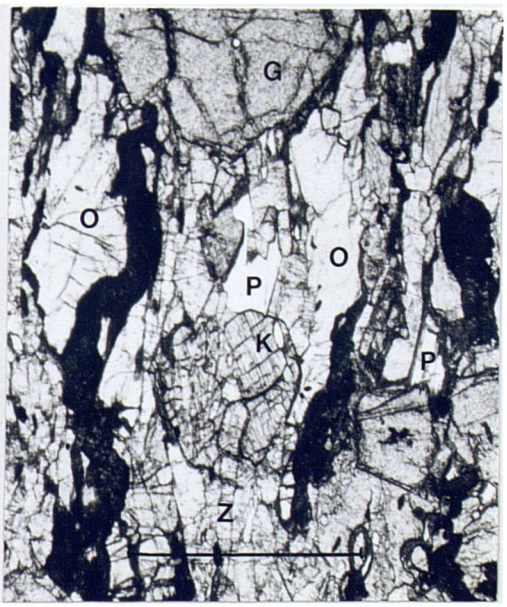

2·47

FIGURE 2.48 Omphacite in heavily altered massive green gneiss, with exsolution lamellae of another (omphacitic?) pyroxene. Scale bar 0.3 mm.

FIGURE 2.49 Textural relationships of corona in altered charnockitic gneiss. A bead-like corona of garnets (G) rims a very fine-grained granular mass of amphibole + plagioclase + quartz (A) which has probably replaced omphacite. Inclusions of ilmenite and rutile (black), apatite and zircon also appear. Outside the garnets there is a fine-grained mass of biotite (B), surrounded by microperthite, clouded with zoisite, white mica and biotite (F).

FIGURE 2.50 Breccia of grey-gneiss fragments in a matrix of amphibolite (A) on the margin of a websterite body. Gjörlanger.

2.48

2.49

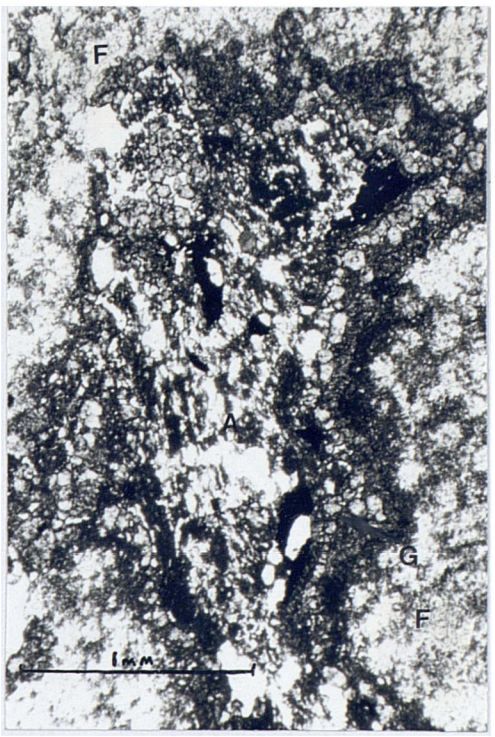

2.50

FIGURE 2.52 Garnetite veins, bordered by omphacite-pyroxenite (pale green) cutting websterite in roadcut by route 607, Gjörlanger.

FIGURE 2.53 Fine interbanding of garnet, omphacite and amphibole-rich bands (omphacite paler green than amphibole) near eastern end of websterite outcrop, Gjörlanger. This example lies below and left of the hammer in figure 2.62. Sample 79/9a comes from one of these bands. Hammer head for scale, lower frame.

2·52

2·53

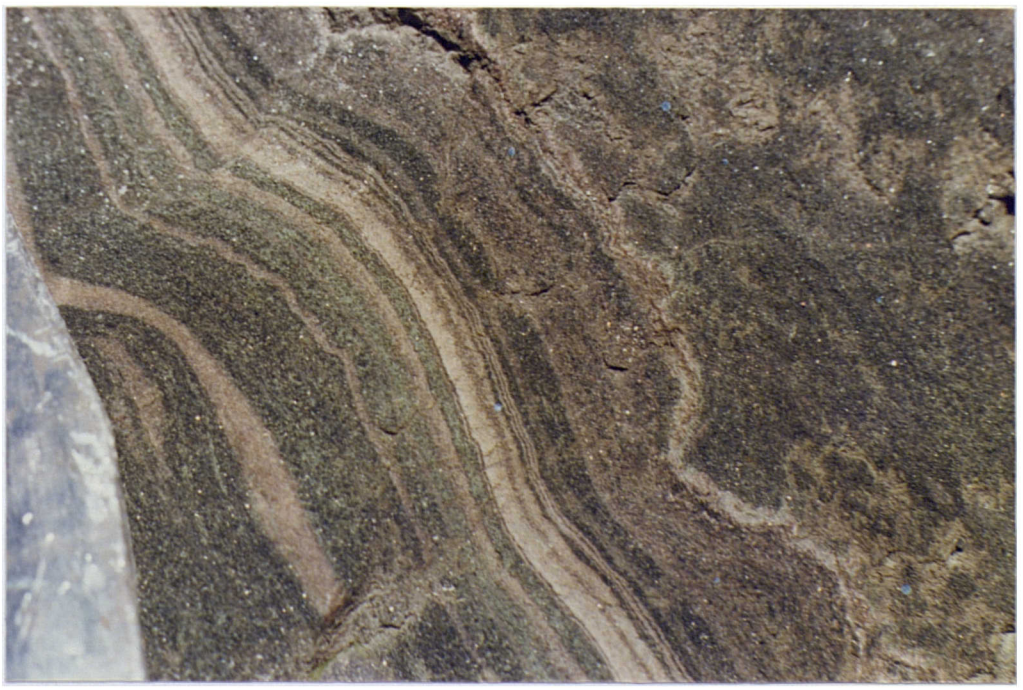

FIGURE 2.54 Textural relationships in websterite. Anhedral oxide is rimmed by chlorite (C), amphibole (A) or garnet (G). A small relic of pleonaste spinel (dark grey) lies in the oxide mass with a small chlorite growing into it (pale grey). To its right is a large mass of garnet (G) with chlorite and amphibole inclusions. An amphibole at the top of the frame has oxide speckling in its core, typical of replacement products of the early pyroxenes. Specimen D45 from south of Gjörlangerelva.

FIGURE 2.55 Typical "atoll" garnet from eclogite D116 in the Basal Gneisses east of Breidvatnet. Note the biotite-feldspar symplectites after phengite and marginal diopside-plagioclase symplectite surrounding the omphacite. Scale bar 0.3 mm.

FIGURE 2.56 Garnet from eclogite in the Basal Gneisses with glaucophane inclusions (G) and omphacite inclusion (O). Scale bar 0.3 mm.

2·54

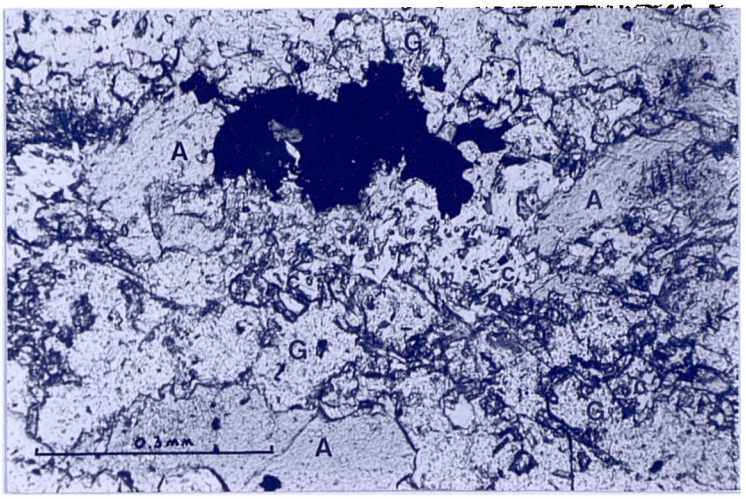

2·55

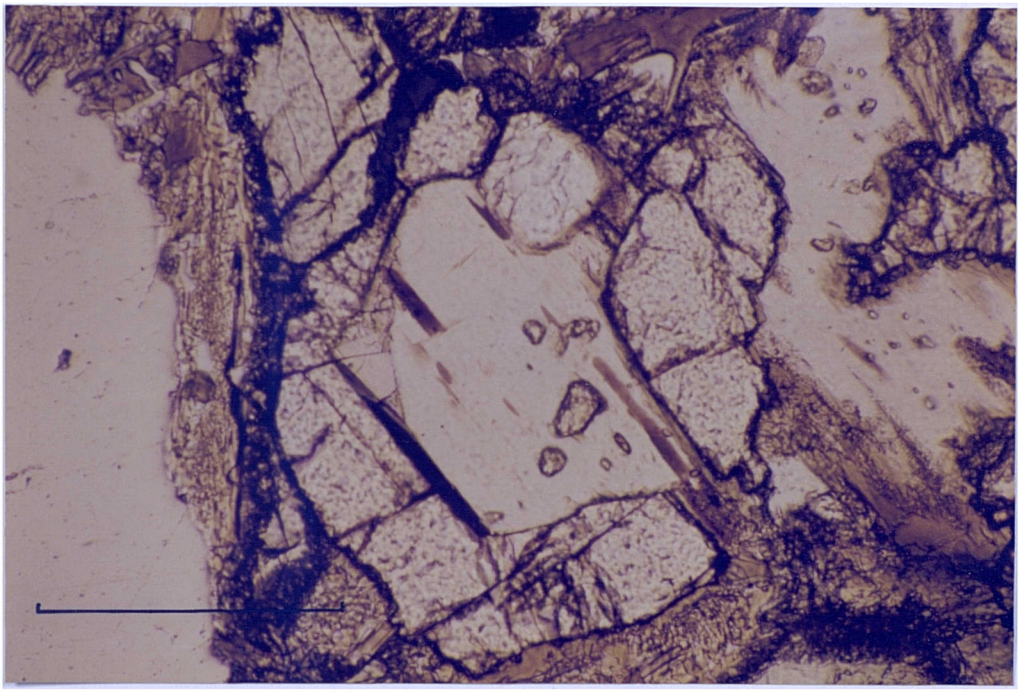

2·56

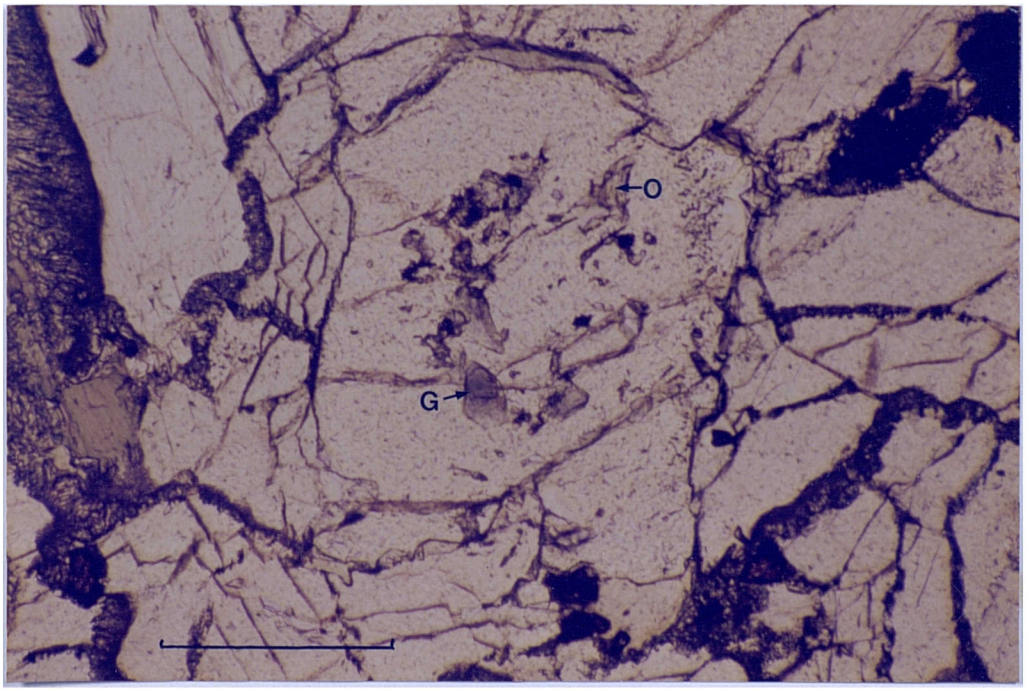

FIGURE 2.57 Relationship of younging direction (arrowed) and S_1 fabric to grade layering (S_0) in metacumulate from north of Instetjörna.

FIGURE 2.58 Recumbant F_2 fold from west of the summit of Vardheia, Vardheia Unit.

FIGURE 2.59 Tight isoclinal F_2 folds defined by omphacite, zoisite or garnet-rich layers in eclogite. Bogevik, Tyssedalsvatnet.

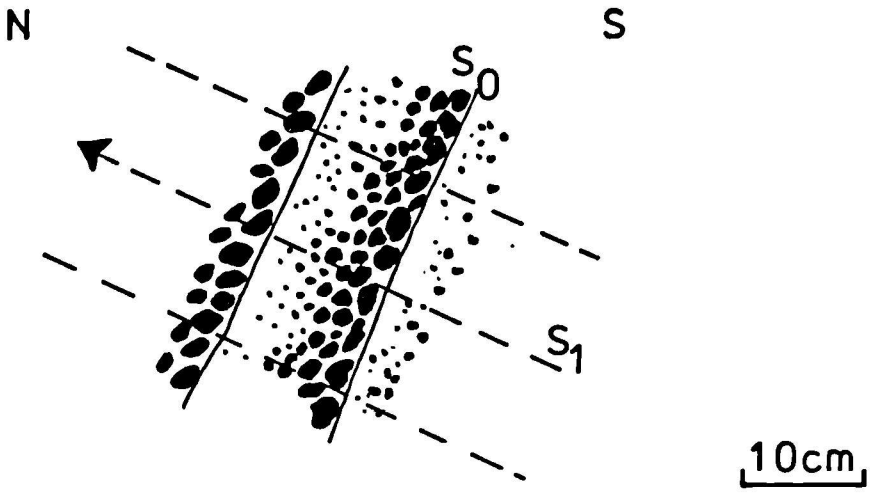

Figure 2.57

Figure 2.58

Figure 2.59

FIGURE 2.60 F_2 chevron folds folding S_1 foliation in garnet amphibolite (retrograded eclogite). North slopes of Haheia, Flekke Unit.

FIGURE 2.61 F_3 fold in grey gneisses, Gjörlanger. Intrusive breccia bordering websterite lies in the core of the fold.

FIGURE 2.62 F_3 fold deforming garnet-rich banding in websterite body, Gjörlanger. The garnetite bands are probably related to the veins shown in figure 2.52.

2·60

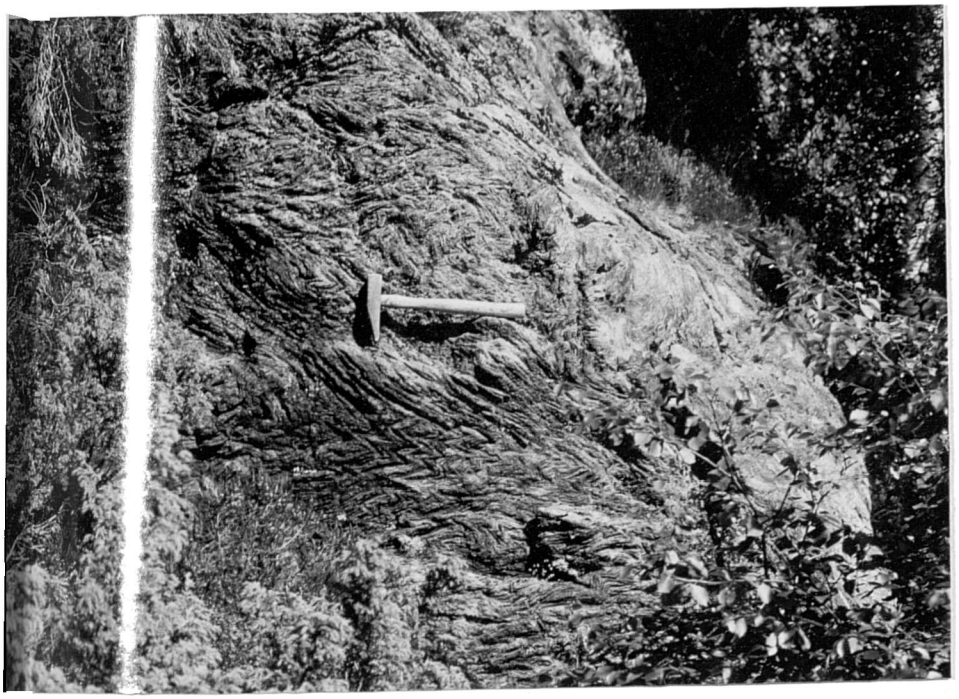

2·61

2·62

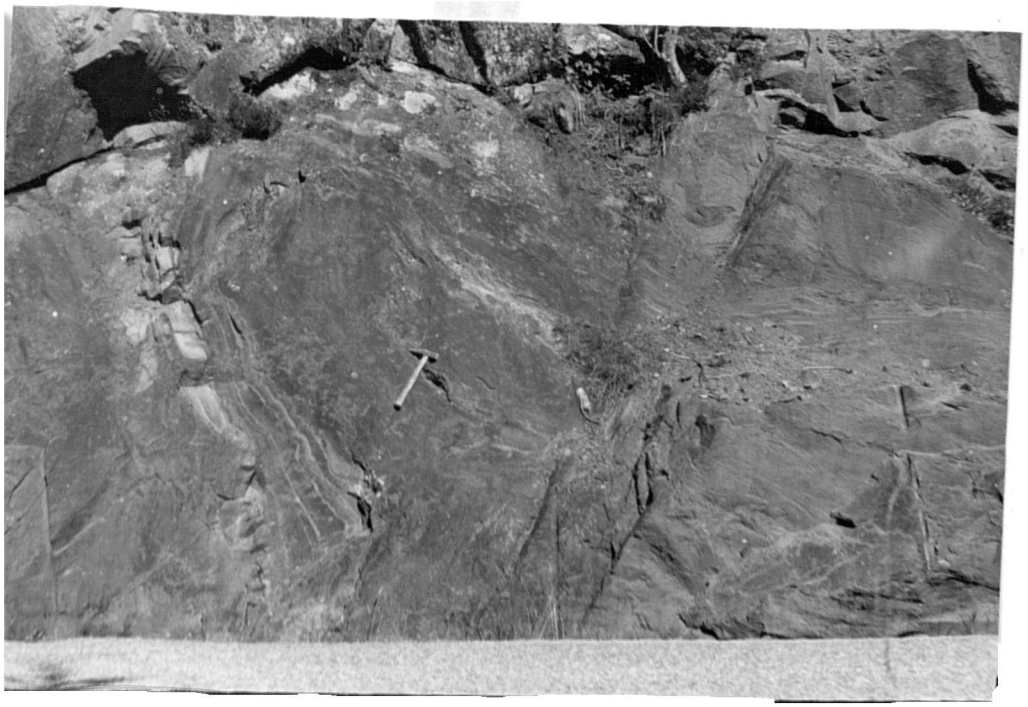

FIGURE 2.63 F_3 fold in orthogneisses of Basal Gneisses with limb folded around open upright F_4 fold. Roadcut on route 57, south end of Breidvatnet.

FIGURE 2.64 Open, upright folding of F_4 phase in meta-psammites of the Vardheia Unit south of Asnes, Gjörlangerfjord.

Figure 2.63

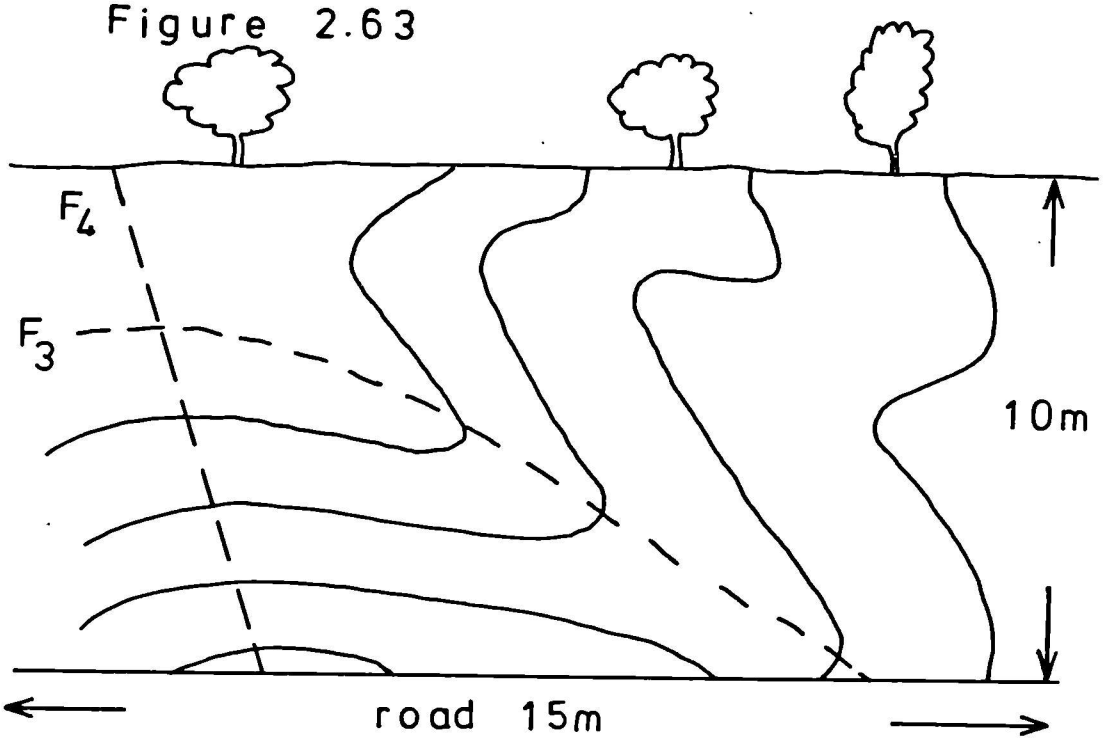

2.6

FIGURE 2.65 Equal area stereographic projections for poles to foliation S_1, contoured by the Mellis method. Each circle represents 1 point and occupies 1% of the total area.

A. All measurements for the study area.
B. All measurements to the east of Haheia.
C. All measurements to the west of Haheia.
D. Orientations of lineations. Open square - axes to minor folds (F_2). Filled square - mineral lineations, augen elongation. Also plotted is the S-Pole girdle fitted to the highest concentrations of points A, B and C.

Figure 2.65 A

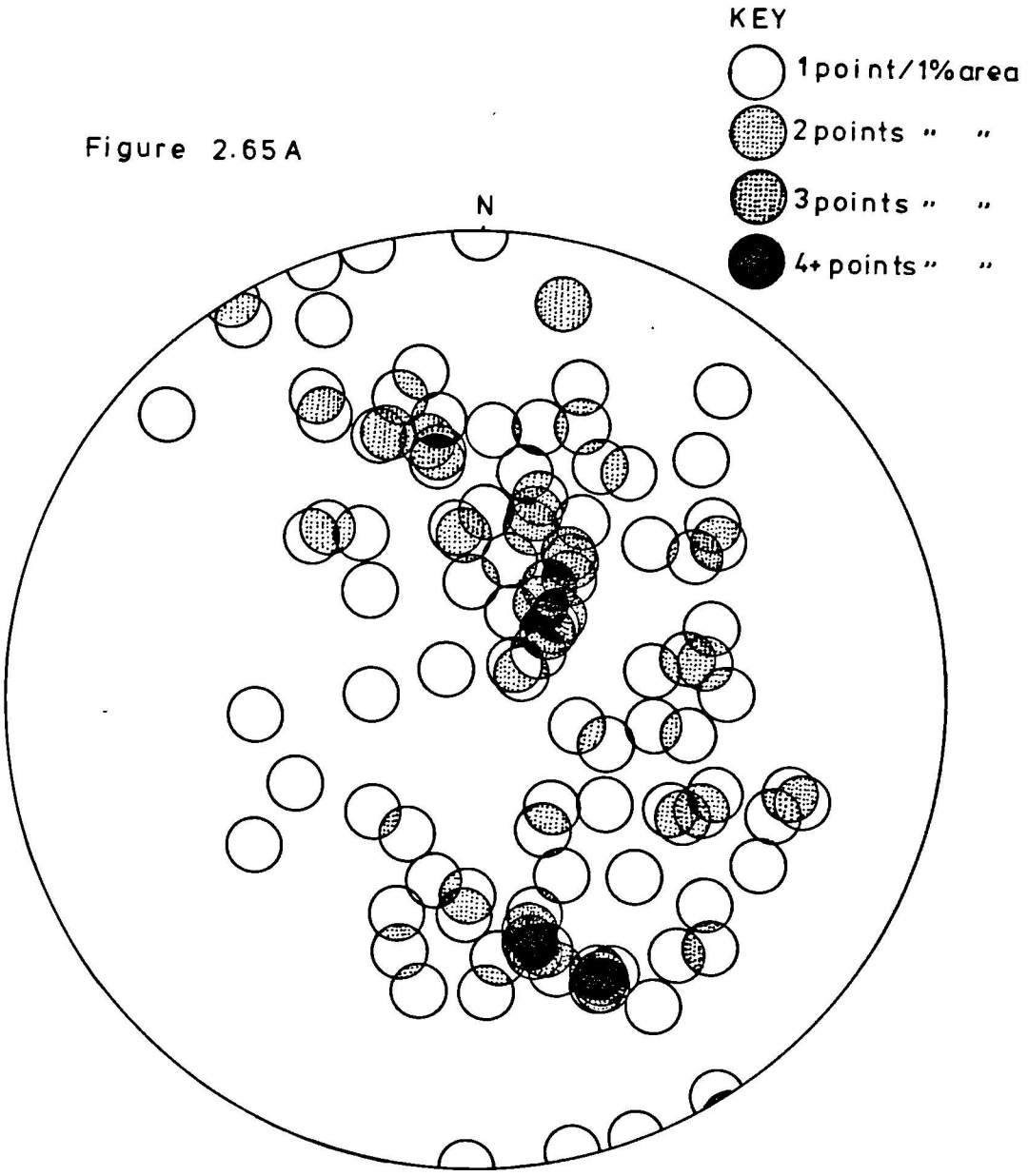

Figure 2.65B

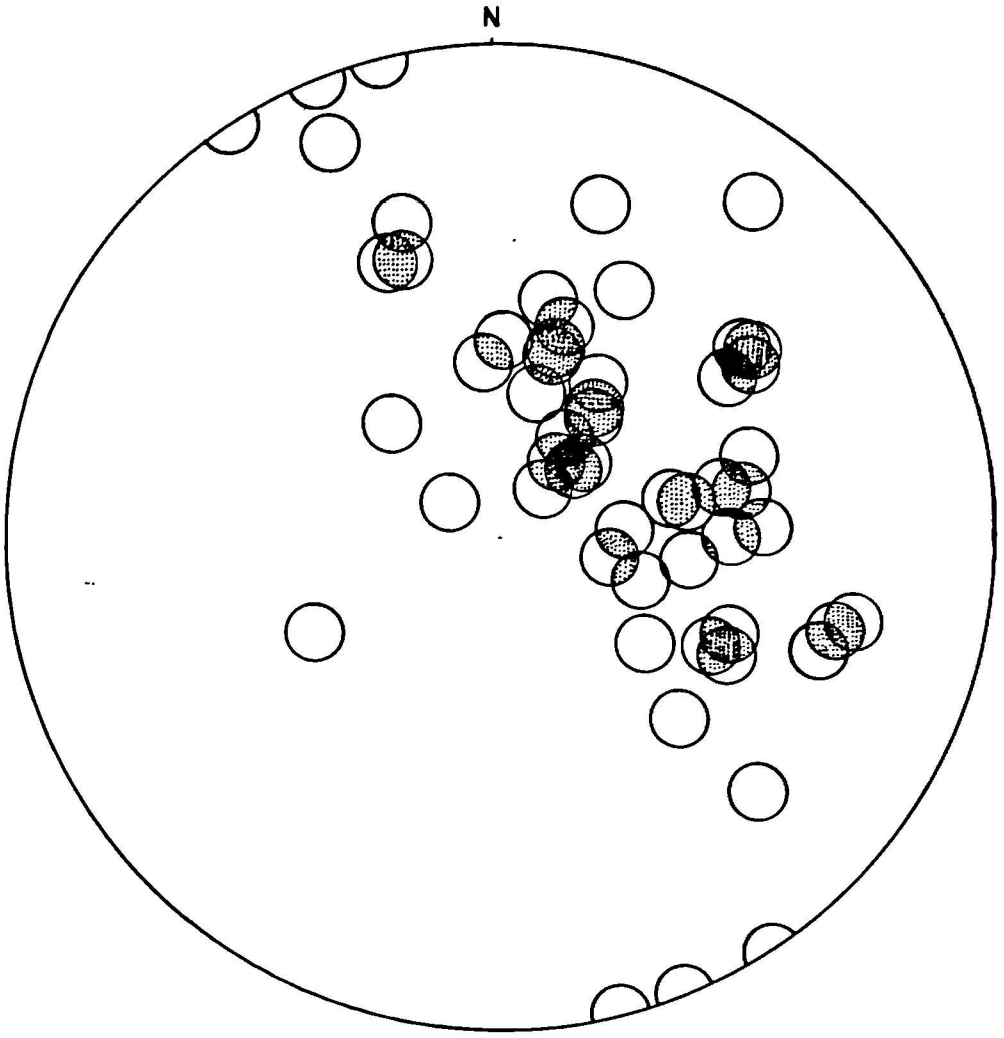

Figure 2.65C

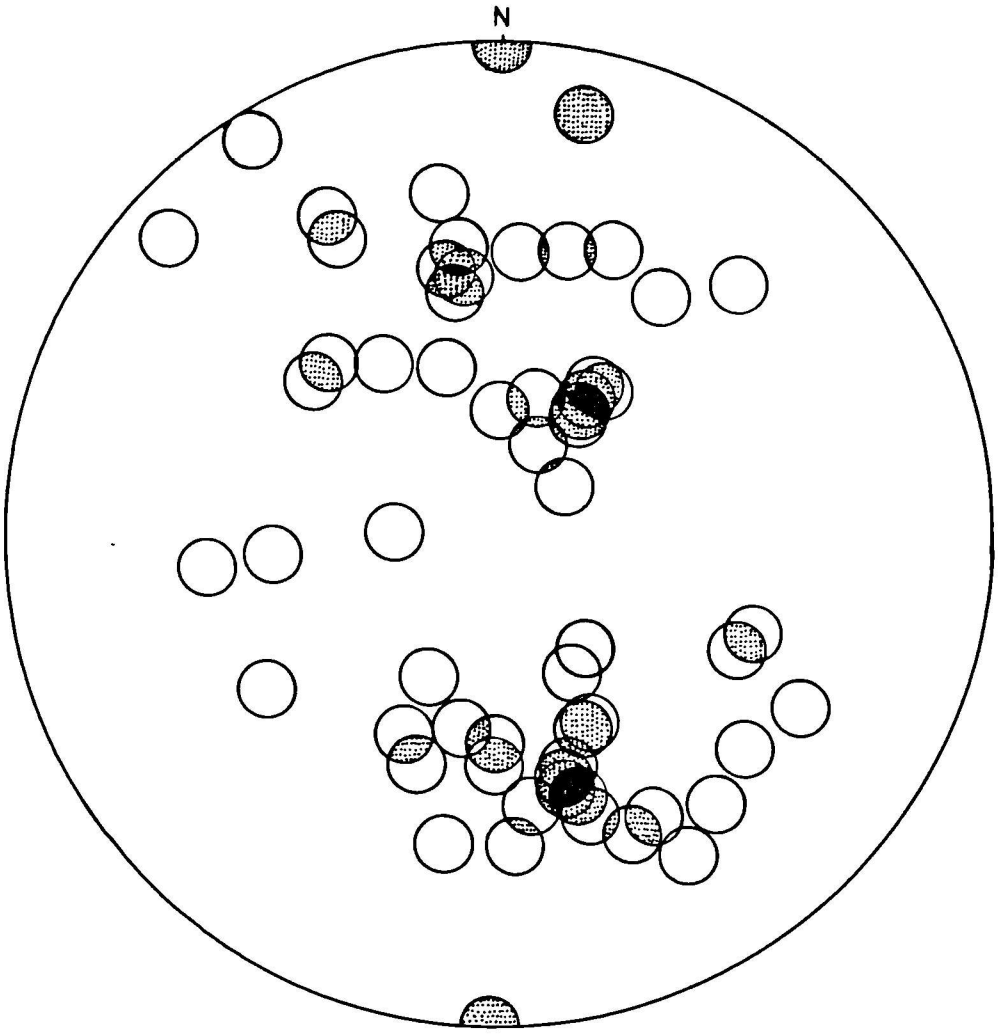

Figure 2.65D

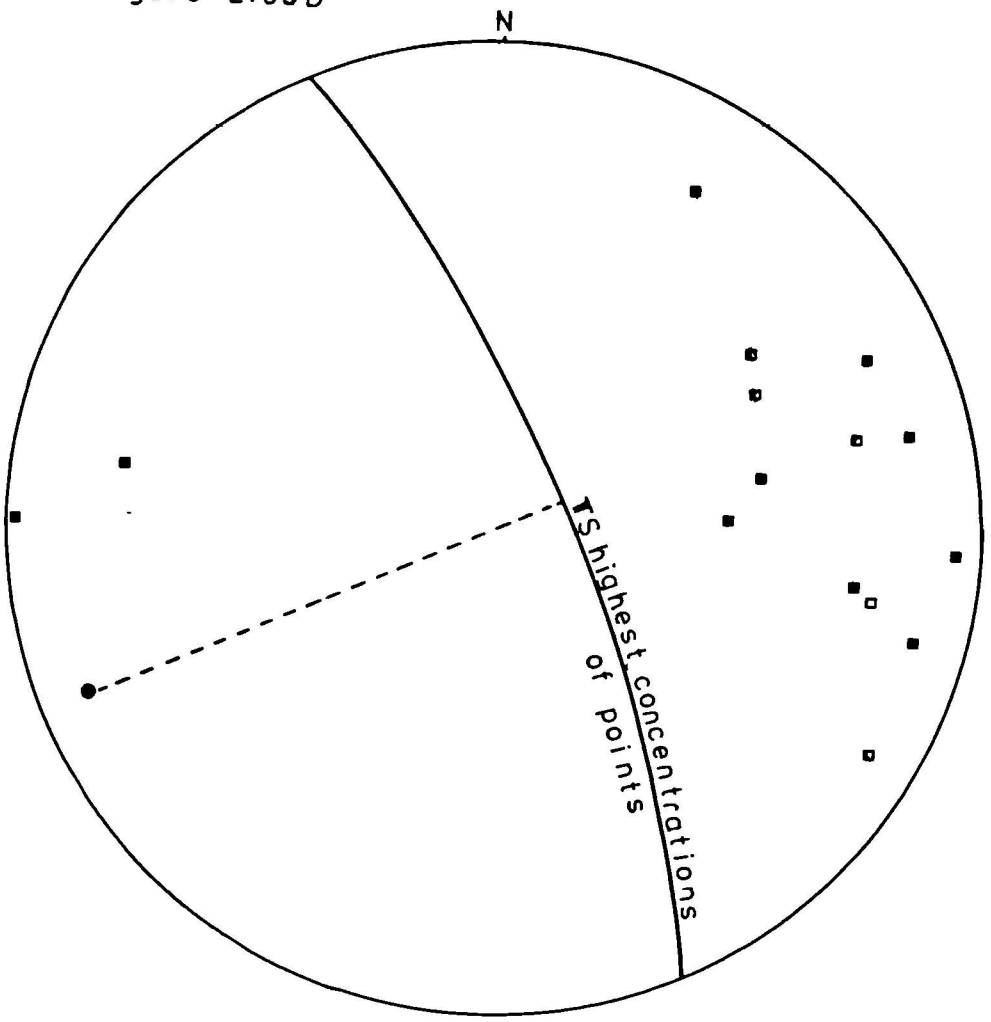

FIGURE 2.66 Typical quartz-phengite-albite-garnet assemblage associated with S_1 in psammitic gneiss, with marginal development of biotite + K-feldspar + quartz (B) around the phengite (P). Plane-polarised light, scale bar 1 mm.

FIGURE 2.67 Tectonic disruption of garnet corona in meta-anorthositic gabbro from north of Sördal. Note gaps between clots of garnet, which are filled with quartz (Q) or barroisite (B). Core of the corona consists of omphacite (dark, symplectic rims) and barroisite. Scale 1 mm.

FIGURE 2.68 F_3 bending of S_1 phengite causing undulose extinction and formation of sub-grains in adjacent albite and quartz. Phengitic grey gneiss, Gjörlanger. Crossed polars, scale bar 1 mm.

2·66

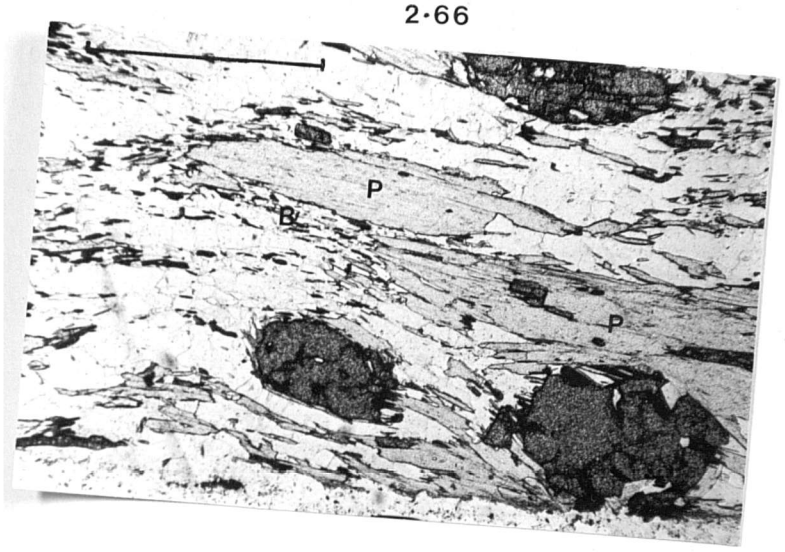

2·67

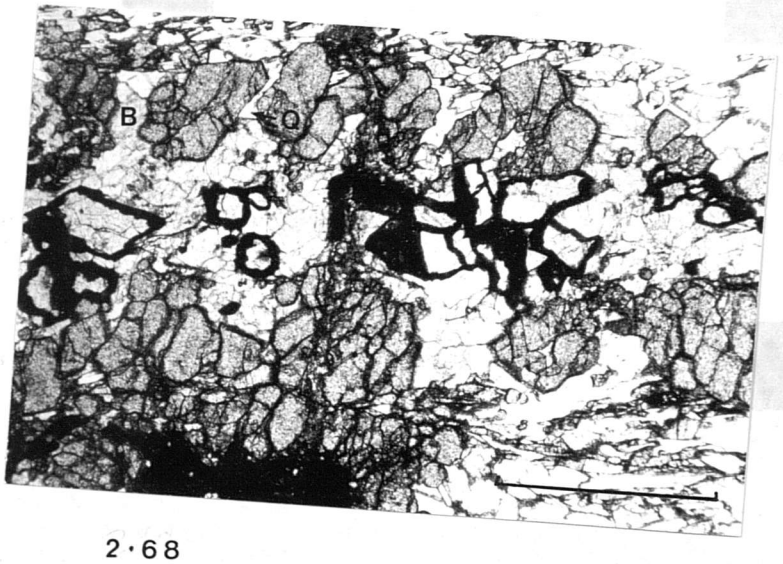

2·68

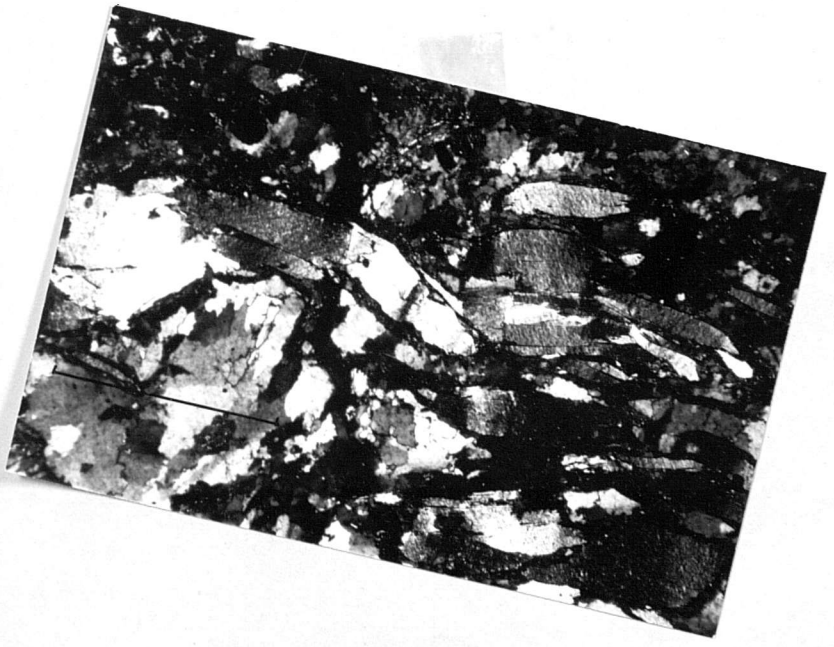

FIGURE 2.69 S_1 foliation formed by chlorite, olivine and oxide in chlorite peridotite, deformed by F_3 crenulations. Post S_1 anothophyllite (A) and later talc (T) is fractured or bent by F_3. Note fractures in anthophyllite and undulose extinction in talc. From roadcut by Flekke school. Crossed polars, scale bar 1 mm.

FIGURE 2.70 Heavily strained and granulated quartz and feldspars in mylonitic gneiss, east shore of Breidvatnet near boundary between Basal Gneisses and Gjörlanger Unit.

2·69

2·70

FIGURES AND TABLES

CHAPTER 3

FIGURE 3.01 Major element concentrations of Gjörlanger Unit lithologies plotted against the differentiation index of Thornton and Tuttle (1960). Analyses have been recalculated to 100% water-free.

Symbols:-

Open circles = Basal Gneisses
Closed circles = Grey Gneisses
Open squares = K-poor gneisses
Closed squares = Massive green gneisses
Close triangles = Metabasic dyke rocks

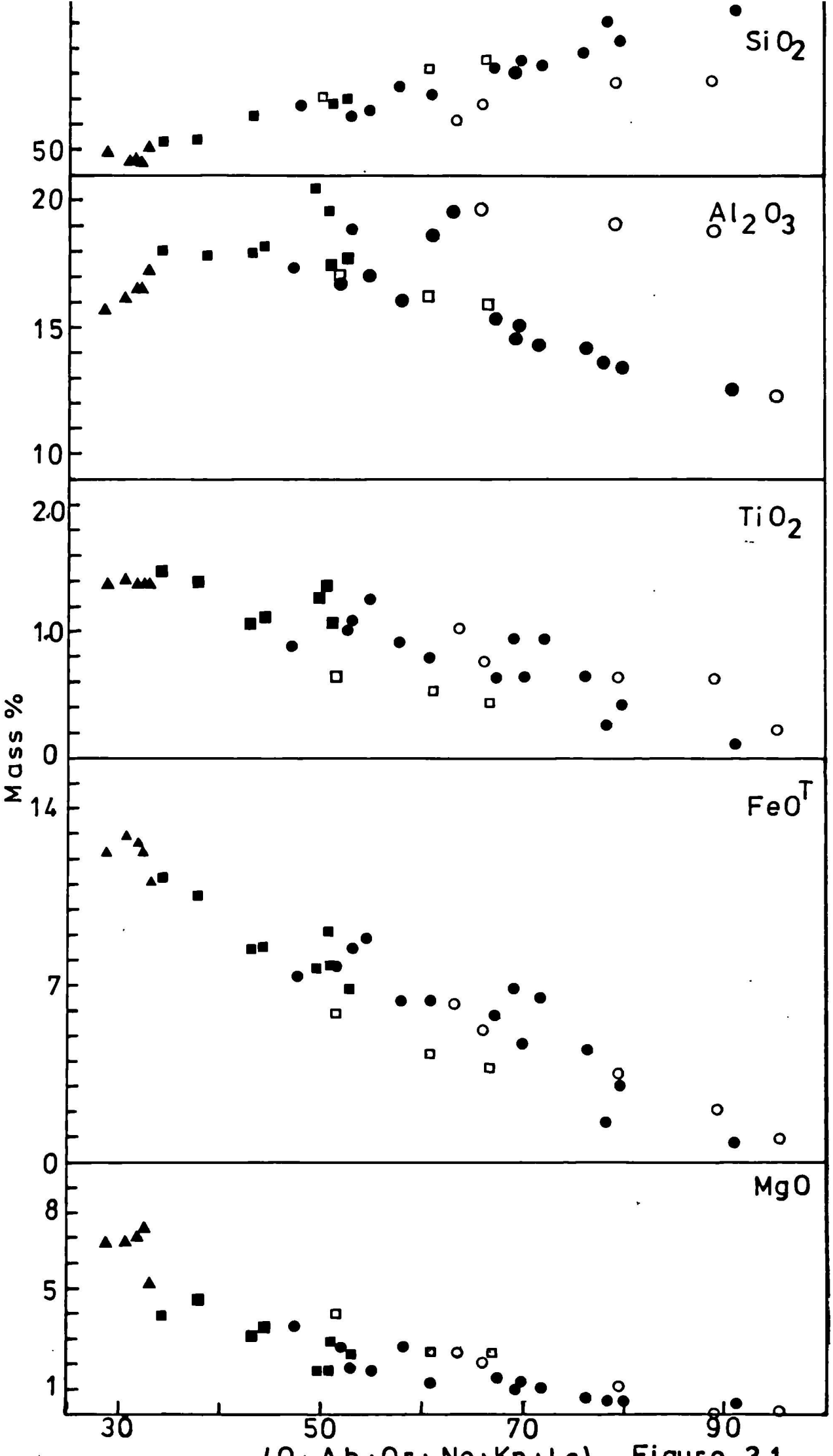
SiO2
50
Al2O3
20
15
10
TiO2
2.0
1.0
0
Mass %
FeO^T
14
7
0
MgO
8
5
1
30
50
70
90
(Q+Ab+Or+Ne+Kp+Lc)

Figure 3.1

Figure 3.1 Cont.

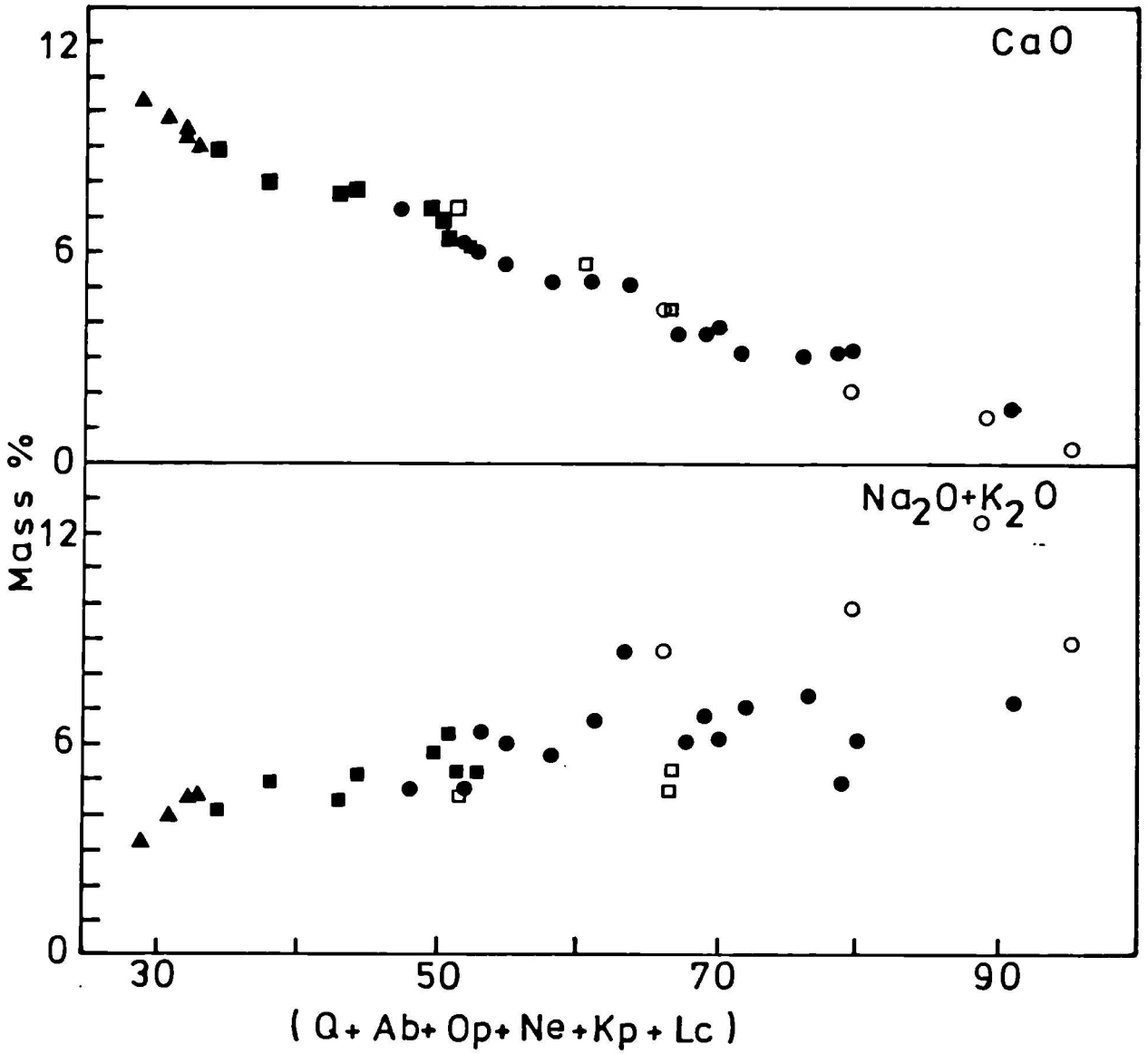

Figure 3.2

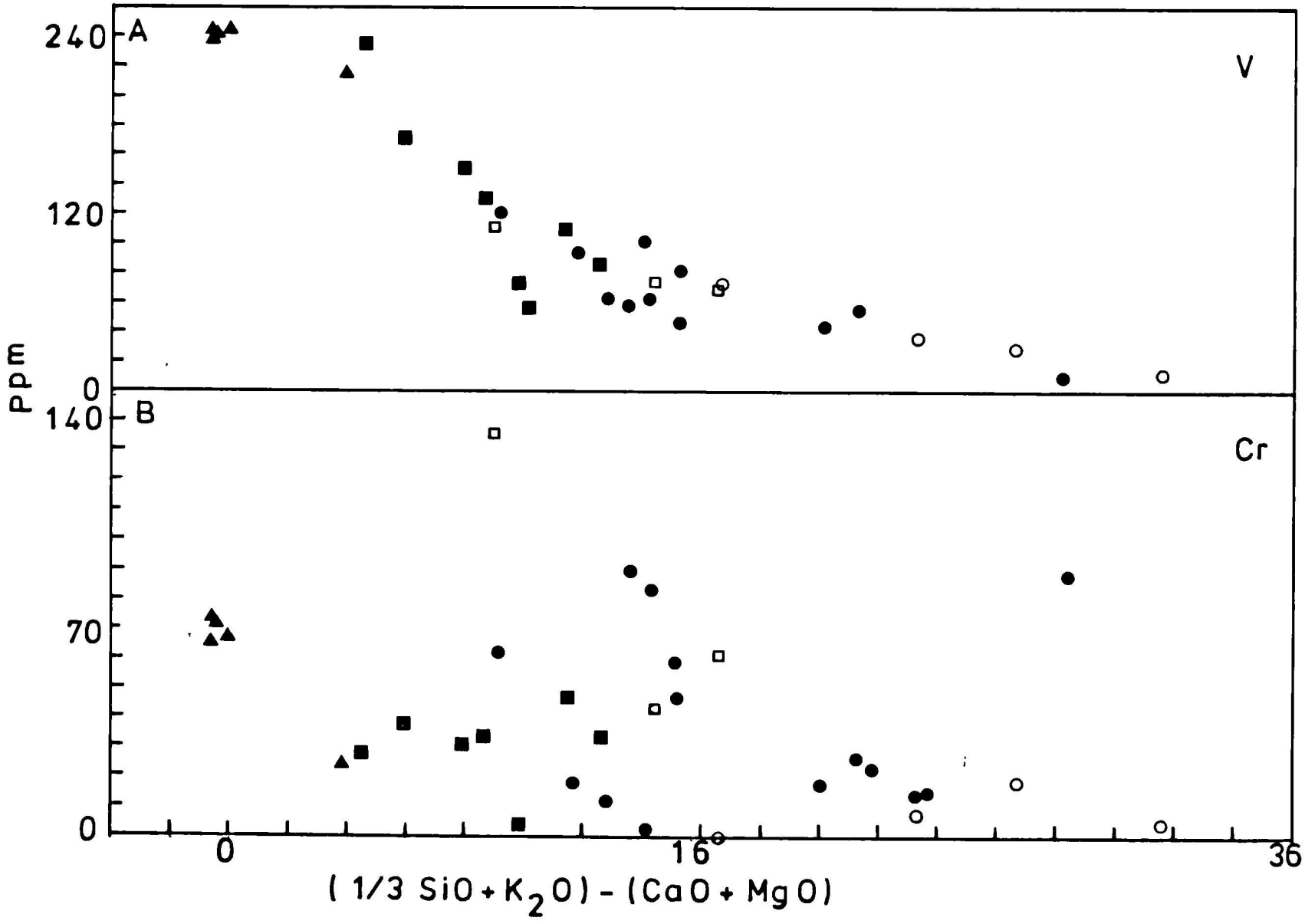

Figure 3.2 Cont.

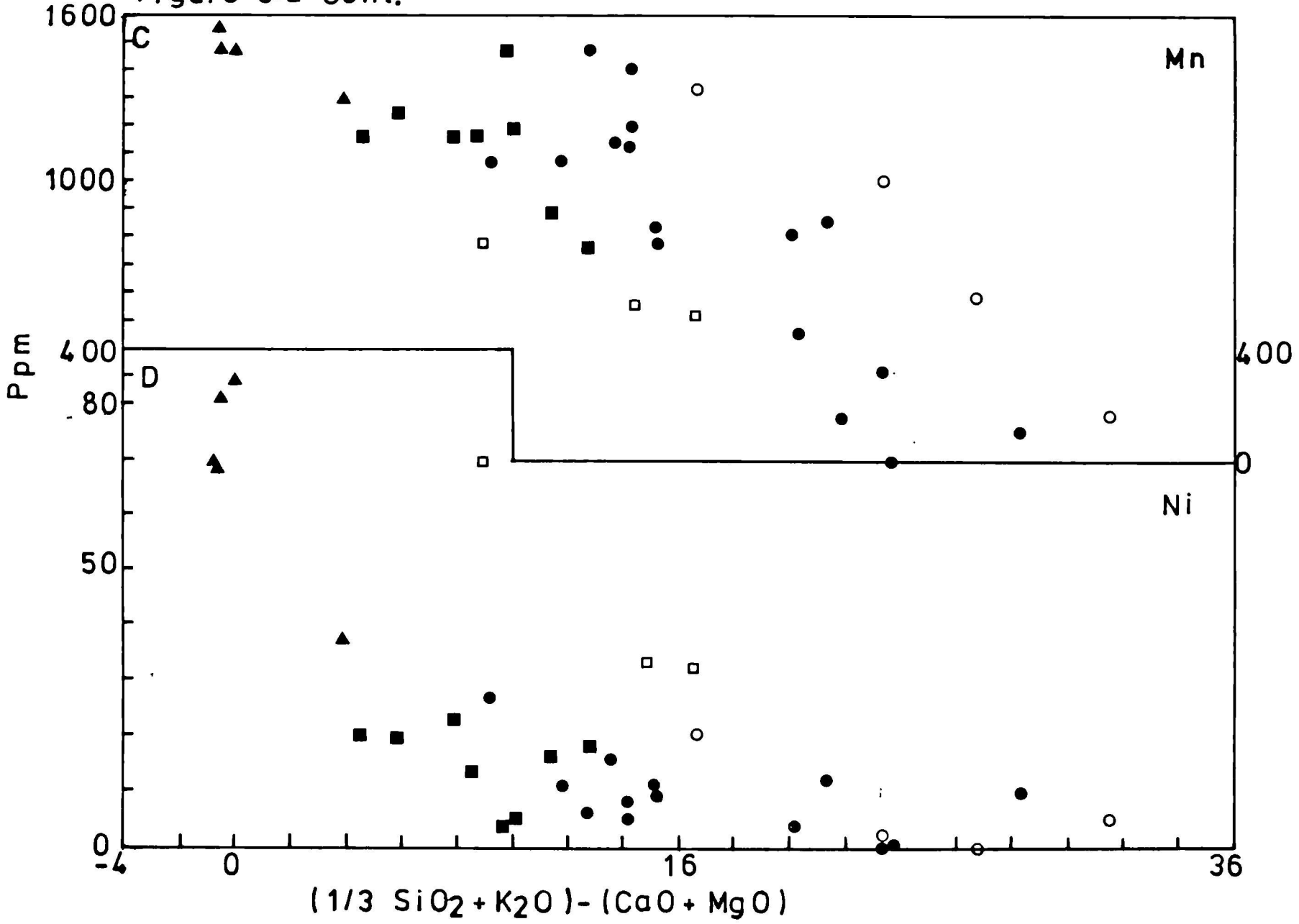

Figure 3.2 Cont.

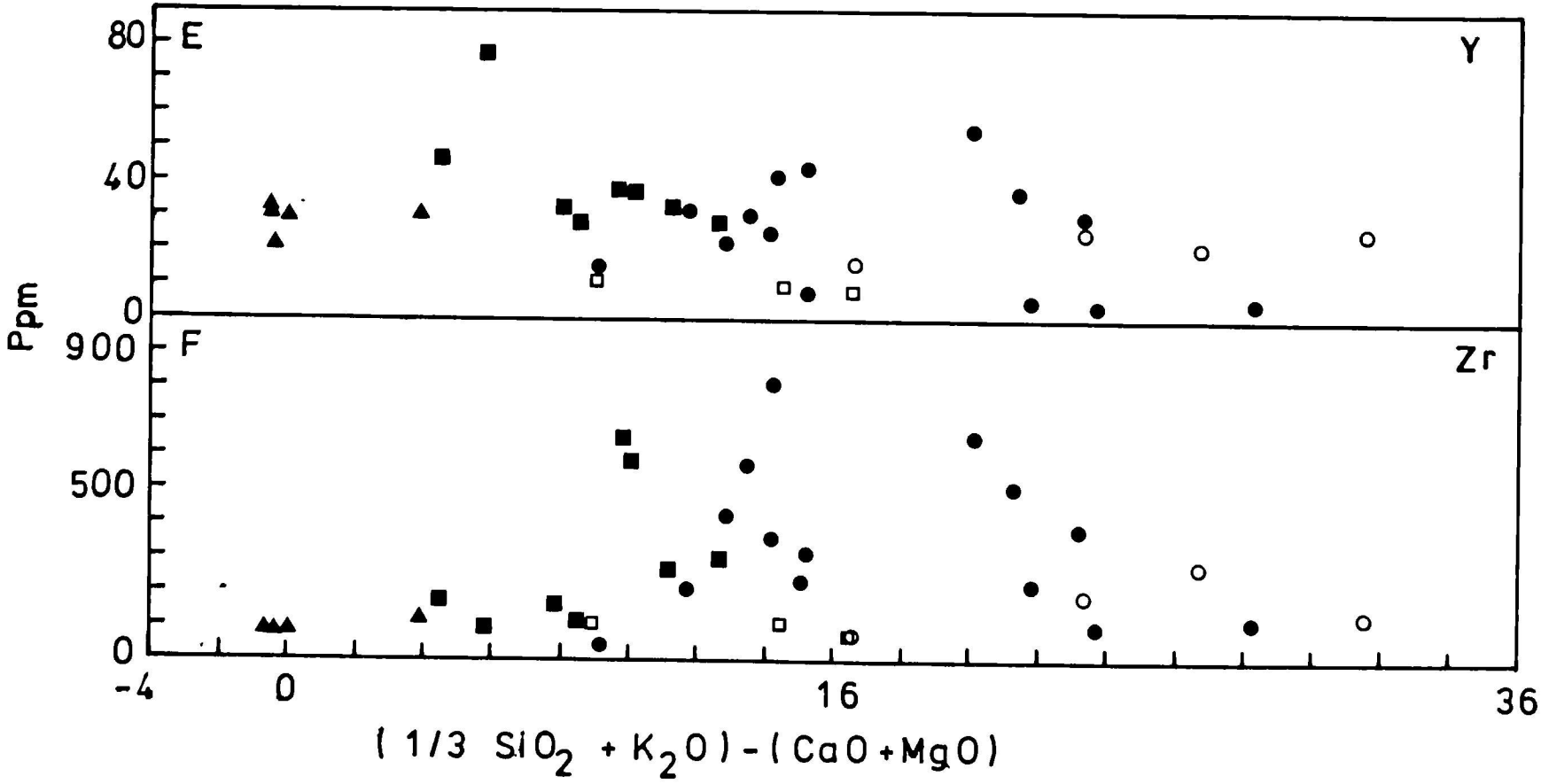

Figure 3.2 final continuation.

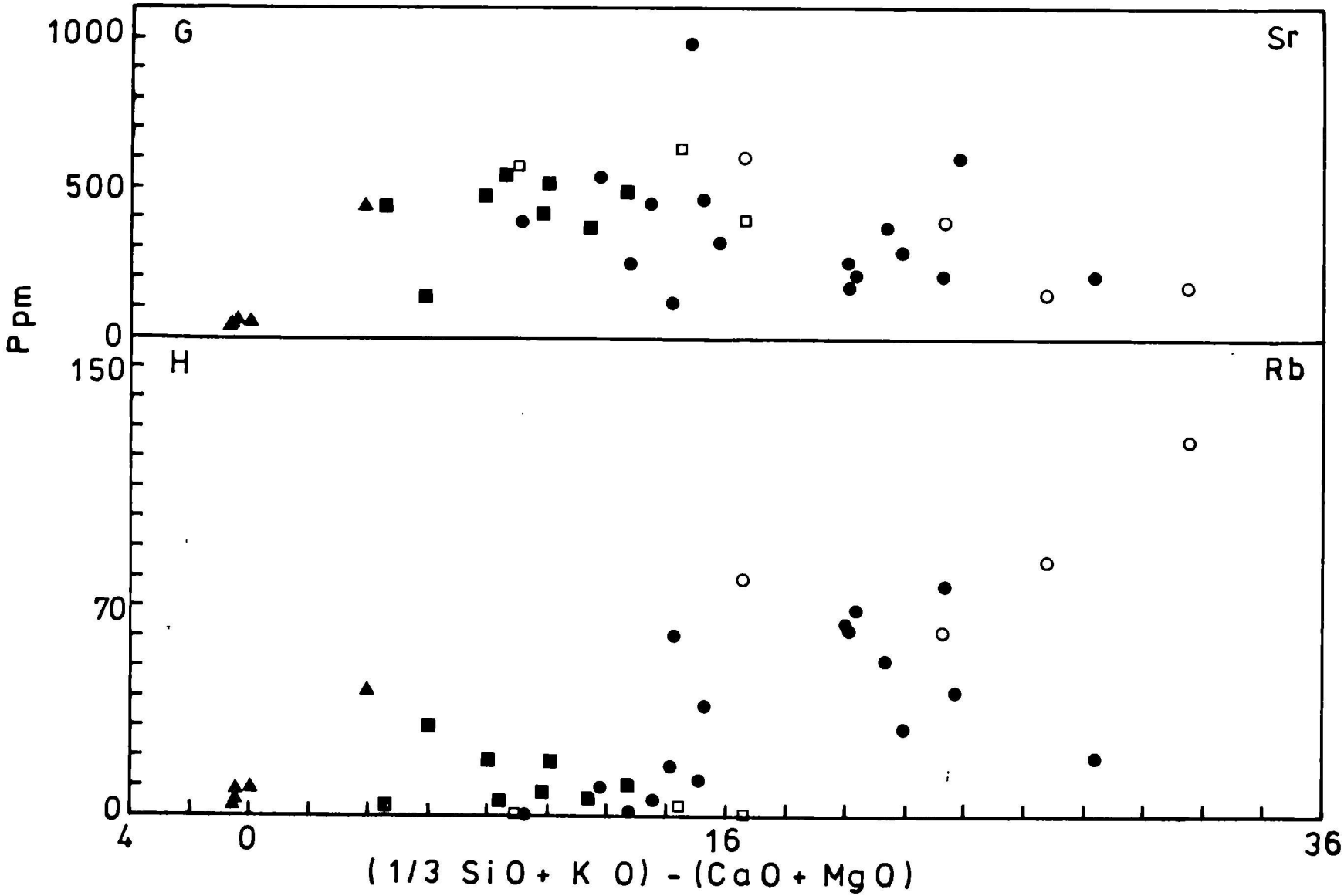

FIGURE 3.03 AFM and K_2O-Na_2O-CaO plots for compositions of rocks from the Gjörlanger Unit and Basal Gneisses. Symbols as for figure 3.01.

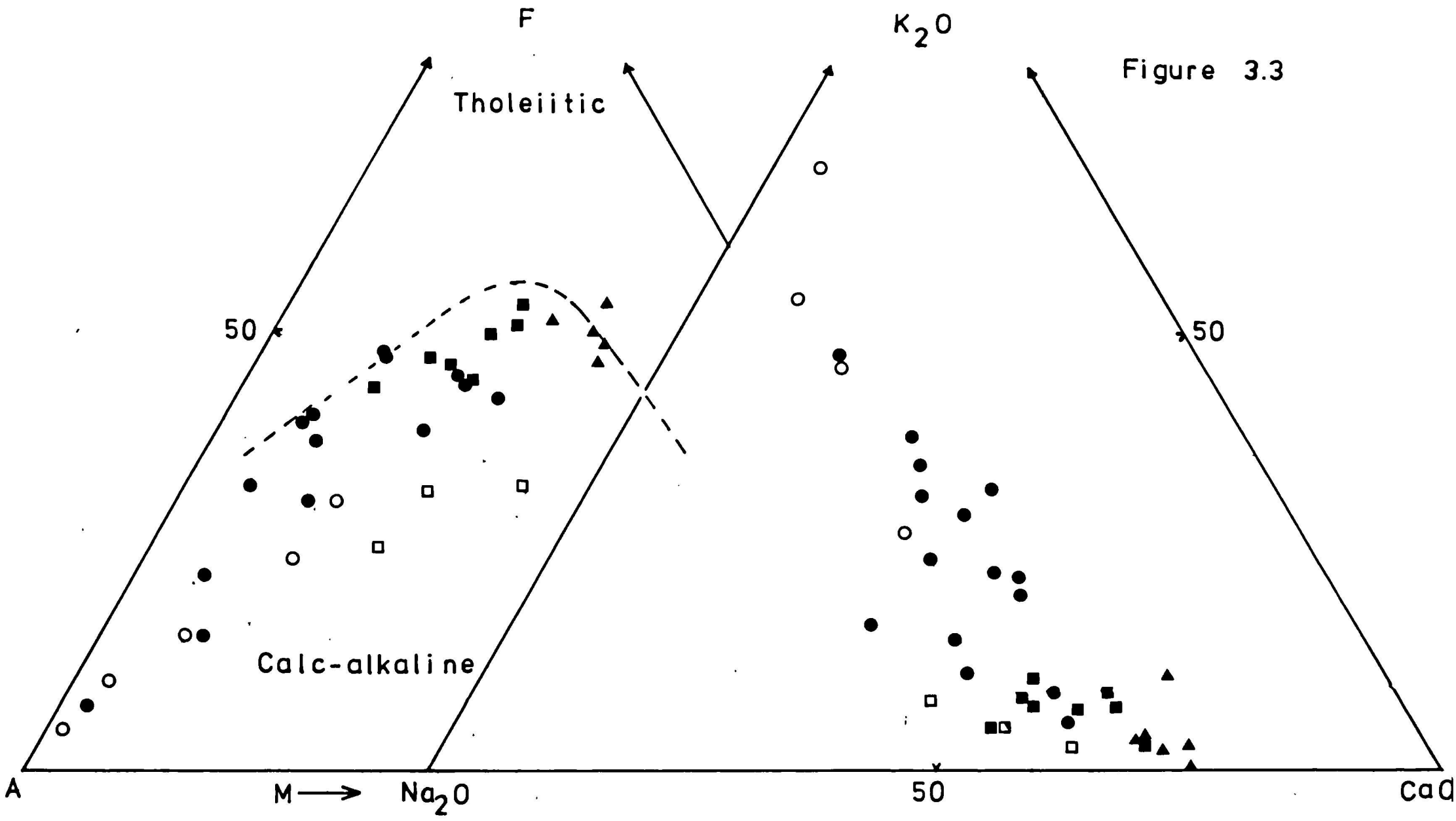

Figure 3.3

FIGURE 3.04 Normative feldspar triangular diagrams (after Streckeisen, 1976a) with compositions of rocks from the Gjörlanger Unit and Basal Gneisses. Symbols as for figure 3.01.

"Quartz-feldspar rocks"
"Feldspar rocks"

Numbers along Or-An join correspond to the composition classification of Streckeisen (1976a).

Figure 3.4A

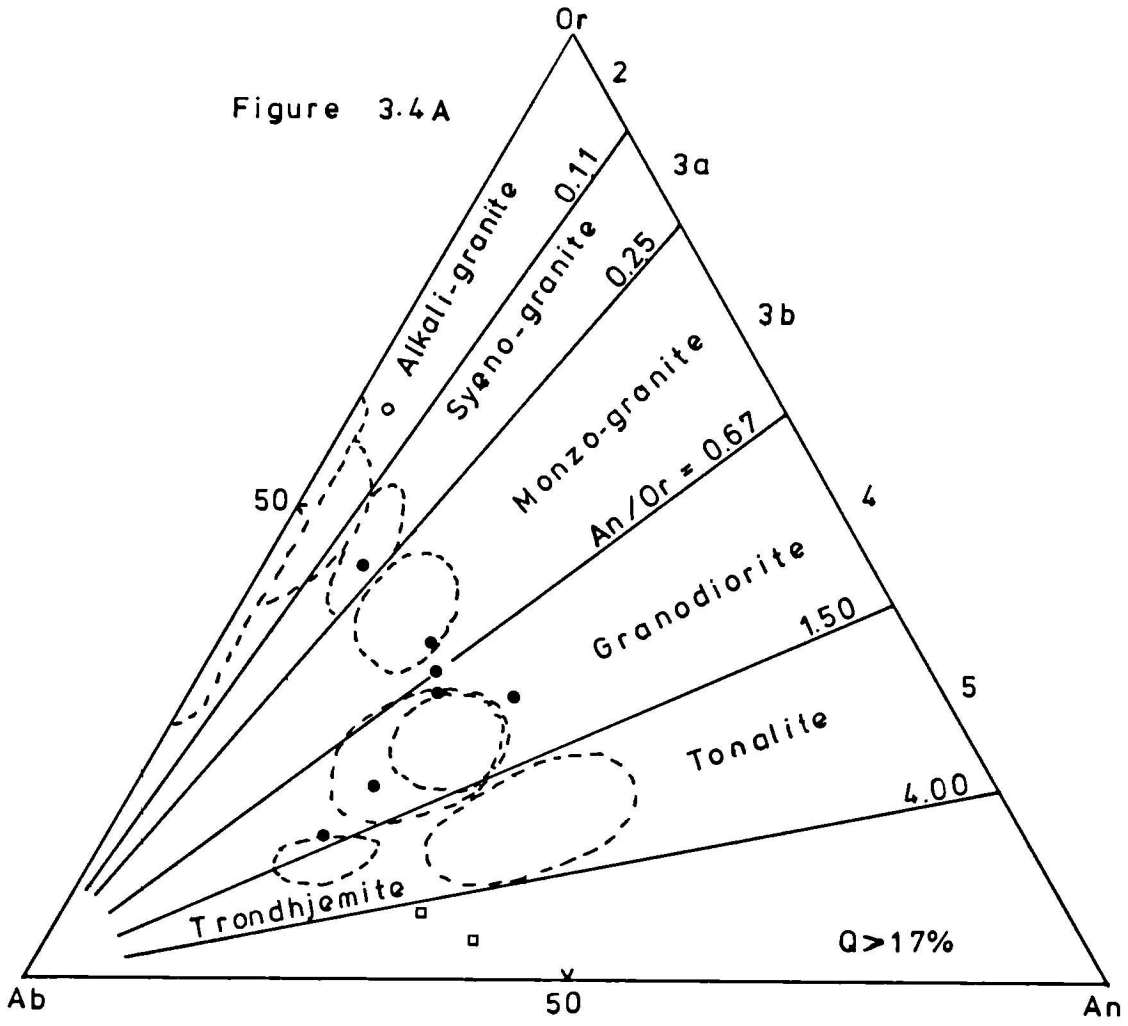
Or
2
3a
3b
4
5
0.11
0.25
An/Or = 0.67
1.50
4.00
Alkali-granite
Syeno-granite
Monzo-granite
Granodiorite
Tonalite
Trondhjemite
Q>17%
50
50
Ab
An

Figure 3.4B

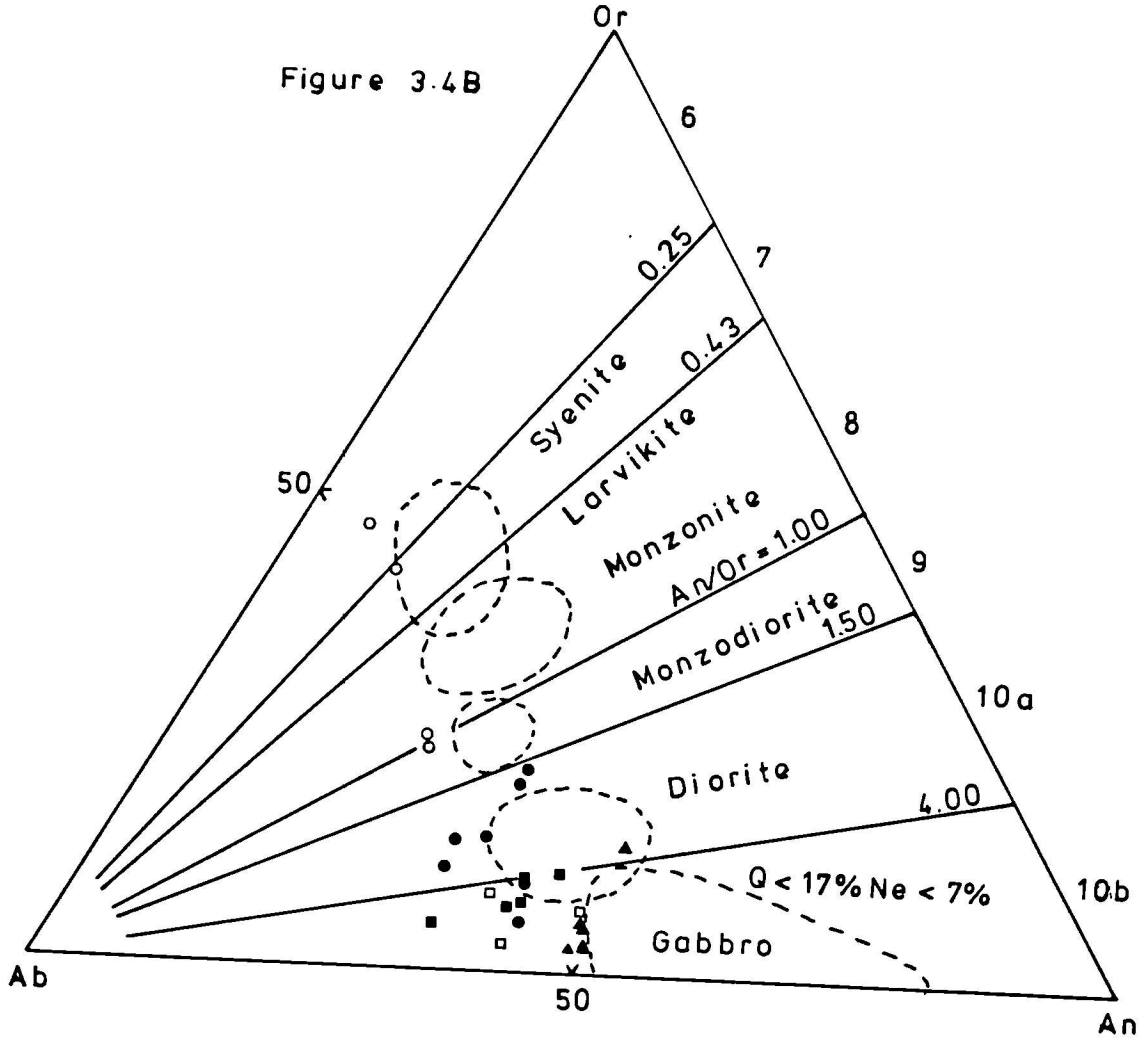
Or
6
7
8
9
10a
10b
0.25
0.43
1.00
1.50
4.00
50
Syenite
Larvikite
Monzonite
An/Or = 1.00
Monzodiorite
Diorite
Q < 17% Ne < 7%
Gabbro
Ab
50
An

FIGURE 3.05 Classification of Gjörlanger Unit and Basal Gneiss lithologies using "immobile" elements. fields are those of Floyd and Winchester (1978).

Abbreviations:
Sub-AB - sub-alkali basalt
AB - alkali basalt
A - andesite
TA - trachyandesite
Ba - basanite, nephelinite
T - trachyte
RD + D - rhyodacite + dacite
R - rhyolite
C + P - comendite + pantellerite
Ph - phonolite

Plotted numbers are equivalent plutonic compositions from figure 3.4.

Figure 3.5A

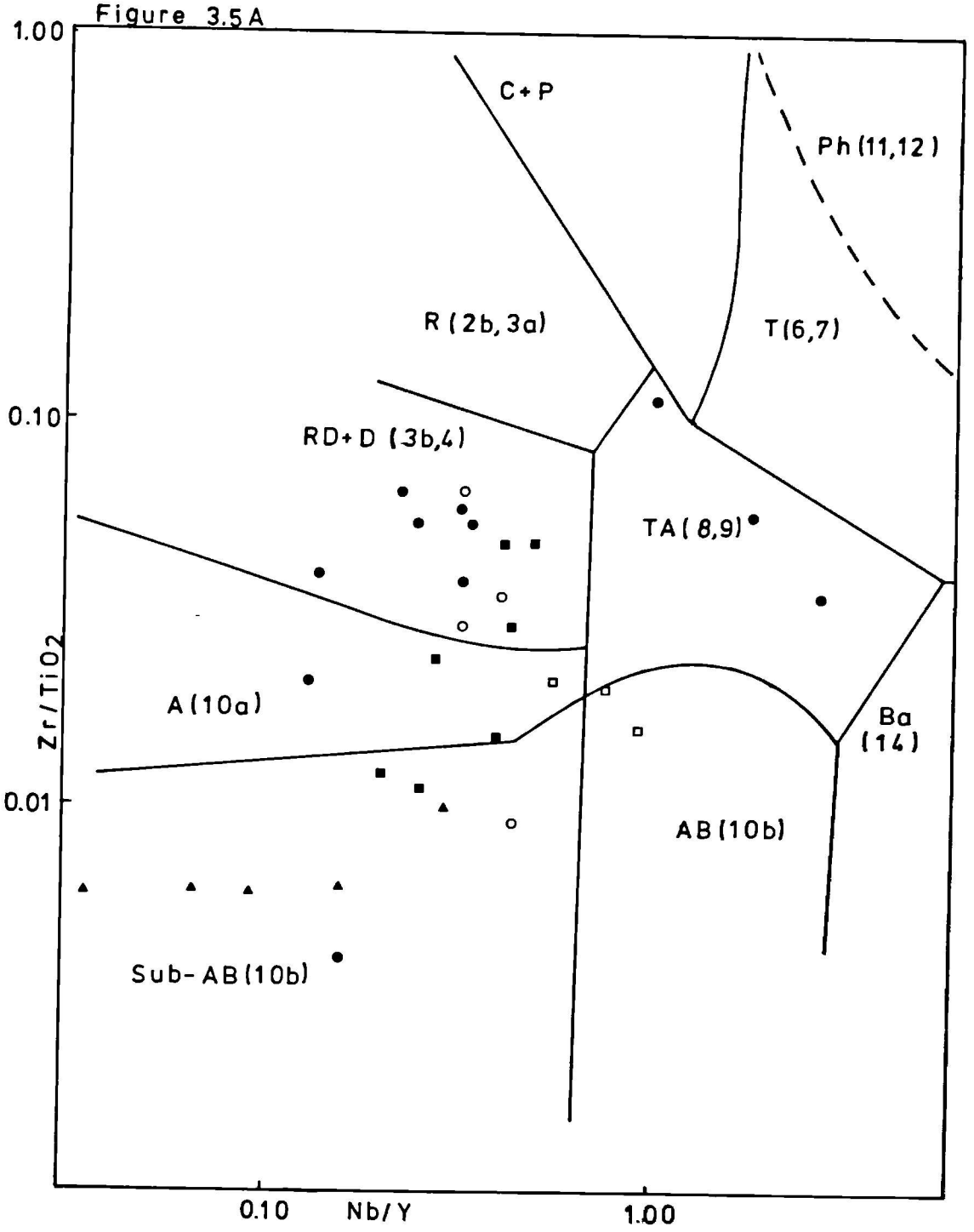
1.00
0.10
0.01
Zr/TiO2
0.10
Nb/Y
1.00
C+P
Ph(11,12)
R(2b,3a)
T(6,7)
RD+D(3b,4)
TA(8,9)
A(10a)
Ba
(14)
AB(10b)
Sub-AB(10b)

Figure 3.5 b

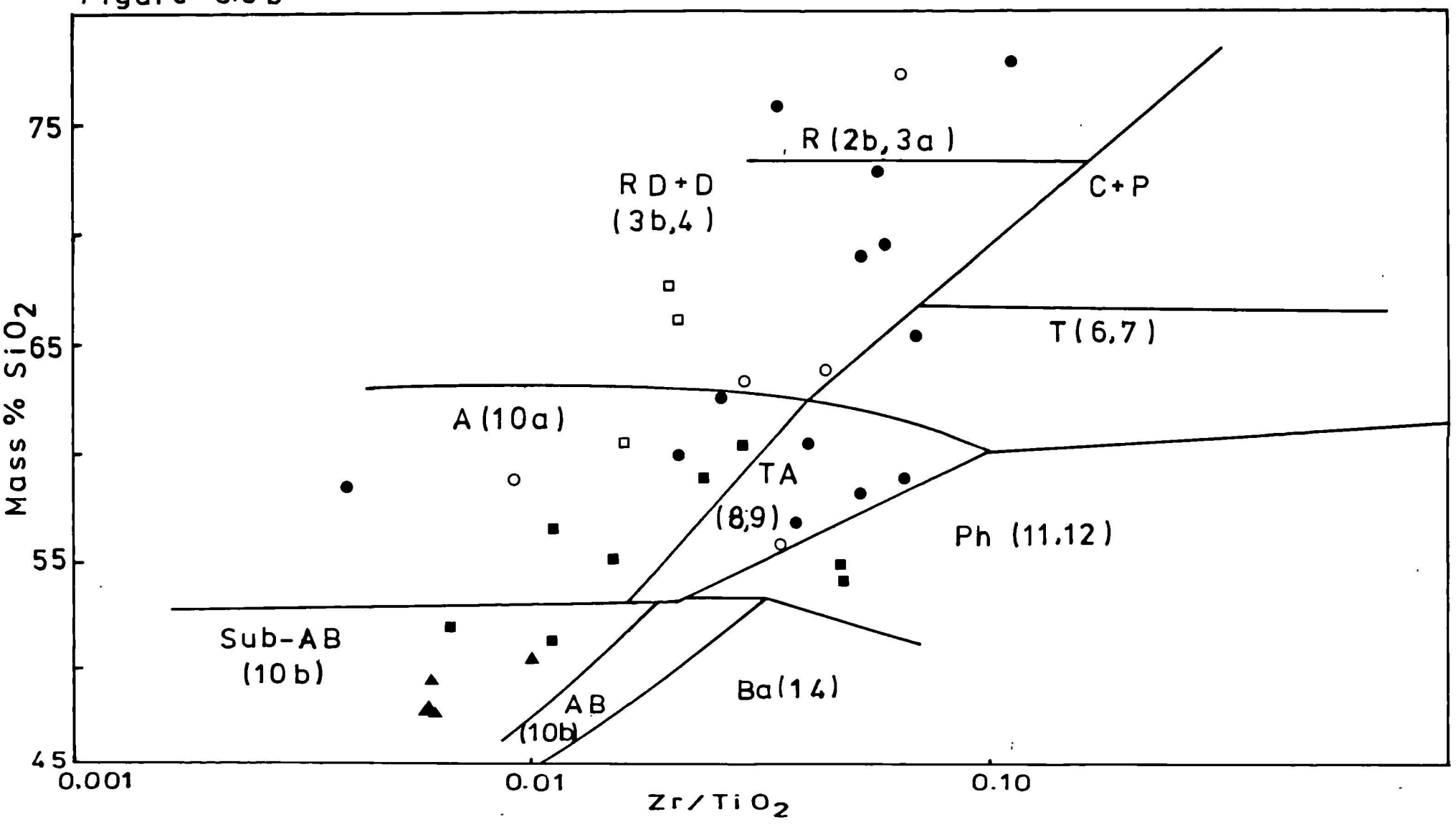
75
65
55
45
Mass % SiO2
0.001
0.01
0.10
Zr/TiO2
R (2b, 3a)
RD+D
(3b,4)
C+P
T (6,7)
A (10a)
TA
(8,9)
Ph (11,12)
Sub-AB
(10b)
AB
(10b)
Ba (14)

FIGURE 3.06

A Silica vs alkalis plot for rocks of the Gjörlanger Unit and Basal Gneisses. Solid line separates fields for alkaline and subalkaline rocks. Hatched lines define field for high-alumina-basalt trend of Kuno (1960).

B. SiO_2 vs CaO plot for Gjörlanger Unit and Basal Gneisses. Vertical hatched line X indicates Peacock index for Gjörlanger Unit grey and massive green gneisses, line Y Peacock index for K-poor gneisses.

Symbols as for figure 3.01.

Figure 3.6

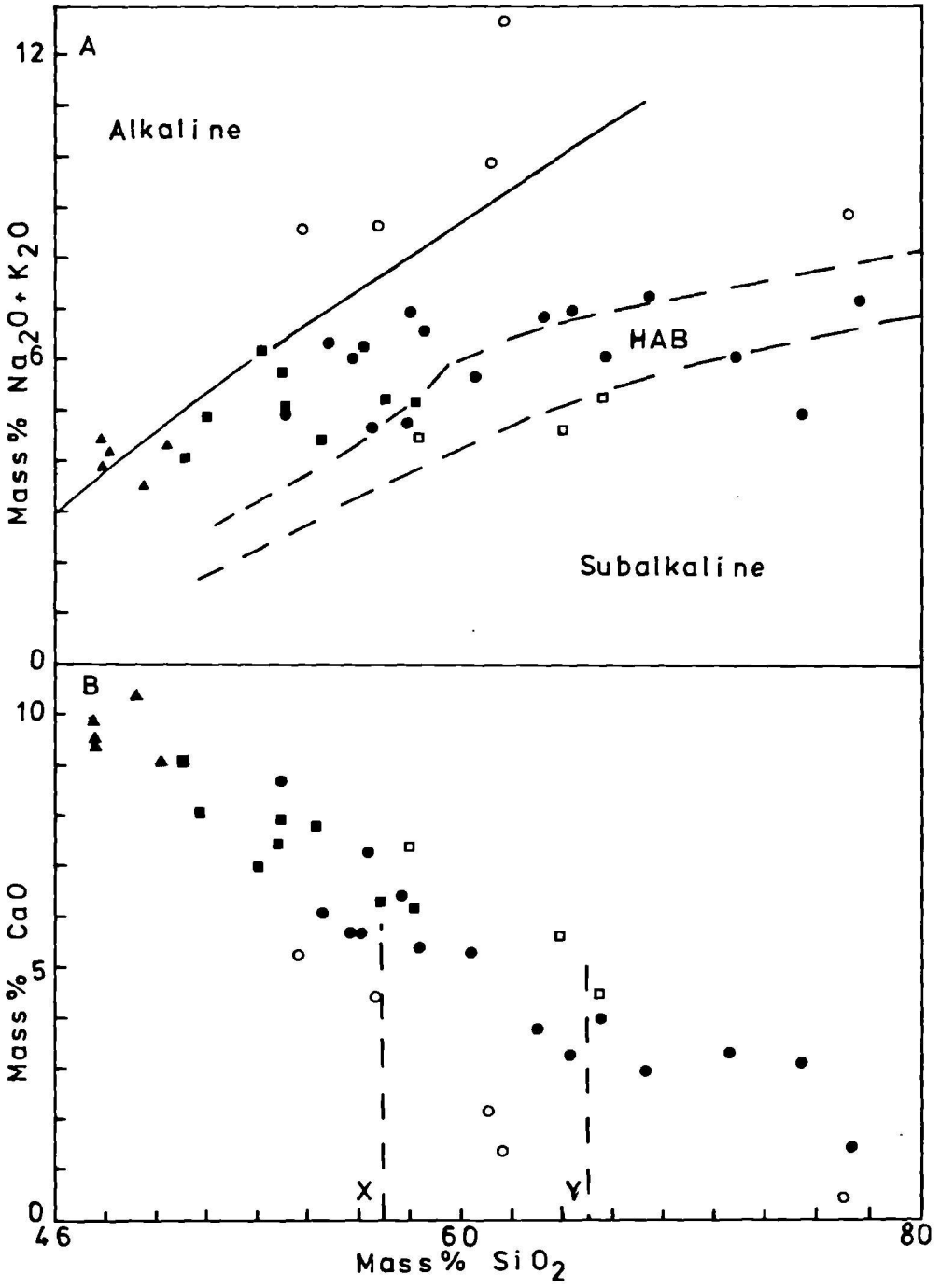
A
Alkaline
HAB
Subalkaline
Mass% Na2O+K2O
12
6
0
B
10
5
0
Mass% CaO
X
Y
46
60
80
Mass% SiO2

FIGURE 3.07 Normative nepheline-olivine-quartz projection for rocks of the Gjörlanger Unit and Basal Gneisses. Solid line divides alkaline and subalkaline fields of Irvine and Baragar (1971). Hatched line represents the critical plane of silica undersaturation. Symbols as in figure 3.01.

Figure 3.7

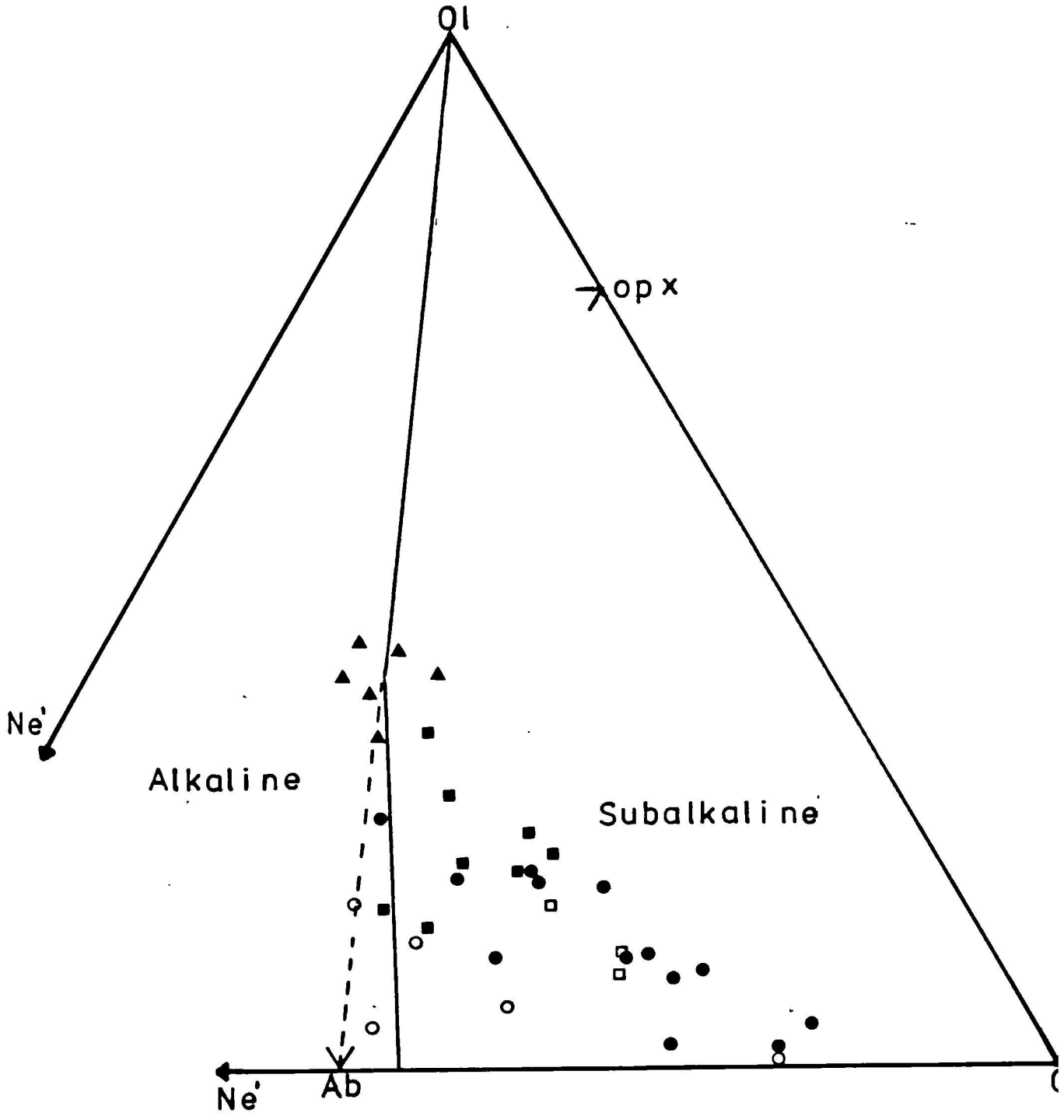

FIGURE 3.08 Al_2O_3 vs normative plagioclase plot for gneisses of the Gjörlanger Unit and Basal Gneisses. Solid line separating theoleiitic and calc-alkaline fields comes from Irvine and Baragar (1971). Symbols as for figure 3.01.

Figure 3.8

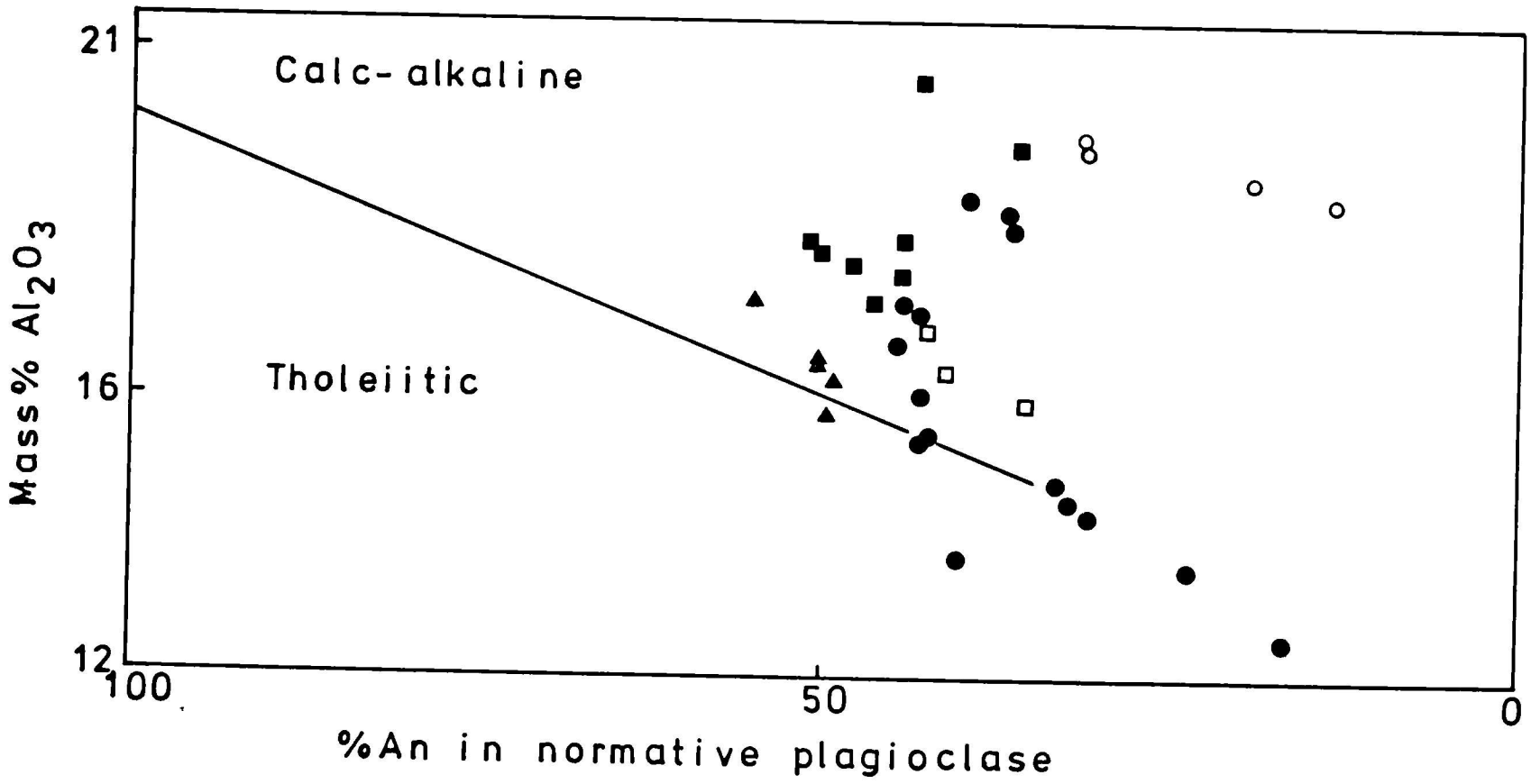
21
16
12
Calc-alkaline
Tholeiitic
Mass% Al_2O_3
100
50
0
%An in normative plagioclase

FIGURE 3.09 SiO_2 vs K_2O plots for gneisses of the Gjörlanger Unit and Basal Gneisses with compositional fields of other rock suites.

A. Comparison with anorthosite-mangerite-rapakivi granite suites.
Solid line - Nain, Labrador (de Waard + Wheeler 1971).
Dashed line - Jotun-Bergen suite, Norway (Kolderup, 1921; Deitrickson, 1958; Batty and McRitchie, 1975; Austrheim, 1978).
Dash-dot line - Roaring Brook, Marcy Massif, Adirondacks (de Waard, 1970).
Dotted line - Morin series, Quebec (Philpotts, 1966).

B. Comparison with:-
Long dashed line - Madras charnockites (Howie, 1955; Subramaniam, 1959).
Short dashed line - Archaean grey gneisses (Tarney, 1976).
Dash-double dot line - Tuolumne Intrusive Series, Sierra Nevada Batholith (Bateman and Chappel, 1979).

Symbols as for figure 3.01.

Figure 3.9

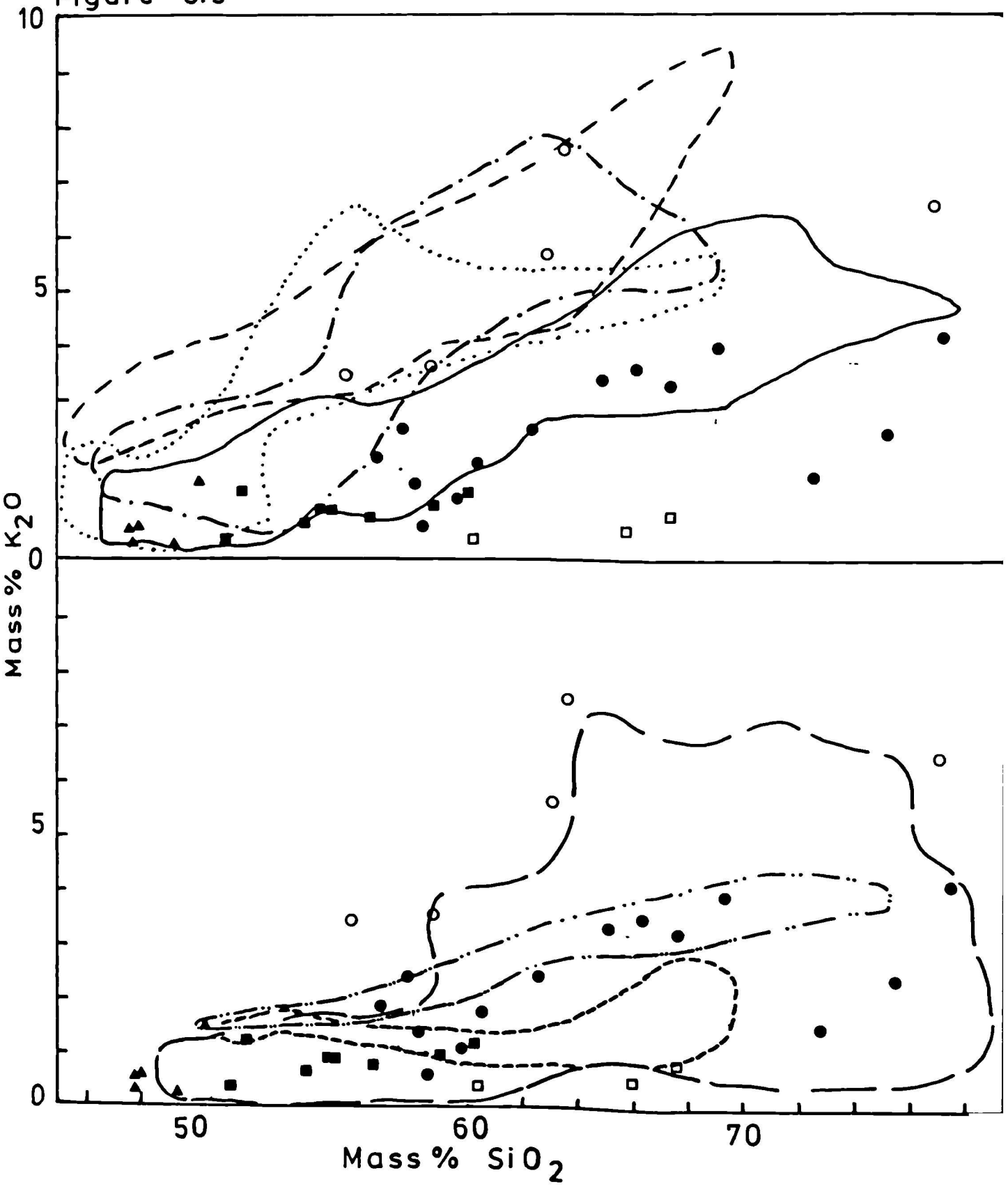

FIGURE 3.10 Triangular Rb-Ba-Sr diagram of el Bouseily and el Sokkary (1975) with compositions of gneisses from the Gjörlanger Unit and Basal Gneisses (excluding the dyke-rocks). Symbols as for figure 3.01.

Figure 3.10

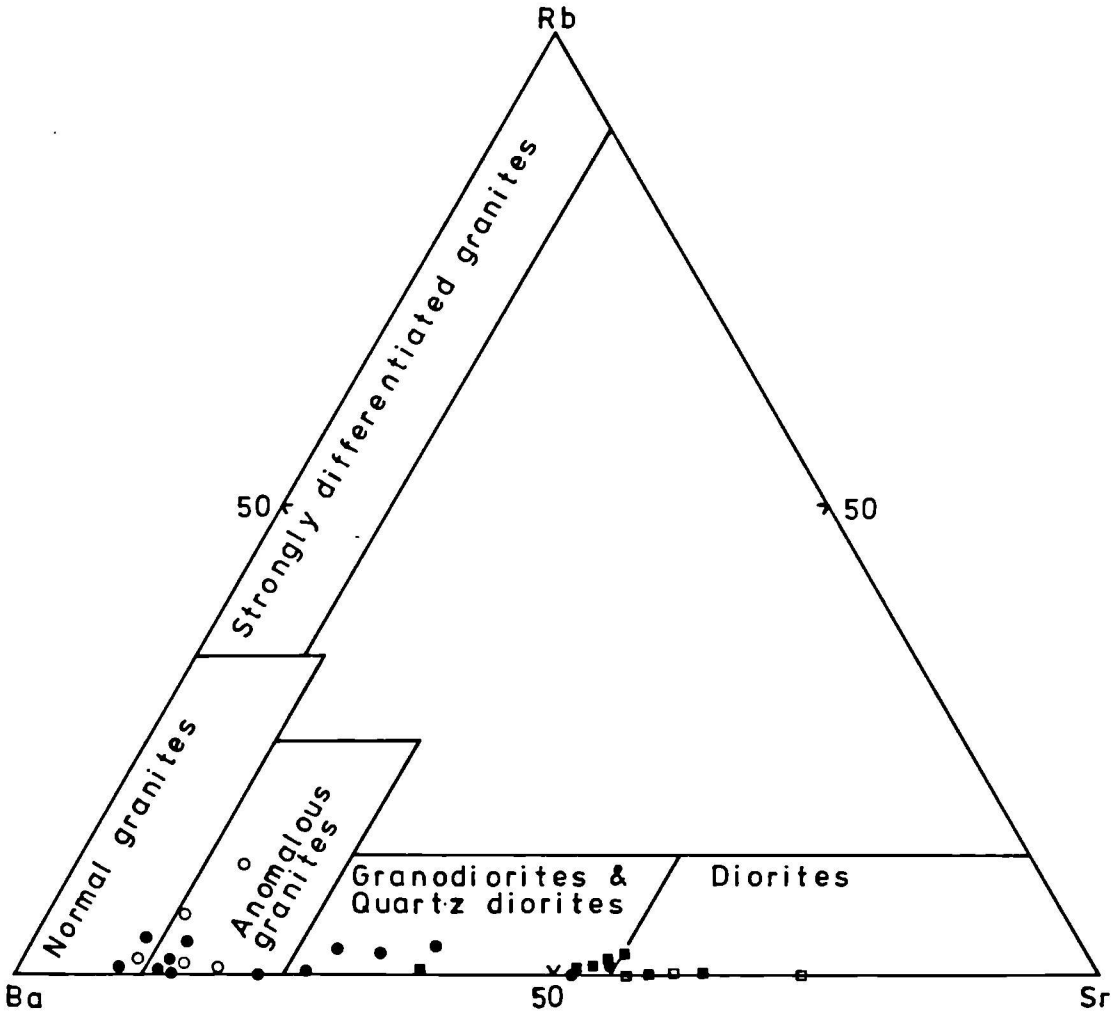
Rb
50
50
Strongly differentiated granites
Normal granites
Anomalous granites
Granodiorites &
Quartz diorites
Diorites
Ba
50
Sr

FIGURE 3.11 Log linear plot of Ba vs Sr for gneisses of the Gjörlanger Unit and Basal Gneisses (excluding dyke-rocks). Solid lines are of constant Ba/Sr ratio. Symbols as for figure 3.01.

Figure 3.11

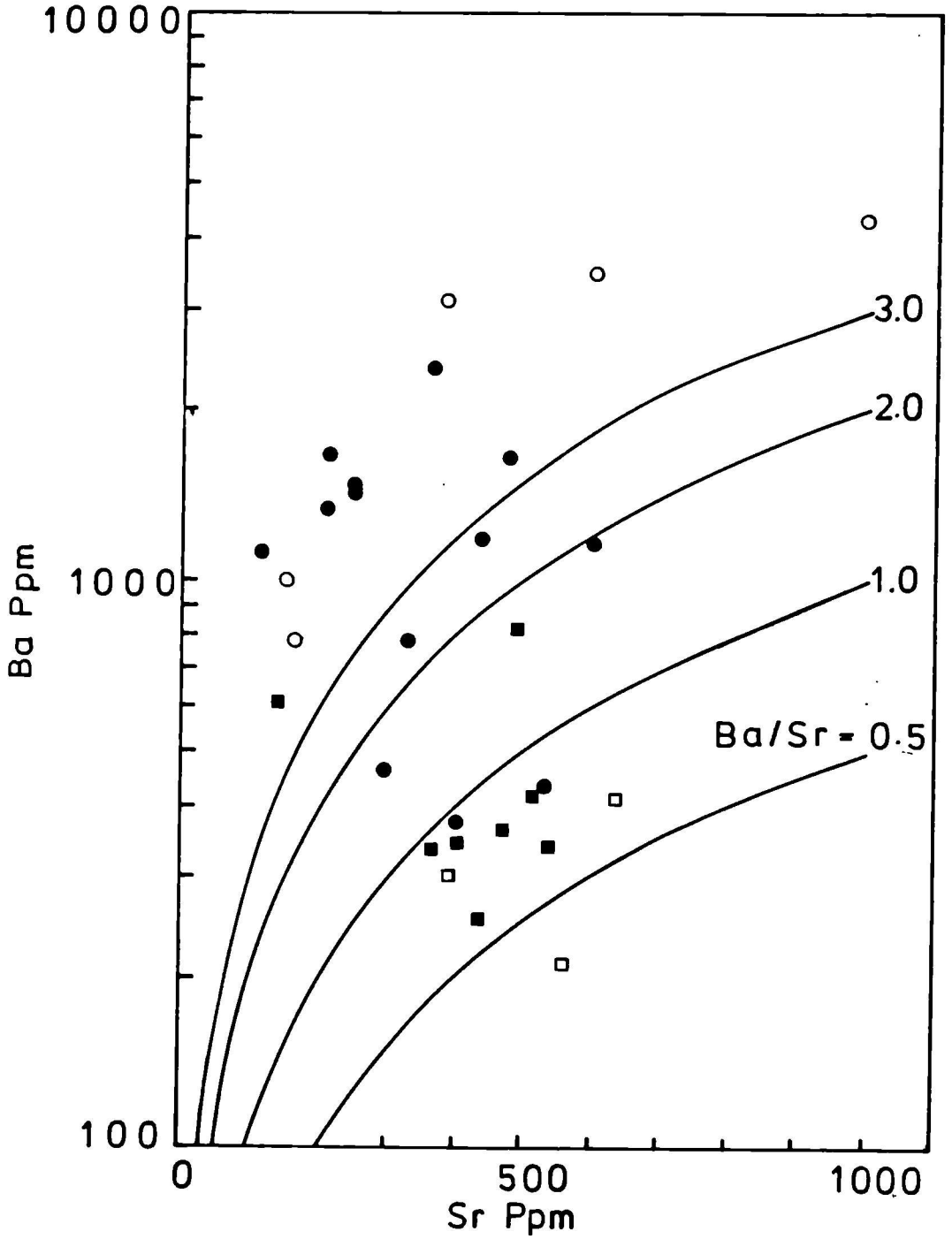

FIGURE 3.12 Log-log plot for K vs Rb (with lines of constant K/Rb ratio for reference) showing compositions of lithologies from the Gjörlanger Unit and Basal Gneisses. Symbols as for figure 3.01.

Figure 3.12

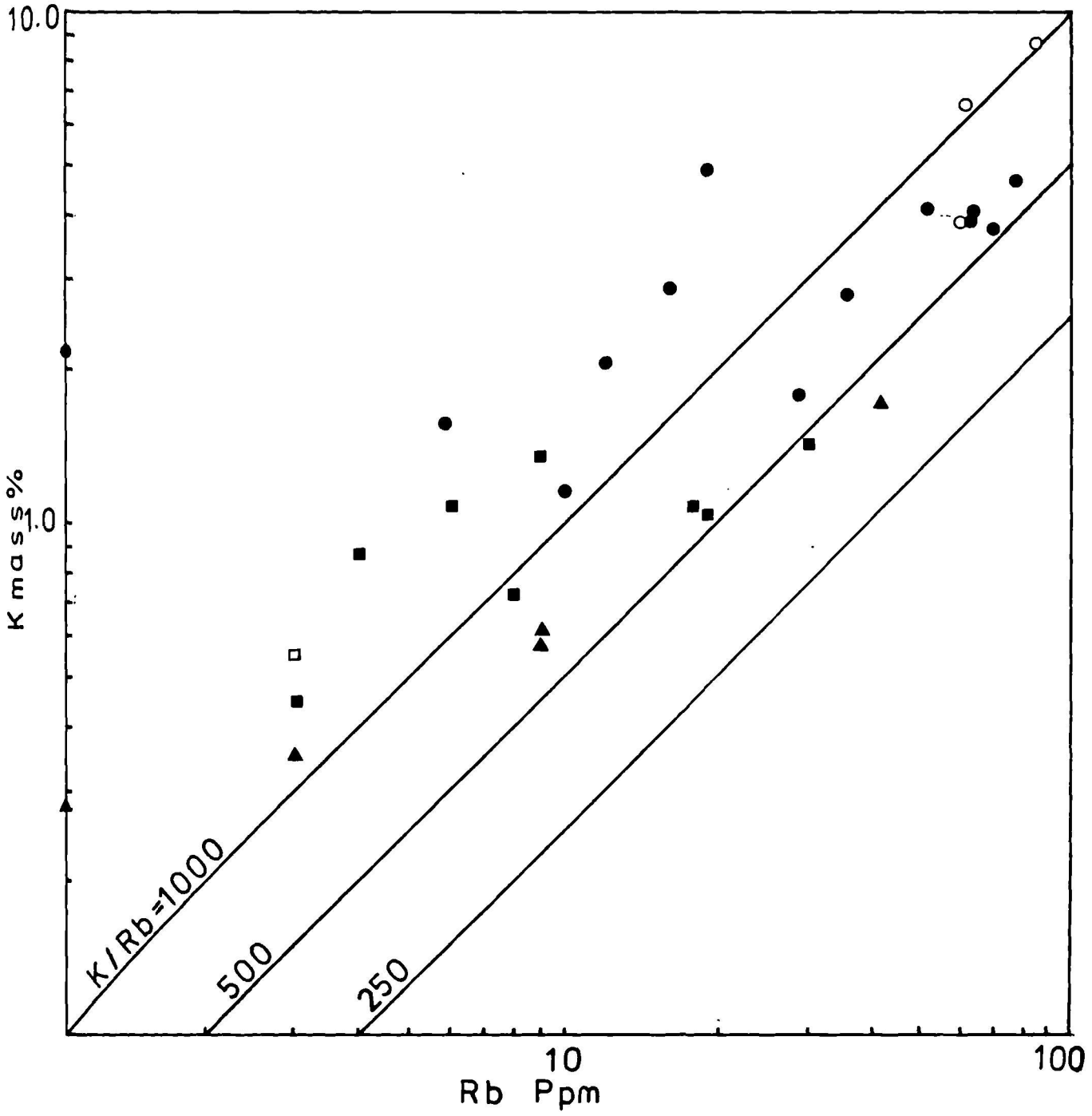

FIGURE 3.13 Rb vs Sr for rocks of the Gjörlanger Unit and Basal Gneisses with solid lines of constant Rb/Sr ratio. Symbols as for figure 3.01.

Figure 3.13

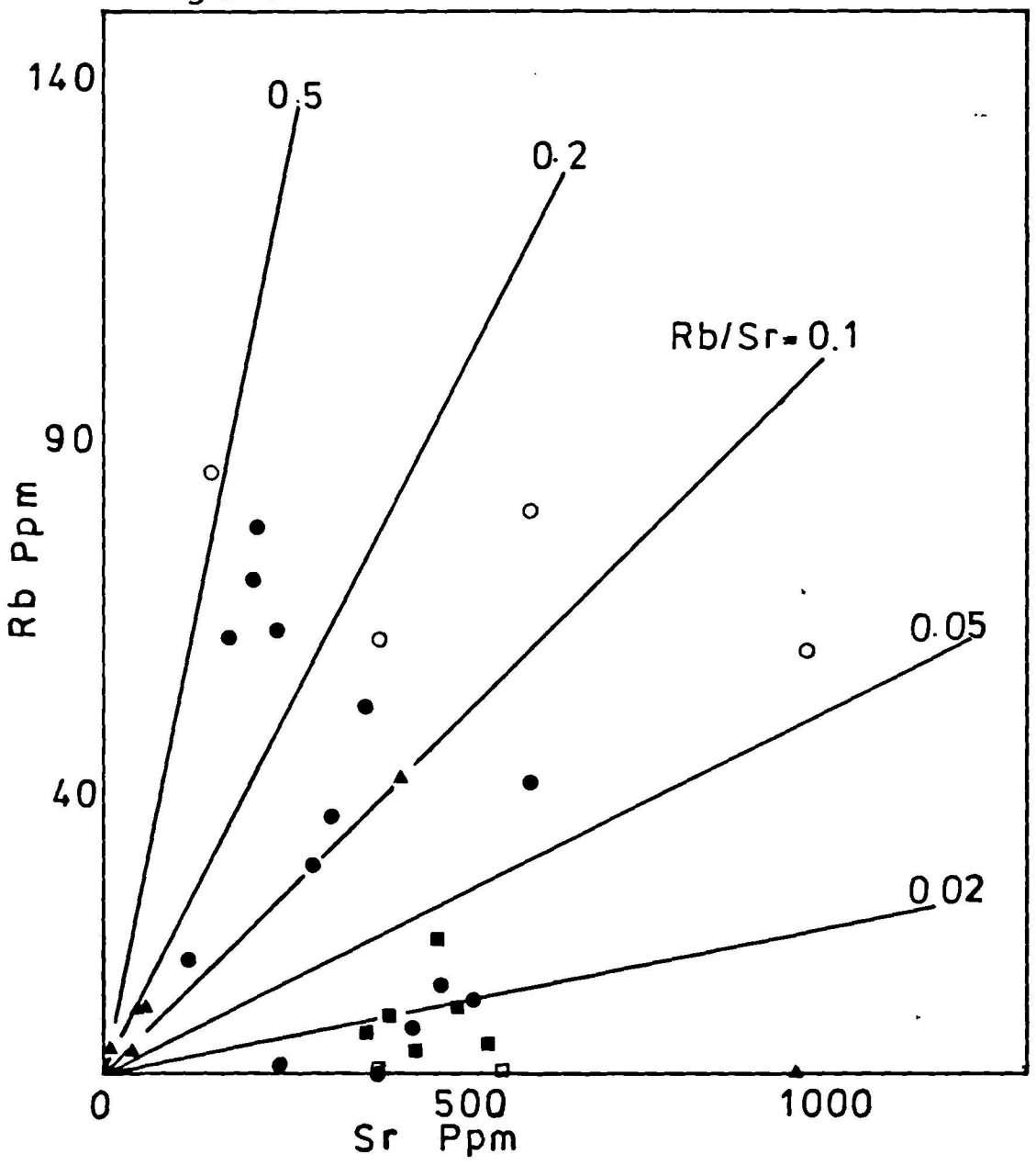

FIGURE 3.14 Isochron diagram for the Rb-Sr system for selected grey gneisses from the Gjörlanger Unit. Samples marked "DG-" come from a single outcrop by the junction of routes 57 and 607 to the south of Flekke (see figure 1.01). Reference isochrons are for 1500 Ma and 1200 Ma.

Figure 3.14

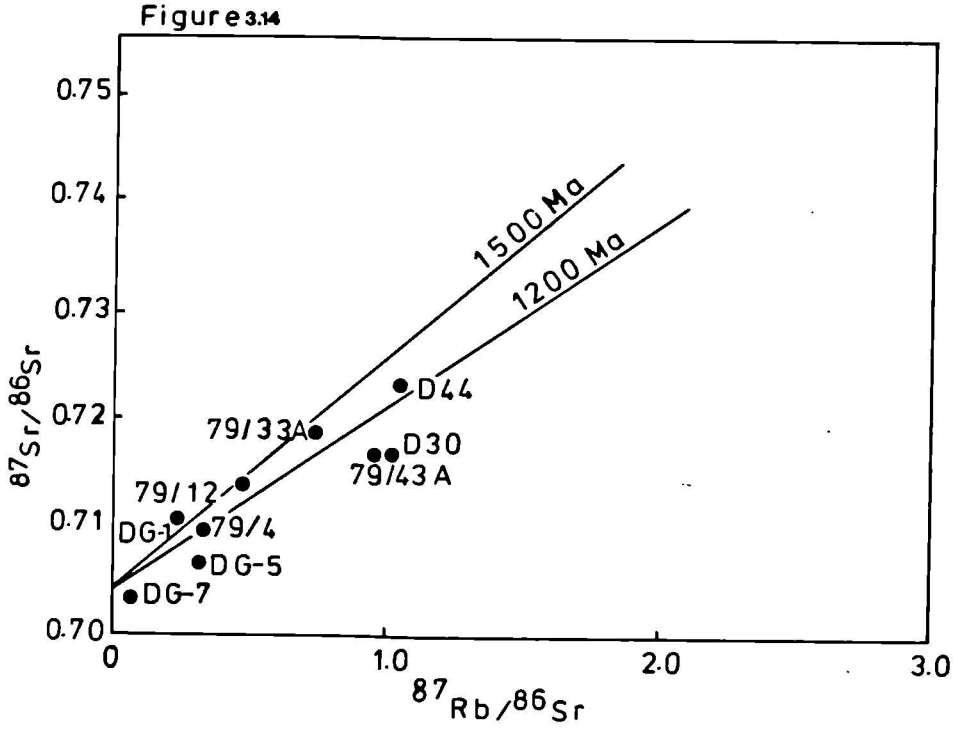
0.75
0.74
0.73
0.72
0.71
0.70
$^{87}Sr/^{86}Sr$
1500 Ma
1200 Ma
D44
79/33A
D30
79/43A
79/12
DG-1
79/4
DG-5
DG-7
0
1.0
2.0
3.0
$^{87}Rb/^{86}Sr$

FIGURE 3.15 Compositional variation across a metabasic (eclogite) dyke in a roadcut by the road from Gjörlanger to Solvik. See figure 2.37 for sample locations.

Squares - dyke-rocks
Circles - immediately adjacent grey gneiss

Figure 3.15

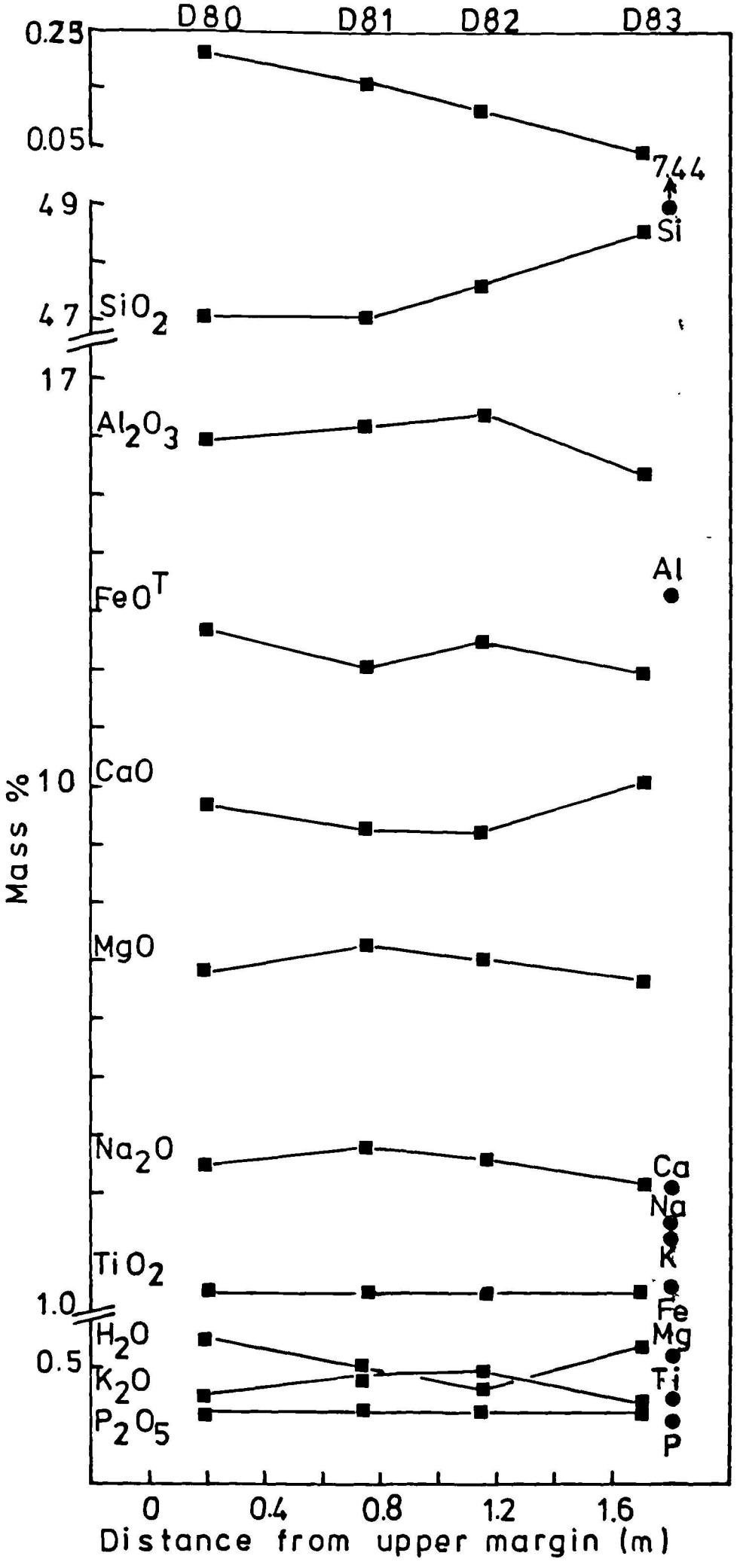
D80
D81
D82
D83
0.25
0.05
49
47
17
1.0
0.5
7.44
Si
Al
Ca
Na
K
Fe
Mg
Ti
P
SiO_2
Al_2O_3
FeO^T
CaO
MgO
Na_2O
TiO_2
H_2O
K_2O
P_2O_5
Mass %
0
0.4
0.8
1.2
1.6
Distance from upper margin (m)

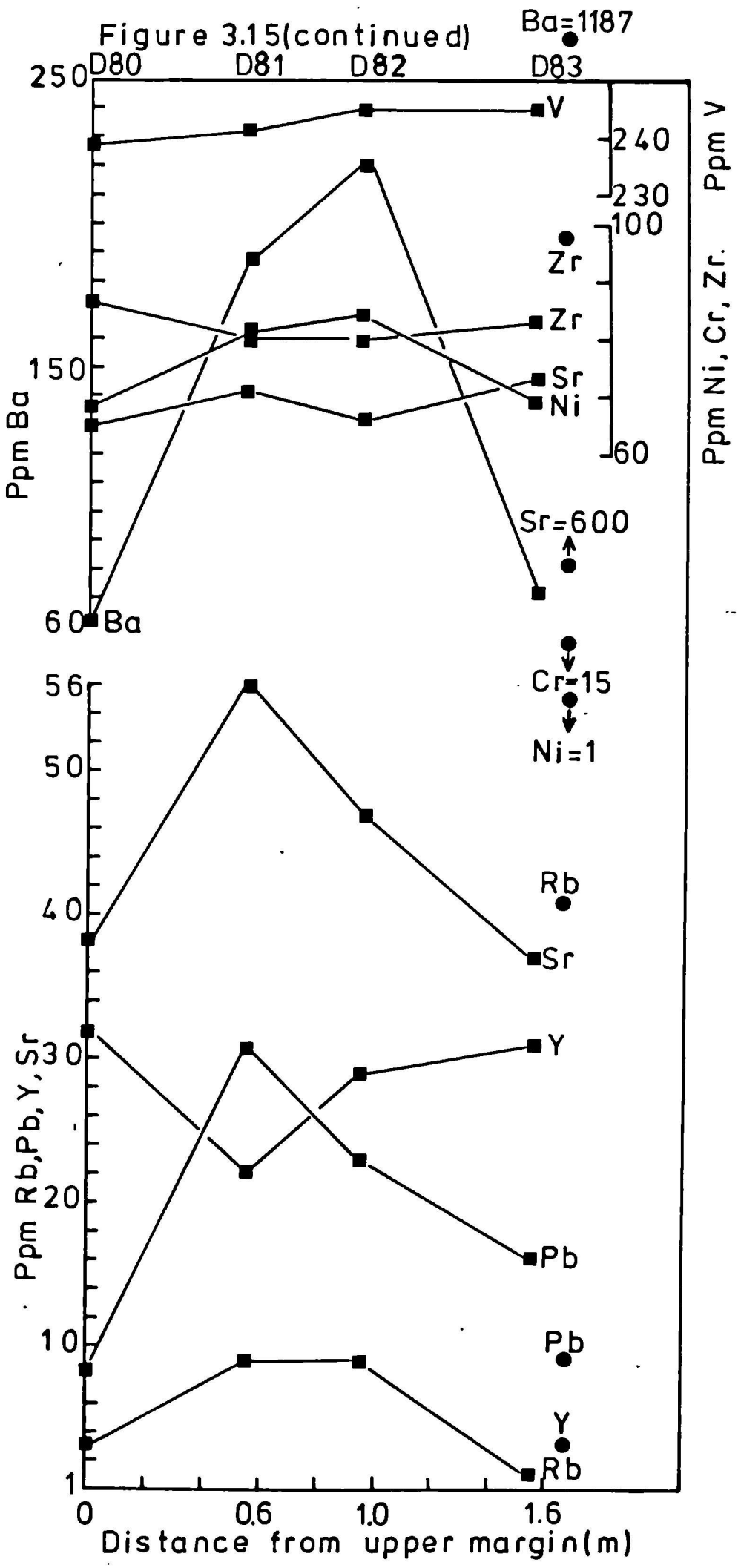
Figure 3.15(continued)
Ba=1187
D80
D81
D82
D83
250
150
60
Ba
Ppm Ba
V
Zr
Zr
Sr
Ni
240
230
100
60
Ppm V
Ppm Ni, Cr, Zr.
Sr=600
Cr=15
Ni=1
56
50
40
30
20
10
1
Rb
Sr
Y
Pb
Pb
Y
Rb
Ppm Rb,Pb, Y, Sr
0
0.6
1.0
1.6
Distance from upper margin(m)

FIGURE 3.16 Variation diagrams for metabasites of Gjörlanger Unit and Basal Gneisses with major and trace element compositions plotted against the modified Larsen index of Nockolds and Allen (1953). Solid lines are trends for the gneisses of the same lithological units.

Upright triangles - basic dykes
Inverted triangles - concordant basic sheets
Diamonds - eclogites/amphibolites in Basal Gneisses

Figure 3.16

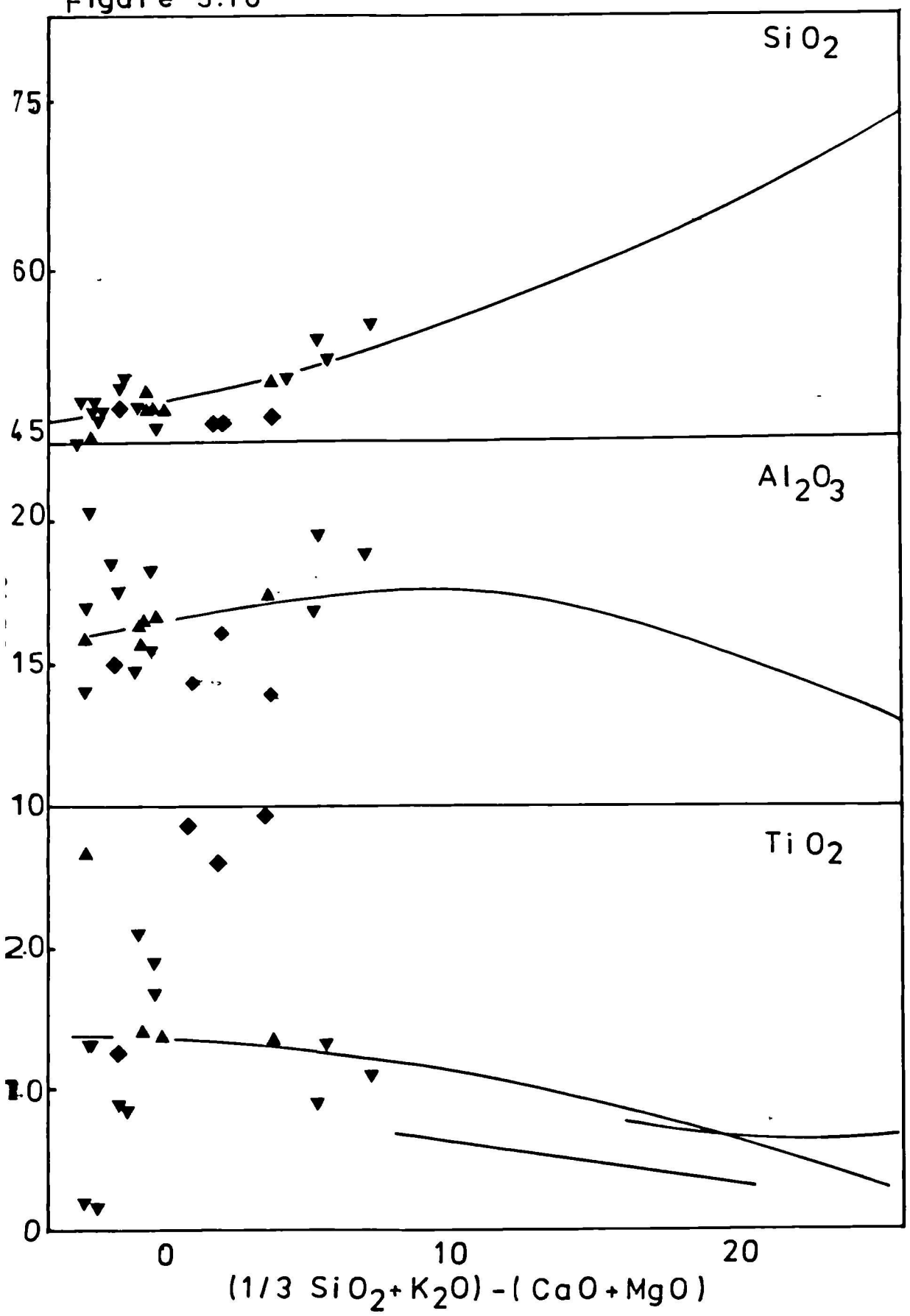
SiO2
75
60
45
Al2O3
20
15
10
TiO2
2.0
1.0
0
0
10
20
(1/3 SiO2+K2O)-(CaO+MgO)

Figure 3.16 (continued)

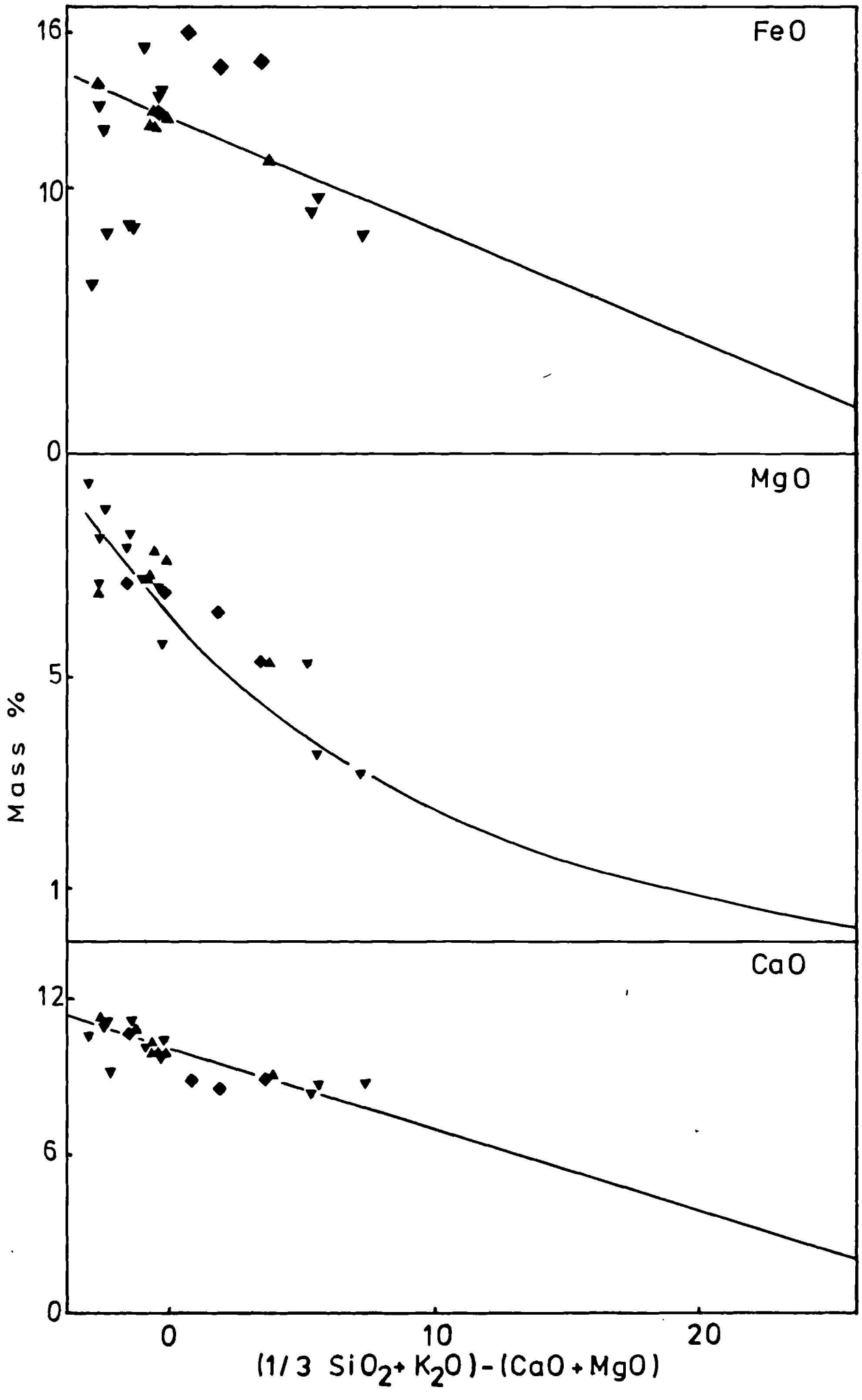

Figure 3.16 continued

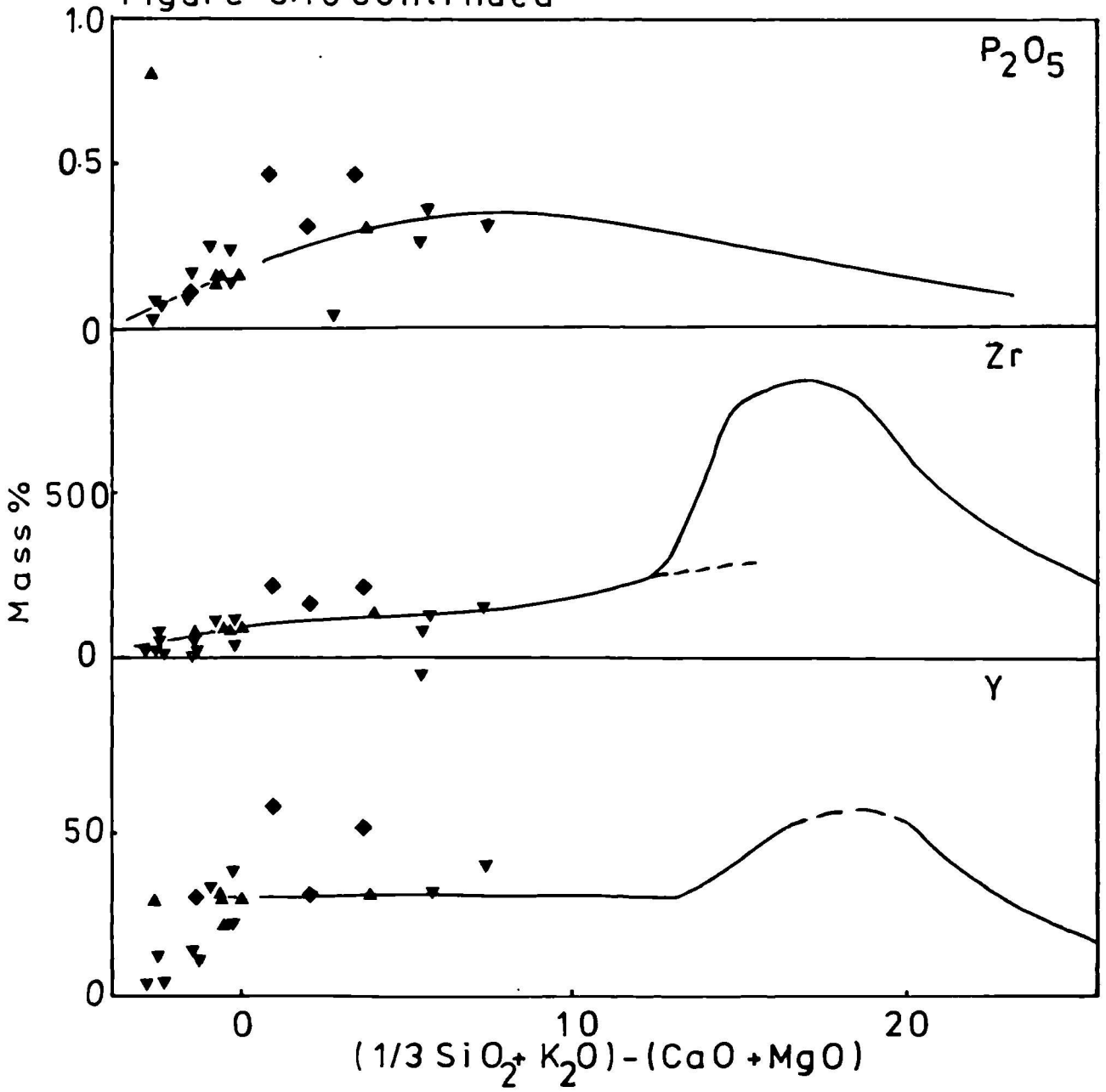

Figure 316 final continuation

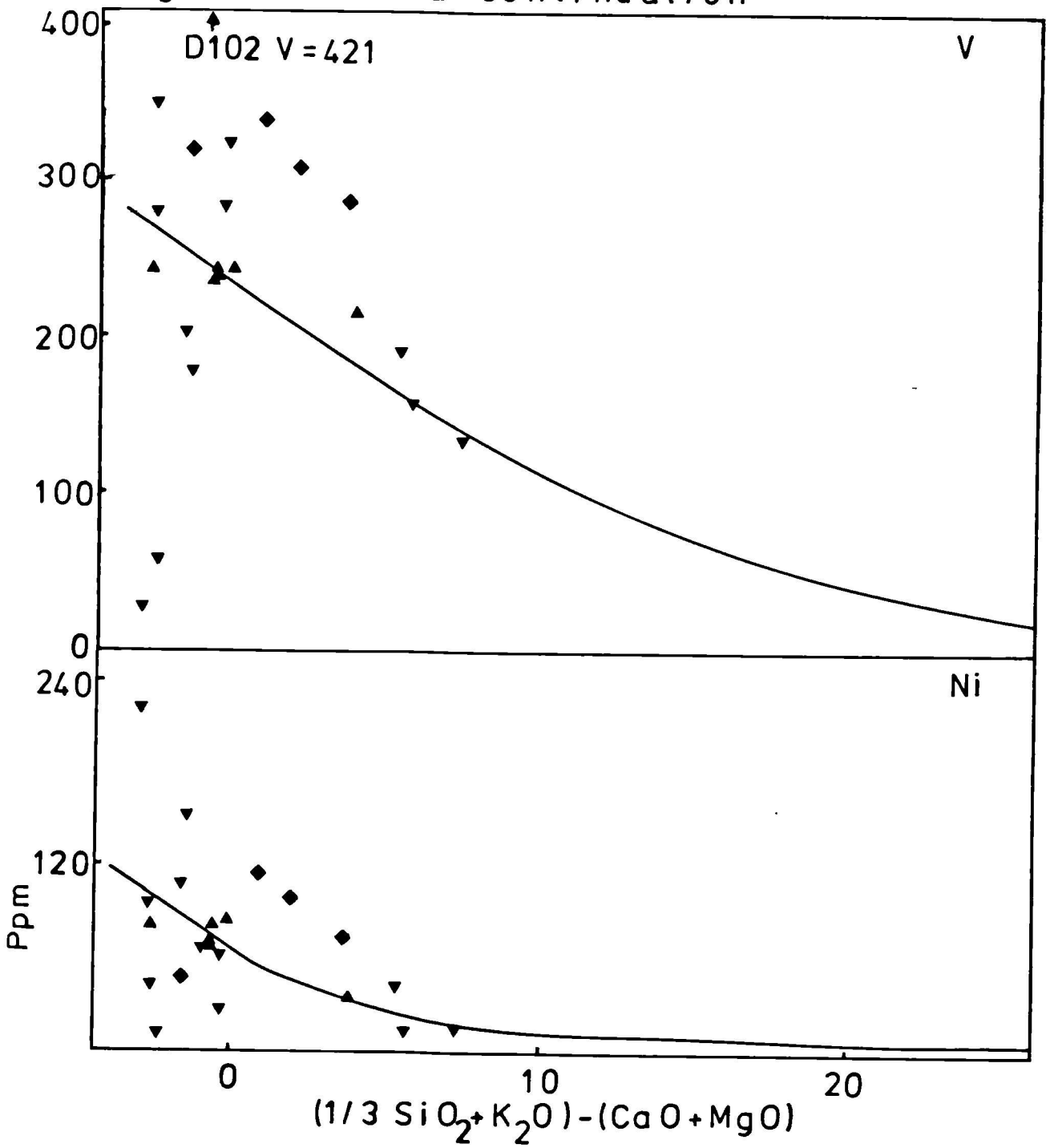

FIGURE 3.17 Metabasites of the Gjörlanger Unit and Basal Gneisses plotted on "immobile element" discrimination diagrams of Floyd and Winchester (1975). Symbols as for figure 3.16.

Abbreviations:-

CAB - continental alkali basalt
CTB - continental tholeiitic basalt
OAB - oceanic alkali basalt
OTB - oceanic tholeiitic basalt

Figure 3.17A

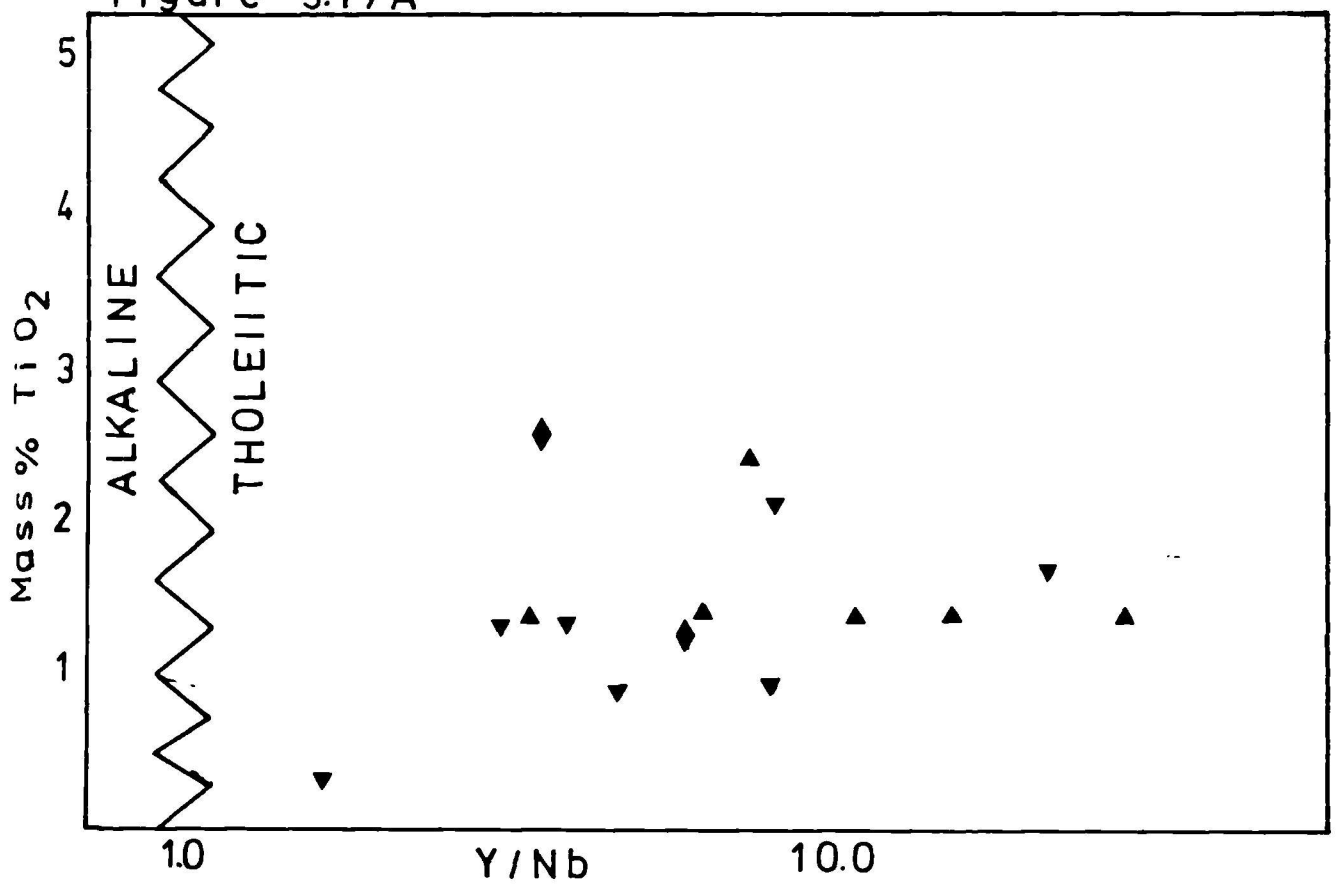

Figure 3.17B

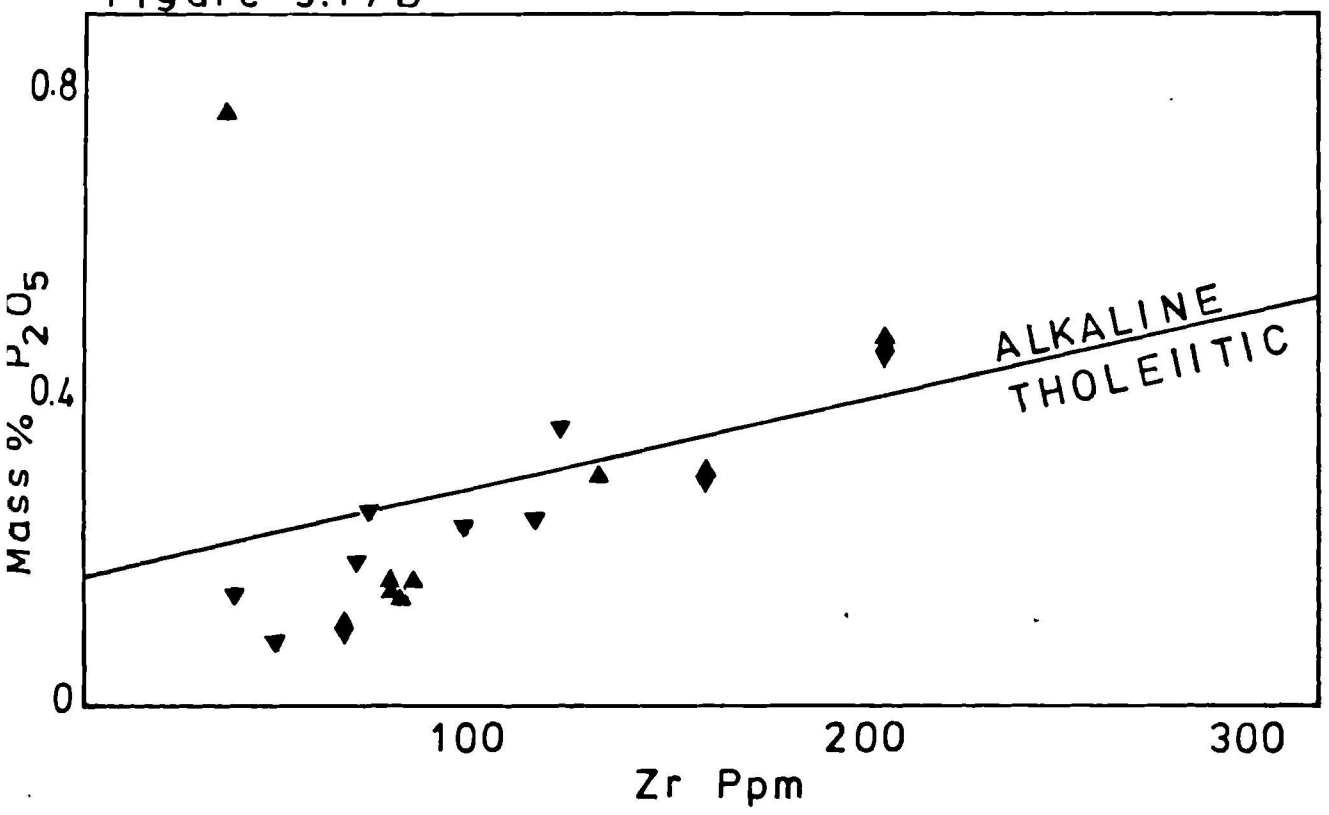

Figure 3.17c

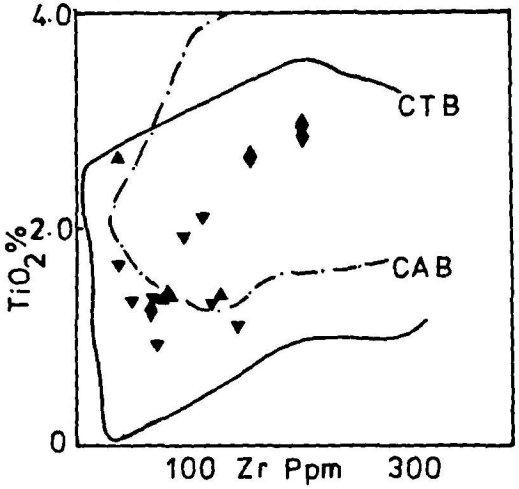

Figure 3.17e

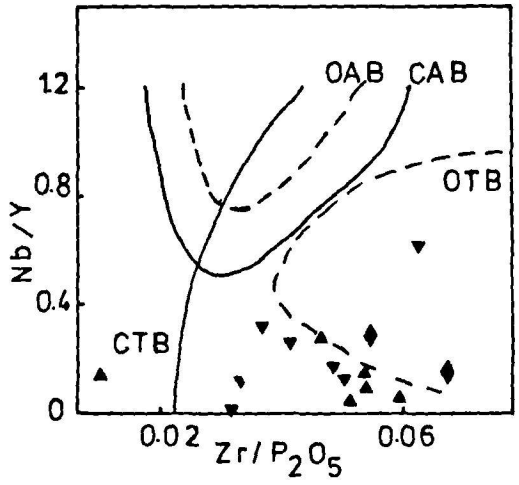

Figure 3.17d

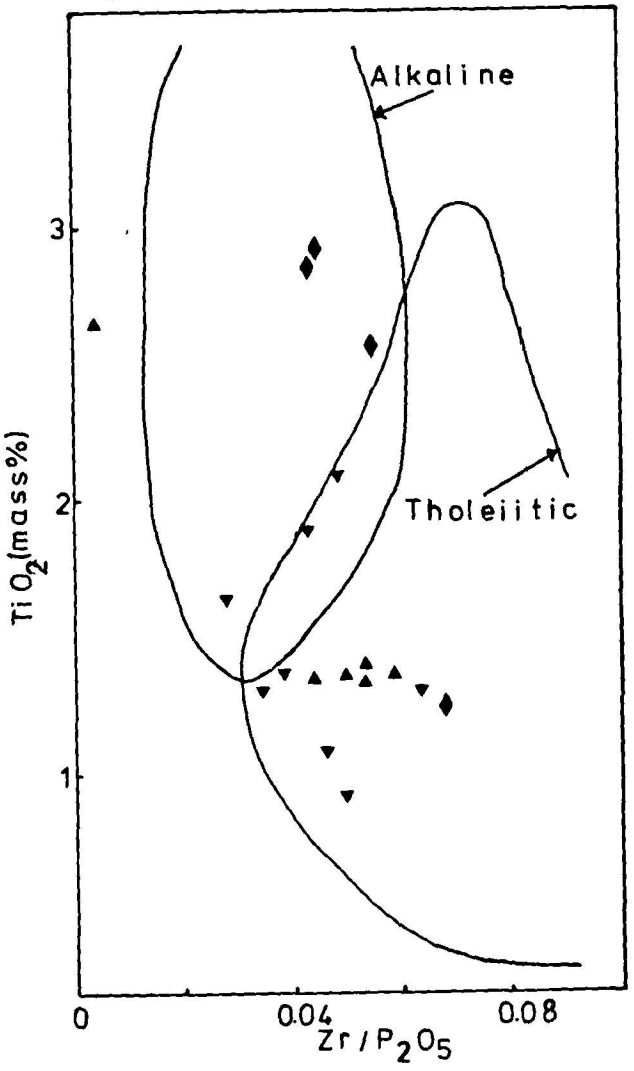

FIGURE 3.18 Metabasites of Gjörlanger Unit and Basal Gneisses plotted on "immobile element" plots of Pearce and Cann (1973). Symbols as for figure 3.16.

Abbreviations:-

OFB - ocean floor basalt
WPB - within plate basalt
CAB - calc-alkali basalt
LKT - low-K tholeiite

Figure 3.18 A

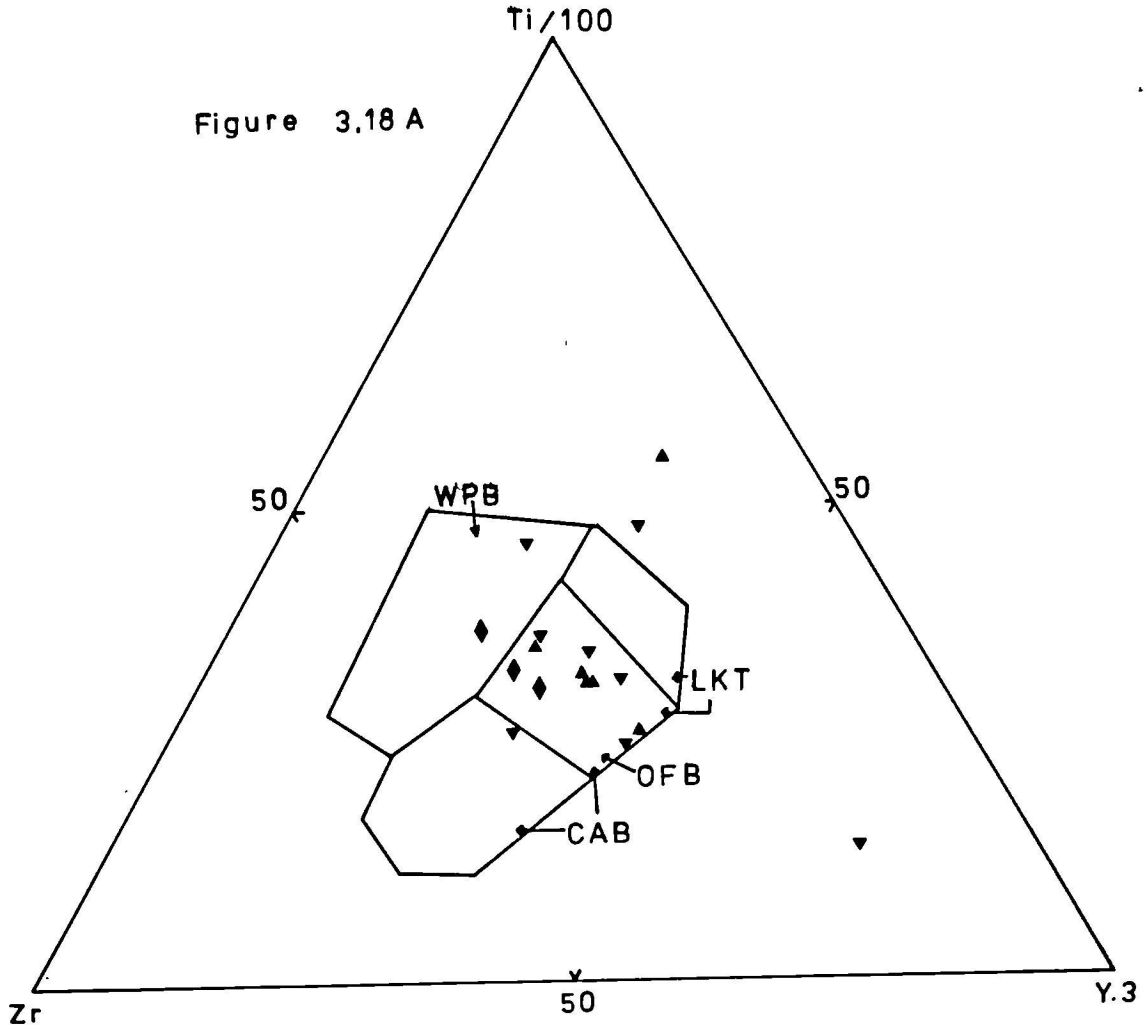

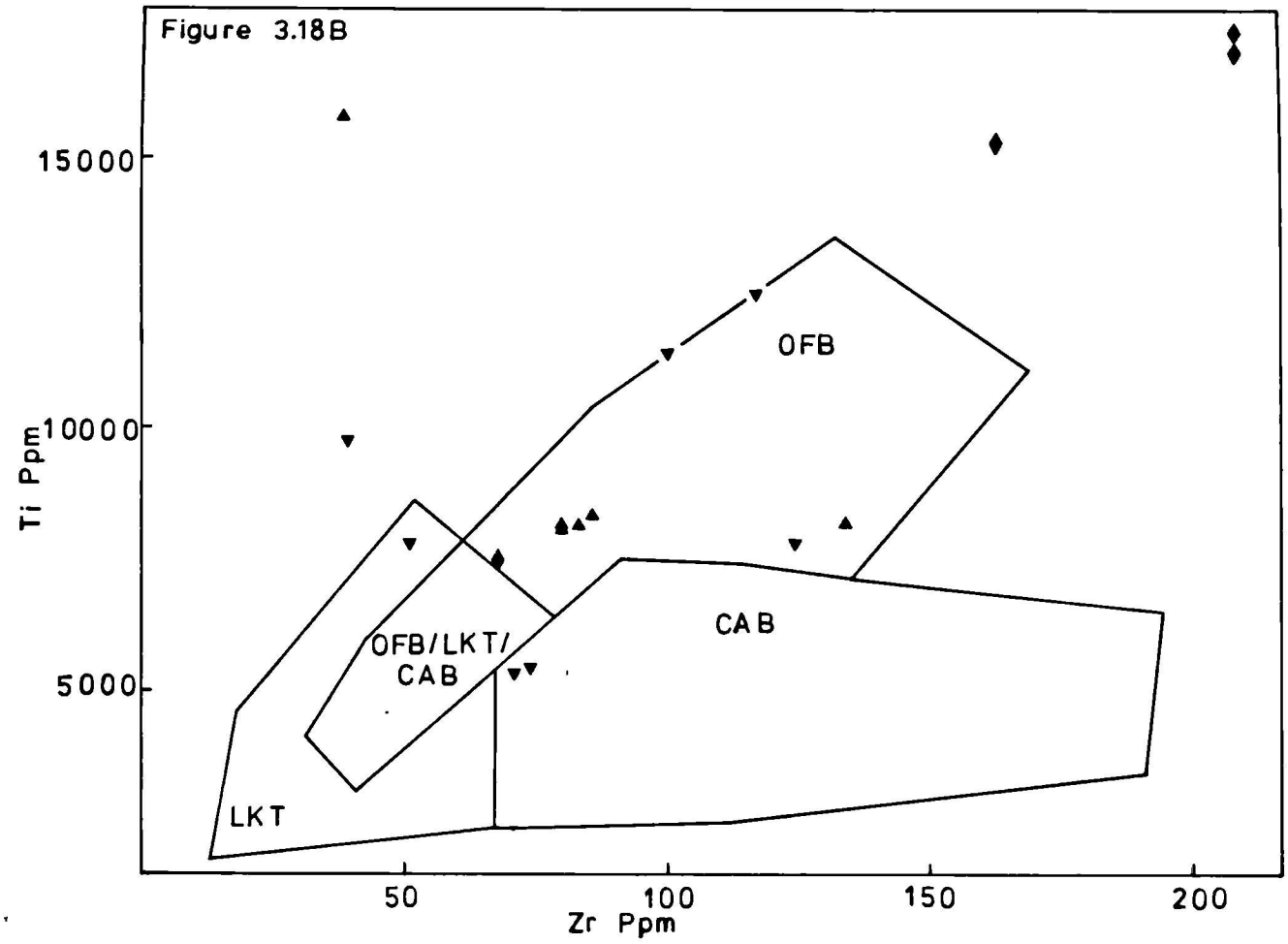
Figure 3.18B
15000
10000
5000
Ti Ppm
OFB
CAB
OFB/LKT/
CAB
LKT
50
100
150
200
Zr Ppm

FIGURE 3.19 Ca-Mg-Fe and AFM diagrams comparing the compositions of websterites in the Gjörlanger Unit with orthopyroxene eclogites from Möre og Romsdal, BGR (from Smith, 1976 and D A Carswell, unpublished data).

Symbols:- squares = orthopyroxene eclogites
circles = Dalsfjord websterites

Enclosed fields:- Solid line Mg-Cr peridotites and pyroxenites BGR.
Dashed line Fe-Ti peridotites and pyroxenites, BGR (from Carswell et al, 1983).

Figure 3.19 A+B

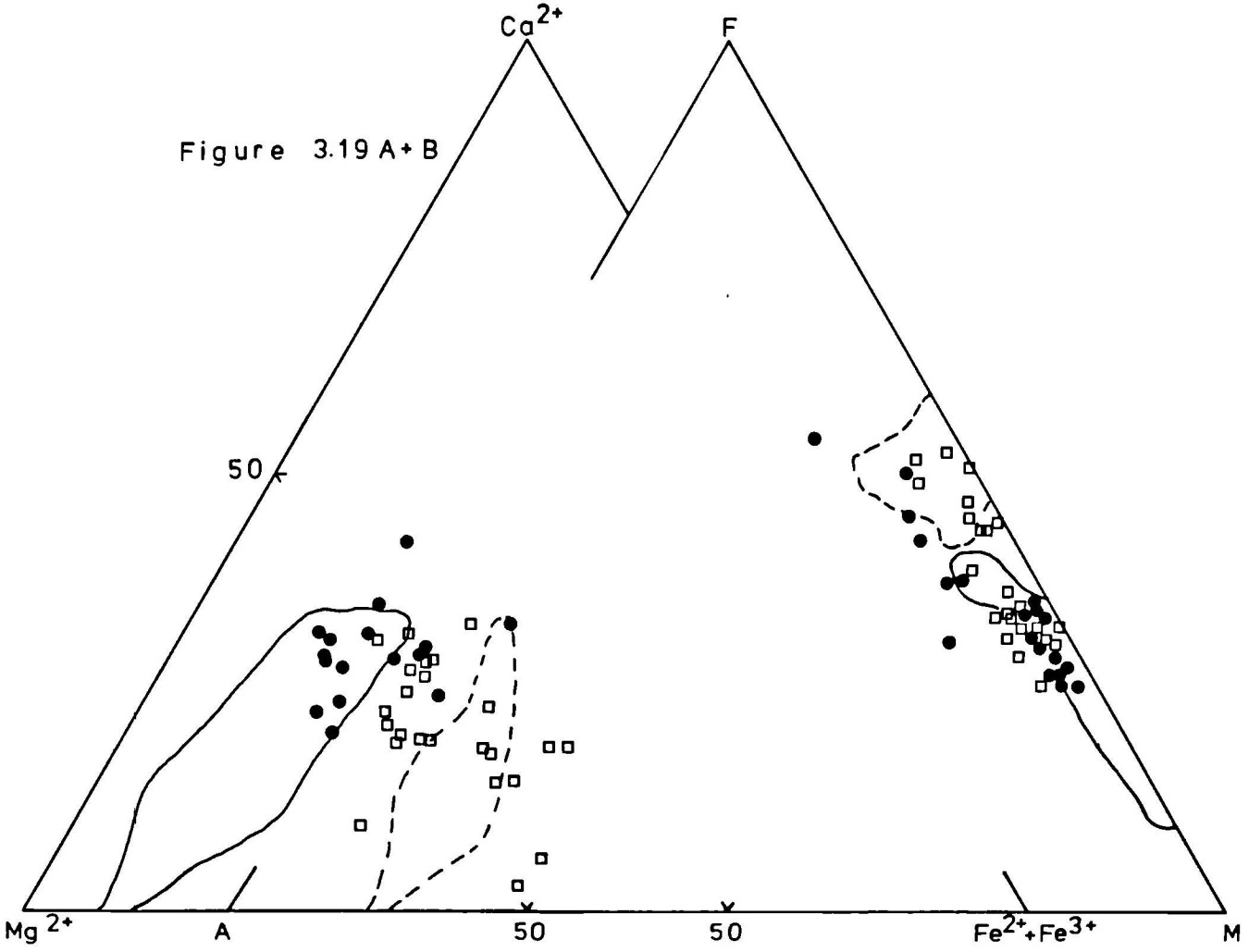

FIGURE 3.20 Variation diagrams comparing the compositions of Dalsfjord websterites with other pyroxenites from the BGR.

Symbols:-

Closed circles	-	Dalsfjord pyroxenites (this work).
Open circles	-	Dalsfjord pyroxenites (A Korneliussen, pers comm, 1981).
Closed triangles	-	Orthopyroxene eclogites (D A Carswell, pers comm, 1982).
	-	Orthopyroxene eclogites (Smith, 1976).

Figure 3.20A

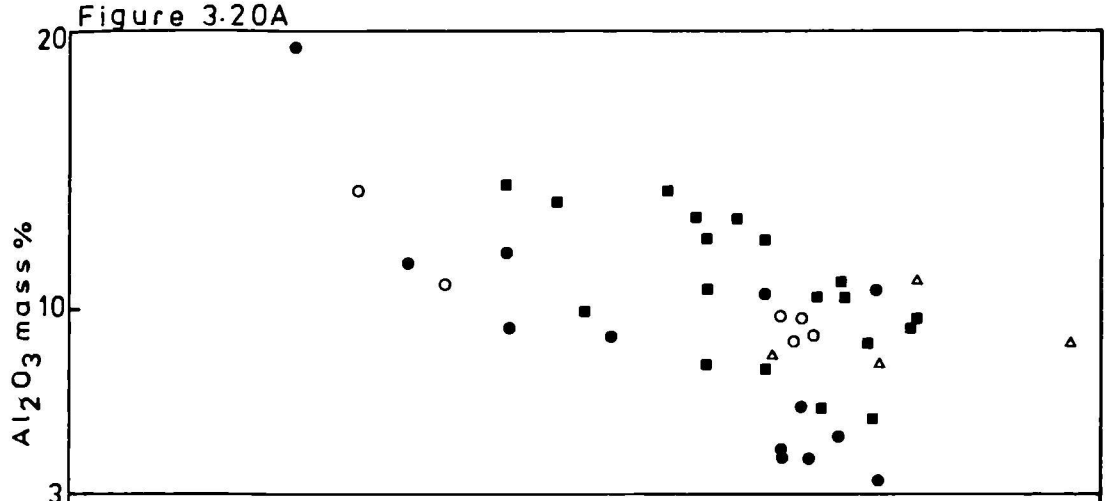

Figure 3.20B

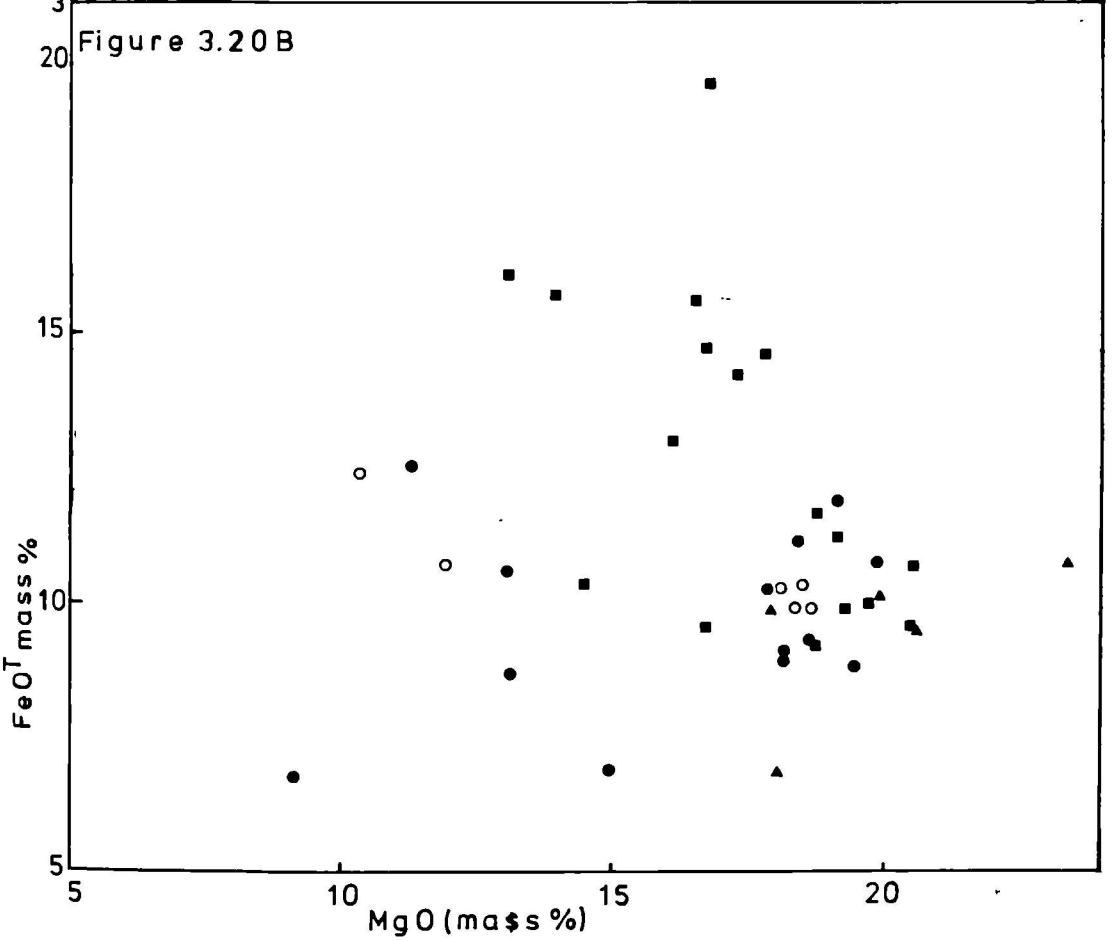

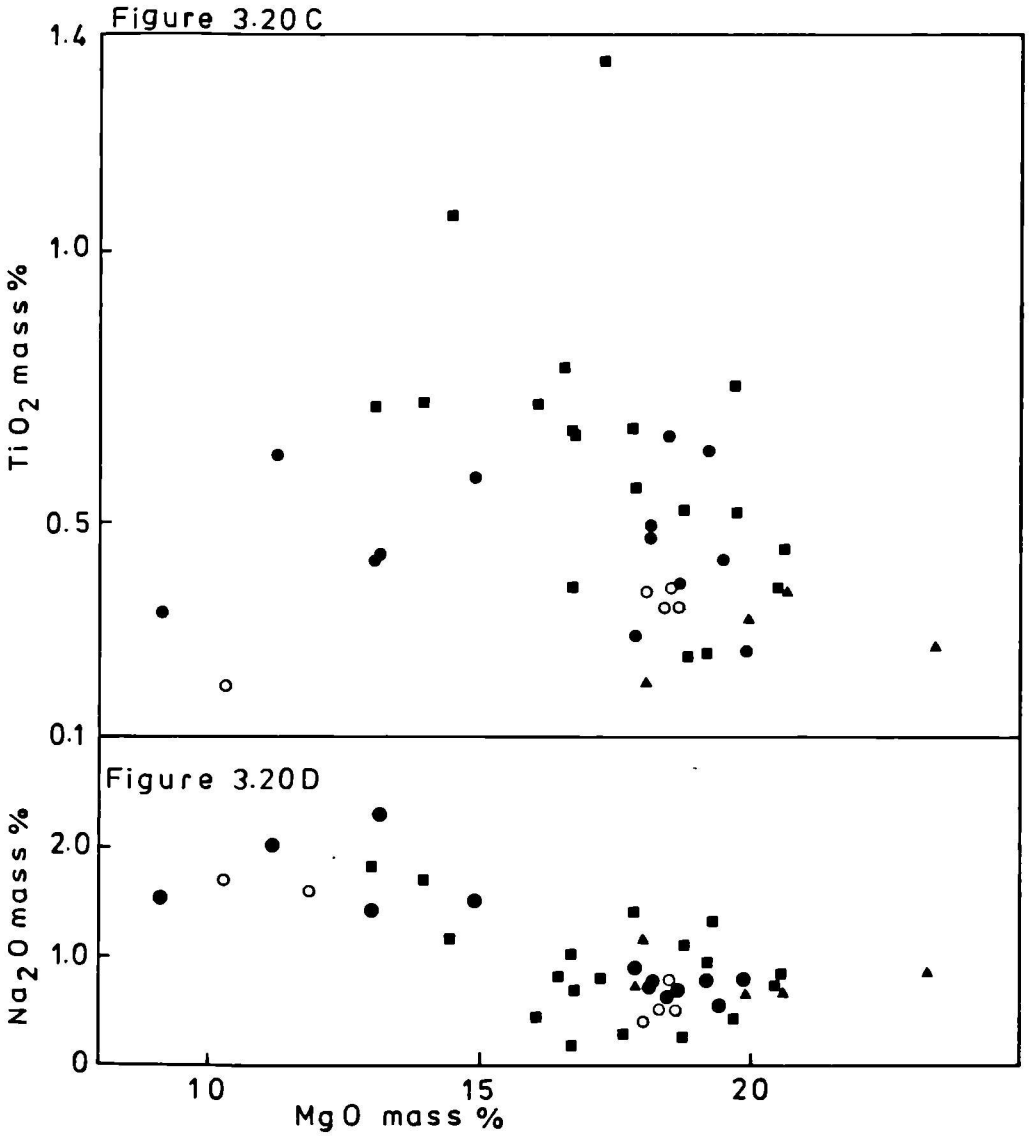
Figure 3.20 C
1.4
1.0
0.5
0.1
Ti O2 mass %
Figure 3.20 D
2.0
1.0
0
Na2O mass %
10
15
20
Mg O mass %

FIGURE 3.21 Compositional variation across a zoisitite pod and its blackwall reaction selvage against the host dunite. Sketch at the top of the diagram is true-scale traced from a rock slab. Solid lines are sharp boundaries, dashed lines are gradational.

Mineral abbreviations:-

Anthoph = anthophyllite
Ol = olivine
Chl = chlorite
Hbl = hornblende
Gt = garnet

Figure 3.21

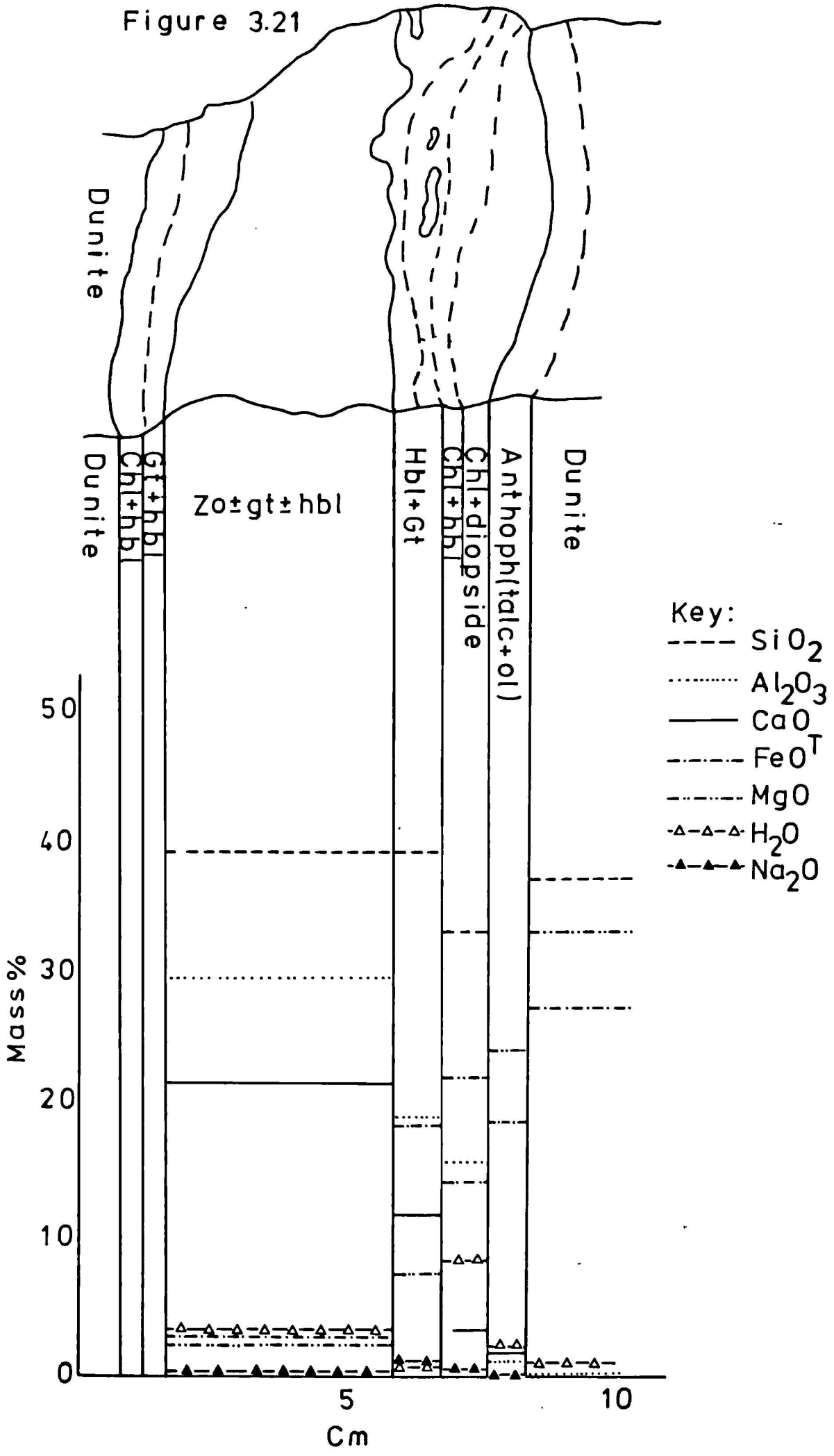
Dunite
Dunite
Chl+hbl
Gt+hbl
Zo±gt±hbl
Hbl+Gt
Chl+hbl
Chl+diopside
Anthoph(talc+ol)
Dunite
Key:
SiO2
Al2O3
CaO
FeOT
MgO
H2O
Na2O
Mass%
50
40
30
20
10
0
5
10
Cm

Figure 3.22

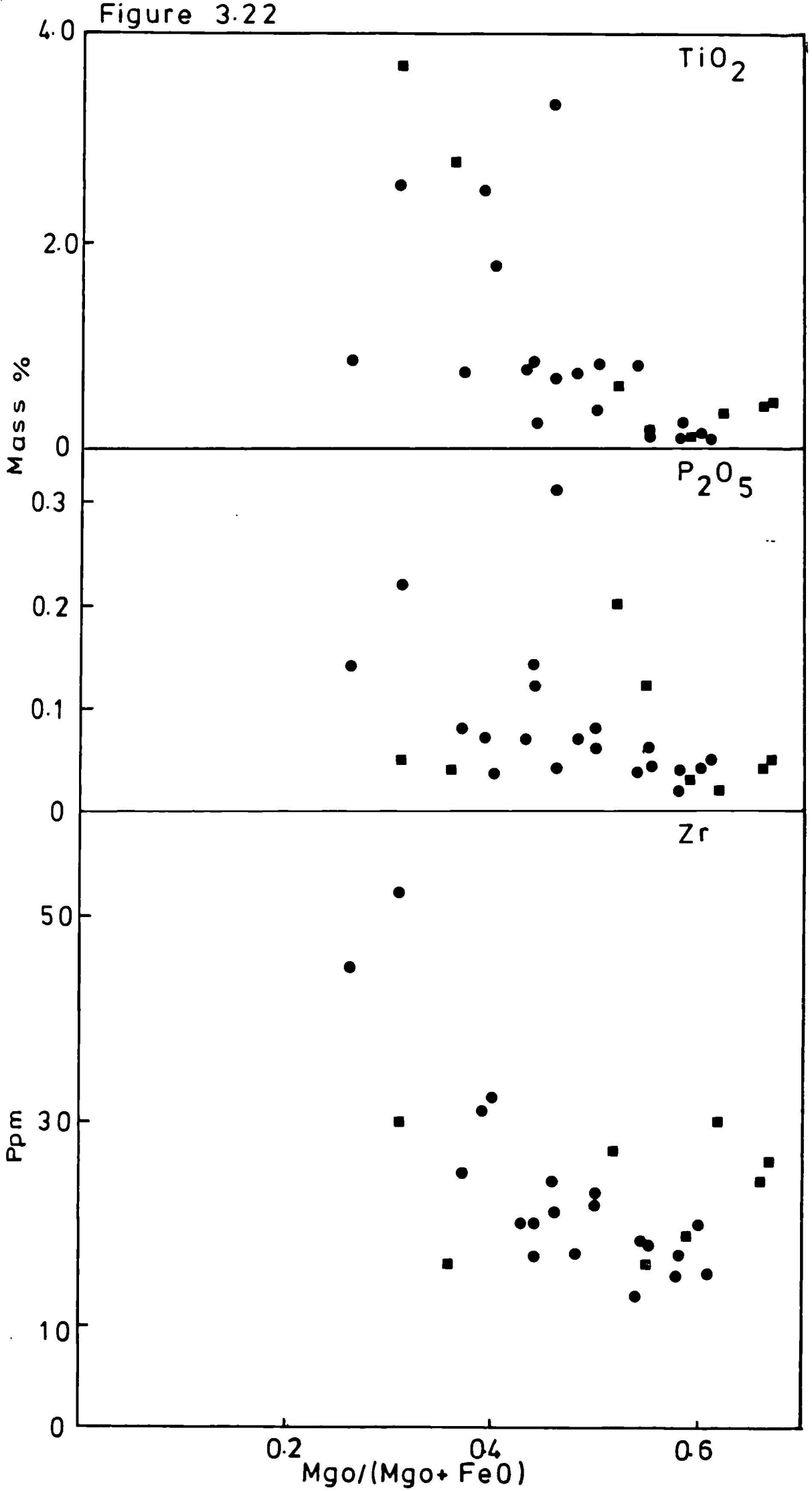
4.0
2.0
0
TiO_2
Mass %
0.3
0.2
0.1
0
P_2O_5
50
30
10
0
Zr
Ppm
0.2
0.4
0.6
Mgo/(Mgo+ FeO)

TABLE 3.1 - Major element analyses and CIPW norms of gneisses, Gjörlanger Unit and Basal Gneisses.

Unit	Gjörlanger Unit																						Basal Gneisses				
Sample	fine grained grey gneisses									massive or augen gneisses (gmεγ)						massive green gneisses								K-poor gneisses					
Mass %	79/4	D26	D30	D97	D99	DG-1	DG-2	DG-5	DG-7	79/12	79/33A	79/43A	D44	D78	D79	79/43B	D110	D112	D113	D114	D115	D120	D184	D23	D24	D121	79/37	79/44A	79/45	79/46	D117
SiO_2	61.66	59.29	65.75	56.39	58.64	77.48	59.81	57.13	57.74	66.08	64.78	67.40	68.69	72.25	74.36	51.44	58.68	56.40	54.44	54.02	54.79	50.95	59.96	66.99	60.26	65.43	58.57	76.12	63.51	62.57	55.27
Al_2O_3	15.80	16.65	15.24	18.77	17.60	12.56	18.47	16.99	18.30	14.49	14.70	15.28	14.20	13.51	13.41	17.78	17.32	18.07	18.04	19.54	20.37	18.09	17.72	15.82	17.03	16.23	19.63	12.47	18.83	10.01	19.49
TiO_2	0.90	0.98	0.63	1.07	0.87	0.10	0.77	1.23	1.07	0.94	0.93	0.63	0.63	0.38	0.28	1.38	1.06	1.05	1.09	1.36	1.26	1.44	1.03	0.42	0.64	0.49	0.76	0.18	0.62	0.64	1.01
Fe_2O_3	1.17	1.78	1.53	1.20	1.43	0.08	1.76	6.40	5.30	1.63	1.69	1.50	0.70	1.31	0.56	0.88	0.98	1.12	1.94	1.80	2.04	2.56	0.14	1.33	1.84	1.04	1.93	0.33	0.69	1.66	1.58
FeO	5.27	6.08	4.40	7.31	6.07	0.59	4.69	3.17	3.04	5.09	5.35	3.30	3.75	1.91	1.01	9.55	6.87	7.38	6.67	7.40	5.76	8.84	6.65	2.55	4.19	3.24	3.39	0.44	1.43	1.96	4.84
MgO	2.74	2.77	1.48	1.88	3.72	0.22	1.33	1.76	1.47	1.05	1.13	1.40	0.80	0.61	0.66	4.51	2.84	3.23	3.38	1.88	1.74	3.91	2.41	2.26	4.11	2.47	2.06	0.15	0.57	1.13	2.50
CaO	5.14	6.34	3.73	5.02	7.23	1.45	5.32	5.55	5.66	3.20	3.77	3.98	2.92	3.28	3.13	7.99	6.30	7.72	7.80	6.97	7.44	8.98	6.13	4.40	7.32	5.50	4.39	0.43	1.39	2.11	5.16
Na_2O	3.28	3.72	2.79	4.54	4.06	3.07	4.83	3.63	4.94	3.43	3.52	2.88	3.33	4.55	2.62	3.65	4.26	3.60	4.15	5.55	4.85	3.54	3.98	4.47	4.16	4.11	5.11	2.66	5.14	4.31	5.23
K_2O	2.30	1.01	3.16	1.79	0.59	4.08	1.71	2.33	1.31	3.46	3.26	3.17	3.81	1.48	2.30	1.18	0.91	0.73	0.86	0.61	0.89	0.37	1.14	0.75	0.32	0.46	3.48	6.37	7.43	5.51	3.29
P_2O_5	0.25	0.42	0.15	0.20	0.17	0.30	0.15	0.52	0.23	0.23	0.24	0.17	0.16	0.07	0.07	0.38	0.26	0.34	0.31	0.39	0.33	0.33	0.27	0.12	0.22	0.14	0.31	0.01	0.12	0.27	0.54
S	0.04	0.00	0.00	0.02	0.01	0.00	0.01	0.01	0.02	0.00	0.02	0.00	0.00	0.03	0.05	0.15	0.02	0.02	0.07	0.06	0.03	0.11	0.06	0.00	0.02	0.01	0.00	0.06	0.02	0.00	0.06
H_2O+	0.80	0.51	0.92	0.55	0.18	0.29	0.96	1.35	0.87	0.92	0.46	0.51	0.40	0.27	0.02	0.41	0.54	0.43	0.73	0.35	0.64	0.65	0.57	0.66	0.21	0.44	0.26	0.30	0.27	0.58	0.36
Total	99.46	99.67	99.85	99.92	100.51	100.23	99.92	100.23	100.10	100.63	99.96	100.28	99.43	99.67	99.27	99.48	100.15	100.23	99.63	100.12	100.29	100.01	100.26	99.82	100.38	99.63	100.06	99.53	100.09	99.85	99.50
ap	0.58	0.97	0.34	0.46	0.39	0.69	0.34	1.20	-	0.53	0.56	0.39	0.37	0.16	0.16	0.88	0.60	0.79	0.72	0.91	0.77	0.77	0.63	0.28	0.51	0.32	0.72	0.02	0.28	0.63	1.25
py	0.07	0.00	0.00	0.03	0.01	0.00	0.01	0.05	-	0.00	0.04	0.00	0.00	0.06	0.89	0.28	0.04	0.04	0.13	0.11	0.06	0.29	0.11	0.00	0.04	0.19	0.00	0.11	0.04	0.00	0.11
il	1.71	1.86	1.19	2.03	1.65	0.19	1.46	2.33	-	1.78	1.76	1.19	1.19	0.72	0.53	2.62	2.01	1.99	2.07	2.58	2.39	2.73	1.96	0.79	1.22	0.93	1.44	0.34	1.18	1.22	1.92
or	13.65	5.96	18.67	10.57	3.48	24.11	10.10	13.77	-	20.45	19.27	18.73	22.52	8.75	13.59	6.97	5.38	4.31	5.08	3.60	5.26	2.19	6.74	4.43	1.89	2.72	20.57	37.64	43.91	32.56	19.44
ab	27.76	31.48	23.61	38.42	34.36	25.98	40.87	30.71	-	29.02	29.79	24.37	28.18	38.50	22.17	30.89	36.05	30.46	35.12	46.96	41.04	30.80	33.68	37.82	35.20	34.78	43.24	22.51	43.49	36.47	43.74
an	21.57	25.72	17.52	25.55	27.51	5.23	23.67	23.18	-	13.92	14.68	18.63	12.55	12.07	15.07	28.65	25.45	30.92	28.06	26.60	31.18	31.93	27.12	20.88	26.85	24.48	19.75	2.07	6.11	8.70	19.99
c	0.00	0.00	0.80	0.00	0.00	1.18	0.00	0.00	-	0.00	0.00	0.28	0.00	0.00	1.08	0.00	0.00	0.00	0.00	0.00	0.00	0.00	0.00	0.00	0.00	0.00	0.22	0.44	0.09	2.27	0.00
mt	1.69	2.58	2.22	1.74	2.07	0.12	2.55	3.17	-	2.36	2.45	2.17	1.01	1.89	0.81	1.27	1.42	1.62	2.81	2.61	2.96	3.71	0.20	1.93	2.67	1.51	2.79	0.48	1.00	2.41	2.29
di wo	0.96	1.23	0.00	1.25	3.03	0.00	0.73	0.39	-	0.19	1.02	0.00	0.37	1.56	0.00	3.55	1.71	2.12	3.59	2.27	1.49	4.36	0.64	0.07	3.52	0.79	0.00	0.00	0.00	0.00	0.87
di en	0.46	0.56	0.00	0.39	1.54	0.00	0.26	0.13	-	0.05	0.31	0.00	0.11	0.72	0.00	1.56	0.71	0.98	1.74	0.76	0.59	1.99	0.24	0.04	2.10	0.45	0.00	0.00	0.00	0.00	0.44
di fs	0.48	0.66	0.00	0.98	1.41	0.00	0.47	0.27	-	0.14	0.75	0.00	0.28	0.82	0.00	1.98	1.01	1.22	1.79	1.58	0.92	2.35	0.41	0.02	1.04	0.31	0.00	0.00	0.00	0.00	0.41
hy en	6.36	6.33	6.68	4.28	7.72	0.55	3.04	4.25	-	2.56	2.50	3.48	1.88	0.79	1.64	6.74	6.37	7.14	6.68	5.28	3.74	7.75	5.76	5.59	8.13	5.70	5.13	0.37	1.42	2.81	0.00
hy fs	6.66	7.41	5.77	9.72	7.89	0.85	5.39	8.60	-	6.31	6.09	3.78	4.98	0.91	0.83	8.53	9.01	9.64	6.90	6.81	5.83	9.16	9.86	2.87	4.03	3.95	3.37	0.12	0.99	1.17	0.00
qz	16.58	14.21	25.01	3.80	5.59	41.01	9.91	10.20	-	22.26	20.14	26.64	25.53	32.79	42.42	0.00	9.74	8.42	4.82	0.00	3.26	1.23	12.12	24.36	13.06	23.14	2.38	35.08	1.23	10.43	0.00
ol fo	0.00	0.00	0.00	0.00	0.00	0.00	0.00	0.00	-	0.00	0.00	0.00	0.00	0.00	0.00	2.05	0.00	0.00	0.00	0.45	0.00	0.00	0.00	0.00	0.00	0.00	0.00	0.00	0.00	0.00	4.05
ol fa	0.00	0.00	0.00	0.00	0.00	0.00	0.00	0.00	-	0.00	0.00	0.00	0.00	0.00	0.00	2.86	0.00	0.00	0.00	1.03	0.00	0.00	0.00	0.00	0.00	0.00	0.00	0.00	0.00	0.00	4.16
ne	0.00	0.00	0.00	0.00	0.00	0.00	0.00	0.00	-	0.00	0.00	0.00	0.00	0.00	0.00	0.00	0.00	0.00	0.00	0.00	0.00	0.00	0.00	0.00	0.00	0.00	0.00	0.00	0.00	0.00	0.28
DI	57.99	51.66	67.29	52.80	47.73	91.10	60.94	54.69	-	71.73	69.19	69.75	76.22	79.65	78.19	37.86	51.26	43.20	44.22	50.57	49.56	34.22	52.54	66.62	50.15	60.64	66.19	95.23	89.09	79.46	63.46

TABLE 3.2 - Whole-rock trace element analyses of gneisses, Gjörlanger Unit and Basal Gneisses

Unit	Gjörlanger Unit																													
Sample	Fine grained grey gneisses									Massive or augen gneisses (grey)			massive green gneisses										K-poor gneisses							
ppm	79/4	D26	D30	D97	D99	DG-1	DG-2	DG-5	DG-7	79/12	79/33A	79/43A	D44	D76	D79	79/43B	D110	D112	D113	D114	D115	D120	D184	D23	D24	D121	79/37	79/44A	79/45	79/46	D117
Ni	11	12	-	6	27	10	10	8	16	12	4	-	ND	ND	1	19	16	13	23	4	5	20	16	32	69	33	20	5	0	2	5
Mn	797	1083	-	1477	1086	105	840	1205	1150	865	808	465	310	155	ND	1251	897	1180	1171	1479	1197	1171	776	534	784	566	1341	162	591	1004	1407
Cr	46	17	-	12	61	80	59	63	89	27	18	-	14	23	15	37	48	33	36	4	ND	26	33	61	136	43	0	4	18	7	2
V	60	95	-	61	120	11	47	61	59	56	44	-	-	-	-	109	109	131	151	65	57	235	82	69	111	74	71	11	29	36	100
Nb	-	4	-	7	2	4	1	9	7	12	-	-	5	5	8	-	9	7	13	19	15	9	12	6	1	5	7	8	-	8	10
Zr	233	210	-	415	35	111	359	606	568	496	646	-	375	216	98	94	251	116	102	651	549	177	298	84	101	104	70	129	277	183	356
Y	44	31	-	22	13	4	7	41	25	36	55	-	29	5	3	77	33	8	33	39	37	46	28	8	11	9	16	25	20	25	25
La	765	433	-	1422	376	1339	1649	1126	1194	2243	1465	-	1609	462	1107	601	339	383	365	349	418	252	825	301	211	417	3405	772	998	3113	4316
Sr	323	525	177	247	398	209	479	115	438	368	249	210	214	291	600	138	366	540	471	401	511	435	495	395	561	635	601	164	152	385	591
Rb	36	16	62	1	ND	19	12	16	6	52	63	70	77	29	41	30	6	4	19	8	16	3	9	ND	ND	3	79	125	85	61	60
Pb	26	10	-	11	6	21	21	15	16	18	17	-	18	8	9	23	9	12	10	10	13	7	12	3	9	4	19	13	7	14	17
K/Rb	741	1220	620	21300	-	2578	1700	1775	2616	803	625	545	558	613	687	470	1800	2175	542	900	583	1500	1511	-	-	1833.3	515.18	616.0	1015.29	1057.21	645.0
Rb/Sr	0.111	0.019	0.350	0.004	-	0.091	0.025	0.139	0.007	0.141	0.253	0.333	0.360	0.100	0.068	0.217	0.016	0.007	0.040	0.020	0.035	0.007	0.018	-	-	0.005	0.131	0.762	0.559	0.159	0.061
Ba/Rb	21.81	43.30	-	1422.00	-	70.47	137.49	70.38	199.00	43.15	23.25	-	21.94	15.93	28.95	20.003	56.5	95.75	19.211	43.625	23.222	84.0	91.666	-	-	139	43.861	6.176	11.741	51.033	71.933

TABLE 3.3 - Average compositions of gneisses from the Gjörlanger Unit and the Basal Gneisses with some other suites for comparison.

	Gjörlanger Unit/Basal Gneisses												Av-crust	Tuolumne		Madras Charnockites								Mangerites			
	1		2		3		4		5		6		7	8		9		10		11		12		13	14		15
Mass%	$\bar{x}$	o	$\bar{x}$	o	$\bar{x}$	o	$\bar{x}$	o	$\bar{x}$	o	$\bar{x}$	o	$\bar{x}$	$\bar{x}$	o	$\bar{x}$	o	$\bar{x}$	o	$\bar{x}$	o	$\bar{x}$	o		$\bar{x}$	o	$\bar{x}$
n	23		7		4		8		5		4		-	22		9		6		8		7		1	3		?
SiO_2	60.07	6.26	59.55	2.81	66.73	1.46	55.09	2.97	67.86	5.02	59.98	3.29	60.30	66.41	4.68	74.12	2.41	68.73	5.11	62.32	4.09	50.81	1.80	55.50	57.13	0.33	58.06
Al_2O_3	16.94	1.91	17.20	1.20	14.67	0.40	18.37	0.97	15.20	1.47	19.24	0.33	15.60	15.59	0.78	12.49	1.85	14.39	1.62	15.44	0.45	15.11	2.43	14.31	18.59	0.36	16.7
Fe_2O_3	1.79	1.45	7.32	1.04	5.61	1.11	8.67	1.36	3.67	1.41	4.22	1.60	7.20	1.67	0.54	3.37	1.12	5.10	2.12	6.73	1.93	14.61	2.11	2.93	2.84	0.87	3.00
FeO	5.58	2.06												2.02	1.26									2.29	2.46	0.59	5.68
MgO	2.17	1.10	2.14	0.79	1.10	0.21	2.99	0.90	2.02	1.30	1.57	0.76	3.90	1.52	1.02	0.84	0.50	1.44	0.94	2.58	1.32	5.36	1.67	0.87	1.75	0.11	0.73
MnO	-	-	-	-	-	-	-	-	-	-	-	-	-	-	-	0.03	0.04	0.12	0.08	0.07	0.05	0.24	0.18	0.08	0.09	0.01	0.23
CaO	5.64	1.90	5.50	0.95	3.47	0.43	7.42	0.87	4.73	1.55	3.26	1.56	5.80	3.78	1.46	2.00	1.47	3.12	1.11	4.54	1.60	9.04	0.92	2.08	3.33	0.06	3.41
Na_2O	3.89	0.71	3.97	0.71	3.29	0.25	4.20	0.65	3.98	0.70	4.95	0.37	3.20	3.85	0.34	2.94	1.14	3.71	0.28	3.89	0.28	2.49	1.11	3.66	5.06	0.10	4.81
K_2O	1.84	1.17	1.78	0.77	3.43	0.25	0.84	0.25	1.06	0.74	4.93	1.69	2.50	3.31	0.65	3.81	1.22	2.11	0.95	2.86	1.71	0.54	0.29	6.17	5.63	0.16	5.30
P_2O_5	0.28	0.01	0.26	0.13	0.20	0.04	0.33	0.04	0.12	0.06	0.31	0.15	0.24	0.16	0.05	0.04	0.05	0.06	0.05	0.24	0.15	0.24	0.12	0.14	0.42	0.03	0.22
ppm																											
Ni	12	7	13	6	4	5	15	7	27	25	7	8	75	5	4	-	-	-	-	-	-	-	-	5	-	-	-
Mn	-	-	1091	212	612	232	1140	202	408	287	1086	324	-	-	-	-	-	-	-	-	-	-	-	-	-	-	-
Cr	38	26	52	28	15	10	27	15	56	43	7	7	100	8	7	-	-	-	-	-	-	-	-	5	-	-	-
V	91	53	75	24	25	25	125	56	51	44	59	29	-	73	48	-	-	-	-	-	-	-	-	70	-	-	-
Nb	9	5	4	3	5	5	11	5	6	3	6	4	-	8	1	-	-	-	-	-	-	-	-	-	18	1	-
Zr	344	218	368	237	379	239	292	200	121	49	222	107	165	121	22	-	-	-	-	-	-	-	-	1000	729	52	-
Y	33	16	27	13	30	20	40	15	7	3	22	4	33	11	6	-	-	-	-	-	-	-	-	100	26	3	-
Ba	908	577	988	449	1349	829	442	172	516	347	2973	1221	425	744	199	-	-	-	-	-	-	-	-	1000	3176	123	-
Sr	348	134	361	133	260	64	420	119	496	132	532	309	375	562	93	-	-	-	-	-	-	-	-	140	626	12	-
Rb	25	24	12	11	66	9	12	9	15	17	71	11	90	129	19	-	-	-	-	-	-	-	-	-	67	5	-
Pb	15	6	16	7	13	8	12	5	7	3	14	5	13	17	3	-	-	-	-	-	-	-	-	-	-	-	-
K/Rb	887		1788		626		844		851		837		232	309	-	-	-	-	-	-	-	-	-	-	1013	-	-
Rb/Sr	0.072		0.03		0.25		0.03		0.03		0.13		0.24	0.23	-	-	-	-	-	-	-	-	-	-	0.11	-	-
Ba/Rb	36		83		20		37		34		42		5	6	-	-	-	-	-	-	-	-	-	-	47	-	-
Ba/Sr	2.61		3		5		1		1		6		1	1	-	-	-	-	-	-	-	-	-	7	5	-	-

TABLE 3.4 - Rb-Sr isotopic analyses of grey gneisses, Gjörlanger Unit.

Sample	Rb/Sr	$^{87}Rb/^{86}Sr$	$^{87}Sr/^{86}Sr$	S.D. (2 σ)	Description
79/4	0.111	0.33236	0.70969	0.00025	Fine-grained, foliated
79/12	0.159	0.46146	0.71390	0.00031	Coarse augen gneiss
79/33A	0.253	0.73273	0.71816	0.00020	Charnockitic, slightly hydrated
79/43A	0.333	0.96515	0.71670	0.00023	Charnockitic, slightly hydrated
D30	0.350	1.01440	0.71687	0.00021	Fine-grained, foliated
DG-1	0.077	0.22226	0.71064	0.00020	Phengite-bearing alaskite
DG-5	0.109	0.31678	0.70678	0.00037	Fine-grained, foliated
DG-7	0.019	0.05524	0.70358	0.00029	Fine-grained, foliated
D44	0.360	1.04255	0.72318	0.00024	Coarse augen gneiss
NBS987			0.71037	0.00024	Standard strontium carbonate

TABLE 3.5 - Major element analysis and CIPW norms of metabasites, Gjörlanger Unit and Basal Gneisses

Unit	Gjörlanger Unit																	Basal Gneisses			
Sample	Dykes						Concordant sheets in gneisses														
Mass%	D46	D80	D81	D82	D83	D134	D1	D38	D77	D95	D101	D102	D103	D104	D105	D108	D123	D129	79/38A	79/38B	D69	D116
SiO_2	44.91	47.17	47.16	47.76	48.67	50.38	53.44	48.02	49.61	47.07	47.51	48.25	51.65	47.66	55.08	44.60	47.94	49.70	47.31	46.62	48.03	46.26
Al_2O_3	15.81	16.07	16.32	16.51	15.49	17.36	16.63	13.95	18.54	20.45	16.89	14.82	19.38	15.34	18.87	17.97	22.80	17.22	14.02	14.45	14.96	15.99
TiO_2	2.65	1.39	1.34	1.35	1.36	1.36	0.91	1.33	0.89	0.17	1.30	2.09	1.30	1.89	1.08	1.63	0.19	0.83	2.92	2.86	1.24	2.56
Fe_2O_3	0.71	3.02	2.19	1.48	0.55	1.19	0.73	2.07	0.93	4.48	1.94	1.83	2.38	0.24	1.95	3.56	0.70	1.99	4.05	2.34	2.58	2.00
FeO	13.28	10.04	10.16	11.27	11.59	10.10	8.41	11.11	7.59	4.32	10.37	13.71	7.44	13.20	6.39	10.29	5.70	6.40	11.12	13.84	10.50	12.59
MgO	6.48	6.89	7.34	7.14	6.79	5.27	5.22	7.72	7.39	9.21	7.60	6.83	3.53	6.68	3.18	5.51	8.54	7.57	5.31	6.64	6.76	6.17
MnO	0.15	0.18	0.14	0.12	0.12	0.17	0.10	0.17	0.08	0.08	0.20	0.23	0.16	0.20	0.14	0.19	0.08	0.13	0.34	0.20	0.22	0.20
CaO	11.10	9.73	9.38	9.31	10.20	9.04	8.25	10.90	11.09	9.07	11.13	10.14	8.57	9.72	7.84	10.19	10.39	10.47	8.98	8.79	10.62	8.51
Na_2O	3.62	3.53	3.88	3.69	3.23	2.90	4.27	3.63	3.13	5.12	2.02	2.08	3.92	3.86	4.15	2.92	2.48	3.76	2.91	2.87	4.50	3.46
K_2O	0.02	0.29	0.48	0.51	0.23	1.42	1.03	0.04	0.39	0.27	0.40	0.02	0.58	0.24	0.82	0.30	0.09	0.12	2.16	0.98	0.06	1.25
P_2O_5	0.77	0.16	0.15	0.16	0.14	0.30	0.25	0.18	0.08	0.06	0.08	0.24	0.36	0.23	0.32	0.14	0.02	0.16	0.46	0.47	0.10	0.30
S	0.05	0.19	0.17	0.16	0.14	0.13	0.10	0.07	0.04	0.05	0.09	0.01	0.05	0.24	0.08	0.07	0.01	0.00	0.24	0.08	0.02	0.10
H_2O^+	0.12	0.31	0.53	0.36	0.74	0.00	0.59	0.43	0.35	0.35	0.44	0.24	1.02	0.21	0.65	0.93	0.55	0.76	0.72	0.28	0.12	0.45
Total	99.67	99.47	99.24	99.82	99.25	99.62	99.93	99.62	100.11	100.70	99.97	100.47	100.34	99.73	100.55	99.30	99.49	99.11	100.54	100.42	99.71	99.84
ap	1.79	0.37	0.35	0.37	0.32	0.69	0.58	0.42	0.89	0.14	0.19	0.56	0.84	0.53	0.74	0.32	0.05	0.37	1.07	1.09	0.23	0.69
py	0.09	0.35	0.32	0.29	0.26	0.24	0.19	0.13	0.07	0.09	0.17	0.02	0.09	0.45	0.15	0.13	0.02	0.00	0.45	0.15	0.04	0.19
il	5.03	2.64	2.54	2.56	2.58	2.58	1.73	2.53	1.69	0.32	2.47	3.97	2.47	3.59	2.05	3.09	0.36	1.58	5.55	5.43	2.35	4.86
or	0.12	1.71	2.84	3.01	1.36	8.39	6.09	0.24	2.30	1.59	2.36	0.12	3.43	1.42	4.85	1.77	0.53	0.71	12.76	5.79	0.35	7.39
ab	20.68	27.99	25.18	26.06	27.33	24.54	36.13	25.91	26.49	22.82	17.09	17.60	33.17	25.99	35.12	24.71	20.99	31.82	24.60	24.29	25.18	23.15
an	26.83	27.15	25.69	26.98	27.09	30.16	23.17	21.65	35.39	32.02	35.84	30.99	33.57	23.88	30.44	35.04	50.81	29.76	18.81	23.65	20.44	24.41
C	0.00	0.00	0.00	0.00	0.00	0.00	0.00	0.00	0.00	0.00	0.00	0.00	0.00	0.00	0.00	0.00	0.00	0.00	0.00	0.00	0.00	0.00
mt	1.03	4.38	3.17	2.15	0.79	1.72	1.06	3.00	1.35	6.49	2.81	2.65	3.45	0.35	2.83	5.16	1.01	2.88	5.87	3.39	3.74	2.90
di) wo	9.69	8.38	8.29	7.58	9.44	5.31	6.74	13.05	7.98	5.25	7.87	7.41	2.75	0.54	2.66	6.09	0.25	8.83	9.49	7.05	13.19	6.62
di) en	4.38	4.56	4.49	3.80	4.47	2.45	3.29	6.85	4.66	4.03	4.23	3.36	1.31	4.26	1.29	3.06	0.16	5.64	4.89	3.28	6.78	3.10
di) fs	5.25	3.52	3.51	3.62	4.84	2.81	3.32	5.82	2.94	0.68	3.38	3.99	1.41	5.23	1.33	2.91	0.07	2.61	4.35	3.69	6.07	3.44
hy) en	0.00	0.00	0.00	0.00	1.38	6.37	4.81	0.00	0.63	0.00	7.35	12.73	7.48	0.00	6.63	0.98	6.18	0.08	0.00	2.35	0.00	0.00
hy) fs	0.00	0.00	0.00	0.00	1.49	7.30	4.86	0.00	0.39	0.00	5.86	15.11	8.04	0.00	6.85	0.94	2.78	0.04	0.00	2.64	0.00	0.00
qz	0.00	0.00	0.00	0.00	0.00	0.00	0.00	0.00	0.00	0.00	0.00	0.00	1.14	0.00	4.81	0.00	0.00	0.00	0.00	0.00	0.00	0.00
ol) fo	8.24	8.83	9.66	9.79	7.75	3.02	3.43	8.68	9.19	13.25	5.15	0.64	0.00	8.67	0.00	6.79	10.46	9.20	5.84	7.64	7.05	8.59
ol) fa	10.87	7.51	8.32	10.27	9.24	3.81	3.82	8.13	6.39	2.45	4.53	0.84	0.00	11.73	0.00	7.16	5.18	4.69	5.72	9.47	6.95	10.49
ne	5.39	1.02	4.14	2.80	0.00	0.00	0.00	2.60	0.00	11.11	0.00	0.00	0.00	3.61	0.00	0.00	0.00	0.00	0.01	0.00	6.98	3.32
$\frac{Ab}{Ab + An}$	0.44	0.51	0.49	0.49	0.50	0.45	0.61	0.54	0.43	0.42	0.32	0.36	0.50	0.52	0.54	0.41	0.29	0.52	0.57	0.49	0.55	0.49
$\frac{MgO}{MgO + FeO^T}$	0.32	0.35	0.38	0.36	0.36	0.32	0.36	0.37	0.47	0.52	0.38	0.31	0.27	0.33	0.28	0.29	0.57	0.48	0.26	0.29	0.34	0.30

TABLE 3.6 - Whole-rock trace element analyses of metabasites, Gjörlanger Unit and Basal Gneisses

Unit	Gjörlanger Unit																		Basal Gneisses			
Sample	Dykes						Concordant sheets in gneisses												Boudins and Sheets			
ppm	D46	D80	D81	D82	D83	D134	D1	D38	D77	D95	D101	D102	D103	D104	D105	D108	D123	D129	79/38A	79/38B	D69	D116
Ni	81	68	81	84	69	37	40	96	107	10	43	66	13	62	14	27	222	152	73	115	47	89
Mn	1483	1561	1431	1482	1478	1300	1156	1654	976	832	1498	1802	1251	1538	1136	1508	627	1107	2667	1665	1582	1508
Cr	109	65	71	66	73	24	45	247	423	15	47	135	11	78	20	8	37	366	99	146	255	135
V	244	239	241	245	245	215	190	349	202	56	280	421	159	283	134	324	25	178	286	340	319	307
Nb	4	5	2	1	2	9	12	8	3	2	8	4	10	ND	7	1	6	2	-	-	5	9
Zr	38	86	80	80	83	134	74	71	46	12	51	117	124	100	149	39	22	28	208	208	68	162
Y	30	32	22	29	31	31	98	31	14	4	13	33	31	38	40	22	4	11	51	59	30	32
Ba	24	61	188	222	72	404	309	9	49	114	101	18	284	94	323	137	41	6	423	302	19	198
Sr	976	38	56	47	37	419	181	60	229	478	395	75	522	27	576	226	349	642	142	150	39	158
Rb	ND	3	9	9	1	42	14	ND	14	1	7	1	9	4	12	ND	3	ND	34	21	2	35
Pb	6	8	31	23	16	10	3	9	7	3	7	5	12	6	8	1	9	6	11	7	2	5
K/Rb	-	700	633	677	2800	166	871	-	328	3100	685	200	766	725	808	-	866	-	770	561	350	428
Rb/Sr	0.001	0.079	0.161	0.191	0.027	0.100	0.077	0.008	0.061	0.002	0.018	0.013	0.017	0.148	0.021	0.002	0.009	0.001	0.239	0.140	0.051	0.222
Y/Nb	7.5	6.4	11.0	29.0	15.5	3.4	8.1	3.8	4.6	2.0	1.6	8.2	3.1	-	5.7	22.0	0.6	5.51	-	-	6.0	3.5

TABLE 3.7 - Major element analyses and CIPW norms of websterites, Gjörlanger Unit

Sample	Websterites													Gt-rich veins		
Mass%	79/8	79/18	D13	D14	D22	D25	D27	D28	D40	D45	D66	D94	D124	79/11B	79/11C	D174
SiO_2	49.60	50.81	51.38	50.58	45.52	50.04	52.54	51.32	48.70	46.87	50.86	52.60	52.23	40.85	51.23	46.16
Al_2O_3	3.45	11.81	6.05	6.11	10.25	8.71	4.35	4.37	19.22	10.30	8.96	11.39	4.26	16.32	4.66	24.36
TiO_2	0.42	0.43	0.62	0.65	0.25	0.57	0.46	0.48	0.33	0.29	0.43	0.61	0.39	0.05	0.42	0.26
Fe_2O_3	1.97	1.63	2.22	4.05	3.11	3.43	2.06	2.28	0.28	2.23	1.60	1.37	1.57	2.95	1.41	1.04
FeO	6.82	9.10	9.73	7.28	7.66	6.78	6.99	6.74	6.41	8.14	7.10	11.10	7.73	14.04	2.62	8.37
MgO	18.94	13.05	18.95	18.14	19.14	14.78	18.03	17.91	9.04	17.75	12.95	11.13	18.44	8.59	13.35	5.72
MnO	0.18	0.19	0.20	0.16	0.11	0.15	0.10	0.14	0.08	0.13	0.18	0.17	0.19	0.53	0.06	0.22
CaO	15.34	10.82	8.97	10.66	10.24	12.94	12.81	14.40	13.08	12.57	13.63	8.41	13.25	12.65	18.91	4.22
Na_2O	0.53	1.39	0.75	0.63	0.74	1.48	0.68	0.73	1.52	0.86	2.26	1.99	0.66	1.02	2.78	0.85
K_2O	0.15	0.47	0.14	0.14	0.21	0.17	0.28	0.22	0.16	0.13	0.57	0.33	0.15	0.09	0.06	6.20
P_2O_5	0.04	0.13	0.06	0.06	0.02	0.05	0.09	0.07	0.05	0.03	0.06	0.03	0.02	0.21	0.08	0.07
S	0.10	0.18	0.06	0.07	0.16	ND	0.01	0.03	0.07	0.29	0.16	ND	0.04	0.06	0.05	0.04
H_2O^+	0.93	0.18	0.02	2.91	1.99	0.20	0.70	1.10	0.59	0.17	0.47	0.47	0.41	0.20	0.32	2.07
CO_2	0.83	ND	-	-	-	-	-	-	-	-	-	-	ND	ND	ND	ND
Total	99.30	100.19	99.15	101.44	99.70	99.30	99.10	99.79	99.53	99.76	99.23	99.60	99.34	97.56	95.95	99.58
ap	0.09	0.30	0.14	0.14	0.05	0.12	0.21	0.16	0.12	0.07	0.14	0.07	0.05	0.49	0.18	0.16
py	0.19	0.34	0.11	0.13	0.29	0.00	0.02	0.06	0.13	0.54	0.30	0.00	0.07	0.11	0.09	0.07
il	0.79	0.82	1.18	1.23	0.47	1.08	0.87	0.91	0.63	0.55	0.82	1.16	0.74	0.09	0.80	0.49
or	0.89	2.78	0.83	0.83	1.24	1.00	1.65	1.30	0.95	0.77	3.37	1.95	0.89	0.53	0.35	36.64
ab	4.48	11.76	6.35	5.33	6.26	12.52	5.75	6.18	12.86	7.28	19.12	16.48	5.58	5.84	10.43	7.19
an	6.59	24.59	12.73	13.43	24.03	16.62	7.99	7.99	45.15	23.86	12.62	21.17	8.22	36.69	0.06	20.48
mt	2.86	2.36	3.22	5.87	4.51	4.97	2.99	3.31	0.41	3.23	2.32	1.99	2.27	4.28	2.04	1.51
di) wo	28.92	11.79	13.10	16.31	11.12	19.73	22.37	26.29	8.11	15.99	22.80	8.49	23.96	9.06	38.93	0.00
di) en	21.52	7.63	9.13	12.28	8.22	14.46	16.40	19.52	5.13	11.45	15.74	4.89	17.23	4.29	31.58	0.00
di) fs	4.56	3.35	2.88	2.39	1.83	3.41	3.85	4.22	2.47	3.12	5.21	3.22	4.57	4.64	2.71	0.00
hy) en	12.28	20.47	35.85	32.90	12.76	15.02	27.66	19.59	10.38	7.43	0.81	22.83	25.47	0.00	0.00	2.27
hy) fs	2.60	8.99	11.30	6.41	2.83	3.54	6.49	4.23	5.00	2.02	0.27	15.02	6.75	0.00	0.00	2.33
qz	0.00	0.00	0.00	1.09	0.00	0.00	1.25	0.00	0.00	0.00	0.00	1.32	0.00	0.00	0.00	0.00
ol) fo	9.37	3.08	1.55	0.00	19.23	5.14	0.00	3.85	4.91	17.75	11.00	0.00	2.26	11.98	1.17	8.39
ol) fa	2.19	1.49	0.54	0.00	4.71	1.33	0.00	0.92	2.61	5.32	4.01	0.00	0.66	14.28	0.11	9.09
$\frac{MgO}{MgO + FeO^T}$	0.69	0.55	0.62	0.62	0.65	0.60	0.67	0.67	0.57	0.64	0.60	0.47	0.67	0.34	0.77	0.38

TABLE 3.8 - Whole-rock trace element analyses of westerites, Gjörlanger Unit

Sample	Websterites													Garnetite Veins		
ppm	79/8	79/18	D13	D14	D22	D25	D27	D28	D40	D45	D66	D94	D124	79/11B	79/11C	D174
Ni	340	326	347	301	394	172	301	263	143	405	186	137	361	69	230	72
Mn	1588	1514	-	-	1277	1584	1236	1449	916	-	1419	2001	1504	4209	314	1708
Cr	2135	1338	1381	1298	338	1374	2338	2121	203	490	966	402	1284	293	2077	135
Y	166	175	-	-	105	188	153	153	112	-	152	107	188	37	154	60
Nb	-	-	6	7	4	4	3	2	1	4	2	7	1	-	-	2
Zr	30	66	53	46	29	33	59	44	31	36	85	88	42	1204	77	969
Y	25	47	16	16	7	15	30	27	5	6	43	52	25	40	2	29
Ba	99	127	76	51	64	32	13	103	81	250	218	108	77	142	113	4882
Sr	81	166	81	81	130	90	59	98	340	325	94	217	54	263	144	199
Rb	5	6	3	2	3	ND	ND	ND	3	3	12	7	7	1	ND	123
Pb	15	ND	ND	4	11	10	1	8	3	5	3	17	8	38	20	9

TABLE 3.9 - Major element analyses and CIPW norms of metaperidotites and associated metabasites, Flekke Unit

Sample	Dunites								Chlorite Peridotites							Metabasite Layers							
Mass%	D9	D10	D43	D111*	D128*	D130*	D146	D149	79/34D	D11	D84	DF4	D144	D145	D163	D140A	D140B	D140C	D141A	D141B	D148	D118	D12
SiO_2	35.55	35.21	36.43	38.77	36.98	40.08	31.66	35.35	38.94	44.16	35.98	31.17	44.76	44.68	35.24	39.91	39.63	33.20	50.15	37.26	40.66	38.02	44.60
Al_2O_3	0.82	0.90	0.18	2.29	1.09	2.77	1.47	0.09	2.06	3.33	6.82	1.82	2.21	2.90	0.76	29.71	19.37	16.04	1.09	0.09	17.01	10.00	13.71
TiO_2	0.20	0.92	0.07	0.31	0.08	0.16	1.74	0.04	0.71	0.30	1.24	1.81	0.15	1.35	0.19	0.24	0.22	0.11	0.10	0.05	0.19	5.05	2.13
Fe_2O_3	10.41	6.95	4.24	4.36	6.08	4.62	11.91	10.46	11.31	9.57	10.91	16.13	7.76	5.25	14.81	1.32	1.90	3.08	4.90	2.78	2.07	2.59	3.64
FeO	16.46	23.40	21.84	10.16	18.97	11.11	19.85	17.68	13.34	14.73	14.35	17.84	15.73	18.35	12.63	1.63	16.66	11.64	14.45	25.02	17.77	20.12	14.84
MgO	29.27	30.57	34.73	35.82	33.64	33.17	27.12	33.89	26.66	23.19	23.50	24.50	25.55	24.14	30.35	2.14	7.62	22.39	24.38	33.81	10.13	7.88	4.32
MnO	0.30	0.30	0.30	0.19	0.31	0.21	0.34	0.28	0.28	0.18	0.17	0.33	0.34	0.29	0.35	0.04	0.69	0.12	0.31	0.31	0.52	0.64	0.30
CaO	0.98	0.14	0.39	2.68	0.69	2.74	0.53	0.07	0.17	0.26	0.18	0.58	0.94	0.21	0.09	21.98	12.10	3.48	1.75	0.07	8.88	10.97	9.68
Na_2O	0.02	0.01	0.07	0.07	0.07	0.07	0.08	0.06	0.01	0.03	0.12	0.01	0.16	0.10	0.04	0.32	1.03	0.48	0.07	0.03	1.23	0.94	4.32
K_2O	0.08	0.02	0.01	0.01	0.00	0.00	0.01	0.00	0.01	0.01	0.07	0.01	0.01	0.01	0.00	0.05	0.18	0.06	0.00	0.00	0.16	0.09	0.08
P_2O_5	0.07	0.06	0.07	0.01	0.04	0.02	0.05	0.06	0.09	0.05	0.17	0.04	0.06	0.07	0.06	0.03	0.03	0.06	0.05	0.07	0.10	2.38	1.37
S	0.04	0.04	0.02	0.02	0.01	0.01	0.07	0.00	0.01	0.20	0.02	0.01	0.04	0.29	0.03	0.00	0.00	0.01	0.10	0.01	0.00	0.07	0.02
H_2O^+	5.60	1.84	0.66	2.51	2.66	4.60	4.95	2.90	3.97	2.98	5.99	5.28	2.35	2.66	5.87	3.44	0.73	8.54	2.14	0.71	1.39	1.08	0.05
CO_2	-	-	-	1.31	0.51	0.51	0.34	-	1.52	-	-	-	-	0.45	-	-	-	-	-	-	-	-	-
Total	99.80	100.36	99.01	98.51	101.13	100.07	100.12	100.88	99.08	99.00	99.52	99.53	100.06	100.35	100.42	100.81	100.16	99.21	99.49	100.21	100.11	99.83	99.06
ap	0.16	0.14	0.16	0.02	0.09	0.05	0.12	0.14	0.21	0.12	0.14	0.09	0.14	0.16	0.14	-	0.07	0.14	0.12	0.16	0.23	5.53	3.18
py	0.07	0.07	0.04	0.04	0.02	0.02	0.13	0.00	0.02	0.37	0.04	0.02	0.07	0.54	0.05	-	0.00	0.02	0.19	0.02	0.00	0.13	0.04
il	0.38	1.75	0.13	0.59	0.15	0.30	3.30	0.08	1.35	0.57	2.35	3.44	0.28	2.56	0.36	-	0.42	0.21	0.19	0.09	0.36	9.59	4.04
or	0.47	0.12	0.06	0.06	0.00	0.00	0.06	0.00	0.06	0.06	0.41	0.06	0.05	0.06	0.00	-	1.06	0.35	0.00	0.00	0.95	0.53	0.47
ab	0.17	0.08	0.59	0.59	0.59	0.59	0.68	0.46	0.08	0.25	1.01	0.08	1.35	0.84	0.34	-	0.44	4.06	0.59	0.25	10.29	7.95	29.26
an	1.91	0.30	0.15	5.90	2.66	7.24	2.30	0.00	0.25	0.96	0.50	2.62	4.27	0.58	0.05	-	47.70	16.87	2.66	0.11	40.42	22.80	17.78
C	0.00	0.75	0.00	0.00	0.00	0.00	0.48	0.02	1.94	2.92	6.36	0.83	0.37	2.51	0.67	-	0.00	9.00	0.00	0.08	0.00	0.00	0.00
mt	15.09	10.08	6.15	6.32	8.81	6.69	17.27	15.15	16.40	13.88	15.82	23.39	11.25	7.61	21.47	-	2.75	4.47	7.10	4.03	3.00	3.75	5.28
di Wo	1.04	0.00	0.55	3.06	0.21	2.60	0.00	0.00	0.00	0.00	0.00	0.00	0.00	0.00	0.00	-	5.06	0.00	2.38	0.00	1.24	6.71	8.89
di en	0.74	0.00	0.36	2.35	0.14	1.95	0.00	0.00	0.00	0.00	0.00	0.00	0.00	0.00	0.00	-	2.04	0.00	1.61	0.00	0.56	2.87	3.12
di fs	0.21	0.00	0.15	0.38	0.05	0.38	0.00	0.00	0.00	0.00	0.00	0.00	0.00	0.00	0.00	-	3.08	0.00	0.58	0.00	0.68	3.85	5.99
hy en	18.73	9.97	3.30	10.11	9.04	17.71	12.08	11.99	45.18	57.76	38.51	22.03	47.18	49.46	30.06	-	0.00	5.22	59.11	4.84	0.00	8.74	0.00
hy fs	5.45	4.67	1.39	1.64	3.20	3.49	4.22	3.38	9.50	18.24	10.03	5.93	16.42	21.83	4.21	-	0.00	1.74	21.53	2.50	0.00	11.72	0.00
ol fo	37.44	46.37	58.05	53.78	52.28	44.12	38.88	50.74	14.87	0.00	14.03	27.32	11.53	7.47	31.91	-	11.87	35.42	0.00	55.62	17.29	5.62	5.35
ol fa	12.01	23.91	26.95	9.63	20.39	9.59	14.96	15.75	3.44	0.00	4.03	8.10	4.42	3.63	4.92	-	19.76	13.04	0.00	31.70	23.11	8.31	11.34
Ne	0.00	0.00	0.00	0.00	0.00	0.00	0.00	0.00	0.00	0.00	0.00	0.00	0.00	0.00	0.00	-	4.48	0.00	0.00	0.00	0.06	0.00	3.95
$\frac{MgO}{(MgO + FeO^T)}$	0.53	0.51	0.57	0.72	0.58	0.68	0.47	0.55	0.53	0.50	0.49	0.43	0.53	0.51	0.54	0.43	0.30	0.61	0.56	0.55	0.34	0.26	0.19
$\frac{Ab}{An + Ab}$	-	-	-	-	-	-	-	-	-	-	-	-	-	-	-	-	-	-	-	-	0.20	0.26	0.62
$\frac{Fe_2O_3}{(Fe_2O_3+FeO)}$	0.39	0.23	0.16	0.30	0.24	0.29	0.38	0.37	0.46	0.39	0.43	0.47	0.33	0.22	0.54	-	-	-	-	-	0.10	0.11	0.20
$\frac{Mgo}{(MgO + FeO)}$	0.64	0.57	0.61	0.78	0.64	0.75	0.58	0.66	0.67	0.61	0.62	0.58	0.62	0.57	0.71	-	-	-	-	-	0.36	0.28	0.23

* from structurally below the anorthositic troctolites

TABLE 3.10 - Whole-rock trace element analyses of metaperidotites and associated metabasites, Flekke Unit

Sample	Dunites								Chlorite Peridotites							Metabasites							
ppm	D9	D10	D43	D111	D128	D130	D146	D149	79/340	D11	D84	DF4	D144	D145	D163	D140A	D140B	D140C	D141A	D141B	D148	D118	D12
Ni	662	580	788	1643	738	1463	588	714	691	653	471	608	565	539	672	25	111	307	652	738	168	25	14
Mn	2804	2855	2676	1593	2459	1692	2622	2225	2139	1458	1825	2631	2746	2363	2841	373	5200	973	2577	2500	4072	4176	2468
Cr	72	513	261	555	260	464	1642	63	1258	491	992	4083	166	1250	56	5	4	37	85	34	26	ND	10
V	28	191	19	85	24	67	416	17	125	87	389	538	47	363	21	17	13	20	24	9	16	33	21
Nb	2	ND	ND	2	ND	ND	3	1	ND	4	ND	1	ND	3	ND	6	3	ND	ND	ND	2	31	45
Zr	21	24	13	17	14	17	16	17	8	19	20	20	11	26	92	ND	20	17	19	17	50	1345	10559
Y	2	ND	1	2	ND	8	ND	4	7	3	ND	2	2	3	1	ND	6	8	ND	ND	9	281	236
Ba	26	22	ND	ND	9	19	15	ND	62	6	ND	ND	17	9	6	38	42	14	ND	14	10	3	35
Sr	11	3	25	10	3	9	ND	1	4	1	2	ND	8	ND	2	10085	516	22	ND	3	90	272	268
Rb	1	1	2	2	4	ND	2	3	ND	ND	2	6	1	2	ND	4	5	ND	1	3	3	6	2
Pb	3	ND	4	8	5	6	ND	ND	ND	5	4	2	5	3	4	32	6	5	2	5	4	10	13

TABLE 3.11 - Average compositions for peridotite types from the Scandinavian Caledonides after Qvale & Stigh (in press) and Carswell et al. (in preparation)

Type	Qvale & Stigh (in press)			Carswell et al.	
Mass%	1	4a	4b	Eik	Kal
SiO_2	43.95	40.27	42.66	40.28	44.94
TiO_2	0.77	0.23	0.36	0.83	0.36
Al_2O_3	7.88	1.12	10.08	7.78	6.76
Cr_2O_3	0.20	0.38	0.27	0.03	0.29
Fe_2O_3	3.77	3.87	4.02	6.42	2.61
FeO	8.36	4.59	6.92	16.81	8.84
MnO	0.19	0.12	0.19	0.34	0.16
NiO	0.10	0.31	0.11	0.08	0.17
MgO	22.92	37.77	23.36	22.58	27.04
CaO	7.37	1.05	7.06	3.54	6.52
Na_2O	0.73	0.19	0.60	0.12	0.70
K_2O	0.23	0.07	0.05	0.01	0.04
P_2O_5	-	-	-	0.11	0.02
Loss	2.89	9.11	5.19	1.31	1.12
Total	100.46	99.08	100.87	100.26	99.63
$\frac{MgO}{MgO + FeO}$	0.71	0.89	0.77	0.57	0.75

Features:

1. Layers and lenses within basic intrusions of Caledonian or Precambrian age. Usually cumulates highly variable composition with high Si, Al, Ti, Ca and alkalis, low Mg, Cr and Ni.

4a Low-Al "alpine type", usually massive meta harzburgites in Caledonian or Precambrian supracrustals. Al_2O_3 3-8%, low CaO and alkalis, high Mn, Cr and MgO/MgO + FeO, MnO 0-12%. Depleted upper mantle?

4b High-Al "alpine type" layered, associated with ortho- or paragneisses metabasites and (in the BGR) anorthosites. Higher CaO, TiO_2 and alkalis and lower MgO (MgO + FeO than 4a. Lower oceanic crust(?) or related to anorthosites?

EiK Average of 9 garnet peridotites, Eiksundal Complex (Fe-Ti type).

Kal Average of 16 garnet peridotites, Kalskaret (Mg-Cr type).

TABLE 3.12 - Whole-rock major element analyses and CIPW norms of unfoliated meta-anorthositic troctolites and related rocks, Flekke Unit

Locality			Gjörlanger				Hellevik					Sördal							Instetj		Flekke		
Sample	Igneous		Coronitic or pseudomorphic												Fe-Ti ore rich				coronitic/pseudomorphic				
Mass%	D96	D143	D35	D36	D49	D86	D37A	D37B	D131	D132	D133	D39	D156	D42	79/41A	79/41B	79/41C	D155	D127	D142	D5	D6	D7
SiO_2	47.66	47.78	42.77	47.97	47.74	46.39	48.68	46.92	47.14	47.22	46.21	46.83	42.60	42.68	1.68	36.38	30.81	33.76	46.06	46.57	48.20	45.23	44.18
Al_2O_3	21.05	21.16	18.72	21.14	15.60	20.88	15.65	20.37	20.43	20.77	20.26	19.46	18.21	18.01	6.58	20.79	18.21	14.47	19.06	20.62	24.45	18.47	19.58
TiO_2	0.16	0.08	0.85	0.74	1.76	0.76	0.25	0.69	0.81	0.82	0.25	0.74	2.56	2.48	15.74	1.90	5.37	3.32	0.10	0.08	0.19	0.14	0.37
Fe_2O_3	0.97	0.62	0.97	1.07	ND	0.66	2.29	1.40	1.95	0.92	1.90	1.49	1.62	1.92	40.55	2.30	9.23	19.46	1.81	1.39	0.71	2.52	2.53
FeO	7.45	6.96	18.70	9.36	11.65	9.54	9.12	9.35	8.69	10.44	10.65	9.37	15.52	14.04	30.73	25.50	24.89	11.06	8.40	8.84	4.54	8.33	10.34
MgO	9.23	11.06	6.57	5.56	7.81	7.18	12.40	8.02	8.64	8.18	8.45	8.72	6.84	8.85	4.54	3.05	3.31	9.58	11.56	10.22	5.64	12.66	10.39
MnO	0.04	0.09	0.33	0.97	0.13	0.10	0.13	0.11	0.12	0.13	0.17	0.10	0.18	0.14	0.27	0.56	0.47	0.47	0.12	0.13	0.03	0.11	0.10
CaO	9.18	9.61	9.06	8.97	10.93	8.60	7.85	8.77	8.91	8.84	9.46	9.29	8.90	7.41	0.06	11.06	8.94	7.06	8.59	7.68	9.40	7.84	8.06
Na_2O	3.22	2.72	2.00	5.40	4.15	4.90	2.66	3.27	3.20	2.93	2.90	2.89	2.81	3.96	0.01	0.01	0.10	0.97	2.64	2.88	4.98	3.15	3.19
K_2O	0.21	0.12	0.04	0.14	0.12	0.23	0.18	0.20	0.14	0.25	0.04	0.20	0.15	0.40	0.01	0.01	0.02	0.16	0.15	0.19	0.19	0.34	0.22
P_2O_5	0.06	0.05	0.14	0.08	0.04	0.07	0.04	0.04	0.08	0.14	0.12	0.07	0.22	0.07	0.06	0.25	0.06	0.31	0.02	0.04	0.04	0.04	0.06
S	0.01	0.01	ND	0.01	0.16	0.07	0.01	0.04	0.02	0.07	0.03	0.01	0.08	0.07	ND	ND	ND	0.06	0.01	0.01	0.02	0.02	0.02
H_2O^+	0.76	0.45	0.18	0.35	0.44	0.55	1.06	0.40	0.53	0.29	0.25	1.16	0.72	0.61	0.07	0.03	0.29	0.73	0.83	1.42	1.00	0.55	0.45
Total	100.00	100.71	100.33	101.76	100.53	99.93	100.32	99.88	100.66	101.00	100.69	100.33	100.41	100.66	100.60	101.84	101.70	101.41	99.35	100.07	99.39	99.40	99.49
ap	0.14	0.12	0.33	0.19	0.09	0.16	0.09	0.09	0.19	0.33	0.28	0.16	0.51	0.16	-	0.58	0.14	0.72	0.05	0.09	0.09	0.09	0.14
py	0.02	0.99	0.00	0.02	0.30	0.13	0.02	0.08	0.04	0.13	0.06	0.02	0.15	0.13									
il	0.03	0.15	1.61	1.41	3.34	1.44	0.48	1.31	1.54	1.56	0.48	1.41	4.86	4.71									
or	1.24	0.71	0.24	0.83	0.71	1.36	1.06	1.18	0.83	1.48	0.24	1.18	0.89	2.36									
ab	24.45	23.02	16.86	25.26	20.18	21.24	22.51	26.41	27.08	24.79	23.23	24.46	18.55	15.95									
an	42.37	45.18	41.99	33.03	23.59	34.30	30.23	40.32	40.97	42.79	42.15	39.54	36.63	30.19									
C	0.00	0.00	0.00	0.00	0.00	0.00	0.00	0.00	0.00	0.00	0.00	0.00	0.00	0.00									
Mt	1.41	0.90	1.41	1.55	0.00	0.96	3.32	2.03	2.83	1.33	2.76	2.16	2.35	2.78									
di wo	1.16	0.91	0.86	4.57	12.69	3.30	3.53	1.23	1.13	0.07	1.67	2.55	2.54	2.55									
di en	0.71	0.59	0.30	2.16	6.41	1.72	2.25	0.68	0.67	0.04	0.88	1.45	1.09	1.31									
di fs	0.39	0.26	0.58	2.35	5.98	1.50	1.05	0.50	0.40	0.03	0.74	0.98	1.46	1.18									
hy en	0.00	0.70	0.00	0.00	0.00	0.00	10.34	0.00	0.05	1.51	0.00	0.76	0.00	0.00									
hy fs	0.00	0.31	0.00	0.00	0.00	0.00	4.83	0.00	0.03	1.26	0.00	0.52	0.00	0.00									
ol fo	15.61	18.41	11.26	8.19	9.14	11.33	12.82	13.52	14.58	13.19	14.13	13.67	11.18	14.53									
ol fa	9.43	8.92	24.37	9.82	9.40	10.87	6.60	11.04	9.68	12.07	12.96	10.22	16.46	14.50									
ne	0.98	0.00	0.04	11.07	8.09	10.96	0.00	0.68	0.00	0.00	0.71	0.00	2.84	9.51									
$\frac{MgO}{MgO + FeO^T}$	0.52	0.59	0.25	0.35	0.40	0.41	0.52	0.43	0.45	0.42	0.40	0.45	0.29	0.36									
$\frac{ab}{ab + an}$	0.37	0.34	0.28	0.43	0.46	0.38	0.43	0.39	0.40	0.37	0.35	0.38	0.34	0.34									

TABLE 3.13 - Whole-rock trace element analyses of unfoliated meta-anorthositic troctolites and related rocks

Locality			Gjörlanger				Hellevik					Särdal						Instetj	Flekke			
Sample	Igneous		Coronitic or pseudomorphic												Fe-Ti ore-rich				coronitic/pseudomorphic				
ppm	D96	D143	D35	D36	D49	D86	D37A	D37B	D131	D132	D133	D39	D156	D42	79/41A	79/41B	79/41C	D155	D127	D142	D5	D6	D7
Ni	221	252	14	97	120	107	258	136	142	143	84	157	107	182	413	20	93	249	256	252	113	267	213
Mn	798	777	3265	904	1255	877	1080	995	928	1038	1297	956	1395	1106	1928	4040	3435	3563	67	1105	549	980	1211
Cr	32	24	5	193	341	267	82	361	437	447	47	549	203	344	5731	480	1506	1093	39	5	16	42	308
V	22	14	99	155	449	125	72	152	191	180	60	149	394	505	4335	393	1310	848	25	7	15	22	72
Nb	ND	2	ND	ND	ND	3	ND	1	3	ND	ND	6	7	6	ND	8	2	4	ND	2	2	2	ND
Zr	18	15	45	25	32	20	17	21	23	17	20	17	52	31	44	28	26	24	15	13	18	20	22
Y	ND	3	51	8	16	3	5	5	6	3	2	8	1	8	ND	11	1	12	1	ND	5	3	6
Ba	77	52	23	67	88	139	53	77	60	71	ND	121	54	44	ND	ND	4	33	41	48	264	59	90
Sr	272	252	39	487	78	349	86	54	40	30	64	293	91	87	ND	13	ND	121	55	165	1074	119	307
Rb	3	1	ND	ND	ND	ND	2	ND	2	ND	ND	3	6	ND	13	1	6	3	1	8	ND	1	ND
Pb	2	2	6	11	ND	7	ND	7	ND	9	8	4	3	1	4	4	5	13	3	5	1	4	ND

TABLE 3.14 - Whole-rock major element analyses and CIPW norms of foliated metabasites, metadolerites and metadiorites, Flekke Unit

Locality	Gjörlangerfjord							Saurd'fj		Fl'fj	Upper border			Straums		Klibbern	
Sample	79/34a																
Mass%	(1)	px	AMPH	D206	D32	D33	D62	D90	D91	D119	D37	D41	D60	79/26	D57	D68	D71
SiO_2	45.08	45.41	44.75	42.69	46.97	51.38	50.40	49.09	49.51	49.25	50.01	45.10	49.93	49.58	51.90	60.81	56.29
Al_2O_3	14.72	14.51	15.04	14.11	18.88	18.14	24.78	16.14	16.52	24.41	19.81	14.23	16.94	15.51	17.40	18.56	15.13
TiO_2	2.75	3.15	2.74	3.70	0.60	0.37	0.11	0.44	0.42	0.18	0.91	1.67	0.76	2.18	0.76	0.60	0.70
Fe_2O_3	3.26	3.40	3.74	2.67	1.44	1.64	0.98	2.66	1.69	1.20	1.44	2.47	0.85	2.92	1.34	1.71	1.75
FeO	13.70	12.78	13.69	17.56	8.13	5.36	3.13	4.66	4.83	4.38	7.12	13.88	8.79	9.12	6.28	2.84	5.25
MgO	7.65	7.79	8.16	8.06	8.70	8.93	4.49	9.36	9.25	5.43	6.01	9.79	7.91	5.29	6.74	1.99	3.99
MnO	0.20	0.19	0.19	0.22	0.07	0.10	0.01	0.06	0.06	0.06	0.12	0.22	0.12	0.45	0.06	0.06	0.07
CaO	9.93	10.24	9.87	9.29	9.96	9.55	10.31	13.82	14.26	10.92	10.55	8.59	9.73	8.84	8.99	6.05	6.65
Na_2O	2.48	2.70	2.12	1.12	3.04	3.78	3.33	2.11	1.98	3.17	2.73	2.05	3.40	3.20	3.36	5.35	5.47
K_2O	0.15	0.02	0.03	0.03	0.42	0.38	0.40	0.15	0.09	0.23	0.43	0.52	0.57	0.66	1.58	0.50	0.26
P_2O_5	0.04	0.06	0.15	0.05	0.20	0.02	0.03	0.05	0.04	0.12	0.10	0.25	0.09	0.60	0.52	0.21	0.31
S	0.04	ND	ND	0.06	0.05	0.03	0.04	0.05	0.03	0.01	0.02	0.07	0.06	0.28	0.14	0.03	0.91
H_2O^+	0.22	0.54	0.63	0.91	1.09	0.94	1.44	0.97	0.60	1.60	1.37	0.81	0.54	0.89	1.10	0.80	ND
Total	100.22	100.79	100.11	100.47	99.55	100.62	99.65	99.56	99.28	100.96	100.62	99.65	99.69	99.52	100.17	99.51	99.78
ap	0.09	0.14	0.35	0.12	0.47	0.05	0.07	0.12	0.09	0.28	0.23	0.58	0.21	1.39	1.21	0.49	0.72
py	0.08	0.00	0.00	0.11	0.09	0.0[illegible]	0.02	0.09	0.06	0.0[illegible]	0.04	0.13	0.11	0.52	0.26	0.06	1.70
il	5.22	5.98	5.20	7.03	1.14	0.7[illegible]	0.21	0.84	0.80	0.34	1.73	3.17	1.44	4.14	1.44	1.14	1.33
or	0.89	0.12	0.18	0.18	2.48	2.25	2.36	0.89	0.53	1.36	2.54	3.07	3.37	3.90	9.34	2.96	1.54
ab	20.99	22.85	17.94	9.48	23.05	31.99	28.13	17.86	16.76	26.83	23.10	17.35	28.77	27.08	20.43	45.27	46.29
an	28.59	27.42	31.44	33.39	36.63	31.41	50.95	41.13	35.93	51.70	40.53	28.09	29.28	26.01	27.73	25.15	24.15
C	0.00	0.00	0.00	0.00	0.00	0.00	0.20	0.00	0.00	0.00	0.00	0.00	0.00	0.00	0.00	0.00	0.00
mt	4.73	4.93	5.42	3.87	2.09	2.38	1.42	3.85	2.45	1.74	2.09	3.58	1.23	4.23	1.94	2.48	2.54
di wo	8.52	9.60	6.91	5.17	4.79	6.61	0.00	14.24	14.43	0.71	4.66	5.38	7.68	5.82	5.63	1.46	2.84
di en	4.30	5.17	3.61	2.35	2.87	4.51	0.00	10.43	10.21	0.44	2.64	2.84	4.30	3.17	3.47	0.89	1.76
di fs	4.03	4.12	3.11	2.78	1.67	1.59	0.00	2.47	2.98	0.22	1.82	2.39	3.07	2.44	1.83	0.49	0.92
hy en	2.64	2.10	6.64	10.89	0.00	2.12	7.80	6.27	6.86	3.56	9.92	5.90	0.57	10.01	6.95	4.07	8.18
hy fs	2.47	1.67	5.72	12.92	0.00	0.74	3.26	1.49	2.00	1.77	6.85	4.97	0.41	7.72	3.68	2.26	4.25
ol fo	8.49	8.50	7.06	4.79	13.18	10.94	2.37	4.64	4.18	6.67	1.69	10.97	10.39	0.00	4.46 qz	11.93	3.27
ol fa	8.76	7.47	6.71	6.26	8.47	4.24	1.09	1.21	1.34	3.66	1.29	10.18	8.17	0.00	2.60		
ne	0.00	0.00	0.00	0.00	1.45	0.00	0.00	0.00	0.00	0.00	0.00	0.00	0.00	0.00	0.00	0.00	0.00
$\frac{MgO}{MgO + FeO^T}$	0.32	0.33	0.32	0.29	0.48	0.57	0.53	0.57	0.59	0.49	0.42	0.38	0.45	0.31	0.47	0.31	0.37
$\frac{ab}{ab + an}$	0.42	0.50	0.36	0.22	0.39	0.50	0.36	0.34	0.32	0.34	0.36	0.38	0.49	0.51	0.42	0.64	0.66

TABLE 3.15 - Whole-rock trace element analyses of foliated metabasites, metadolerites and metadiorites, Flekke Unit

Locality	Gjörlanger Fjord							Saurd'fj		Fl'fj	Upper Border			Straumsnes		Klibbern	
Sample	79/34A																
ppm	(i)	px	AMPH	D206	D32	D33	D62	D90	D91	D119	D37	D41	D60	79/26	D57	D68	D71
Ni	158	120	156	179	156	170	117	157	146	135	104	45	138	70	112	24	48
Mn	1505	1372	1441	1674	960	926	397	883	785	545	1041	1866	1234	1458	942	461	834
Cr	51	66	57	148	108	167	26	1731	1708	34	228	53	148	156	298	9	81
V	772	728	652	945	122	116	19	165	161	27	160	388	210	239	95	71	131
Nb	ND	8	2	2	1	2	3	1	ND	2	1	5	5	-	4	2	5
Zr	16	30	30	30	27	30	19	26	24	16	62	62	70	215	53	114	79
Y	14	9	17	8	12	7	4	8	14	6	19	27	24	51	15	12	17
Ba	48	54	38	32	215	62	102	ND	36	84	138	146	142	456	1247	311	210
Sr	11	9	8	10	439	434	651	213	229	344	317	133	127	507	2090	893	586
Rb	ND	6	5	10	ND	3	9	1	ND	ND	14	16	18	2	23	ND	4
Pb	ND	15	12	18	9	4	6	4	7	3	8	7	7	12	16	7	7

TABLE 3.16 - EMP analyses of cumulate olivine and plagioclase, anorthositic troctolite D170

	Olivine		Plagioclase	
SiO_2	37.65	37.67	52.68	53.17
Al_2O_3	-	-	29.77	29.64
FeO^T	28.19	26.62	0.02	0.03
MgO	34.59	35.37	-	-
MnO	0.36	0.28	-	-
NiO	0.09	0.08	-	-
CaO	0.01	ND	12.67	12.37
Na_2O	-	-	4.37	4.44
K_2O	-	-	0.17	0.16
Total	100.91		99.70	99.81
Si	0.9984	1.0004	2.3953	2.4111
Al	-	-	1.5954	1.5839
Fe	0.6250	0.5912	0.0006	0.0011
Mg	1.3676	1.4005	-	-
Mn	0.0080	0.0063	-	-
Ni	0.0019	0.0016	-	-
Ca	0.0004	0.0000	0.6172	0.6010
Na	-	-	0.3868	0.3903
K	-	-	0.0098	0.0090
Total	3.0016	3.0000	5.0051	4.9964
O	4	4	8	8

FIGURES AND TABLES

CHAPTER 4

FIGURE 4.01 Compositions of clinopyroxenes in eclogites plotted on the jadeite-augite-acmite diagram of Essene and Fyfe (1967).

Symbols:-
Stars - garnet amphibolite band in eclogite (D206).
Triangles - Kyanite eclogite (D77)
Circles - eclogite band in websterite (79/9a)
Squares - bimineralic eclogite (D205)
Inverted triangles - phengite eclogite with siliceous backveins (D181)
Diamonds - eclogites in Basal Gneisses (79/38b, D116, D69).

Filled symbols = inclusions in garnets
Open symbols = matrix omphacites
Half-filled symbols = symplectic pyroxenes

Figure 4.01

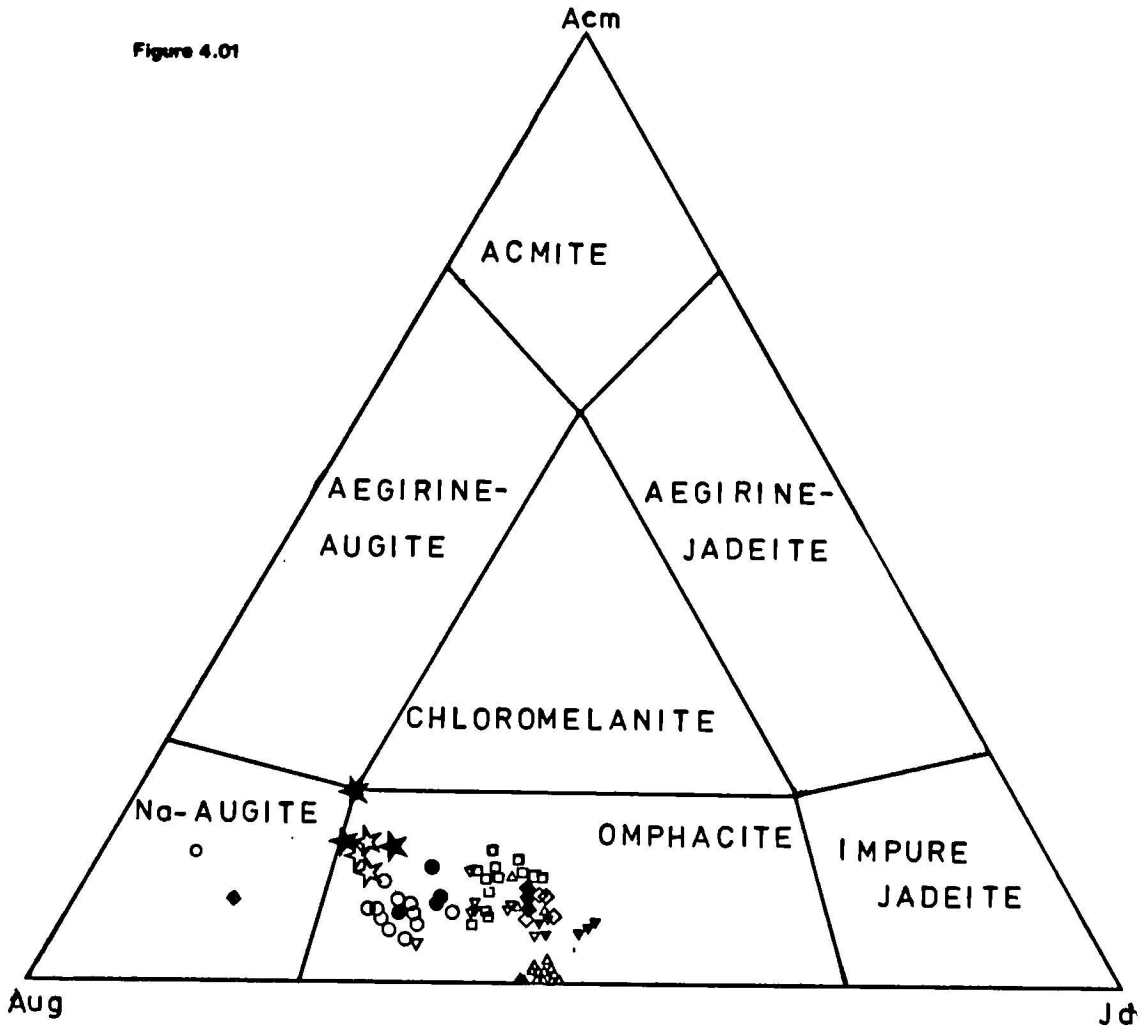
Acm
ACMITE
AEGIRINE-
AUGITE
AEGIRINE-
JADEITE
CHLOROMELANITE
Na-AUGITE
OMPHACITE
IMPURE
JADEITE
Aug
Jd

FIGURE 4.02 Classification of amphiboles in eclogites after Leak (1978), with Fe^{3+} calculated by method of Robinson et al. (1981).

Symbols:-
Circles - kyanite eclogite (D123)
Triangles - bimineralic eclogite (D205)
Inverted triangles - amphibolite band in eclogite (D206)
Diamonds - stage IV amphiboles in other eclogites (79/9a, 79/38b, D116).

Open symbols = matrix amphiboles
Filled symbols = inclusions in garnets

FIGURE 4·02

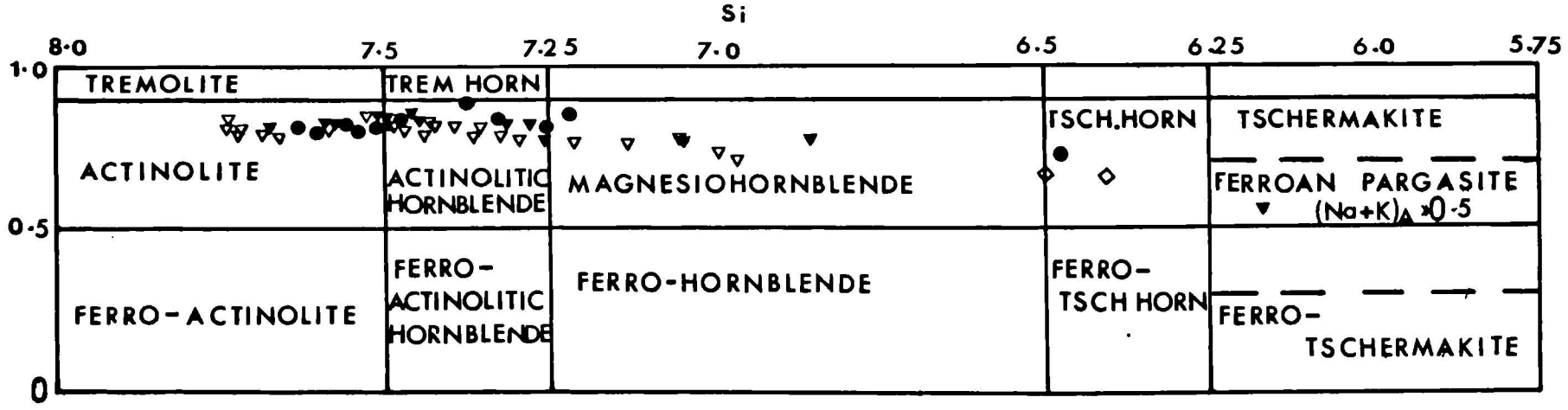

Calcic Amphiboles $(Na+K)_A < 0.5$, $Ti < 0.5$, $(Ca+Na)_B > 1.34$, $Na_B < 0.67$

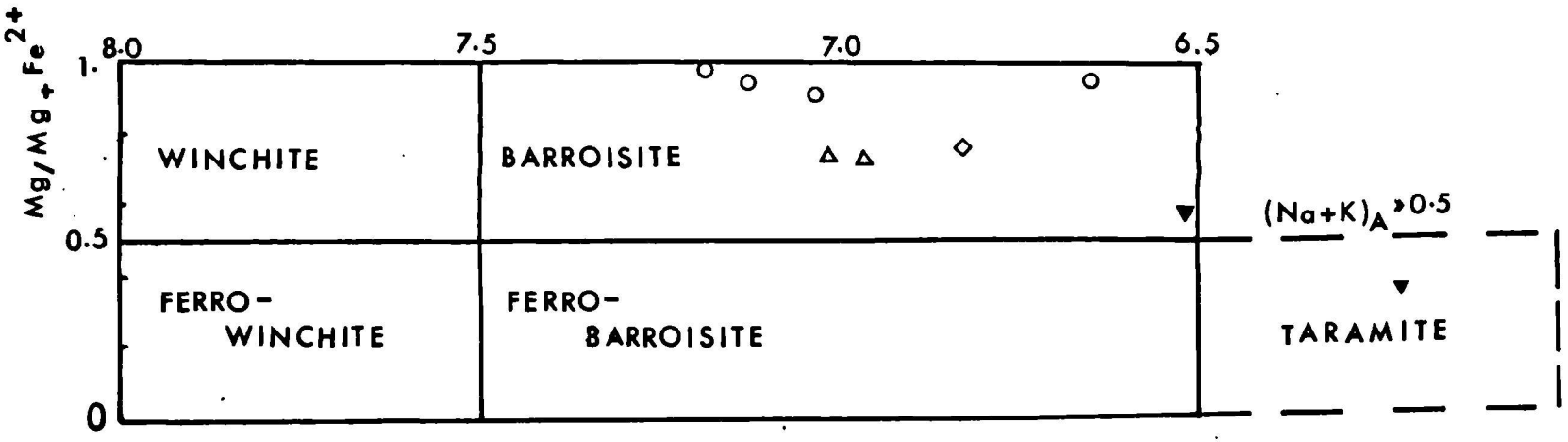

Sodic Calcic amphiboles $(Ca+Na)_B > 1.34$, $.67 < Na_B < 1.34$, $(Na+K) < .5$

FIGURE 4.04 Variation diagrams showing compositions of amphiboles in kyanite eclogite D123. Filled circles are inclusions, open circles are matrix amphiboles. Squares show end-member compositions.

Abbreviations:-
RICH - richterite
EDEN - edenite
NYBO - nyböite
TARA - taramite
TREM - tremolite
HBLD - hornblende
WINCH - winchite
ECKE - eckermanite
KATO - katophorite
PARG - pargasite
GLAUC - glaucophane
BARR - barroisite
TSCH - tschermakite

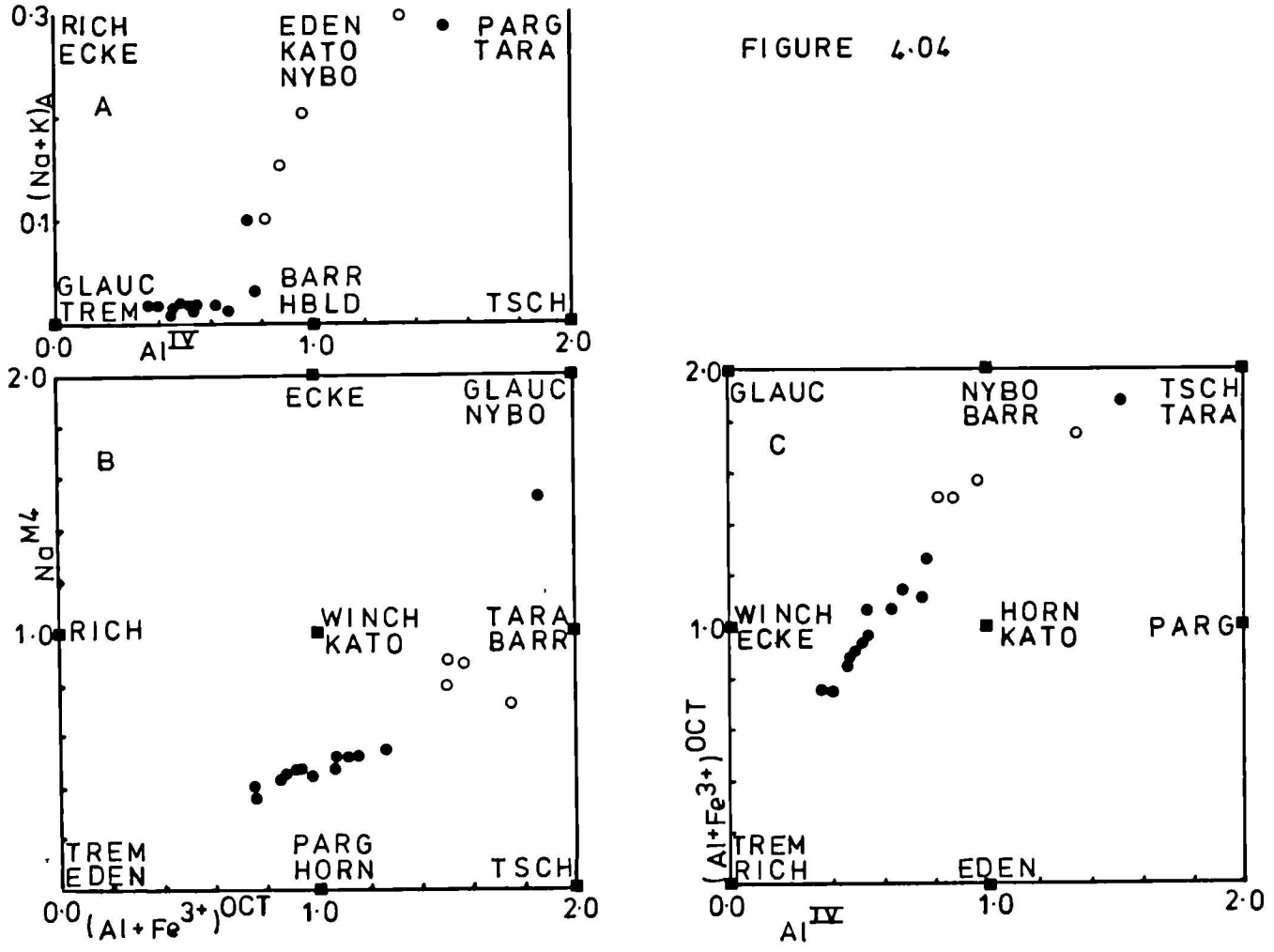
0·3
0·1
(Na+K)A
RICH
ECKE
EDEN
KATO
NYBO
PARG
TARA
A
GLAUC
TREM
BARR
HBLD
TSCH
0·0
AlIV
1·0
2·0
2·0
NaM4
1·0
B
ECKE
GLAUC
NYBO
RICH
WINCH
KATO
TARA
BARR
TREM
EDEN
PARG
HORN
TSCH
0·0
(Al+Fe3+)OCT
1·0
2·0
2·0
1·0
(Al+Fe3+)OCT
C
GLAUC
NYBO
BARR
TSCH
TARA
WINCH
ECKE
HORN
KATO
PARG
TREM
RICH
EDEN
0·0
AlIV
1·0
2·0

FIGURE 4.04

FIGURE 4.05 Garnet in amphibolite band in eclogite from a roadcut between Gjörlanger and Solvik (specimen D206). This is reproduced as a line drawing in figure 4.12. H = Al-rich hornblendic or taramitic amphiboles, A = Si-rich actinolitic amphiboles, C = clinopyroxenes.

4·05

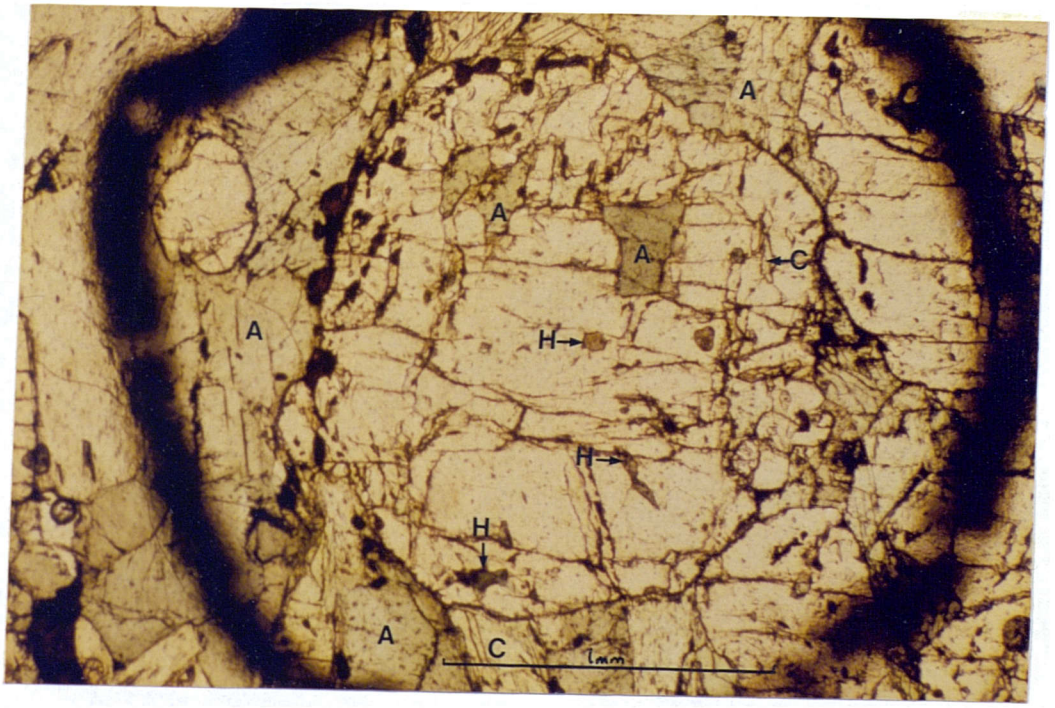

FIGURE 4.06 Variation diagrams showing compositions of amphiboles in bimineralic eclogite D205 (triangles) and interbanded garnet amphibolite D206 (circles). Open symbols are matrix amphiboles, half-filled symbols are pale-coloured amphibole inclusions in garnets and filled symbols are dark amphibole inclusions in garnets. Abbreviations as for figure 4.05.

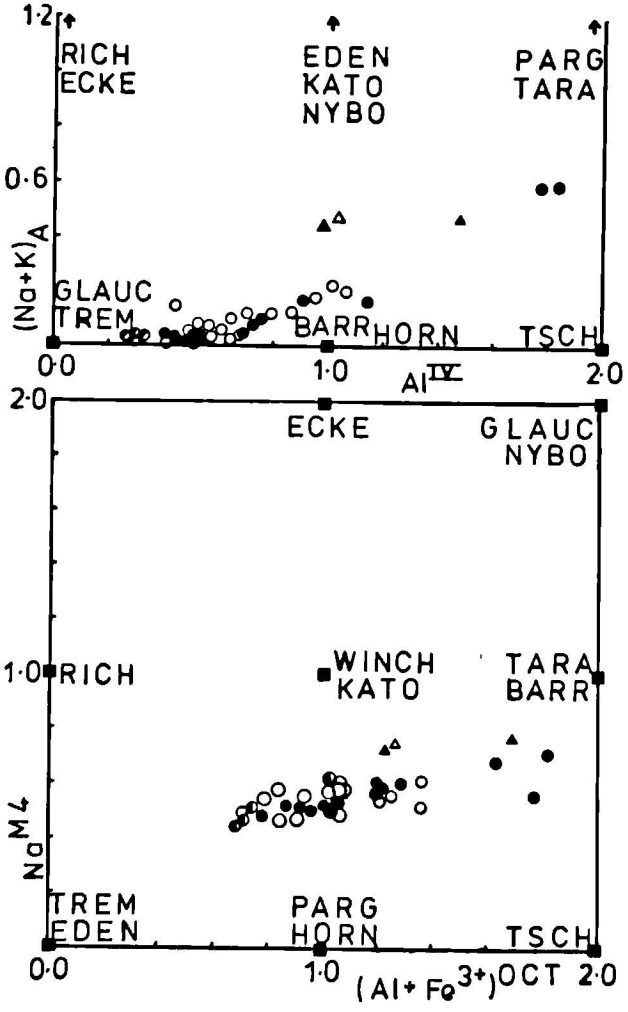
RICH
ECKE
EDEN
KATO
NYBO
PARG
TARA
GLAUC
TREM
BARR
HORN
TSCH
1·2
0·6
0·0
1·0
2·0
(Na+K)A
AlIV
ECKE
GLAUC
NYBO
RICH
WINCH
KATO
TARA
BARR
TREM
EDEN
PARG
HORN
TSCH
2·0
1·0
0·0
NaM4
(Al+Fe3+)OCT

FIGURE 4.06

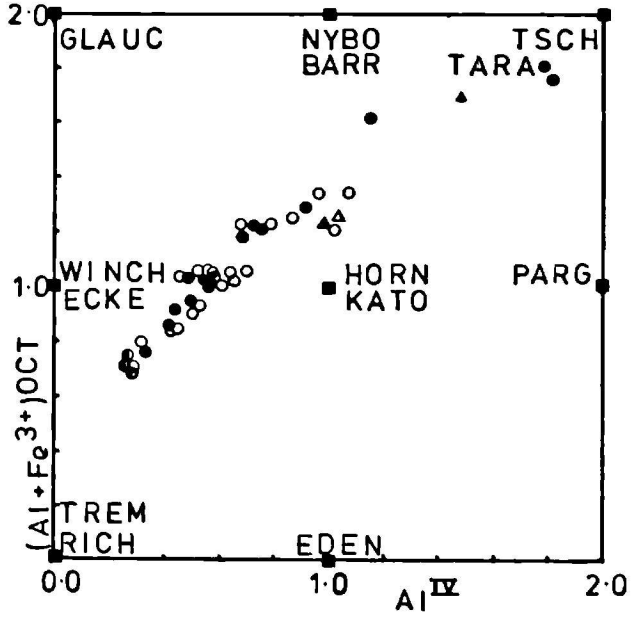
GLAUC
NYBO
BARR
TSCH
TARA
WINCH
ECKE
HORN
KATO
PARG
TREM
RICH
EDEN
2·0
1·0
0·0
(Al+Fe3+)OCT
AlIV

FIGURE 4.07 Compositions of phengites in part of the triangular diagram (8-Si)-Fe^{T}-Mg. Triangles are kyanite eclogites, inverted triangles are phengites from siliceous backveins in the eclogite near Asnes, squares are psammitic gneiss phengites, cross is low-K gneiss D24 and diamonds are phengites from Basal Gneiss eclogites. Filled symbols are core compositions. Open symbols are rims and half-filled symbols secondary phengites.

FIGURE 4.07

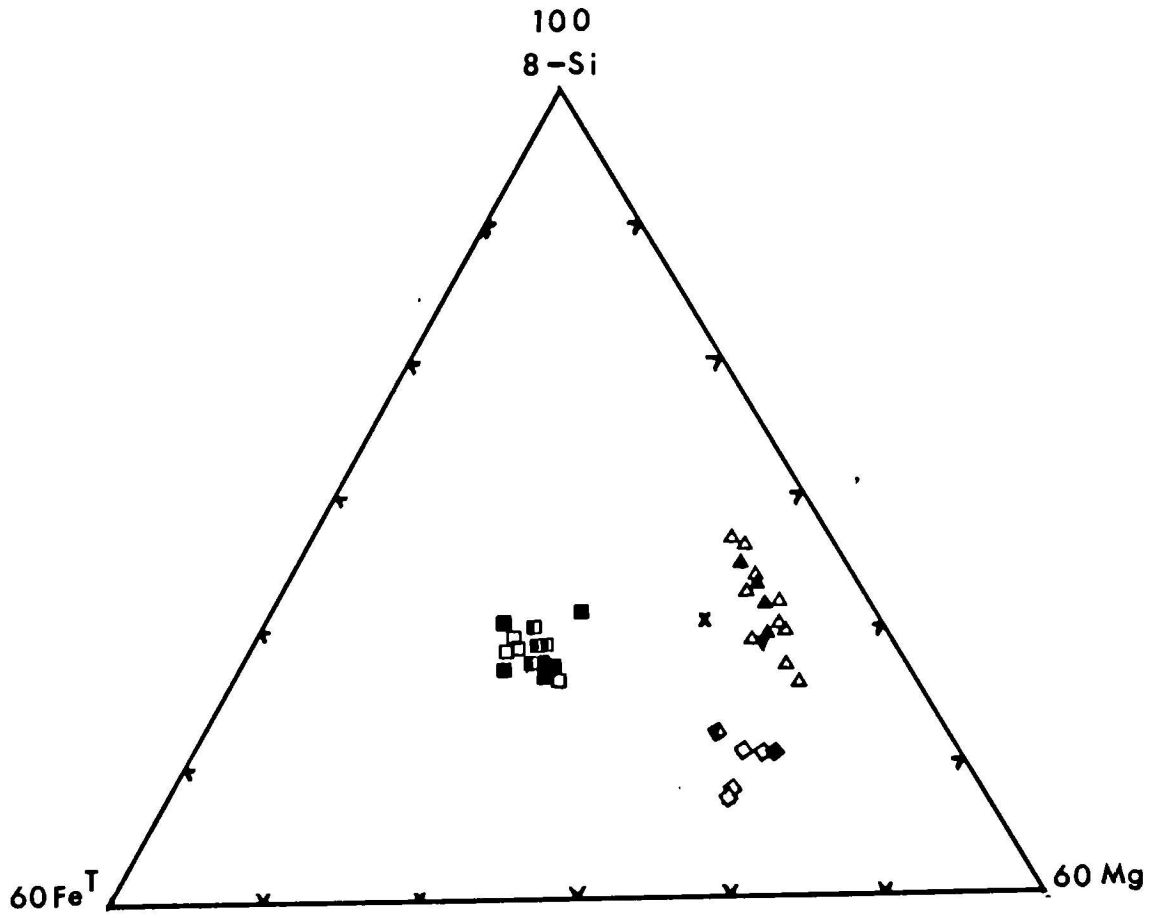

FIGURE 4.09 Compositions of garnets plotted on the diagram of Coleman et al (1965). Straight dashed lines separate fields for "Type B" and "Type C" eclogites of Coleman et al (op cit) and enclosed field is that of garnets in blueschist-eclogites from California.

A. Bimineralic eclogite (D205, 79/34a).
B. Garnet amphibolite band (D206).
C. Kyanite eclogites (D77, triangles; D123, circles).
D. Veined phengite eclogite (D181, squares) and eclogite band in websterite (79/9a, diamonds).
E. Eclogites from the Basal Gneisses (79/38b, circles; D116, diamonds).

Filled symbols - cores
Half-filled symbols - intermediate
Open symbols - rims

Figure 4.09
(final continuation)

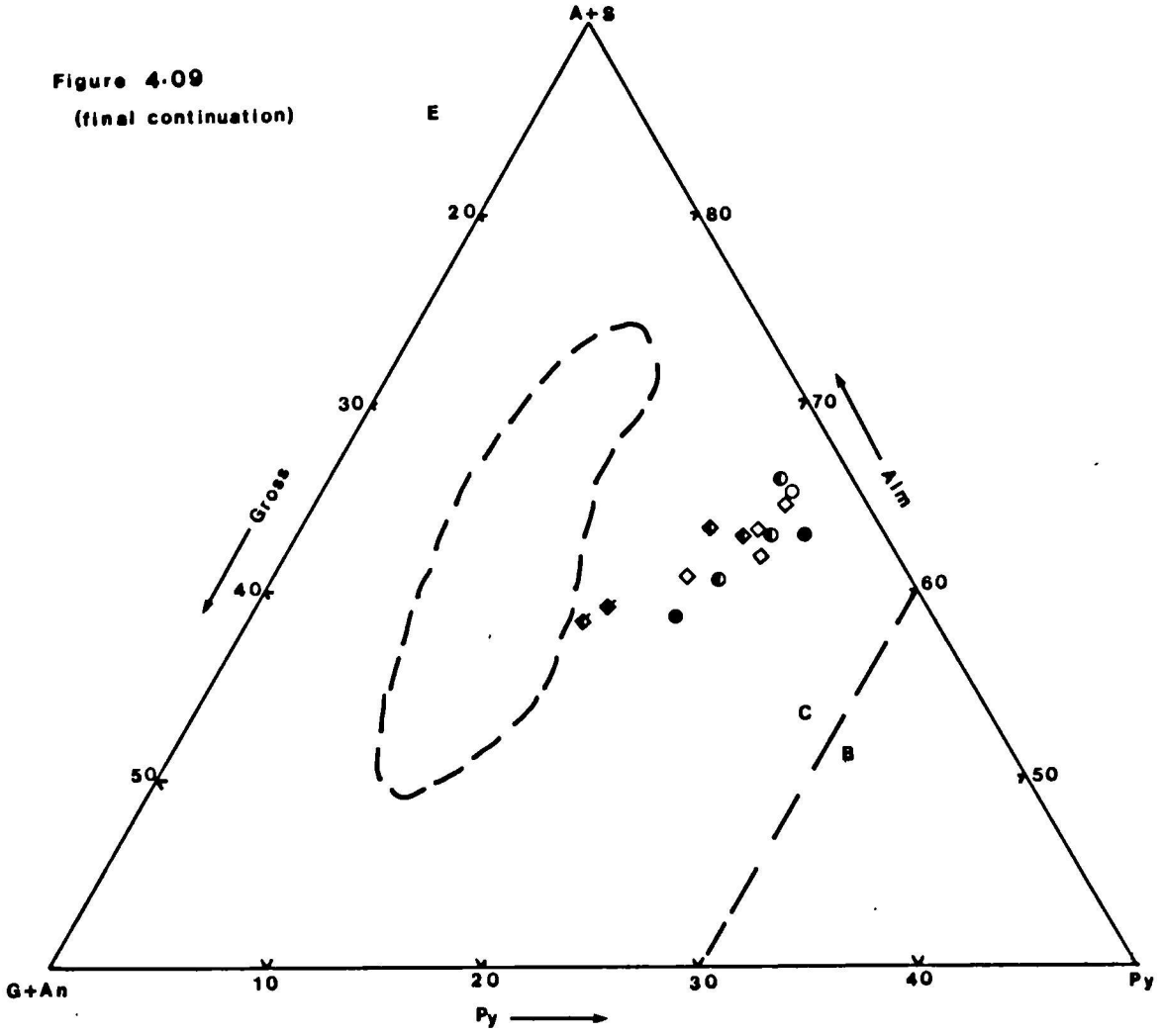

Figure 4·09
(contd)

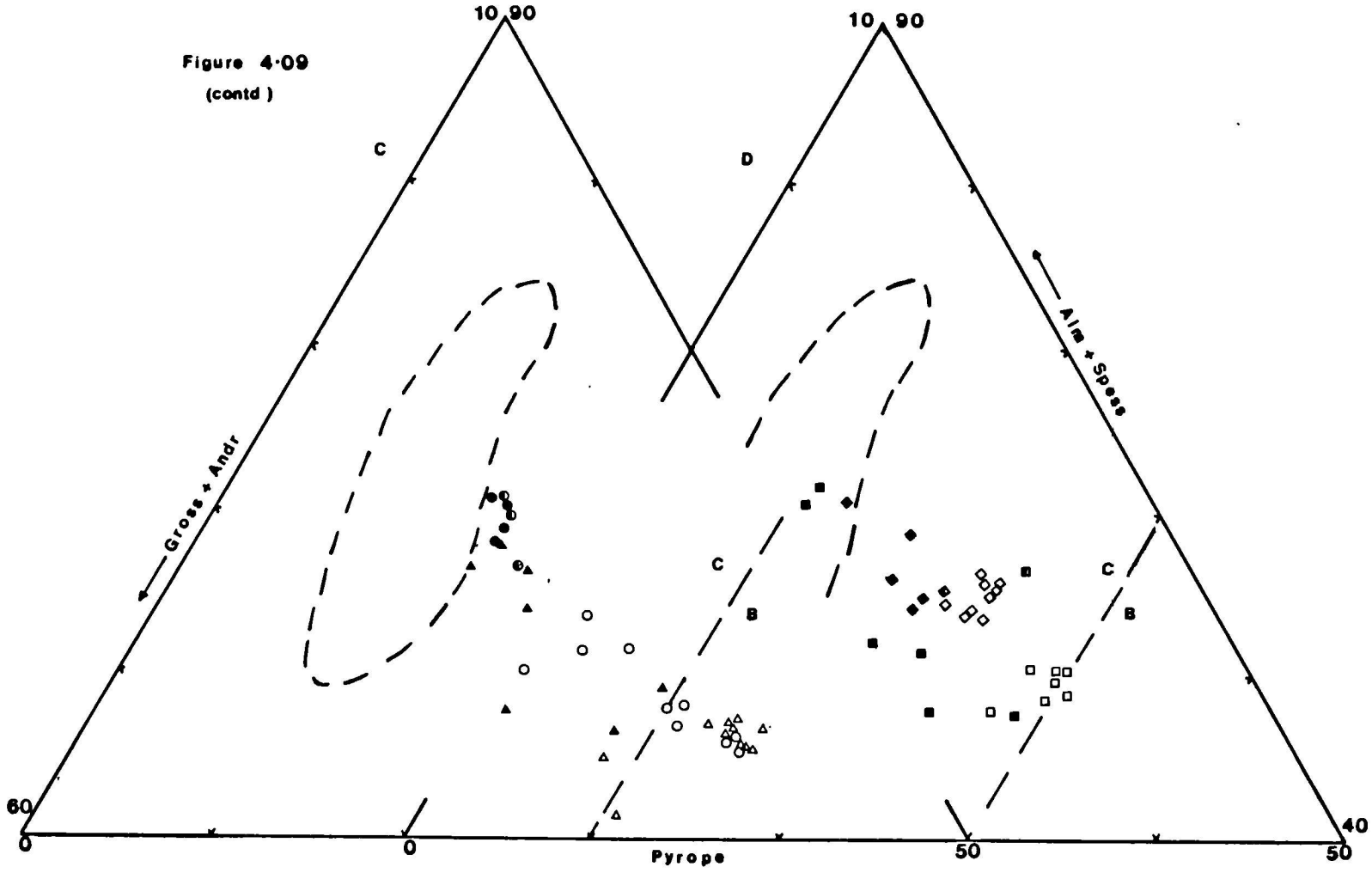

Figure 4-09

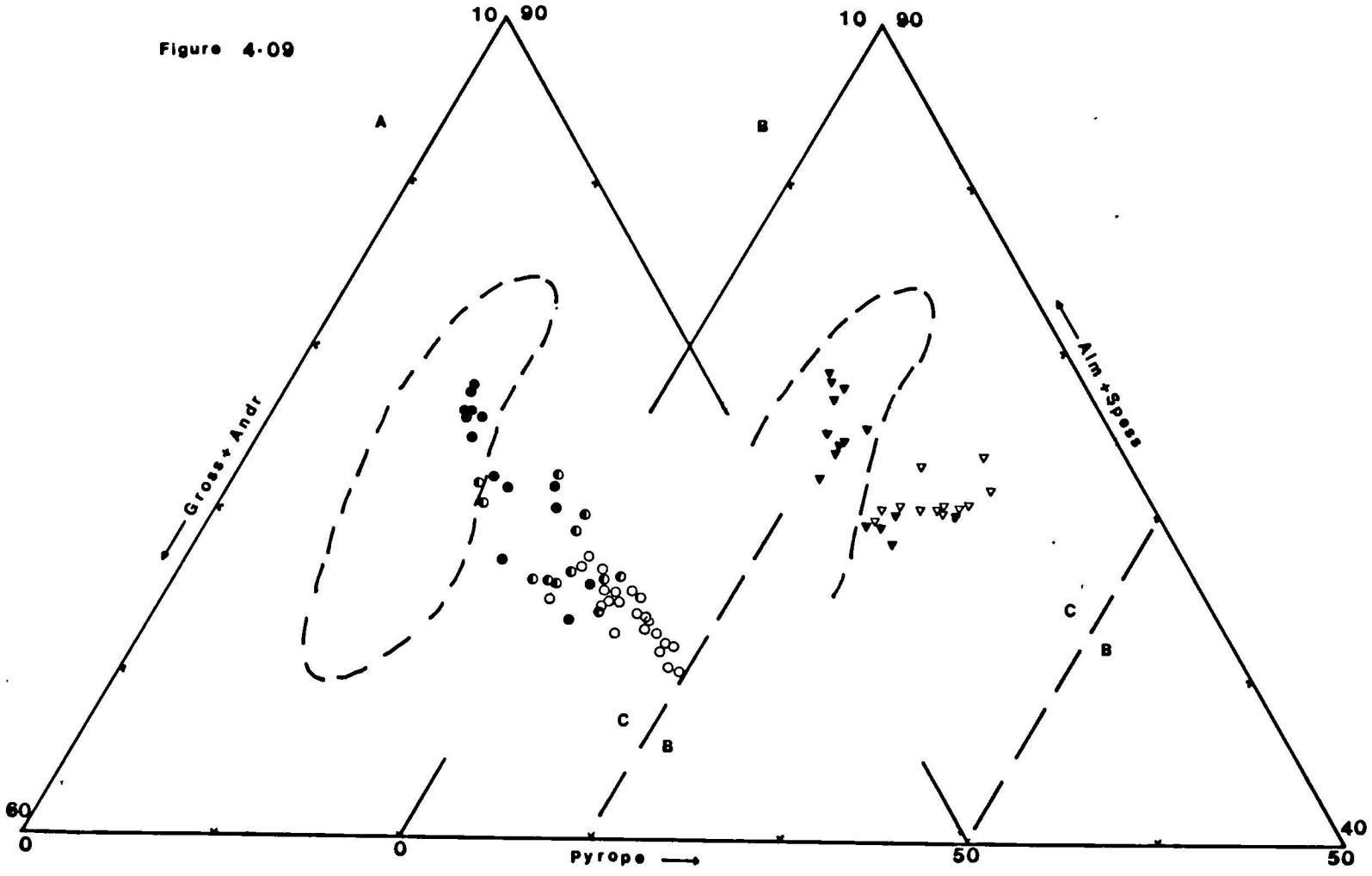

FIGURE 4.10 Compositional maps of garnet in kyanite eclogite D123.

A - Locations of inclusions. Light hatching = amphiboles, light and heavy hatching = zoisite, no hatching = quartz, heavy hatching = kyanite (matrix).
B - FeO/MgO, contour interval 1.0 units.
C - Mno, contour interval 0.1 mass %.
D - Cao, contour interval 1.0 mass %.

Figure 4.10

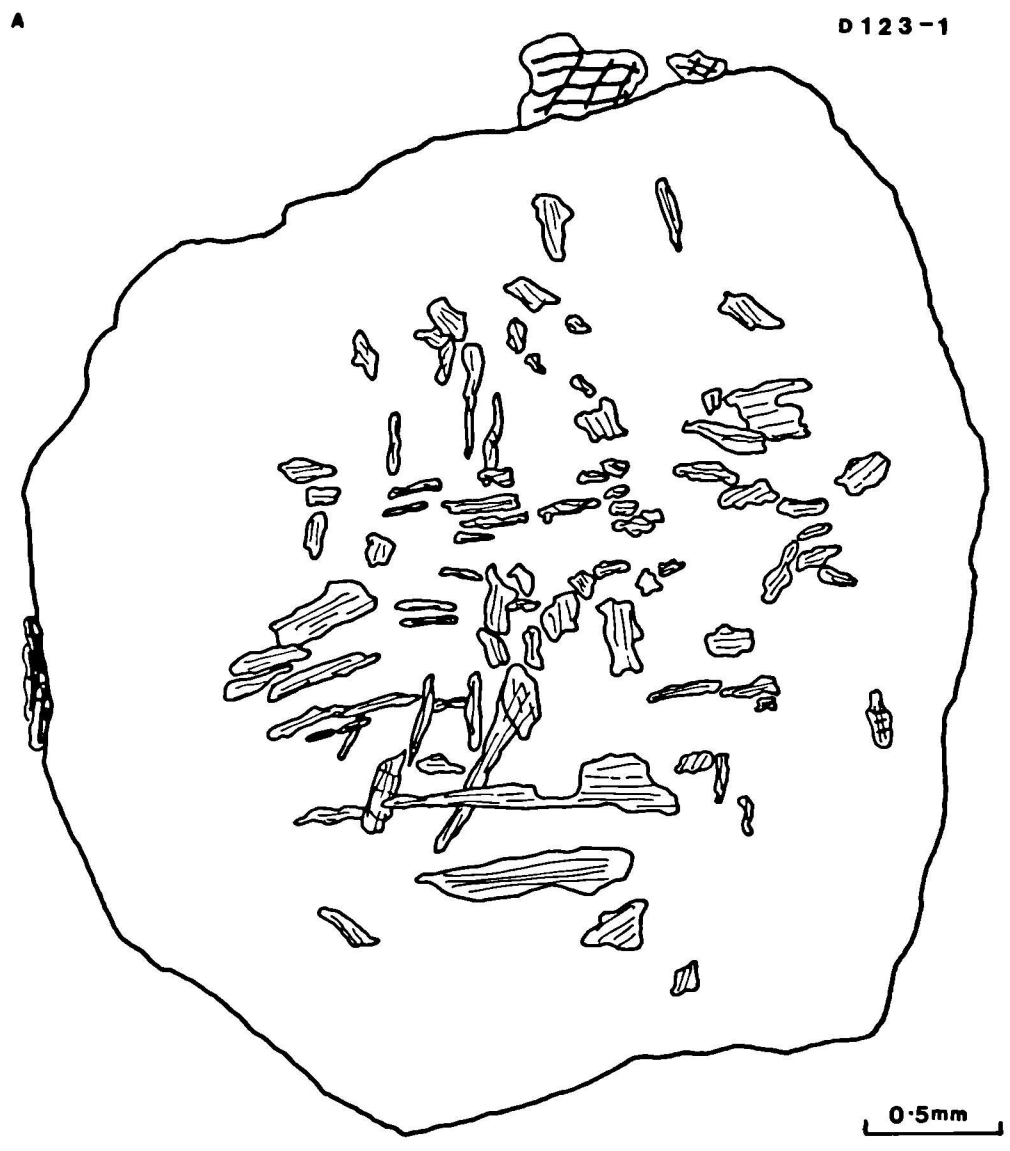

B

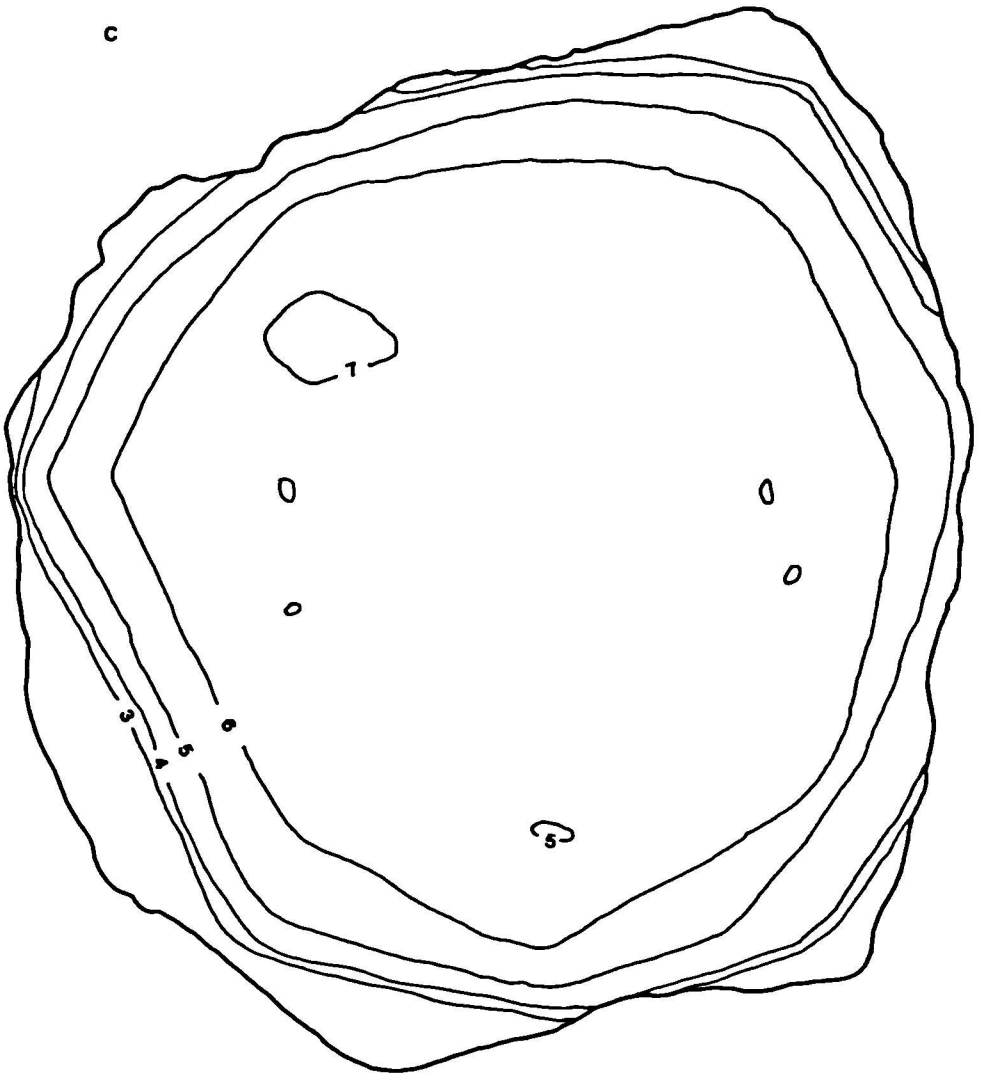
c
7
0
0
0
0
3
4
5
6
5
FeO/MgO

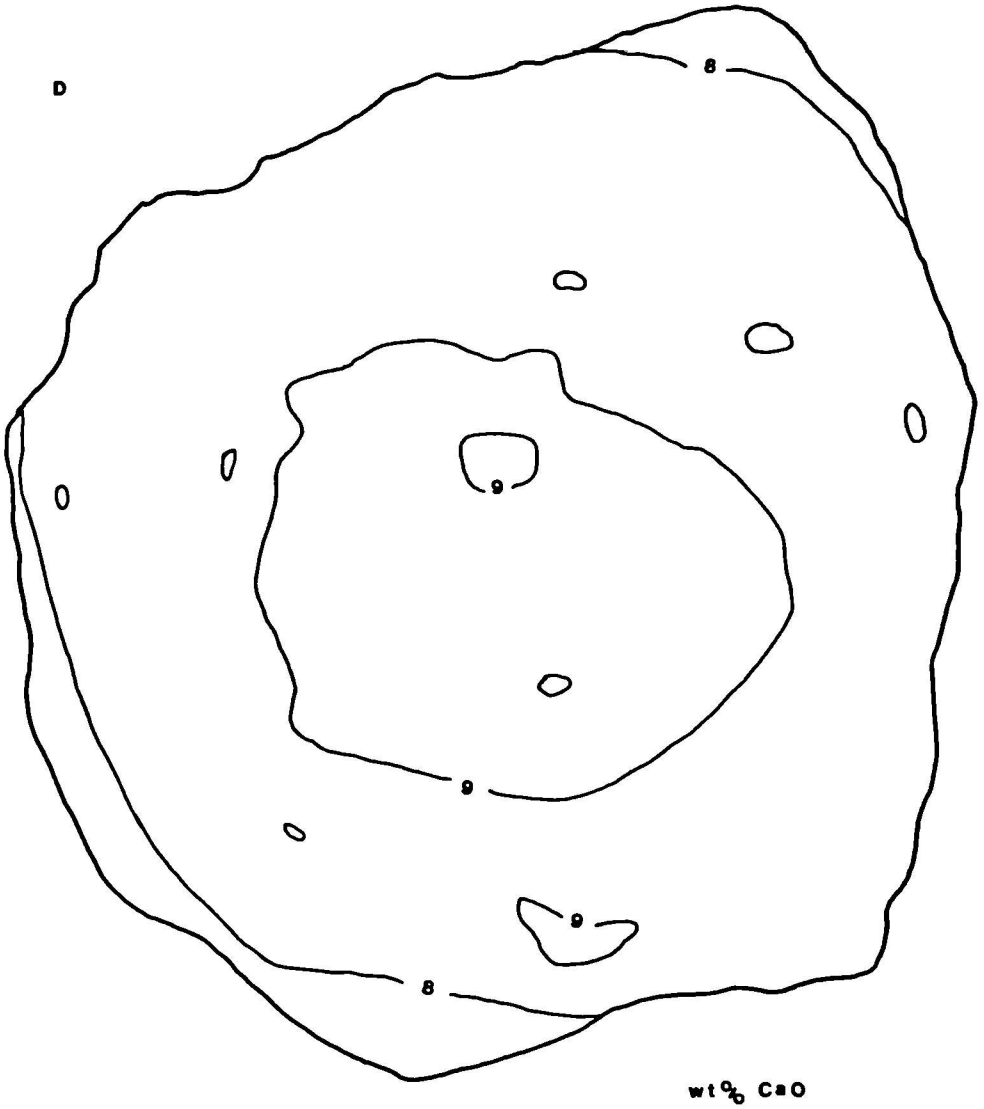
D
8
0
0
9
9
0
9
8
wt% CaO

FIGURE 4.11 Compositional maps of garnet in bimineralic eclogite D205.
A - location of inclusions; light hatching = amphiboles, black = rutile, no hatching = omphacite.
B - MnO, contour interval 0.5 mass %, dash-dot line shows reversal of zoning profile at about 0.2 mass %.
C - CaO, contour interval 0.5 mass %.
D - FeO^{T}/MgO, contour interval 1 unit.

Figure 4.11

A

D205-4

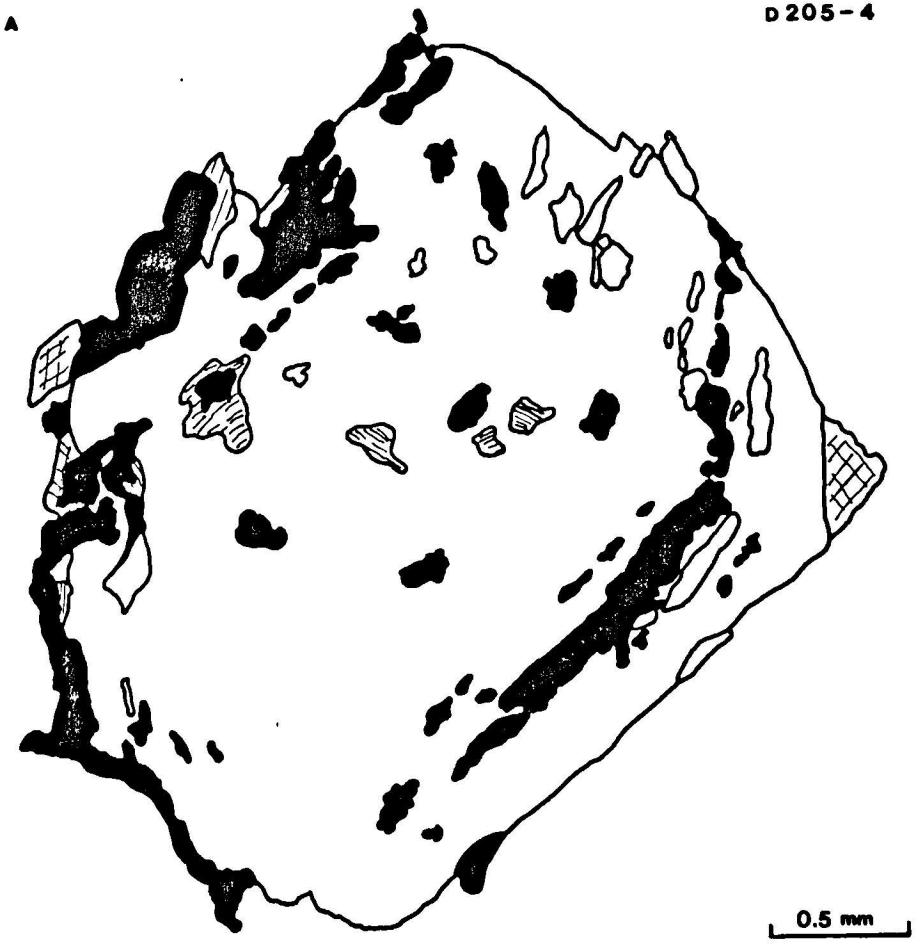

B

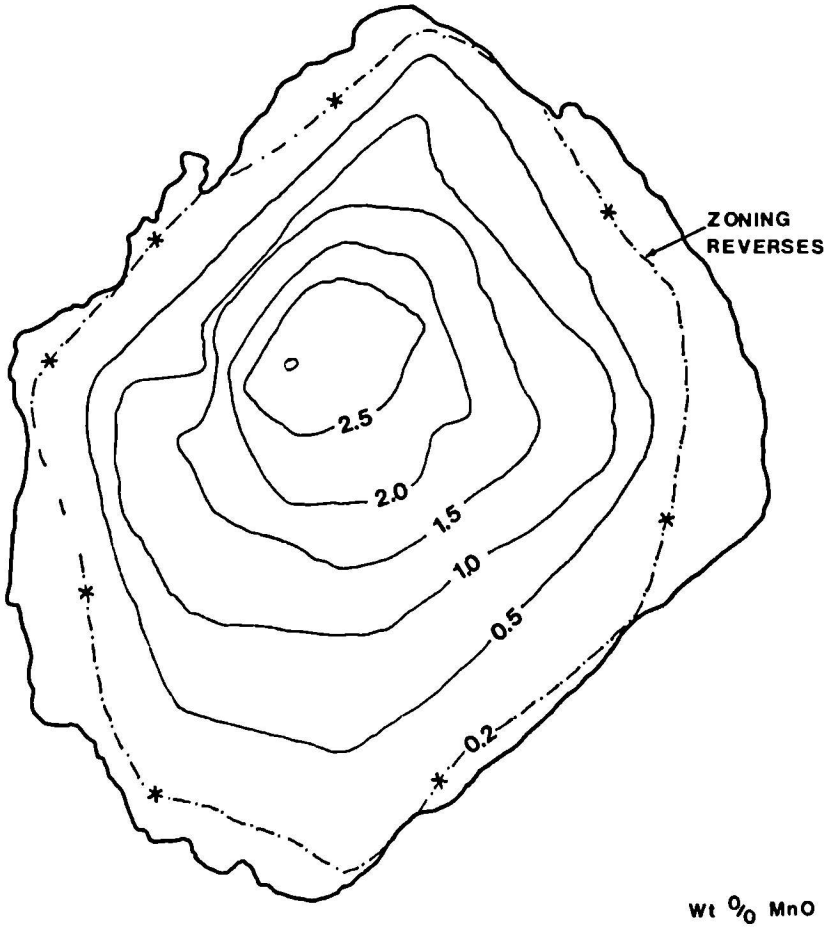

c

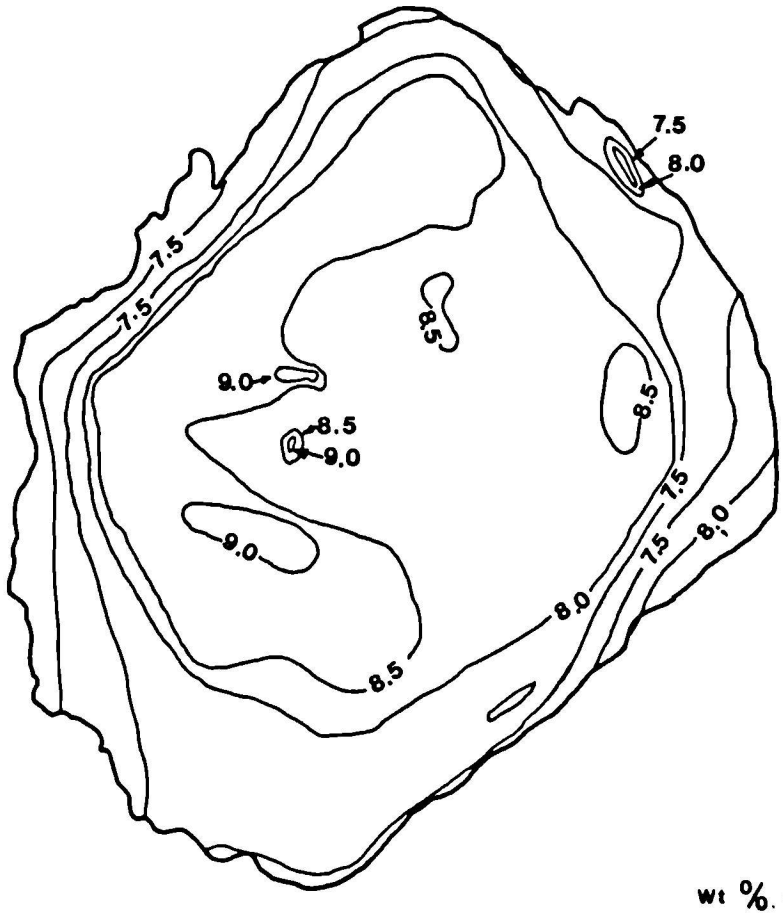

wt %. CaO

D

FeO/MgO

FIGURE 4.12 Compositional map of garnet in garnet amphibolite band D206.

A - location of inclusions: light hatching = amphibole, stipple = apatite, black = rutile, no hatching = omphacite. Garnets outlined by dotted stipple.
B - FeO^T/MgO, contour interval 1 unit.
C - MnO, contour intervals: above 0.5 mass % = mass %. below 0.5 mass % (dashed) 0.1 mass %. Cross shows compositional maximum.
D - CaO, contour interval 1 mass %.

Figure 4·12 A

D206–1

Figure 4·12 B

D 206–1 FeO^T/MgO

0·5 mm

Figure 4·12 C

D 206–1 MnO wt %

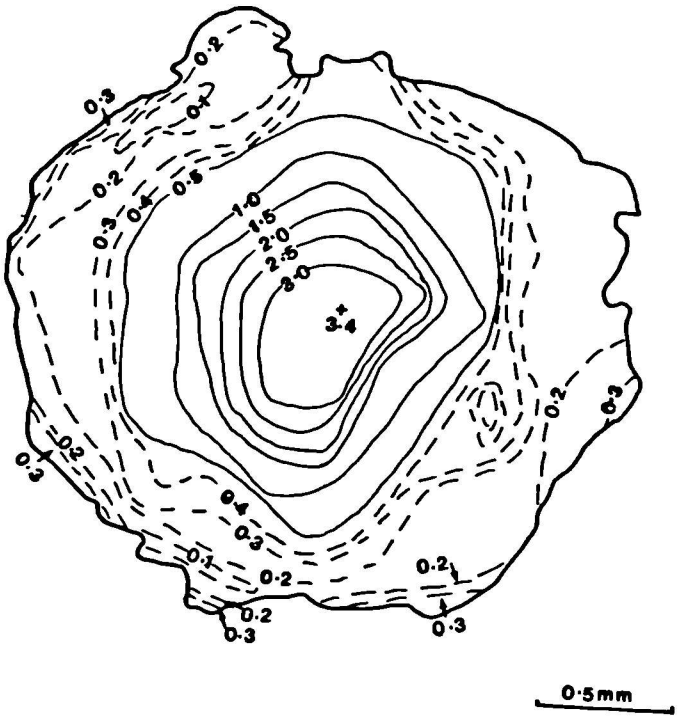

Figure 4·12 D

D206-1 CaO wt %

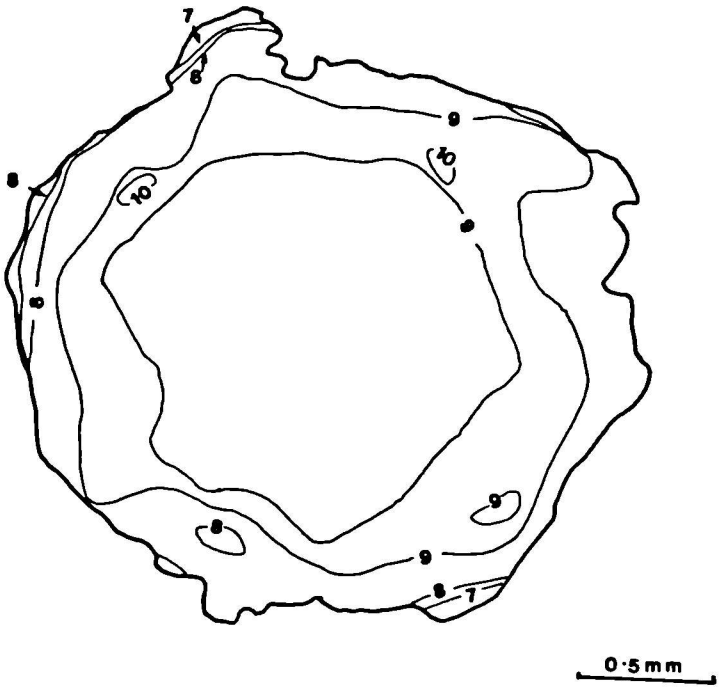

FIGURE 4.13 $LnK_D^{Fe/Mg}$ vs X_{Ca}^{gt} for coexisting garnet and omphacite in eclogites. Isotherms are calculated from the expression of Ellis and Green (1979) at 16 kbars.

Symbols:-
Circles = eclogite band in websterite (79/9a)
X = quartz eclogite (79/16)
Triangles = kyanite eclogite (D77) - note that Fe^{3+} determination for pyroxene is probably too low.
Star = dyke eclogite (D83a)
+ = eclogite with siliceous backveins (D181)
Diamonds = bimineralic eclogite (D205)
Inverted triangles = garnet amphibole band in eclogite (D206)
Squares = eclogites in Basal Gneisses (D69, 79/38b, D116)

Open symbols are rim-rim pairs, filled symbols are inclusion-host pairs. Crosses are rim-rim pairs.

Figure 4.13

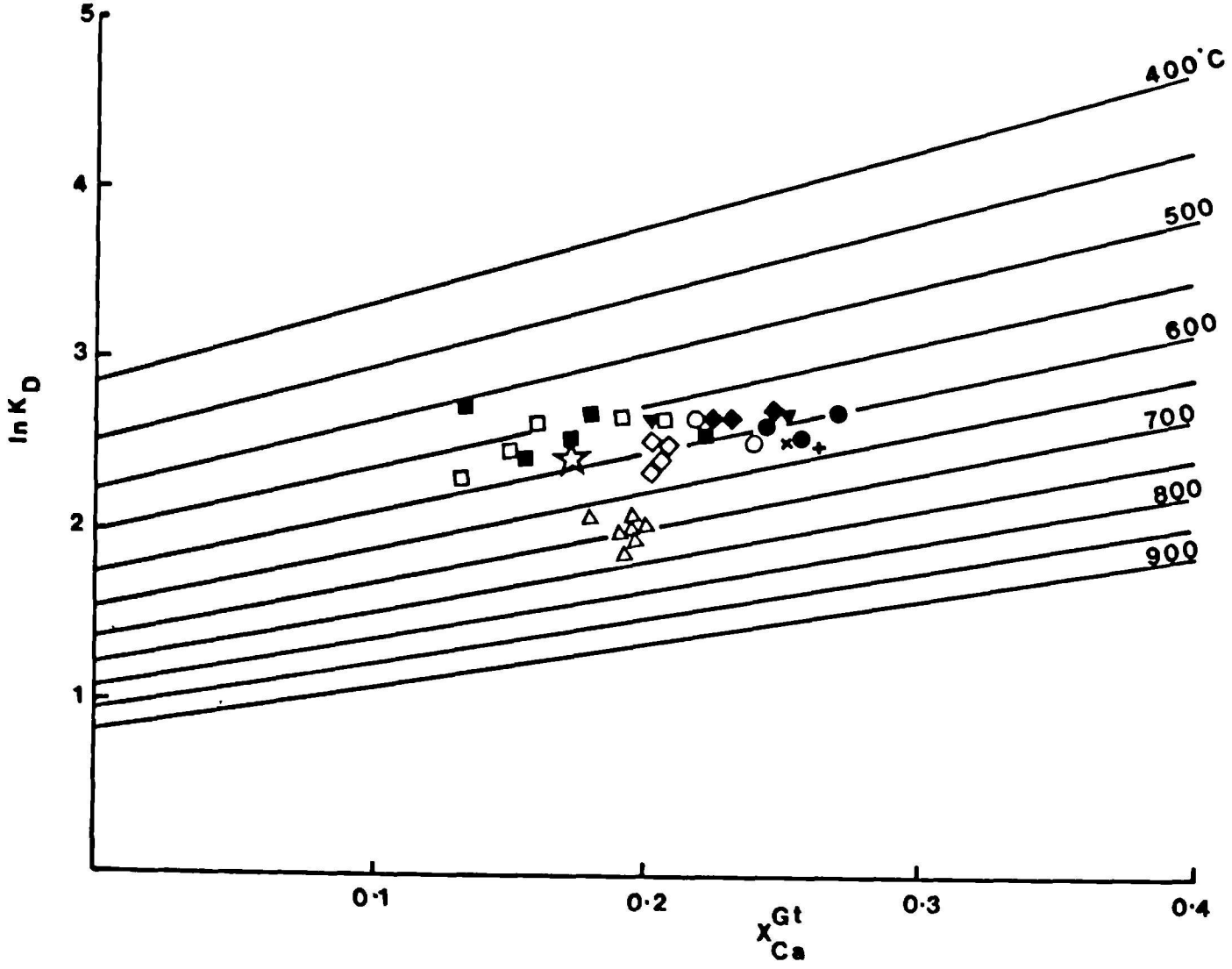

FIGURE 4.14 $LnK_D^{Fe/Mg}$ vs X_{Ca}^{gt} for coexisting garnet and amphibole in eclogites. Isotherms are calculated from the expression of Graham and Powell (1984).

Symbols:-
Circles = eclogite band in websterite (79/9a)
Triangles = kyanite eclogite (D123)
Diamonds = bimineralic eclogite (D205)
Inverted triangles = garnet amphibolite band in eclogite (D206)

Open symbols are rim-rim pairs, closed symbols are dark-coloured hornblende inclusions in garnets, horizontally half-filled symbols are actinolitic inclusions in garnets, vertically half-filled symbols are secondary (stage IV) matrix amphiboles.

Figure 4.14

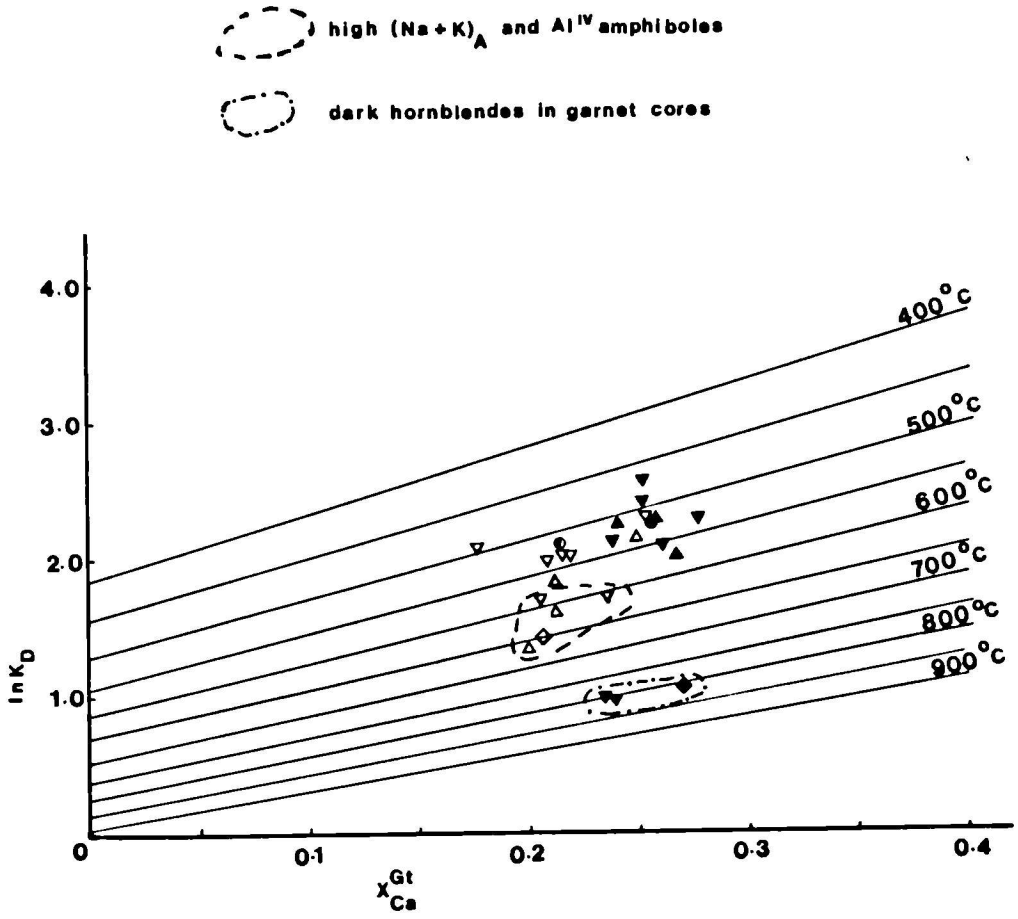
high $(Na+K)_A$ and Al^{IV} amphiboles
dark hornblendes in garnet cores
4.0
3.0
2.0
1.0
0
0·1
0·2
0·3
0·4
$\ln K_D$
X_{Ca}^{Gt}
400°C
500°C
600°C
700°C
800°C
900°C

FIGURE 4.15 Fe/Mg ratios of coexisting garnets and phengites. Isotherms are also isopleths for $K_D^{Fe/Mg}$ with temperatures calculated from the expression of Green and Hellman (1982) for a basaltic composition at 16 kbars.

Symbols:-
Circle = Basal Gneiss eclogite 79/38b
Inverted triangle = Basal Gneiss eclogite D116
Triangles = kyanite eclogite D77
Square = eclogite with siliceous backveins D181

Figure 4.15

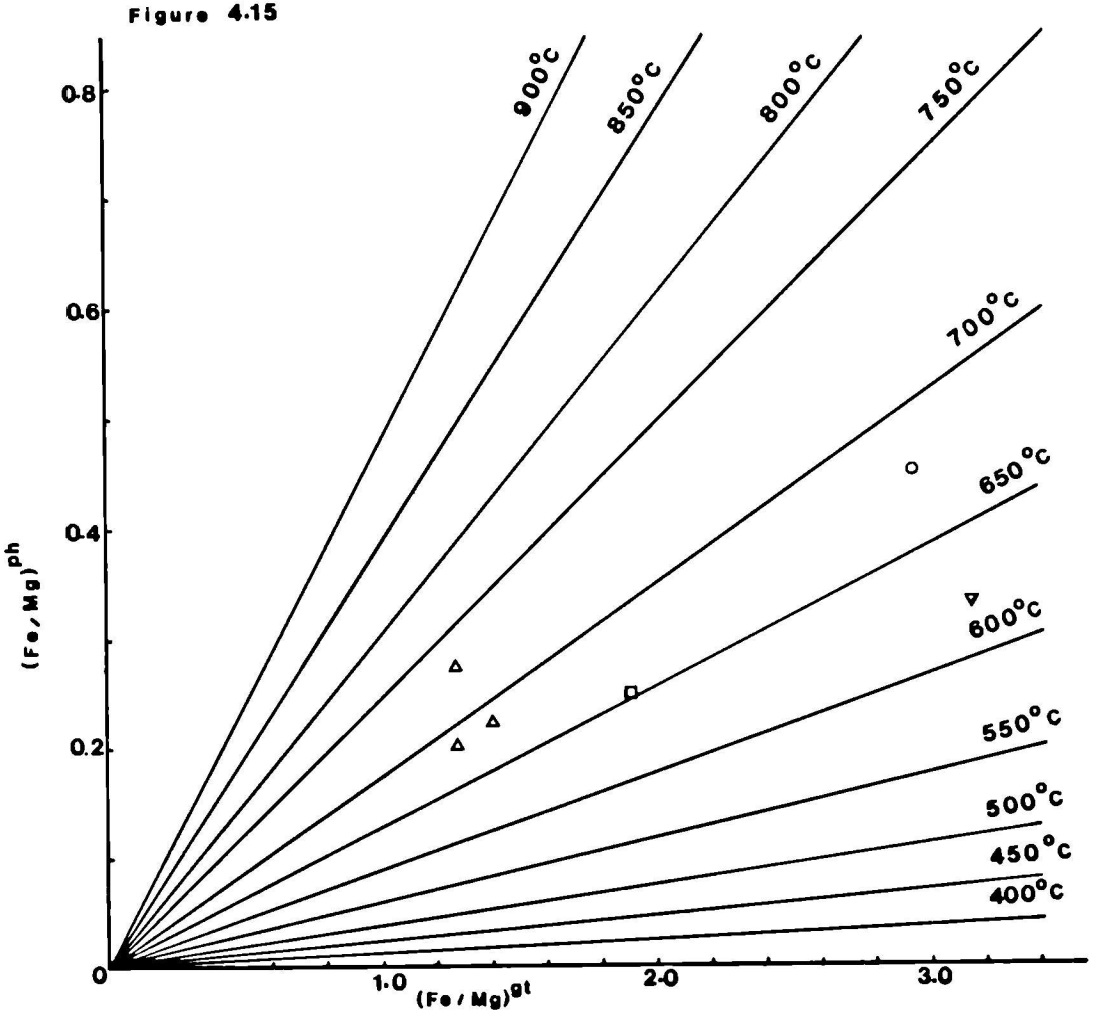
900°C
850°C
800°C
750°C
700°C
650°C
600°C
550°C
500°C
450°C
400°C
0.8
0.6
0.4
0.2
0
1.0
2.0
3.0
(Fe/Mg)ph
(Fe/Mg)gt

FIGURE 4.16 Schematic diagram illustrating high-pressure breakdown relationships of hornblende showing possible up-pressure evolution of early (stage I) amphiboles from the eclogites. After Essene et al (1970).

Figure 4.16

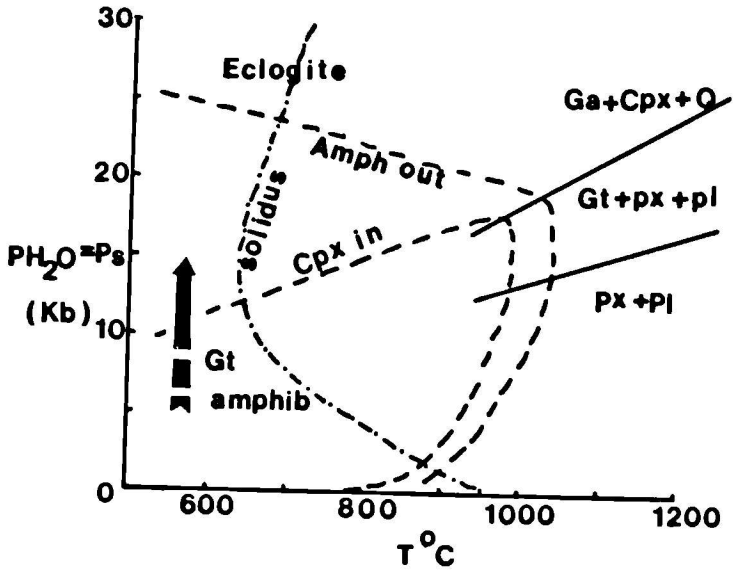
30
20
10
0
Eclogite
Amph out
solidus
Cpx in
Ga+Cpx+Q
Gt+px+pl
Px+Pl
Gt
amphib
PH2O=Ps
(Kb)
600
800
1000
1200
T°C

FIGURE 4.17 Petrogenetic grid for metamorphic conditions of eclogites. Numbered curves are:-

1: Albite-jadeite + quartz (Holland, 1980)
2: Lower stability $DiJd_{40}$ + quartz (Holland, 1983)
3: Lower stability $DiJd_{15}$ + quartz (Holland, 1983).
4: Paragonite = jadeite + kyanite + H_2O (Holland, 1979b).
5: Paragonite + $DiJd_{40}$ + kyanite + H_2O (Holland, 1979b).
6, 7, 8: Kyanite = sillimanite, kyanite = analusite, andalusite = sillimanite (Robie and Hemingway, 1984).
9: Margarite + quartz = kyanite + zoisite + vapour
10: Margarite + quartz = anorthite + kyanite + vapour
11: Anorthite + vapour = zoisite + kyanite + quartz (9, 10, 11 from Jenkins, 1984).
12: Zoisite + kyanite = liquid + vapour (Goldsmith, 1982).
13: Lawsonite = zoisite + kyanite + quartz (Newton and Kennedy, 1963).
14: Zoisite + quartz = anorthite + grossular + vapour (Newton, 1966).
15: Almandine + rutile = ilmenite + kyanite + quartz (Bohlen et al, 1983).
16: Muscovite + quartz = sanidine + sillimanite + vapour (extrapolated from Evans, 1965).
17: "Wet" eclogite solidus (Hill and Boettcher, 1968).
18: Maximum stability of glaucophane (Maresch, 1977).

A - Range of garnet-hornblende temperatures for stage I amphiboles (Graham and Powell, 1984).

Dashed lines - range of garnet-clinopyroxene temperatures for eclogites above top of Basal Gneisses (Ellis and Green, 1979). Dash-dot lines - range of garnet-clinopyroxene temperatures for Basal Gneiss eclogites.

Figure 4.17

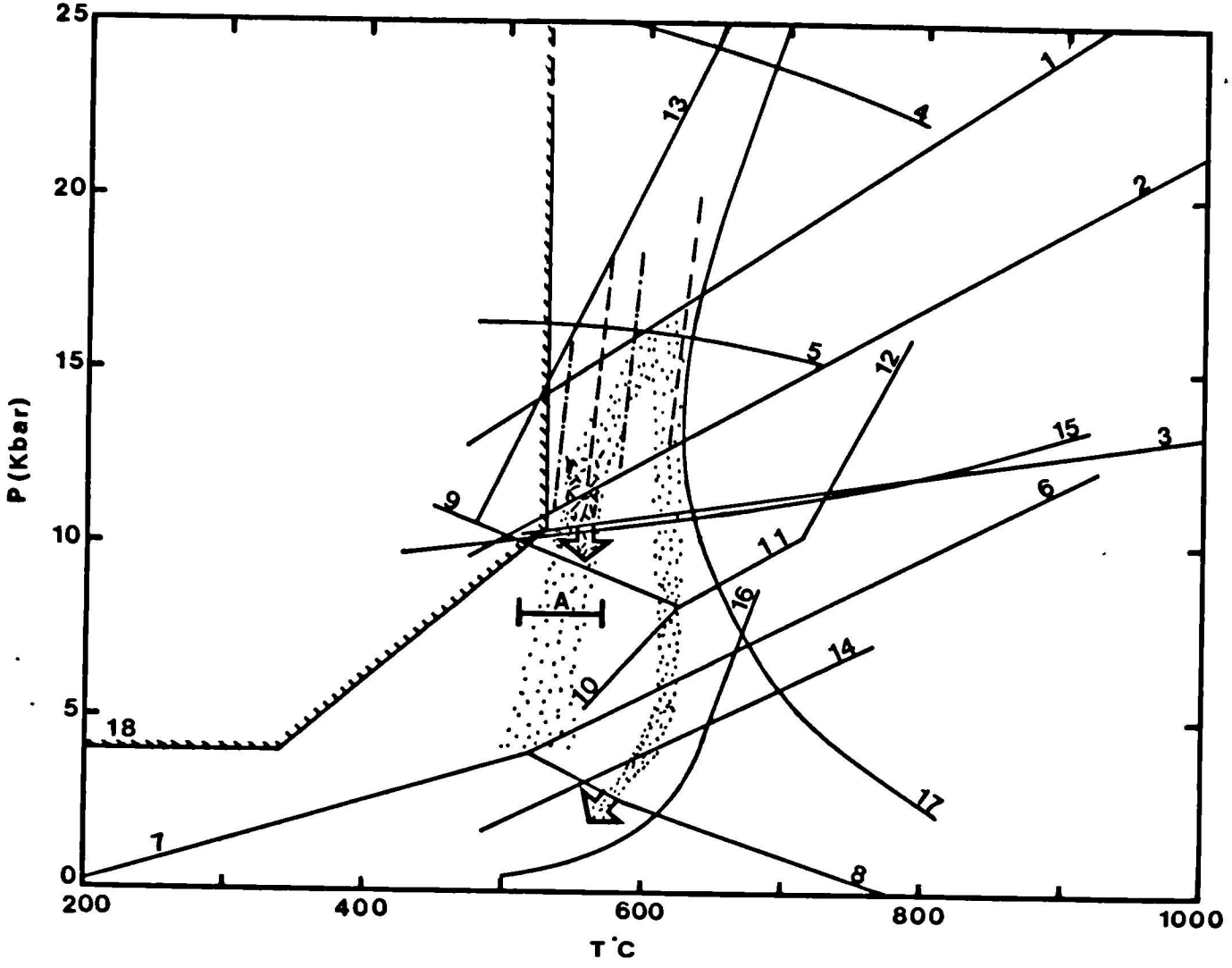
25
20
15
10
5
0
P(Kbar)
200
400
600
800
1000
T°C
1
2
3
4
5
6
7
8
9
10
11
12
13
14
15
16
17
18
A

FIGURE 4.18 Compositions of clinopyroxenes from coronites.

A - jadeite-diopside-tschermak's diagram of White (1964) with dashed line dividing fields for granulite and eclogite pyroxenes.
B - part of the jadeite-augite-acmite diagram of Essene and Fyfe (1967).

Symbols:-
Open diamond = jadeite, coronite D187
Closed diamond = igneous augites from anorthositic troctolite D170
Circles = partially transformed augites, D194.
X = vein omphacite
+ = symplectised vein omphacite.
Triangles = omphacites from jadeite-bearing coronite 6-5.5.
Inverted triangles = omphacites from kyanite-bearing coronite D132.
Squares = omphacites from bimineralic coronite-eclogite.

In latter 3, filled symbols are in the mafic site, open symbols in the plagioclase site and half-filled symbols inclusions in garnet.

Figure 4.18

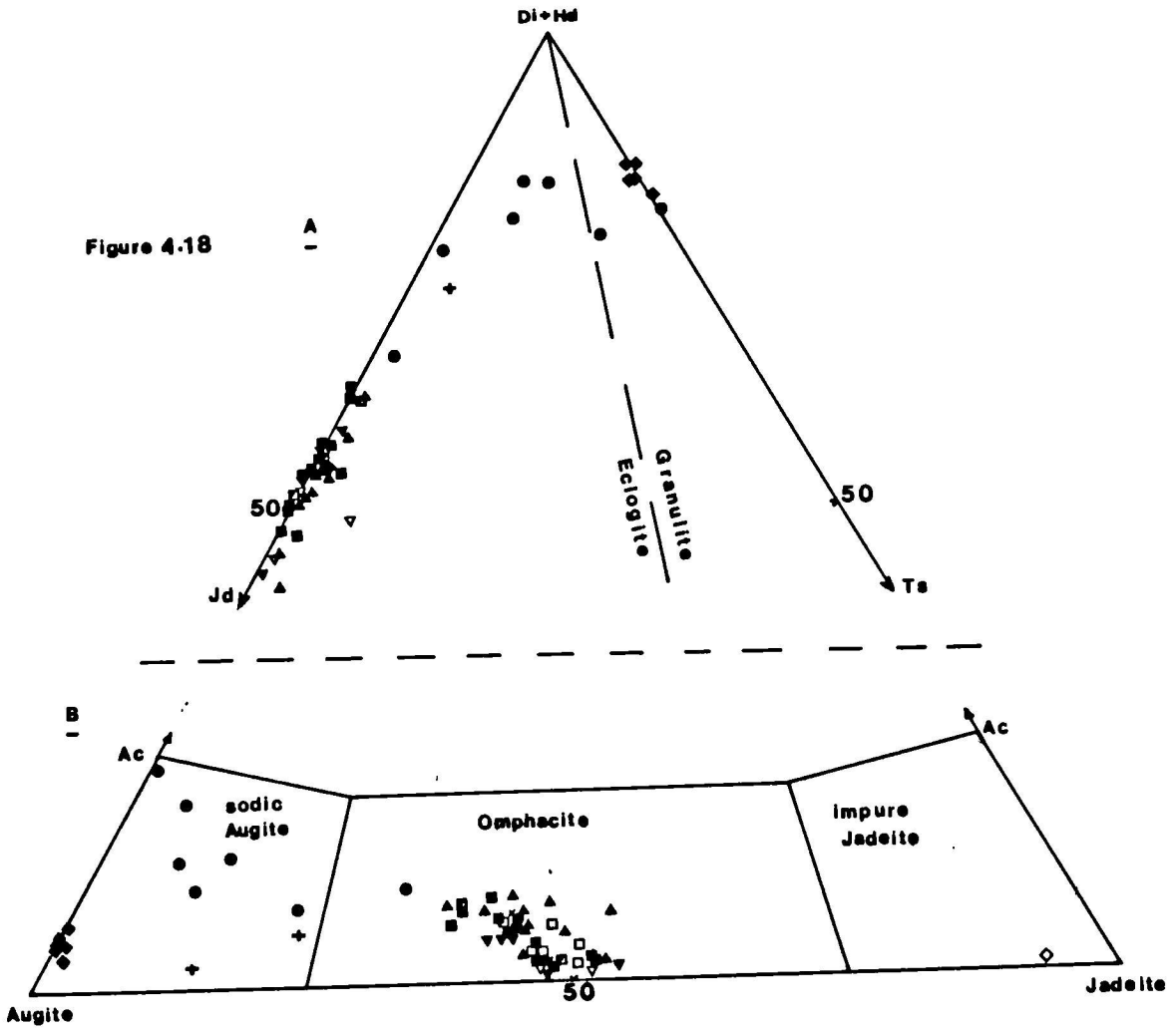
A
Di+Hd
50
50
Jd
Ts
Granulite
Eclogite
B
Ac
Ac
sodic
Augite
Omphacite
impure
Jadeite
50
Augite
Jadeite

FIGURE 4.19 Compositions of pyroxenes from the anorthositic troctolite (D170) projected onto the pyroxene quadrilateral isotherms are from Lindsley (1983), at 10 Kbars.

Symbols:-
Squares = cores
Circles = rims
Triangles = symplectite pyroxenes

Solid tie-lines link coexisting rim and core pairs, dashed tie-line links a pair of symplectite pyroxenes.

Figure 4-19

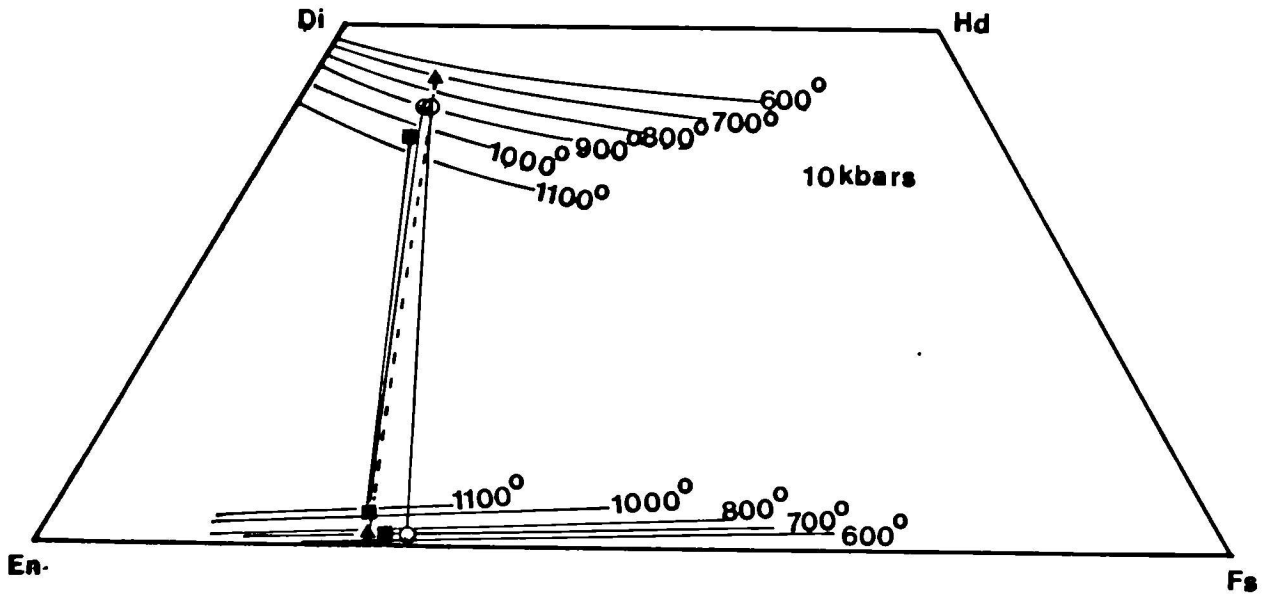
Di
Hd
600°
700°
800°
900°
1000°
1100°
10 kbars
1100°
1000°
800°
700°
600°
En
Fs

FIGURE 4.20 Compositions of garnets in coronites.

a - jadeite-bearing coronite. Open symbols are compositions from the clear, inner zone, while filled symbols are from the outer, inclusion-rich zone. Dashed line separates fields for the two zones. Specimen 6-5.5.

b - bimineralic coronite-eclogite D192 and kyanite-bearing eclogite D132 (circles). For D192 filled symbols represent cores of indiviudal garnets in a corona, with open symbols for rims. Tie-lines link cores and rims in the same grains, while "A" indicates the presence of amphibole inclusions. For D132 the garnets are discreet grains in the plagioclase sites. Filled symbols are cores, open symbols rims.

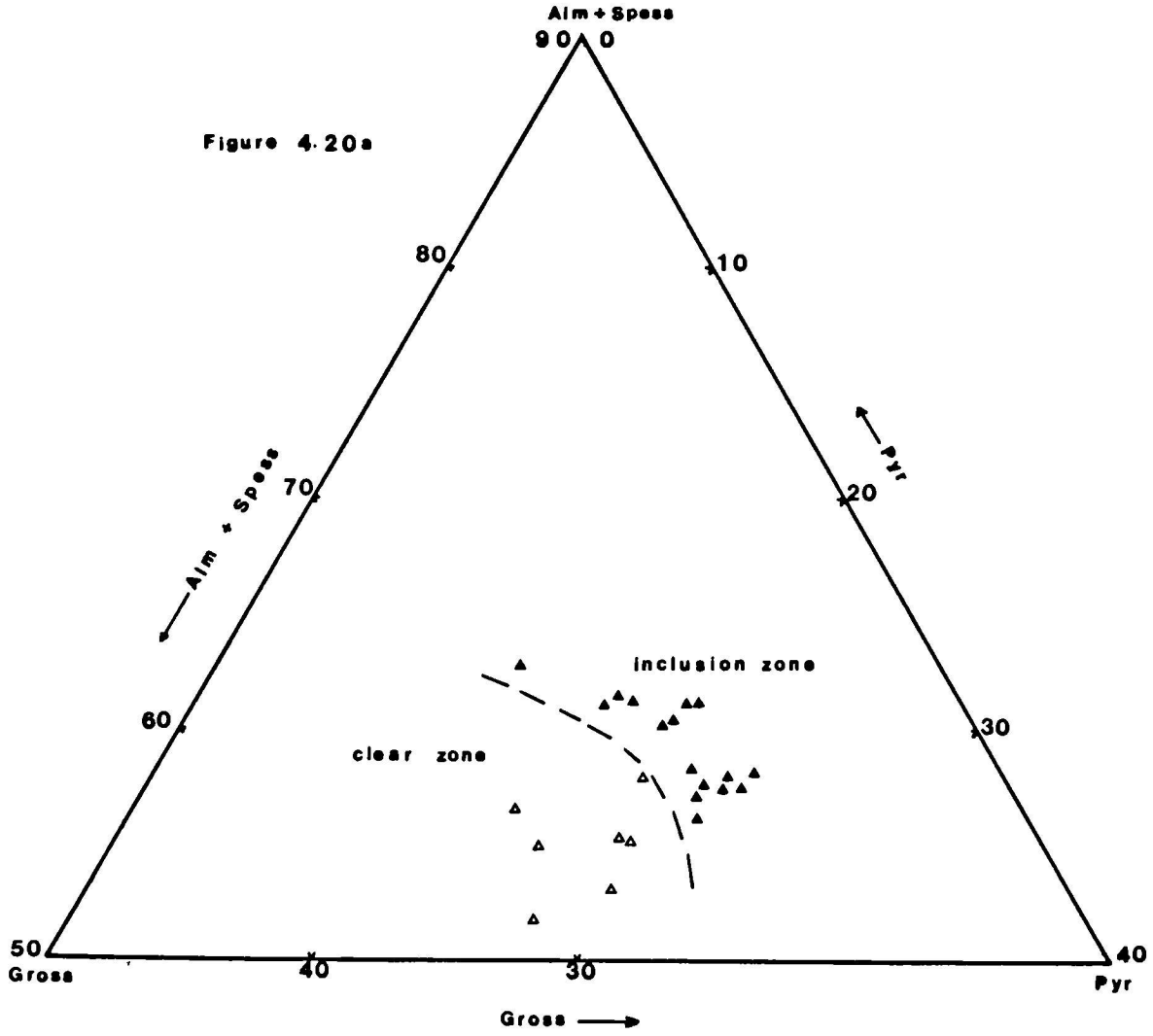
Alm + Spess
90
0
80
10
70
20
60
30
50
40
40
30
Gross
Pyr
Alm + Spess
Pyr
inclusion zone
clear zone
Gross

Figure 4.20a

FIGURE 4.21 Compositional variation across a garnet corona in jadeite-bearing coronite 6-5.5.

Figure 4·21

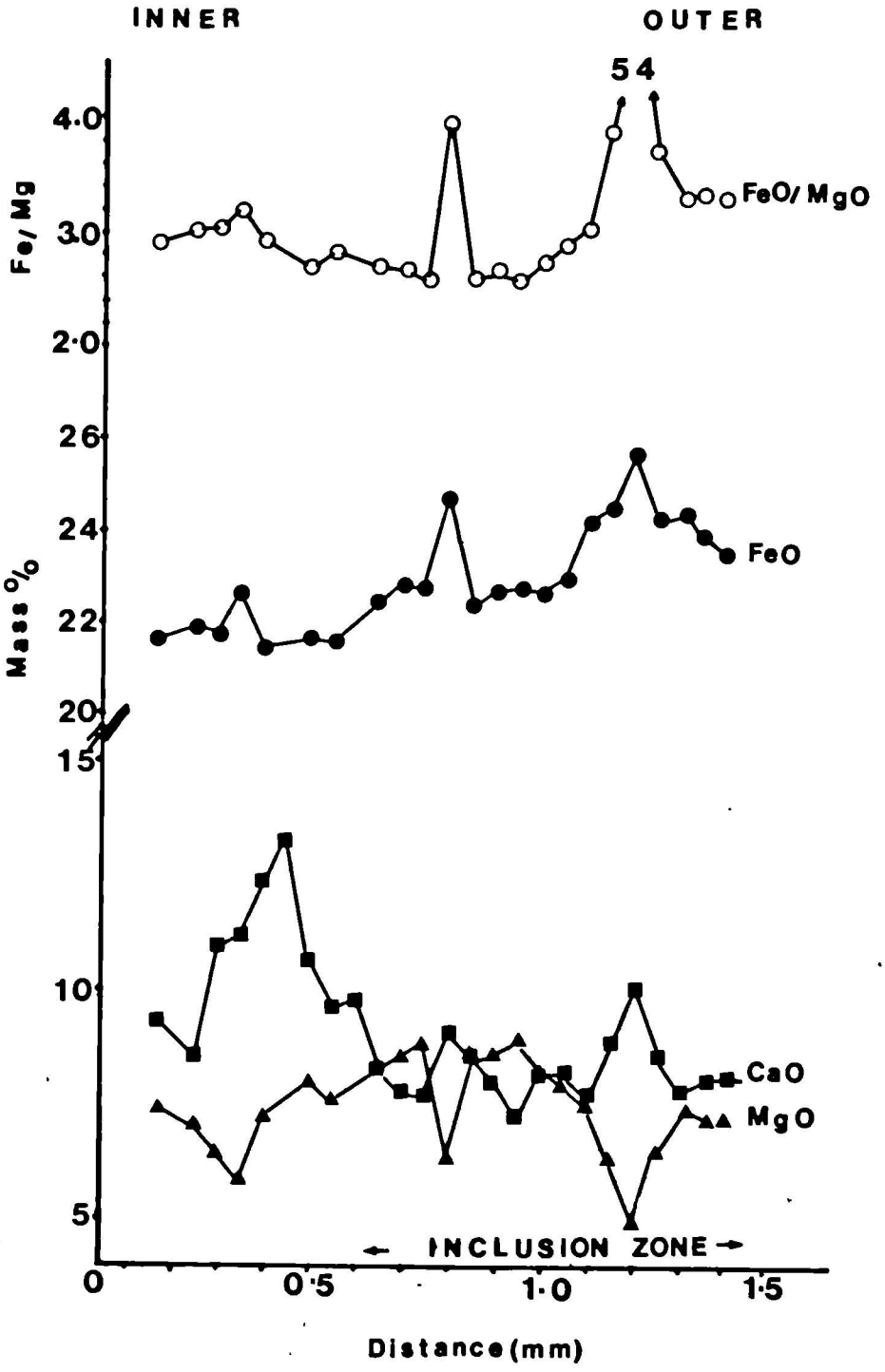
INNER
OUTER
54
4·0
3·0
2·0
Fe/Mg
FeO/MgO
26
24
22
20
15
Mass %
FeO
10
5
CaO
MgO
INCLUSION ZONE
0
0·5
1·0
1·5
Distance (mm)

FIGURE 4.22 Compositional variation across a garnet corona in a kyanite-bearing coronite. Plotted values are raw X-ray counts per second.

Figure 4·22

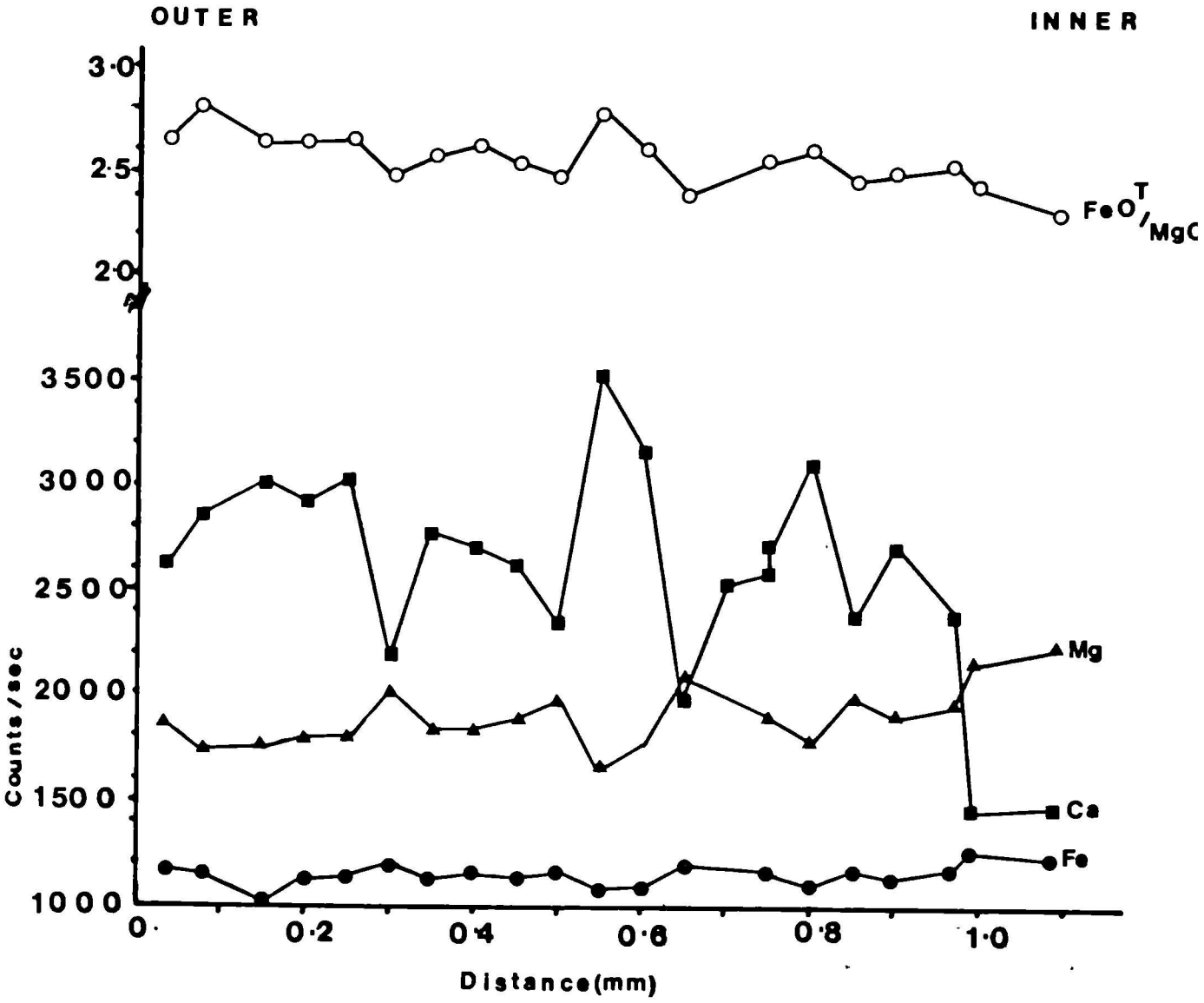
OUTER
INNER
3·0
2·5
2·0
FeO^T/MgO
3500
3000
2500
2000
1500
1000
Counts/sec
Mg
Ca
Fe
0·
0·2
0·4
0·6
0·8
1·0
Distance(mm)

FIGURES 4.23 Calcium variation across a garnet grain from within a granular garnet corona in bimineralic coronite-eclogite D192. Values are raw X-ray counts per second with two calibrated values for reference. The peak corresponds to a zone of omphacite inclusions.

Figure 4.23

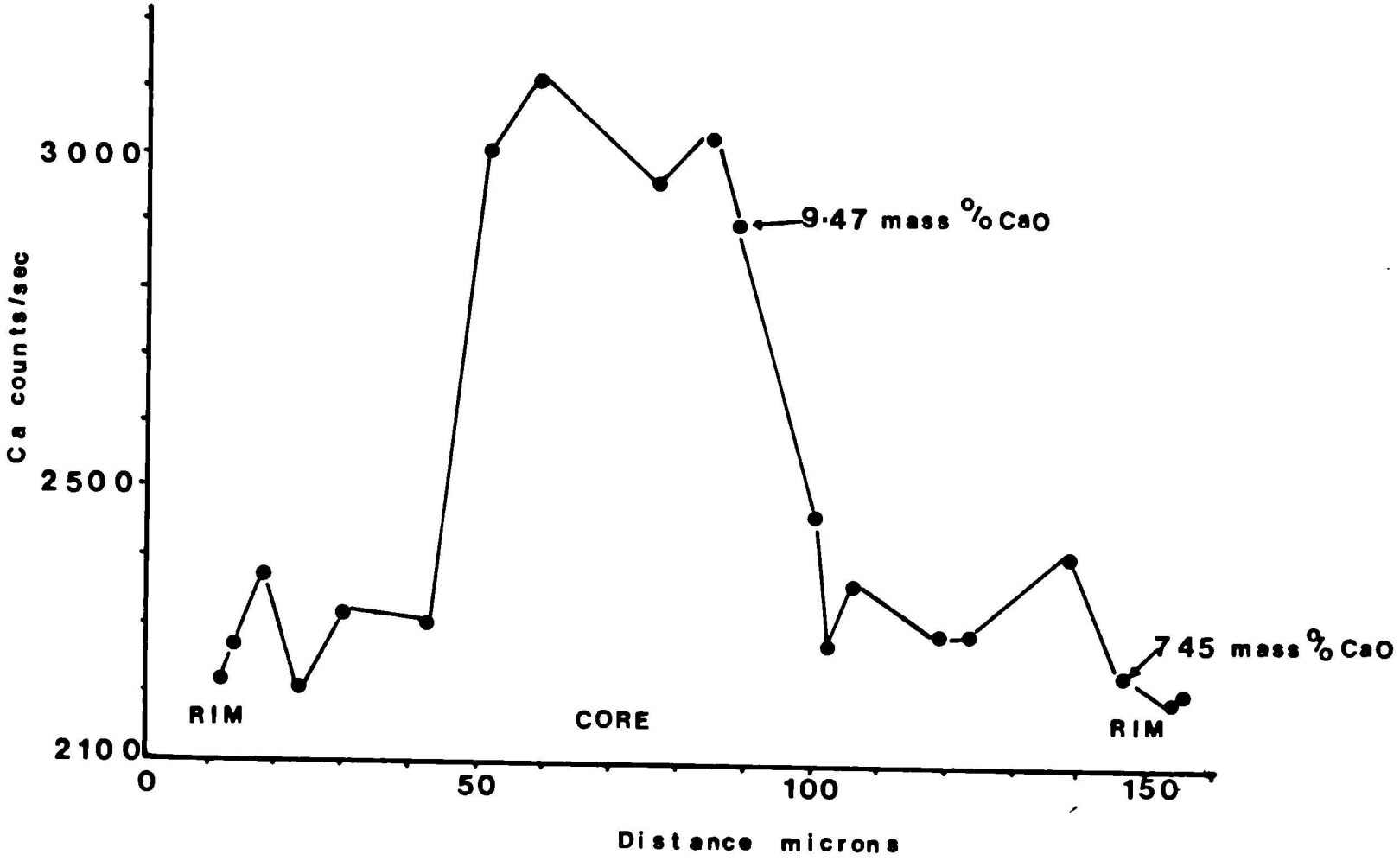
3000
2500
2100
Ca counts/sec
9·47 mass % CaO
7·45 mass % CaO
RIM
CORE
RIM
0
50
100
150
Distance microns

FIGURE 4.24 Histograms showing various compositional parameters for coronite types. J = jadeite bearing, K = kyanite-bearing, E = bimineralic coronite-eclogite, I = preserved igneous assemblage, A = coronite rich in Ca-amphibole, MCI = colour index, f = frequency.

Figure 4·24

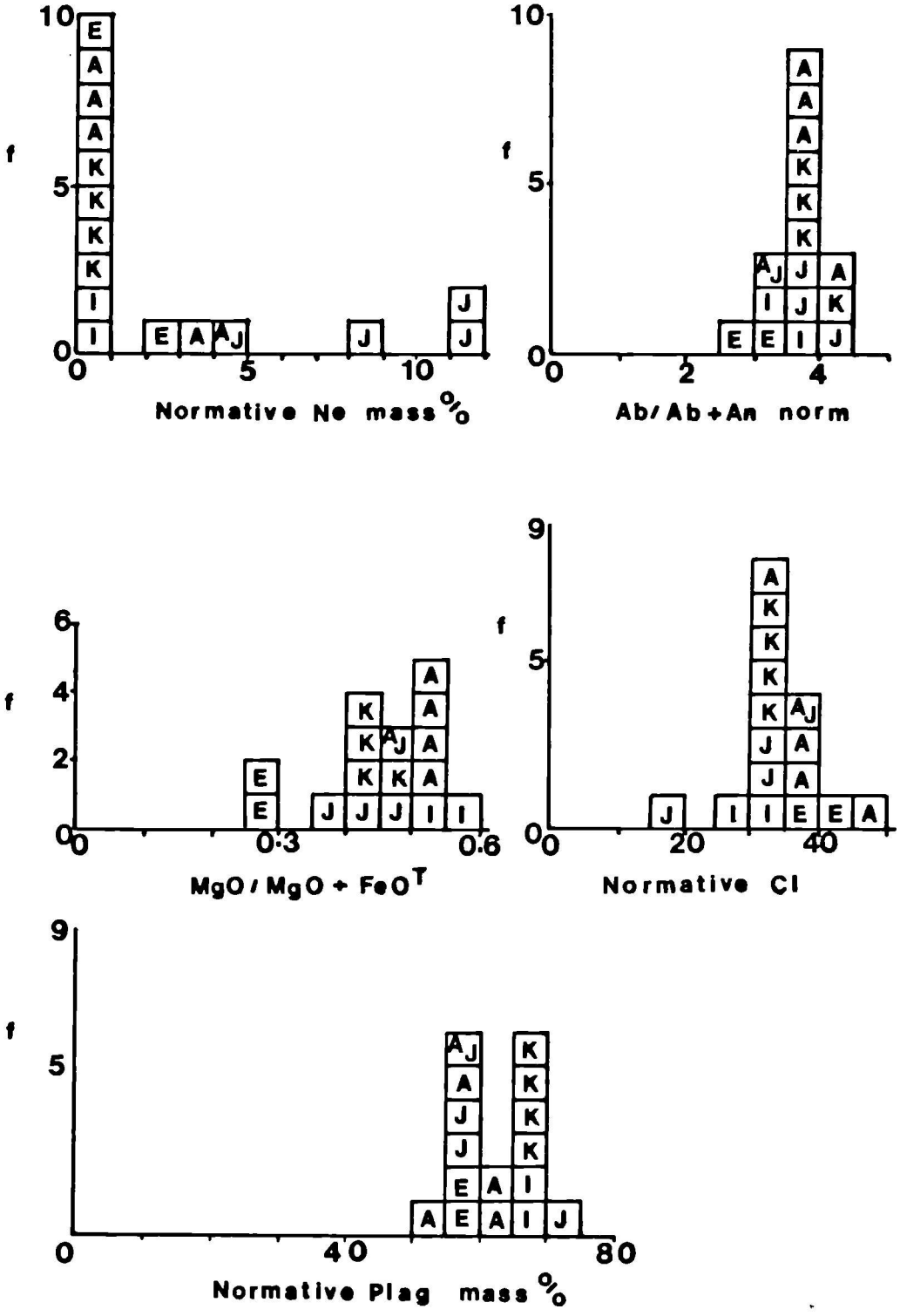
f
Normative Ne mass %
Ab/Ab+An norm
MgO/MgO+FeO^T
Normative Cl
Normative Plag mass %

FIGURE 4.25 ACF diagram showing relationship of mineral paragenesis to bulk-rock composition. Circles are jadeite-bearing coronites, squares are kyanite-bearing coronites, triangles are bimineralic coronitic-eclogies and the diamond is an anorthositic troctolite with preserved igneous assemblage. In garnet field stipple becomes lighter from core towards rim compositions. In omphacite field, stipple is heavier in grains from plagioclase sites.

Figure 4·25

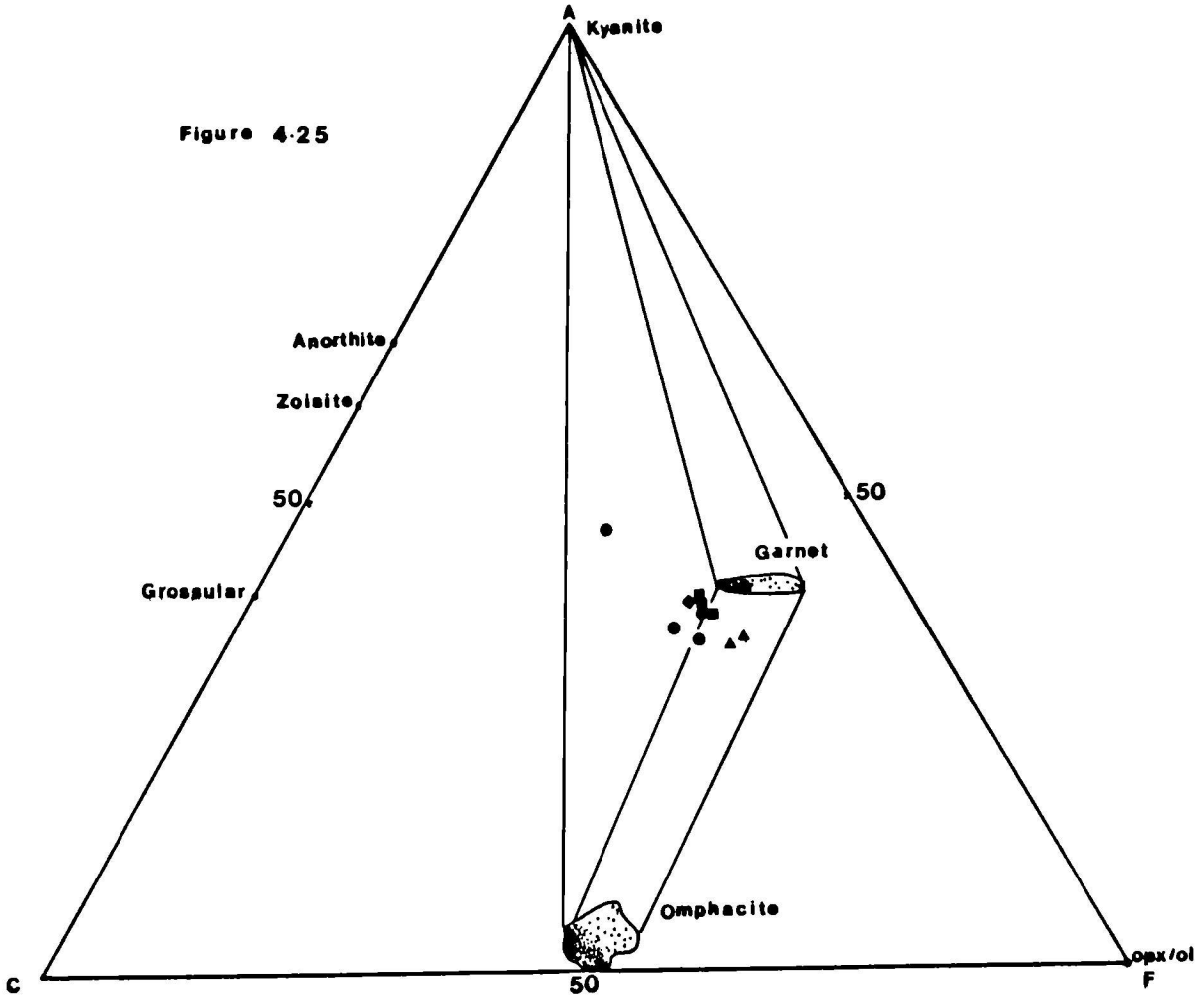
A
Kyanite
Anorthite
Zoisite
50
Grossular
50
Garnet
Omphacite
C
50
opx/ol
F

FIGURE 4.26 Schematic diagram illustrating evolution of pyroxenes from the anorthositic troctolites during cooling from the solidus to granulite-facies and post-granulite-facies conditions, with relation to variations in tschermak's molecule and enstatite content. Isopleths are from Gasparik (1984). C = core compositions, R = rims, S = symplectites.

Figure 4·26

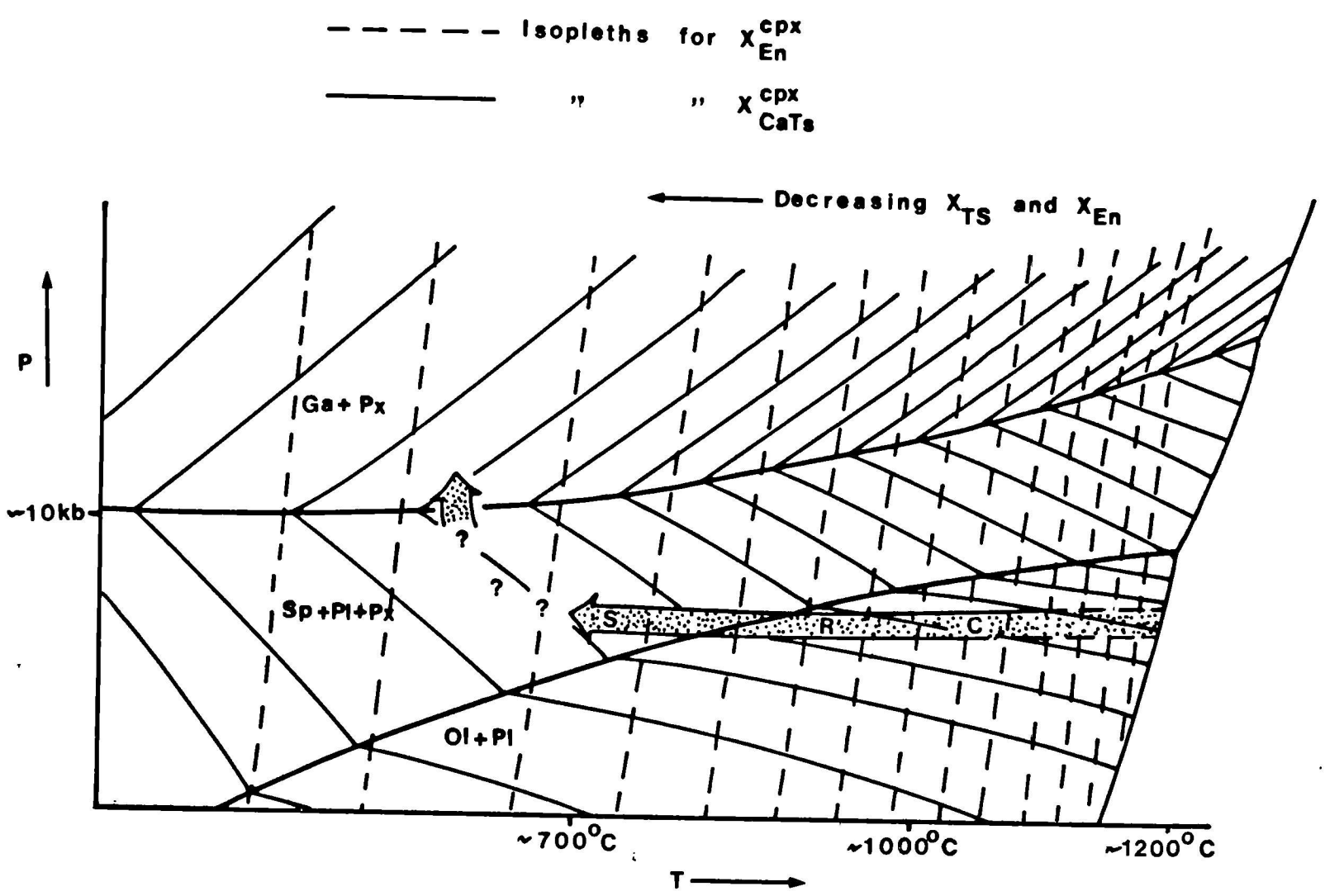
Isopleths for X^{cpx}_{En}
" " X^{cpx}_{CaTs}
Decreasing X_{TS} and X_{En}
P
~10kb
Ga + Px
Sp+Pl+Px
Ol+Pl
?
?
?
S
R
C
~700°C
~1000°C
~1200°C
T

FIGURE 4.27 Metamorphic evolution of jadeite- and kyanite-bearing coronites, mainly inferred from petrographic observations. Garnets have stippled borders.

Abbreviations:-
Al-cp : aluminous clinopyroxene
Al-op : aluminous orthopyroxene
ol : olivine, Ky : kyanite
Jd : jadeite, Pg : paragonite, ZO : zoisite
Omph : omphacite, Am : amphibole, Tc : talc
Rt : rutile, Aug : augite, Ilm : ilmenite
Plag : plagioclase, Neph : nepheline

Figure 4·27

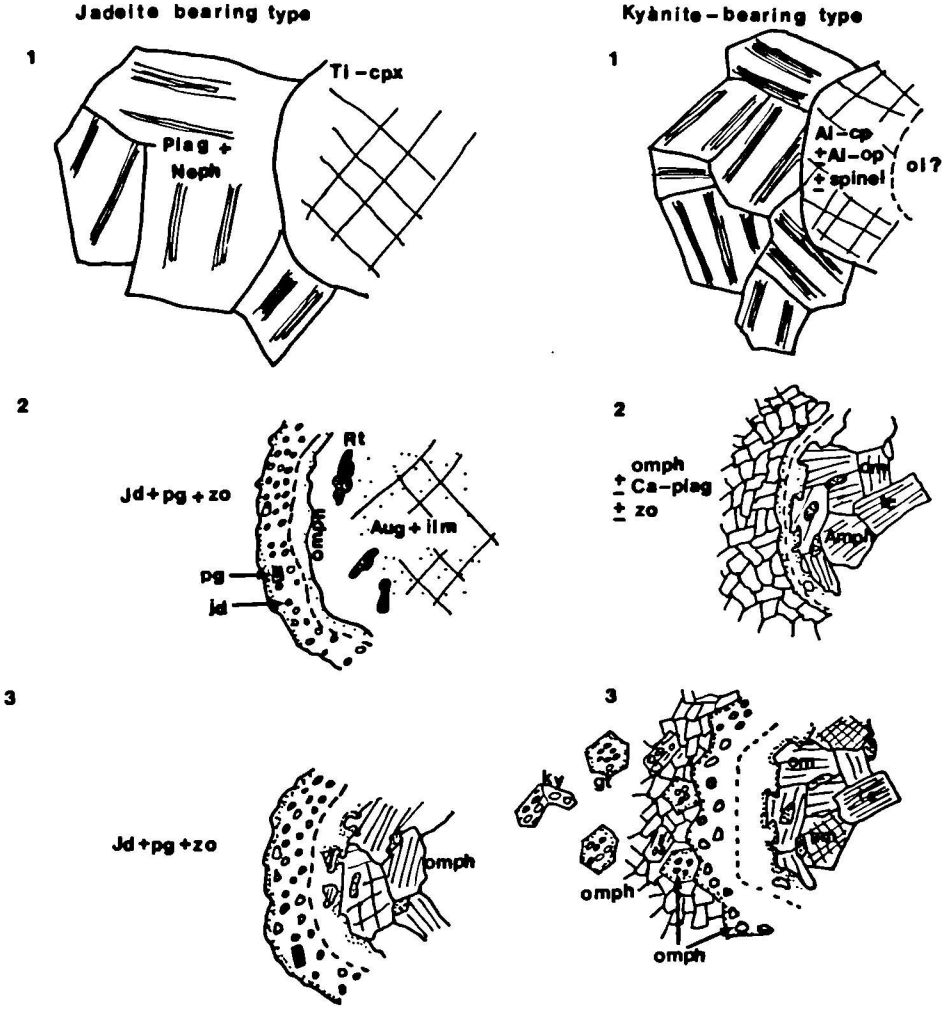
Jadeite bearing type
Kyanite-bearing type
1
Ti-cpx
Plag +
Neph
1
Al-cp
+Al-op
±spinel
ol?
2
Jd+pg+zo
Rt
omph
Aug+ilm
pg
jd
2
omph
±Ca-plag
±zo
dm
ky
Amph
3
Jd+pg+zo
omph
3
ky
gt
omph
omph
dm
ky

FIGURE 4.28 $LnK_D^{Fe/Mg}$ vs X_{Ca}^{gt} for coexisting garnet and omphacite in the coronites. Isotherms have been calculated from the expression of Ellis and Green (1979) at 16 Kbars.

Symbols:-
Circles = bimineralic coronite-eclogite (D192)
Squares = jadeite-bearing coronites (6-5.5)

Open symbols are from mafic sites, half-filled symbols from plagioclase sites and filled symbols are for inclusion-host pairs.

Figure 4-28

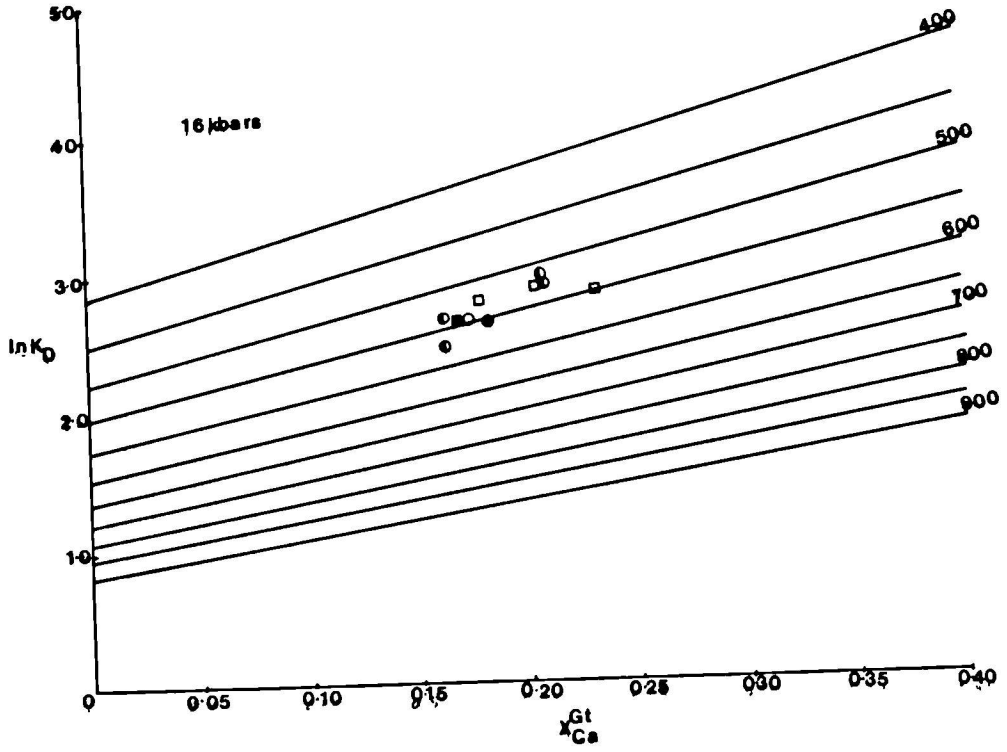
16 kbars
400
500
600
700
800
900
5·0
4·0
3·0
2·0
1·0
0
ln K_D
0·05
0·10
0·15
0·20
0·25
0·30
0·35
0·40
X_Ca^Gt

FIGURE 4.29 Petrogenetic grid constraining the evolution of the coronites. Numbered curves are:-

1: Albite = jadeite + quartz (Holland, 1980)
2: Albite + nepheline = 2 jadeite (Gasparik, 1985)
3: Paragonite = jadeite + kyanite + vapour
4: Paragonite + $DiJd_{45}$ + kyanite + vapour
5, 6, 7: Kyanite = sillimanite, kyanite = andalusite, sillimanite = andalusite (Robie and Hemingway, 1984).
8: ilmenite + kyanite + quartz = almandine + rutile (Bohlen et al, 1983)
9: Margarite + quartz = zoisite + kyanite + vapour (Jenkins, 1984).
10: Zoisite + kyanite = margarite + anorthite (Perkins et al, 1980)
11: Zoisite + kyanite = anorthite + corundum + vapour (Perkins et al, 1980)
12: Garnet in high alumina basalt composition (Green, 1967).
13: Olivine out in olivine tholeiite (Green and Ringwood, 1967).
14: Garnet = spinel + anorthite in CMAS (Gasparik, 1984).
15: Anorthite + forsterite + spinel in CMAS (Gasparik, 1984).
16: Curve 13, modified parallel to CMAS curve 15.
17: Dry solidus for olivine tholeiite (Green and Ringwood, 1967).
18: "Wet" eclogite solidus (Hill and Boettcher, 1968).

Dash-dot lines bracket range of temperatures from garnet-clinopyroxene thermometry (Ellis and Green, 1979). Stippled arrow; possible post intrusive evolution of anorthositic troctolites prior to high-pressure metamorphism.

Figure 4·29

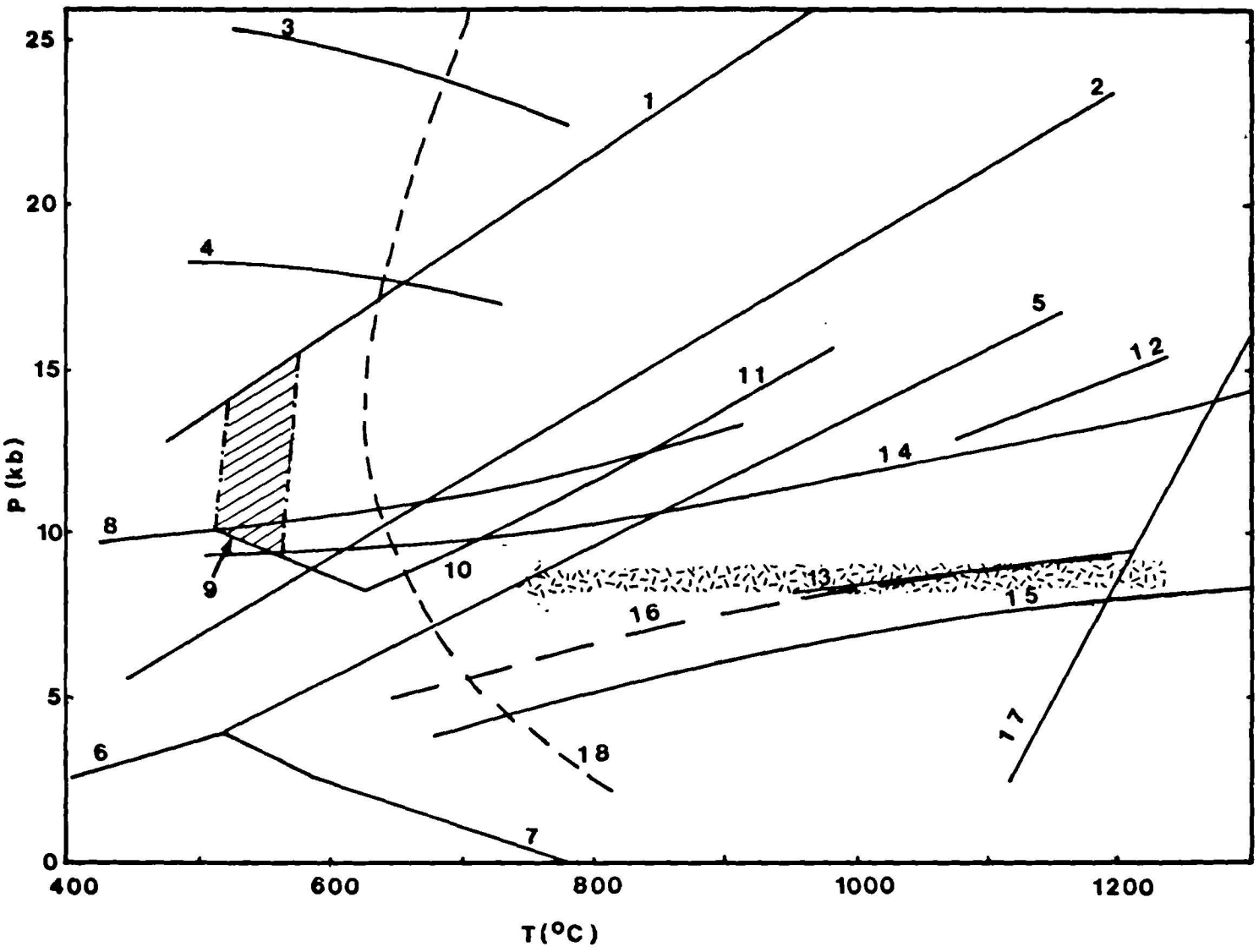
25
20
15
10
5
0
P (kb)
400
600
800
1000
1200
T(°C)
1
2
3
4
5
6
7
8
9
10
11
12
13
14
15
16
17
18

FIGURE 4.30 Schematic illustration of the different mineral assemblages likely to be encountered during up-pressure evolution of a basaltic protolith at high and low temperatures.

Figure 4.30

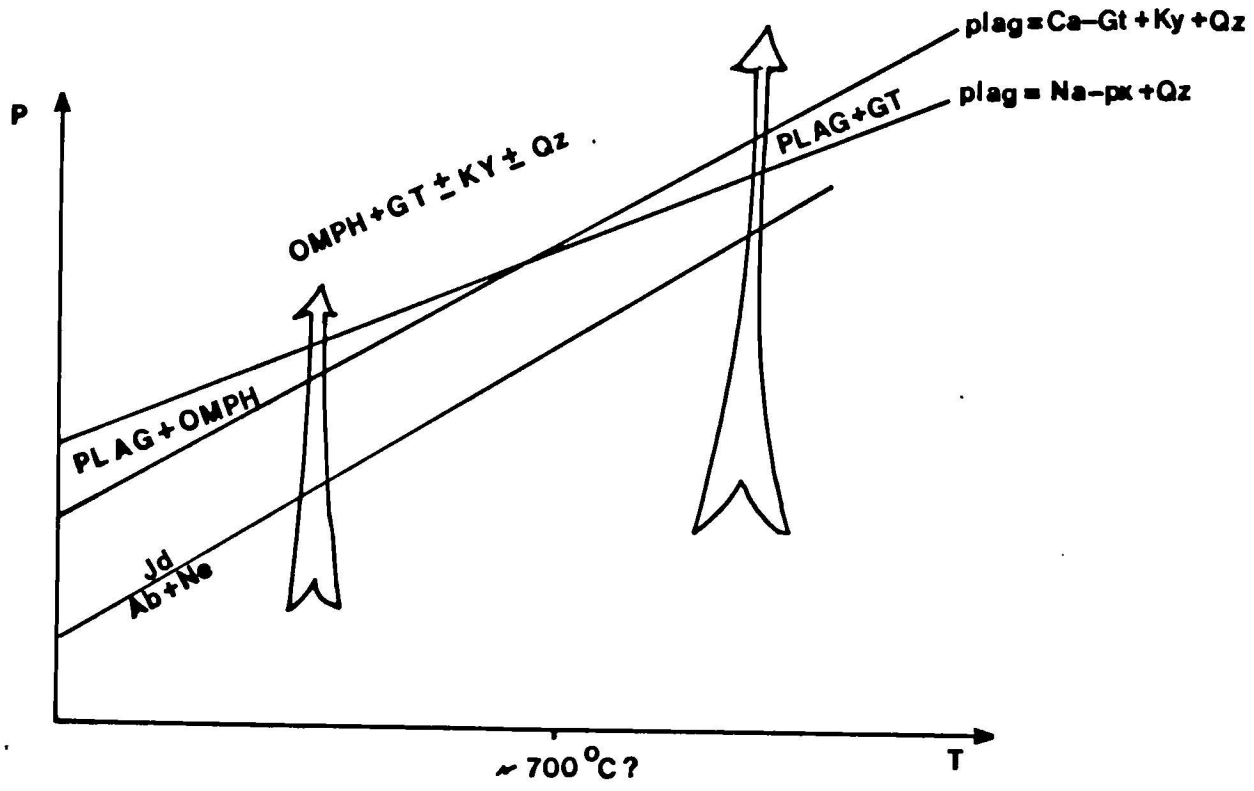
plag=Ca–Gt+Ky+Qz
plag=Na–px+Qz
P
OMPH+GT ± KY ± Qz
PLAG+GT
PLAG+OMPH
Jd
Ab+Ne
~700 °C?
T

FIGURE 4.31 Compositions of pyroxenes from a charnockitic gneiss (D99 - circles), a basaltic dyke (D134 - triangles) and two websterite samples (79/8 - inverted triangles; D45 - diamonds). Filled symbols are core compositions (usually pigmented). Open symbols are rim compositions or unpigmented pyroxenes. For D99 symbols with vertical lines are granular inclusions (possibly formed by granule exsolution). Tie-lines join pairs of coexisting pyroxenes.

Figure 4·31

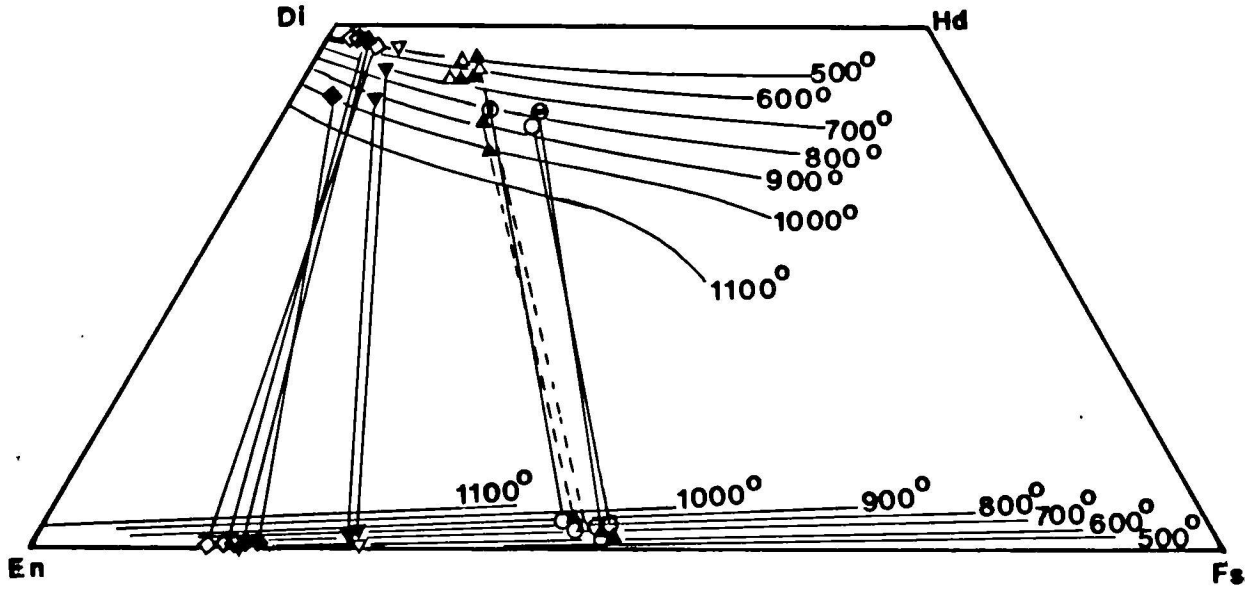
Di
Hd
En
Fs
500°
600°
700°
800°
900°
1000°
1100°
1100°
1000°
900°
800°
700°
600°
500°

FIGURE 4.32 Schematic diagram showing possible evolution of the websterites in relation to reactions in the CMASH system involving pyroxenes, spinel, olivine, amphibole, chlorite and garnet. Reaction curves are after Obata and Thompson (1981).

Figure 4·32

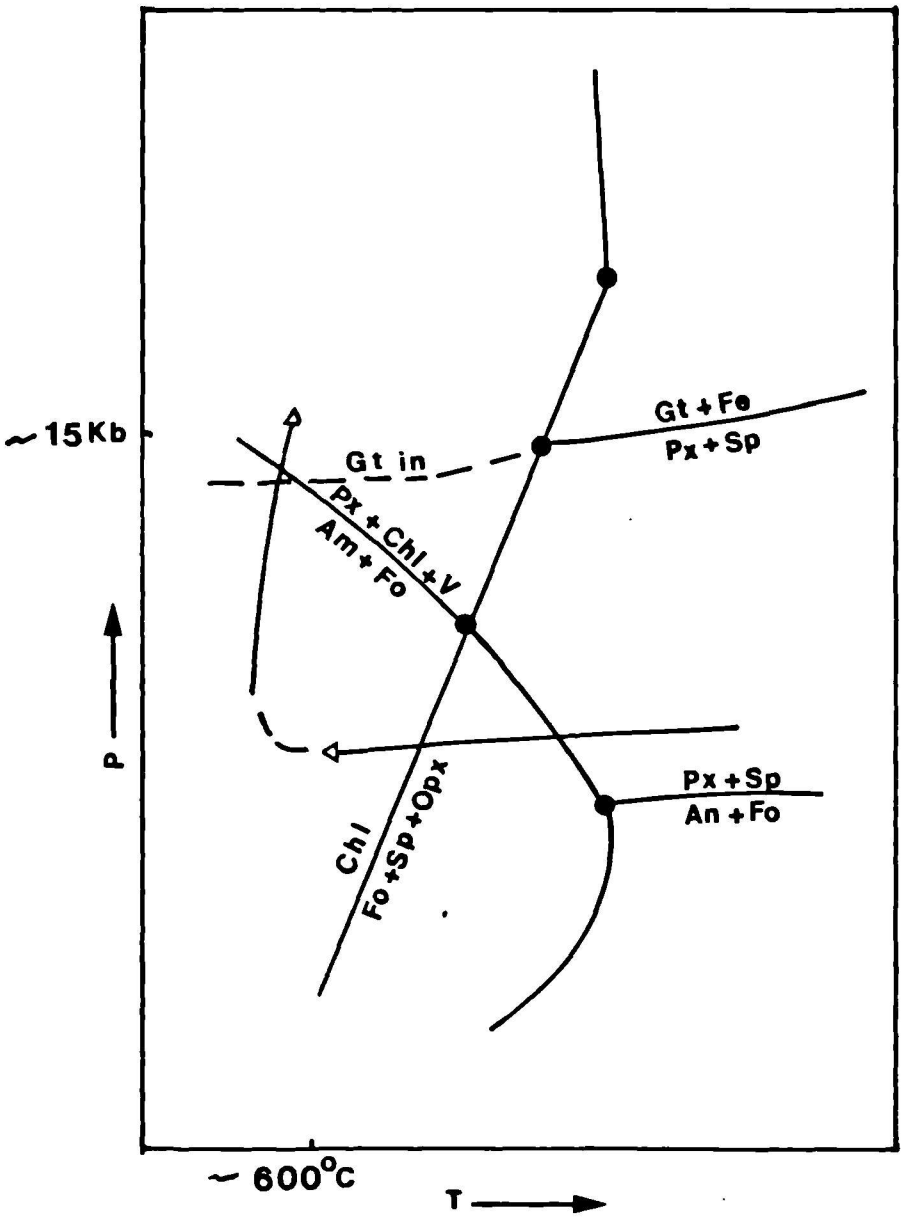
~15Kb
P
Gt in
Gt + Fe
Px + Sp
Px + Chl + V
Am + Fo
Px + Sp
An + Fo
Chl
Fo + Sp + Opx
~600°C
T

FIGURE 4.33 Compositions of garnets and omphacites in low-K gneiss D24 (Gjörlanger Unit) and psammitic phengite-gneiss D178 (Vardheia Unit). Triangles are for D24 analyses with open symbols for rims and filled symbols for cores. Squares are for D178, withopen symbols for garnet rims, half-filled symbols for the mddles of garnet atolls, symbols with a dot for inner rims of garnet atolls and filled symbols for the cores of "solid" garnets. Fields for garnets in eclogites (this work) and omphacites in eclogites (this work) are shown for reference.

Figure 4-33

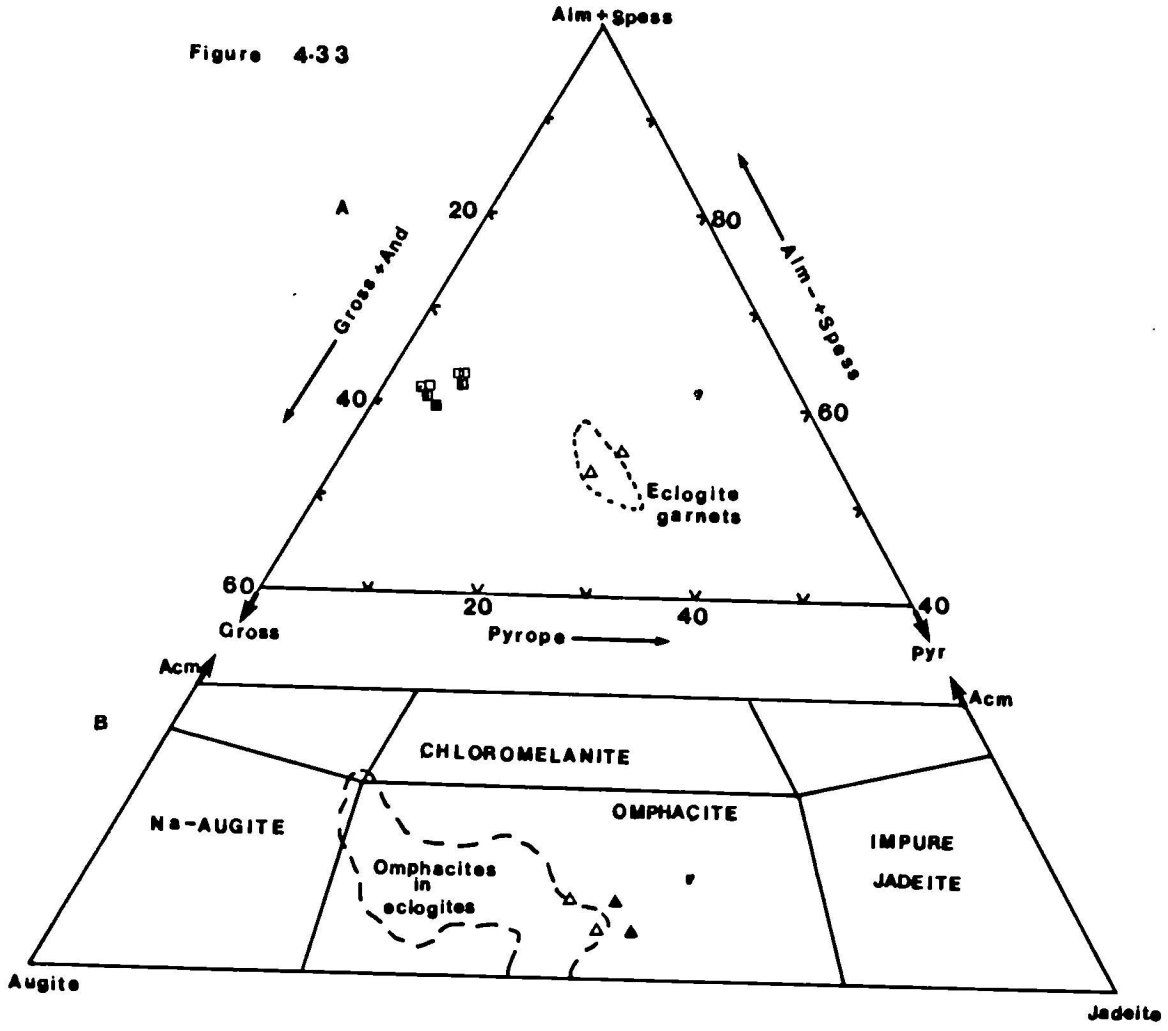
Alm+Spess
A
20
80
Gross+And
Alm+Spess
40
60
Eclogite garnets
60
20
40
40
Gross
Pyrope
Pyr
Acm
Acm
B
CHLOROMELANITE
OMPHACITE
Na-AUGITE
IMPURE JADEITE
Omphacites in eclogites
Augite
Jadeite

FIGURE 4.34 Petrogenetic grid constraining the metamorphic conditions for the low-K gneisses. Curves are:-

1: Albite = jadeite + quartz (Holland, 1980).
2: $DiJd_{50}$ + quartz minimum stability (Holland, 1983).
3: Paragonite = jadeite + kyanite + vapour (Holland, 1979b).
4: Paragonite + zoisite + quartz = liquid (Franz + Althaus, 1977).
5: Jadeite + lawsonite = paragonite + zoisite + quartz (Holland, 1979b).
6: Lawsonite + albite = paragonite + zoisite + quartz (Holland, 1979b).
7: Lawsonite = zoisite + kyanite + quartz (Perkins et al, 1980).
8: Ilmenite + kyanite + quartz = garnet + rutile (Bohlen et al, 1983).
9: Zoisite + kyanite + quartz + vapour = zoisite + kyanite + vapour + liquid (Goldsmith, 1982).
10: Zoisite + kyanite + quartz = anorthite + vapour (Jenkins, 1984).
11: Margarite + quartz = anorthite + kyanite + vapour (Jenkins, 1984).
12: Zoisite + kyanite + vapour = margarite + quartz (Jenkins, 1984).
13, 14, 15: Al-silicate stability (see figure 4.29).
16: "Wet" tonalite solidus (Stern et al, 1975).

Dash-dot line - isopleth for $K_D^{Fe/Mg}$ for a garnet-omphacite pair, K_D = 13.2, X_{Ca}^{gt} = 0.24 (Ellis and Green, 1979).
Stippled area - best estimate of peak metamorphic conditions for low-K gneiss.

Figure 4·34

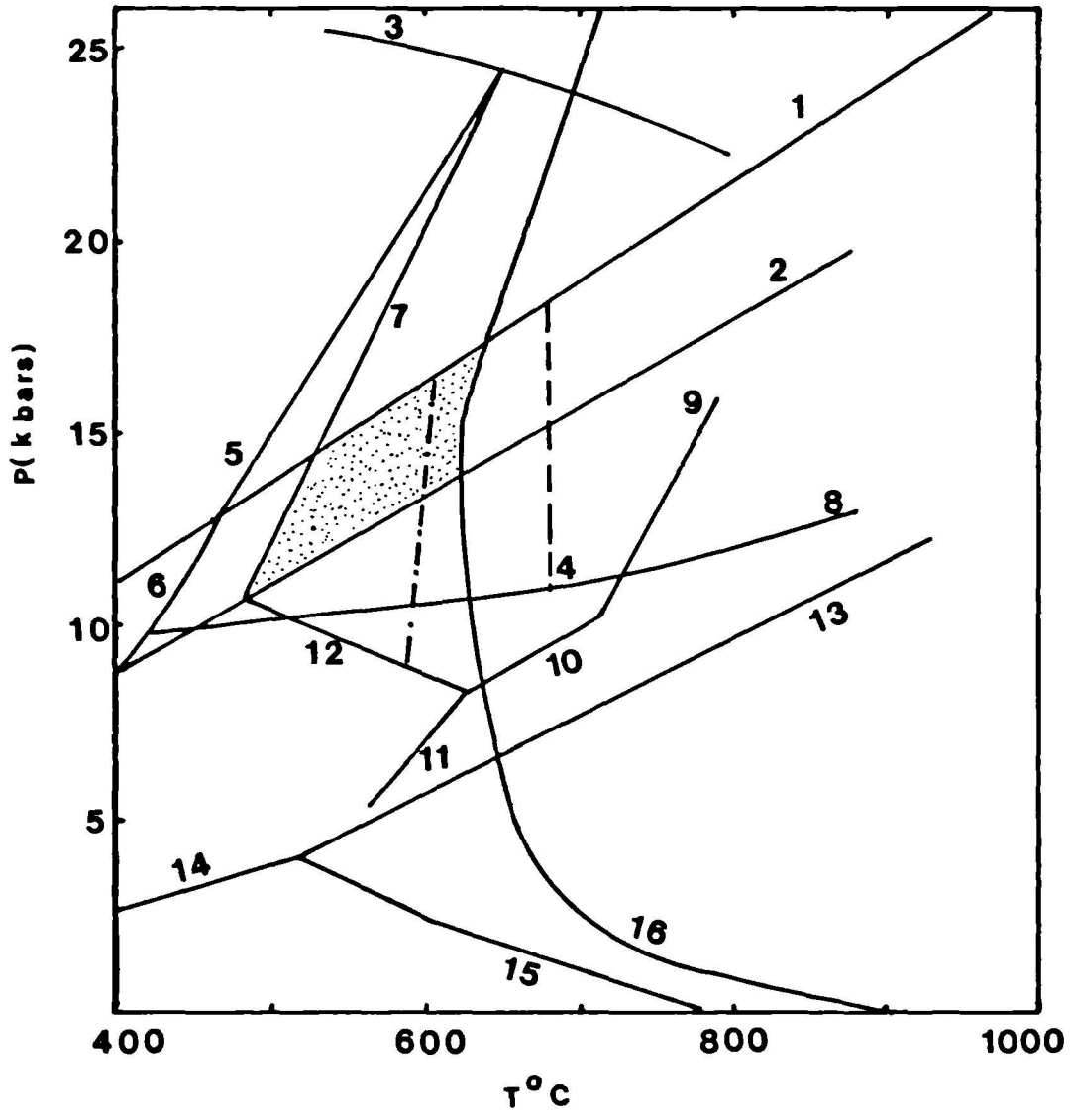
25
20
15
10
5
P(k bars)
400
600
800
1000
T°C
1
2
3
4
5
6
7
8
9
10
11
12
13
14
15
16

FIGURE 4.35 Petrogenetic grid constraining the metamorphic conditions for the psammitic phengite-gneisses. Number curves are:-

1: Albite = jadeite + quartz (Holland, 1980).
2: Staurolite + annite + quartz = almandine + muscovite (extrapolated from Rao and Johannes, 1979).
3: Zoisite + quartz = anorthite + grossular + kyanite + H_2O (Newton, 1966).
4: Epidote (PS_{33}) + quartz = garnet + anorthite + Fe-oxide + quartz + H_2O (Liou, 1973).
5: Minimum stability of phengite Si^{4+} = 3.3 (extrapolated from Velde, 1967).
6: "Wet" granite solidus (Stern et al, 1975).

Dash-dot lines - isopleths for $K_D^{Fe/Mg}$ for two garnet/phengite pairs (FeO = FeO^T) calculated from the expression of Green and Hellman (1982) for a low Ca pelite.

Stippled field - best estimate of peak metamorphic conditions for the psammitic phengite gneisses.

Figure 4·35

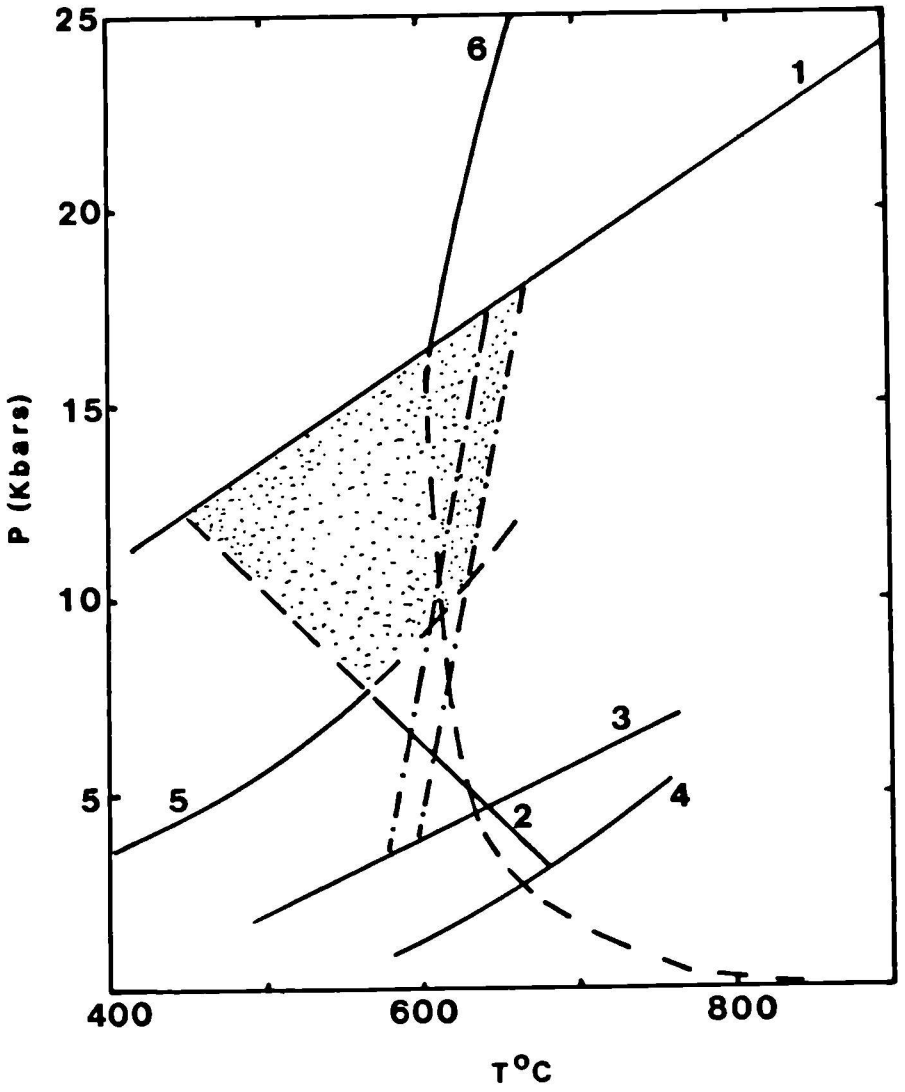

FIGURE 4.36 Summary petrogenetic grid illustrating the thermal evolution of the Hellevik-Flekke area from intrusion of the Flekke unit layered complex through granulite-facies metamorphism (M_1), amphibolite-facies metamorphism (M_2) and eclogite-facies metamorphism and subsequent uplift-related retrogression (M_3, M_4), with a possible period of near surface serpentinisation and rodingite-formation between M_1 and M_3. Stippled areas represent P-T conditions recorded by preverved mineral assemblages. See figures 4.17 and 4.29 for sources of reaction curves.

Figure 4·36

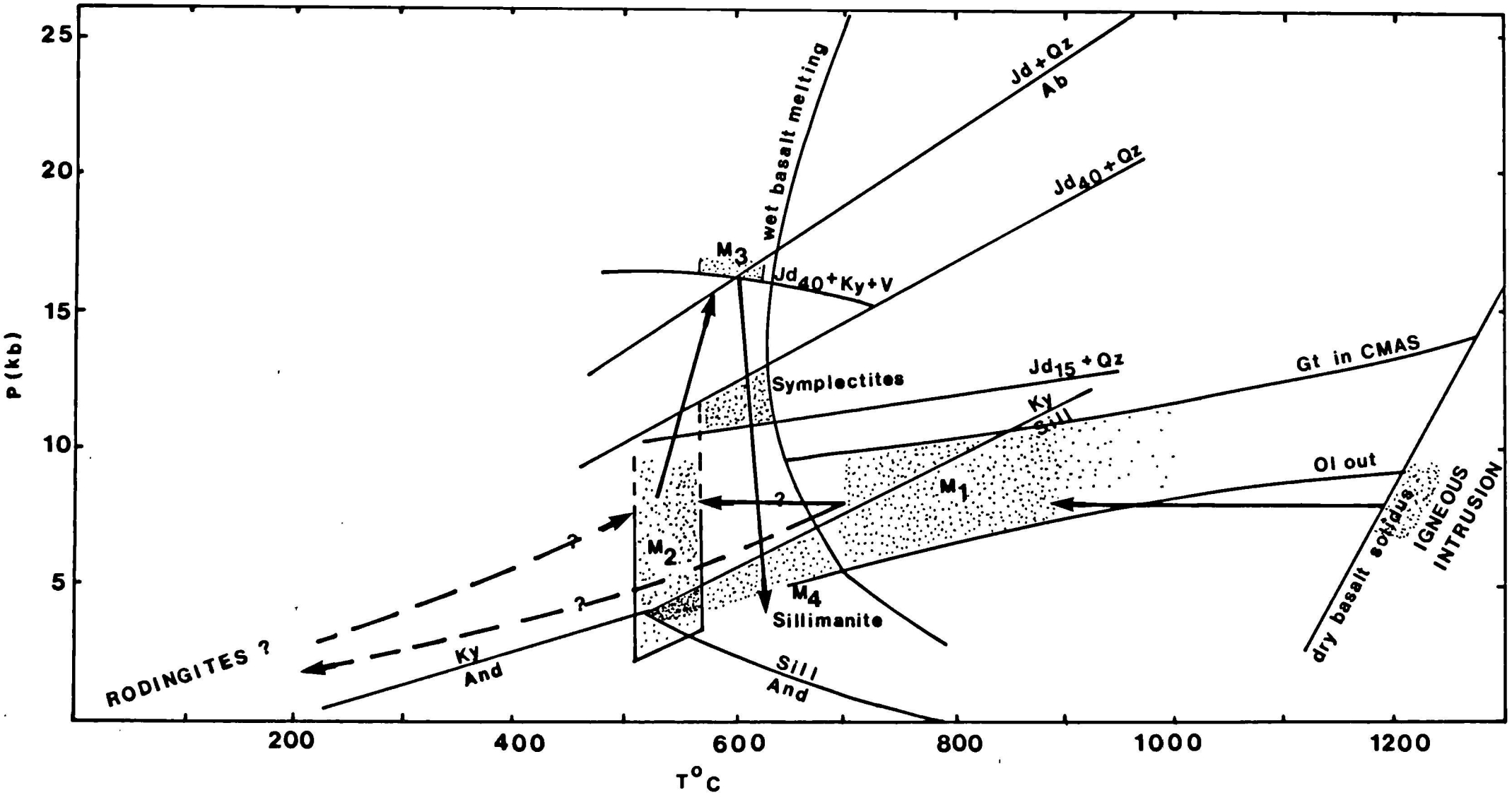
25
20
15
10
5
P (kb)
200
400
600
800
1000
1200
T°C
wet basalt melting
Jd + Qz
Ab
Jd40 + Qz
M3
Jd40 + Ky + V
Symplectites
Jd15 + Qz
Gt in CMAS
Ky
Sill
Ol out
M1
M2
M4
Sillimanite
dry basalt solidus
IGNEOUS INTRUSION
RODINGITES ?
Ky
And
Sill
And
?
?
?

TABLE 4.1 EMP analyses of clinopyroxenes from eclogites

	79/38b		D116						D69			79/9a										79/16		D77										
Sample	PBI	PBK	PAA	PAB	PAC	PAD	PAF	SME	PCR	PCQ	PCP	PAA	PAB	PAC	PAO	PAP	PAO	PAQ	PAF	PAI	PAL	PAR	PAM	PAX	PDA	PDC	PDH	PDN	PCW	PCX	PDD	PDE	PDF	PDJ	PDK	PDO
Stage	IIIR	II	II	II	IIIR	IIIR	IIIR	IV	IIIc	IIII	IIIR	II	II	II	II	IIIc	IIII	IIIR	IIIR	IIIR	IIIR	IIIR	IIIR	IIIR	IIIc	IIIc	IIIc	IIIc	IIIR	IIIR	IIIR	IIIR	IIIR	IIIR	IIIR	IIIR
SiO_2	55.44	55.69	55.67	56.01	56.37	55.99	55.86	53.75	56.20	56.76	56.83	55.52	55.65	55.35	55.68	55.72	55.91	55.37	55.82	55.69	46.94	55.57	55.49	55.75	56.48	56.44	56.73	56.39	56.75	56.39	56.61	56.53	56.56	56.54	55.87	56.04
TiO_2	0.07	0.07	0.00	0.00	0.00	0.00	0.00	0.00	0.04	0.02	0.04	0.02	0.04	0.04	0.02	0.06	0.06	0.07	0.04	0.04	0.05	0.04	0.43	0.15	0.04	0.04	0.04	0.02	0.06	0.04	0.06	0.04	0.06	0.04	0.06	0.04
Al_2O_3	8.07	7.66	10.11	10.42	10.25	10.18	10.34	4.67	10.72	11.50	11.61	8.18	8.28	8.55	8.82	8.20	9.31	7.51	7.69	6.90	14.43	7.16	8.87	9.48	10.79	11.10	11.30	11.19	11.25	10.84	11.34	10.86	11.40	11.07	10.60	10.04
Cr_2O_3	0.00	0.00	0.00	0.00	0.00	0.00	0.02	0.00	0.00	0.00	0.00	0.02	0.02	0.02	0.02	0.00	0.05	0.03	0.00	0.05	0.03	0.03	0.02	0.00	0.07	0.02	0.09	0.16	0.09	0.02	0.02	0.04	0.16	0.07	0.05	0.32
Fe_2O_3	4.90	4.96	2.97	3.33	3.30	2.56	3.31	3.28	2.64	1.80	2.14	3.06	4.50	3.06	3.29	2.96	2.66	2.33	3.10	2.69	4.77	2.80	3.03	3.49	0.62	0.64	0.27	0.06	0.06	0.00	0.23	0.44	0.12	0.78	2.96	4.08
FeO	3.69	3.76	3.26	3.06	3.01	4.10	3.00	4.40	3.50	2.86	2.87	3.43	2.39	3.20	2.78	3.07	2.97	3.36	2.95	3.37	11.09	2.99	3.17	3.27	2.78	2.56	2.57	2.84	3.08	2.53	2.51	2.85	2.90	2.66	0.52	0.19
MnO	0.03	0.03	0.02	0.03	0.00	0.02	0.02	0.13	0.05	0.00	0.02	0.00	0.00	0.03	0.00	0.00	0.00	0.00	0.00	0.05	0.31	0.00	0.00	0.00	0.03	0.06	0.10	0.03	0.10	0.05	0.06	0.06	0.10	0.06	0.00	0.06
MgO	8.26	8.50	7.80	7.73	7.87	7.91	7.61	11.15	7.60	7.72	7.49	9.29	9.15	9.33	9.23	9.86	8.99	10.11	10.10	10.42	8.17	10.45	8.68	8.35	8.62	8.72	8.65	8.64	8.76	9.10	8.72	8.89	8.50	8.58	9.00	8.75
CaO	13.40	13.41	12.67	12.40	12.24	12.41	12.37	19.25	12.32	12.08	11.73	14.66	14.97	14.65	14.97	15.56	15.14	16.58	16.01	16.31	12.40	16.78	13.89	13.54	13.50	13.12	13.30	13.21	13.23	13.96	13.03	13.40	12.89	12.86	13.67	13.47
Na_2O	6.63	6.56	7.15	7.38	7.48	7.08	7.41	3.28	7.41	7.69	7.89	5.96	6.19	5.95	6.08	5.63	6.15	5.10	5.50	5.12	3.09	5.04	6.41	6.75	6.83	7.00	7.01	6.89	6.90	6.48	6.99	6.79	7.04	7.06	7.07	7.32
Total	100.49	100.64	99.65	100.36	100.52	100.26	99.94	99.91	100.47	100.43	100.69	100.14	101.19	100.19	100.89	101.06	101.25	100.46	101.11	100.64	101.28	100.86	99.99	100.78	99.76	99.69	100.06	99.43	100.29	99.41	99.57	99.90	99.76	99.72	99.81	100.31
Si	1.992	1.999	1.995	1.991	1.999	1.996	1.994	1.970	1.994	2.001	2.000	1.992	1.978	1.983	1.980	1.981	1.979	1.985	1.986	1.994	1.729	1.985	1.988	1.983	2.003	2.000	2.001	2.002	2.000	2.002	2.004	2.001	2.001	2.003	1.980	1.982
Ti	0.002	0.002	0.000	0.000	0.000	0.000	0.000	0.000	0.001	0.001	0.001	0.001	0.001	0.001	0.001	0.002	0.002	0.002	0.001	0.001	0.001	0.001	0.012	0.004	0.001	0.001	0.001	0.001	0.002	0.001	0.002	0.001	0.002	0.001	0.002	0.001
Al^{IV}	0.008	0.001	0.005	0.009	0.001	0.004	0.006	0.030	0.006	0.000	0.000	0.008	0.022	0.017	0.020	0.019	0.021	0.015	0.014	0.006	0.271	0.015	0.012	0.017	0.000	0.000	0.000	0.000	0.000	0.000	0.000	0.000	0.000	0.000	0.020	0.018
Al^{VI}	0.334	0.323	0.422	0.428	0.427	0.424	0.429	0.172	0.442	0.478	0.482	0.338	0.325	0.344	0.350	0.325	0.367	0.302	0.308	0.285	0.356	0.286	0.363	0.381	0.451	0.464	0.470	0.468	0.467	0.454	0.473	0.453	0.475	0.462	0.423	0.401
Cr	0.000	0.000	0.000	0.000	0.000	0.000	0.000	0.000	0.000	0.000	0.000	0.001	0.001	0.001	0.001	0.001	0.001	0.001	0.001	0.001	0.001	0.001	0.001	0.000	0.002	0.001	0.003	0.004	0.003	0.001	0.001	0.001	0.004	0.002	0.001	0.009
Fe^{3+}	0.132	0.134	0.080	0.089	0.088	0.069	0.089	0.091	0.070	0.048	0.057	0.083	0.120	0.083	0.088	0.079	0.071	0.063	0.083	0.073	0.132	0.075	0.082	0.093	0.017	0.017	0.007	0.002	0.002	0.000	0.006	0.012	0.003	0.021	0.079	0.109
Fe^{2+}	0.111	0.113	0.098	0.091	0.089	0.122	0.090	0.135	0.104	0.084	0.084	0.103	0.071	0.096	0.083	0.091	0.088	0.101	0.088	0.101	0.342	0.089	0.095	0.097	0.082	0.076	0.076	0.084	0.091	0.075	0.074	0.084	0.086	0.079	0.016	0.006
Mn	0.001	0.001	0.001	0.001	0.000	0.001	0.001	0.004	0.002	0.000	0.001	0.000	0.000	0.001	0.000	0.000	0.000	0.000	0.000	0.002	0.010	0.000	0.000	0.000	0.001	0.002	0.003	0.001	0.003	0.002	0.002	0.002	0.003	0.002	0.000	0.002
Mg	0.442	0.455	0.417	0.410	0.416	0.420	0.405	0.609	0.402	0.406	0.393	0.497	0.485	0.498	0.489	0.522	0.474	0.540	0.530	0.556	0.449	0.556	0.464	0.443	0.456	0.460	0.455	0.457	0.460	0.482	0.460	0.469	0.450	0.453	0.475	0.461
Ca	0.516	0.516	0.486	0.472	0.465	0.474	0.473	0.756	0.468	0.456	0.442	0.564	0.570	0.563	0.570	0.593	0.574	0.637	0.610	0.626	0.489	0.642	0.533	0.516	0.513	0.498	0.503	0.503	0.500	0.531	0.494	0.508	0.489	0.488	0.519	0.510
Na	0.462	0.456	0.497	0.509	0.514	0.490	0.513	0.233	0.510	0.526	0.538	0.415	0.427	0.413	0.419	0.388	0.422	0.354	0.379	0.355	0.221	0.349	0.445	0.446	0.470	0.481	0.480	0.474	0.472	0.446	0.480	0.466	0.483	0.485	0.486	0.502
Jad	32.95	32.26	41.67	41.96	42.63	42.07	42.35	14.26	43.95	43.78	48.17	33.16	30.57	33.02	33.05	30.89	34.97	29.08	29.63	28.16	8.75	27.29	36.30	37.22	45.11	46.34	46.99	46.84	46.73	44.56	47.31	45.31	47.55	46.23	40.53	38.45
Acm	13.24	13.39	8.01	8.92	8.80	6.88	8.89	9.05	7.04	4.78	5.68	8.25	12.04	8.26	8.81	7.92	7.10	6.29	8.31	7.25	13.23	7.52	8.18	9.34	1.67	1.70	0.71	0.16	0.17	-	0.61	1.18	0.31	2.08	7.90	10.85
Di-tbl	50.97	51.38	48.13	46.38	46.40	47.06	46.74	72.65	46.40	45.57	44.13	55.65	54.96	54.71	55.08	57.54	55.49	62.36	59.72	62.09	21.99	62.79	52.17	50.35	51.20	49.70	50.17	50.21	49.80	53.00	49.25	50.72	48.72	48.71	49.08	46.86

Table 4.1 (contd.)

	D83a			D181		D205								D206		
	PAK	PAM	PAN	PAP	PAQ	PAC	PAD	PAE	PAG	PAF	PAA	PBL		PBZ	PCB	PBH
	IIIc	IIIc	IIIR	IIIR	IIIR	II	II	II	II	II	IIIR	IIIR	PAP			
SiO_2	56.70	56.21	56.10	56.46	56.69	55.66	55.95	56.14	55.83	56.32	56.01	57.04	55.82	54.71	54.95	55.01
TiO_2	0.06	0.04	0.06	0.04	0.04	0.04	0.06	0.04	0.06	0.04	0.04	0.04	0.04	0.04	0.06	0.06
Al_2O_3	10.69	9.10	8.81	11.04	11.17	8.93	9.22	9.35	9.15	10.17	9.29	9.65	9.42	5.14	6.22	5.59
Cr_2O_3	0.04	0.03	0.14	0.02	0.00	0.00	0.00	0.00	0.00	0.00	0.00	0.03	0.00	0.02	0.02	0.00
Fe_2O_3	2.31	2.86	2.88	1.84	1.31	5.03	4.54	4.37	4.70	3.98	2.64	2.92	2.53	5.28	5.01	4.99
FeO	2.33	2.35	2.67	2.17	2.66	2.64	2.54	2.37	2.73	2.61	2.70	2.58	2.55	4.66	4.45	3.67
MnO	0.08	0.10	0.06	0.05	0.06	0.02	0.02	0.00	0.00	0.00	0.00	0.03	0.02	0.02	0.02	0.05
MgO	8.50	9.18	9.14	8.41	8.22	8.04	8.19	8.01	7.93	7.71	8.96	8.63	8.91	9.45	8.89	9.61
CaO	13.16	14.35	14.25	12.94	12.94	13.09	13.28	12.70	12.34	12.32	14.06	13.46	14.09	15.76	14.87	15.71
Na_2O	7.21	6.48	6.44	7.28	7.29	7.08	7.07	7.37	7.35	7.60	6.54	7.01	6.53	5.12	5.69	5.33
Total	101.08	100.71	100.55	100.25	100.38	100.53	100.87	100.35	100.11	100.76	100.24	101.38	99.91	100.20	100.18	100.02
Si	1.992	1.993	1.995	1.994	1.999	1.988	1.988	1.999	1.997	1.995	1.994	2.004	1.993	1.997	1.997	2.000
Ti	0.002	0.001	0.002	0.001	0.001	0.001	0.002	0.001	0.002	0.001	0.001	0.001	0.001	0.001	0.002	0.000
Al^{IV}	0.008	0.007	0.005	0.006	0.001	0.012	0.012	0.001	0.003	0.005	0.006	0.000	0.007	0.003	0.003	0.000
Al^{VI}	0.435	0.373	0.364	0.453	0.463	0.364	0.374	0.391	0.383	0.420	0.384	0.400	0.389	0.218	0.263	0.240
Cr_{3+}	0.001	0.001	0.004	0.001	0.000	0.000	0.000	0.000	0.000	0.000	0.000	0.001	0.000	0.001	0.001	0.000
Fe^{3+}	0.061	0.076	0.077	0.049	0.035	0.135	0.121	0.117	0.127	0.106	0.071	0.077	0.068	0.145	0.137	0.137
Fe^{2+}	0.068	0.070	0.079	0.064	0.078	0.079	0.076	0.071	0.082	0.077	0.080	0.076	0.076	0.142	0.135	0.112
Mn	0.002	0.003	0.002	0.001	0.002	0.001	0.001	0.000	0.001	0.000	0.000	0.001	0.001	0.001	0.001	0.002
Mg	0.445	0.485	0.484	0.443	0.432	0.428	0.434	0.425	0.423	0.407	0.475	0.452	0.474	0.514	0.481	0.521
Ca	0.495	0.545	0.543	0.490	0.489	0.501	0.506	0.485	0.473	0.467	0.536	0.507	0.539	0.616	0.579	0.612
Na	0.491	0.445	0.444	0.498	0.499	0.490	0.487	0.509	0.510	0.522	0.452	0.478	0.452	0.362	0.401	0.376
Jad	42.88	36.83	36.30	44.90	46.36	35.51	36.56	39.18	38.34	41.57	38.07	39.96	38.40	21.68	26.33	23.91
AcM	6.11	7.64	7.71	4.89	3.49	13.53	12.15	11.71	12.65	10.62	7.08	7.71	6.80	14.49	13.70	13.65
Di-Hd	48.84	53.91	53.99	48.43	48.79	49.06	49.54	48.36	47.15	46.31	53.18	50.56	53.28	61.42	57.74	61.03

TABLE 4.02 EMP analyses of amphiboles from eclogites

	D116	79/9a	79/16	D123															
Sample	AAE	AAA	AAC	ADQ	ADN	ADU	ADV	ADO	ADR	ADS	ADT	ADW	ADX	ADY	AAS	AAT	ADK	ADL	ADG	ADH
Stage	IV	IV	IV	I	I	I	I	I	I	I	I	I	I	I	I	I	IVr	IVr	IVr	IVr
SiO_2	43.40	44.75	47.96	49.63	51.78	53.86	50.70	53.16	53.47	53.02	44.50	53.36	53.23	52.84	53.03	51.19	51.33	47.15	51.83	50.49
TiO_2	0.60	0.22	0.27	0.15	0.11	0.05	0.09	0.07	0.07	0.07	0.09	0.05	0.07	0.05	0.07	0.02	0.0	0.11	0.09	0.09
Al_2O_3	13.76	14.71	12.58	6.88	6.59	4.21	7.28	5.03	4.54	5.35	12.55	4.90	4.96	4.19	5.21	4.64	10.80	13.43	9.49	11.73
Fe_2O_3	6.57	3.43	5.37	6.27	6.91	7.20	7.72	5.64	5.24	5.74	11.36	4.84	5.42	3.90	7.12	8.38	5.86	8.25	7.43	6.31
FeO	9.45	9.97	7.03	6.14	5.21	3.98	4.65	6.24	6.62	6.29	7.16	6.88	6.44	7.29	5.12	3.82	1.79	1.63	0.68	2.65
MnO	0.03	0.08	0.06	0.08	0.08	0.10	0.03	0.11	0.11	0.06	0.14	0.05	0.03	0.03	0.00	0.00	0.05	0.05	0.05	0.06
MgO	10.16	10.89	12.32	14.26	15.30	16.41	14.91	16.05	16.16	15.92	10.28	16.14	16.07	16.12	15.81	16.29	15.87	14.48	16.47	14.74
CaO	8.87	9.86	8.09	9.56	9.66	9.97	9.58	9.83	9.95	9.77	8.62	9.74	9.81	9.81	9.69	9.80	8.16	8.51	8.04	7.57
Na_2O	3.98	3.34	3.90	2.08	1.90	1.49	2.01	1.69	1.60	1.71	3.29	1.60	1.68	1.41	1.88	1.67	3.39	3.60	3.30	3.87
K_2O	-	0.24	0.33	0.11	0.07	0.10	0.10	0.10	0.06	0.08	0.10	0.08	0.10	0.10	0.10	0.10	0.18	0.18	0.14	0.19
TOTAL	96.90	97.49	97.39	95.16	98.33	97.37	97.07	97.92	97.82	98.01	98.09	97.64	97.81	95.74	98.03	95.91	97.49	97.39	97.52	97.70
T Si	6.406	6.506	6.829	7.251	7.326	7.627	7.222	7.498	7.550	7.471	6.479	7.542	7.513	7.616	7.462	7.374	7.124	6.647	7.184	7.033
Al^{IV}	1.594	1.494	1.170	0.749	0.674	0.373	0.778	0.502	0.450	0.529	1.521	0.458	0.487	0.384	0.538	0.626	0.856	1.352	0.816	0.967
C Al^{VI}	0.797	1.023	0.939	0.434	0.423	0.329	0.443	0.333	0.305	0.358	0.630	0.357	0.338	0.326	0.325	0.161	0.889	0.876	0.732	0.957
Fe^{3+}	0.728	0.375	0.575	0.688	0.724	0.424	0.827	0.597	0.556	0.607	1.243	0.514	0.575	0.422	0.752	0.908	0.611	0.873	0.774	0.661
Ti	0.066	0.024	0.029	0.016	0.012	0.005	0.010	0.007	0.007	0.007	0.010	0.005	0.007	0.005	0.007	0.002	0.006	0.012	0.009	0.009
Mg	2.234	2.358	2.614	3.103	3.224	3.461	3.163	3.372	3.399	3.341	2.229	3.398	3.378	3.460	3.314	3.495	3.281	3.041	3.400	3.058
Fe^{2+}	1.164	1.210	0.836	0.748	0.606	0.781	0.554	0.690	0.733	0.685	0.871	0.726	0.702	0.786	0.601	0.434	0.207	0.192	0.079	0.308
Mn	0.009	0.010	0.007	0.010	-	-	0.003	-	-	-	0.017	-	-	-	-	-	0.006	0.006	0.006	0.007
B Fe^{2+}	-	-	-	-	0.009	0.071	-	0.044	0.048	0.055	-	0.086	0.057	0.092	-	0.026	-	-	-	-
Mn	-	-	-	-	0.009	0.012	-	0.013	0.013	0.007	-	0.006	0.004	0.004	-	-	-	-	-	-
Ca	1.400	1.532	1.232	1.493	1.461	1.509	1.459	1.482	1.502	1.472	1.342	1.472	1.480	1.511	1.458	1.509	1.211	1.283	1.191	1.127
Na	0.600	0.468	0.768	0.507	0.520	0.408	0.541	0.461	0.437	0.466	0.658	0.437	0.459	0.393	0.512	0.465	0.789	0.717	0.809	0.873
A Na	0.536	0.471	0.307	0.081	-	-	0.013	-	-	-	0.268	-	-	-	-	-	0.121	0.264	0.076	0.170
K	-	0.044	0.060	0.020	0.013	0.018	0.018	0.018	0.011	0.014	0.018	0.014	0.018	0.018	0.018	0.018	0.032	0.032	0.025	0.038
Method	13eCNK	13eCNK	13eCNK	13eCNK	15eK	15eK	13eCNK	15eK	15eK	15eK	13eCNK	15eK	15eK	15eK	13eCNK	15eK	13eCNK	13eCNK	13eCNK	13eCNK

	D205			D206								
Sample	AAE	AAC	AAB	AAG	ACP	ACX	ACG	AAM	AAH	AAI	AAJ	ACS
Stage	I	IVr	IVr	I	I	I	I	II	II	II	II	II
SiO_2	45.22	49.16	48.71	41.01	41.01	47.11	49.44	52.97	49.14	51.53	52.99	53.07
TiO_2	0.48	0.20	0.24	0.44	0.11	0.16	0.20	0.09	0.33	0.11	0.11	0.07
Al_2O_3	14.55	11.48	11.77	14.66	15.91	10.03	7.10	4.78	7.98	6.60	4.90	4.58
Fe_2O_3	6.50	2.03	2.86	8.65	6.90	9.61	6.64	6.20	7.80	7.24	6.51	5.26
FeO	11.63	8.51	8.53	15.76	6.90	6.63	6.96	5.97	7.16	5.71	5.31	6.15
MnO	0.00	0.00	0.00	0.34	0.03	0.02	0.03	0.00	0.02	0.02	0.00	0.02
MgO	8.65	12.87	12.64	4.86	7.94	11.77	13.29	15.82	13.08	14.74	15.81	16.04
CaO	7.92	8.28	8.17	7.95	9.08	8.53	8.88	9.85	9.01	9.41	9.55	9.36
Na_2O	4.43	4.17	4.29	4.31	3.78	2.88	2.35	1.87	2.67	2.12	1.92	1.87
K_2O	0.06	0.18	0.16	0.15	0.15	0.12	0.16	0.24	0.14	0.16	0.13	0.13
TOTAL	99.44	97.45	97.37	98.13	91.81	96.86	95.05	97.79	97.33	97.64	97.23	96.55
T Si	6.518	7.018	6.971	6.215	6.166	6.855	7.256	7.495	7.089	7.317	7.511	7.572
Al^{IV}	1.482	0.982	1.029	1.784	1.834	1.145	0.743	0.505	0.911	0.683	0.489	0.428
C Al^{VI}	0.987	0.947	0.954	0.831	0.982	0.573	0.483	0.292	0.444	0.420	0.329	0.341
Fe^{3+}	0.703	0.282	0.307	0.985	0.779	1.051	0.732	0.659	0.845	0.772	0.693	0.564
Ti	0.052	0.021	0.026	0.050	0.012	0.017	0.022	0.009	0.036	0.012	0.012	0.007
Mg	1.857	2.736	2.694	1.097	1.778	2.551	2.905	3.334	2.811	3.117	3.338	3.409
Fe^{2+}	1.400	1.014	1.019	1.994	1.444	0.805	0.853	0.706	0.862	0.677	0.629	0.678
Mn	-	-	-	0.043	0.004	0.002	0.004	-	0.002	0.002	-	-
B Fe^{2+}	-	-	-	-	-	-	-	-	-	-	-	0.054
Mn	-	-	-	-	-	-	-	-	-	-	-	0.024
Ca	1.220	1.264	1.250	1.288	1.459	1.327	1.394	1.490	1.389	1.428	1.447	1.428
Na	0.779	0.736	0.750	0.712	0.540	0.673	0.607	0.509	0.610	0.572	0.526	0.516
A Na	0.455	0.415	0.437	0.551	0.559	0.137	0.060	0.002	0.135	0.012	-	-
K	0.011	0.033	0.029	0.029	0.029	0.022	0.030	0.043	0.026	0.029	0.023	0.024
Method	13eCNK	13eCNK	13eCNK	13eCNK	13eCNK	13eCNK	13eCNK	13eCNK	13eCNK	13eCNK	13eCNK	15eK

	D206 (cont.)														
Sample	AAW	ABC	ABE	ABG	ABI	ABK	ABN	AAN	AAO	AAP	AAQ	ADC	ADD	ADE	ADF
Stage	IIIr	IIIr	III	IIIr	IIIr	IIIr	IIIr	IIIr	IIIi	IIIi	IVc	IIIr	IIIc	IIIr	IIIc
SiO_2	48.34	47.37	52.46	53.07	53.79	52.75	50.54	52.21	52.25	54.23	34.32	48.93	52.94	49.82	82.01
TiO_2	0.33	0.18	0.40	0.09	0.13	0.13	0.20	0.13	0.15	0.02	0.05	0.18	0.13	0.16	0.16
Al_2O_3	9.88	10.27	5.40	4.36	3.59	5.04	6.89	5.43	5.12	2.93	3.03	9.50	5.08	7.82	5.85
Fe_2O_3	5.07	5.87	5.17	4.98	3.53	5.44	5.53	6.59	3.74	4.76	4.34	6.42	6.18	6.38	6.00
FeO	8.60	8.91	6.77	6.93	7.99	6.71	7.71	5.85	7.63	6.25	6.79	7.22	5.33	7.40	6.46
MnO	0.02	0.03	0.03	0.02	0.00	0.00	0.02	0.00	0.00	0.00	0.00	0.05	0.05	0.06	0.05
MgO	12.59	11.66	15.15	15.70	15.83	15.51	13.91	15.28	14.96	16.87	16.74	12.86	15.67	13.19	14.86
CaO	9.47	9.47	9.49	9.93	9.45	10.08	9.69	9.30	9.23	9.30	9.46	9.02	9.17	9.05	9.37
Na_2O	2.79	2.46	2.16	1.67	1.74	1.79	2.15	2.27	2.41	1.85	1.73	2.77	2.20	2.49	2.23
K_2O	0.13	0.12	0.12	0.10	0.14	0.12	0.11	0.17	0.22	0.16	0.12	0.11	0.11	0.10	0.11
TOTAL	97.22	96.34	97.15	96.86	95.14	97.57	96.75	97.23	95.71	96.37	96.49	97.06	96.98	96.47	97.10
T Si	6.984	6.932	7.474	7.578	7.721	7.488	7.290	7.435	7.559	7.737	7.735	7.044	7.523	7.211	7.422
Al^{IV}	1.016	1.068	0.526	0.422	0.279	0.512	0.710	0.565	0.441	0.263	0.265	0.956	0.476	0.789	0.578
C Al^{VI}	0.665	0.701	0.379	0.311	0.328	0.331	0.459	0.345	0.431	0.229	0.241	0.654	0.373	0.544	0.405
Fe^{3+}	0.550	0.645	0.554	0.534	0.381	0.580	0.599	0.705	0.407	0.510	0.465	0.694	0.660	0.694	0.644
Ti	0.036	0.020	0.044	0.010	0.014	0.014	0.022	0.014	0.016	0.002	0.005	0.019	0.014	0.017	0.017
Mg	2.709	2.542	3.215	3.339	3.386	3.279	2.988	3.241	3.224	3.585	3.557	2.758	3.317	2.844	3.159
Fe^{2+}	1.037	1.088	0.806	0.806	0.892	0.795	0.929	0.695	0.922	0.673	0.729	0.868	0.632	0.894	0.793
Mn	0.002	0.004	0.004	-	-	-	0.002	-	-	-	-	0.006	0.004	0.007	0.006
B Fe^{2+}	-	-	-	0.020	0.066	-	-	-	-	0.071	0.080	-	-	-	-
Mn	-	-	-	0.002	-	-	-	-	-	-	-	-	0.002	-	-
Ca	1.463	1.482	1.445	1.516	1.451	1.529	1.494	1.416	1.428	1.418	1.443	1.388	1.393	1.400	1.430
Na	0.537	0.518	0.554	0.461	0.483	0.470	0.506	0.584	0.572	0.511	0.477	0.612	0.605	0.599	0.570
A Na	0.242	0.178	0.040	-	-	0.021	0.094	0.041	0.102	-	-	0.159	-	0.097	0.045
K	0.024	0.022	0.022	0.018	0.026	0.022	0.020	0.031	0.040	0.029	0.022	0.020	0.019	0.018	0.020
Method	13eCNK	13eCNK	13eCNK	15eK	15eK	13eCNK	13eCNK	13eCNK	13eCNK	15eK	15eK	13eCNK	15eK	13eCNK	13eCNK

TABLE 4.03 EMP analyses of phengites and biotites from eclogites

	79/38b-1		D116			D77													79/38	D116	
	MAC	MAD	MAI	MAJ	MAK	MAG	MAH	MAI	MAJ	MAK	MAL	MAM	MAN	MAP	MAQ	MAR	MAS	MAT	MAU	MAA	MAM	MAQ
	i	c	r	c	r	r	c	r	r	r	r	c	r	r	c	r	r	r	r	s	s	s
SiO_2	49.84	49.34	50.01	50.07	50.41	51.05	48.49	48.04	48.91	49.14	47.87	48.11	47.89	49.21	46.68	48.76	49.88	49.13	49.58	36.04	35.48	35.63
TiO_2	0.57	0.57	0.44	0.54	0.54	0.26	0.30	0.32	0.30	0.30	0.20	0.22	0.22	0.30	0.30	0.30	0.26	0.30	0.28	3.61	1.60	3.75
Al_2O_3	23.51	23.53	25.22	24.73	25.04	27.55	28.36	28.24	27.96	25.57	29.43	29.07	29.25	27.50	28.03	27.82	26.76	27.80	27.73	15.19	17.73	17.92
FeO^T	3.18	3.10	2.68	2.17	2.34	1.46	1.24	1.22	1.08	1.19	1.12	1.23	1.18	1.65	1.23	1.27	1.35	1.38	1.26	17.33	16.88	13.06
MnO	0.00	0.00	0.03	0.00	0.00	0.06	0.06	0.06	0.05	0.06	0.06	0.05	0.05	0.06	0.03	0.03	0.06	0.03	0.05	0.06	0.08	0.08
MgO	3.92	3.89	3.88	3.88	3.96	3.65	3.20	3.25	3.35	3.46	2.99	3.07	2.86	3.37	3.35	3.13	3.73	3.48	3.51	12.34	12.38	13.17
CaO	0.00	0.00	0.00	0.00	0.00	0.00	0.00	0.00	0.01	0.01	0.01	0.00	0.00	0.01	0.00	0.00	0.01	0.01	0.00	0.00	0.09	-
Na_2O	0.41	0.37	0.45	0.48	0.48	0.57	0.89	1.03	0.93	0.84	1.23	1.13	1.16	0.59	1.06	0.54	0.72	0.76	0.81	0.34	0.24	0.39
K_2O	10.46	10.55	10.33	10.56	10.51	9.82	9.72	10.22	9.22	9.59	9.06	9.23	9.24	9.87	9.53	9.81	8.86	9.72	9.77	9.56	9.78	9.76
Si	6.957	6.935	6.864	6.911	6.895	6.821	6.650	6.612	6.705	6.734	6.565	6.595	6.583	6.735	6.675	6.721	6.838	6.709	6.738	5.520	5.427	5.380
Al^{IV}	1.043	1.065	1.135	1.089	1.105	1.179	1.350	1.388	1.295	1.266	1.435	1.405	1.417	1.265	1.325	1.279	1.162	1.291	1.262	2.480	2.573	2.620
Al^{VI}	2.821	2.827	2.940	2.929	2.926	3.155	3.229	3.188	3.217	3.182	3.316	3.286	3.316	3.186	3.199	3.235	3.156	3.179	3.175	0.259	0.620	0.565
Ti	0.050	0.060	0.045	0.056	0.055	0.026	0.031	0.033	0.031	0.031	0.021	0.023	0.023	0.031	0.031	0.031	0.027	0.031	0.029	0.415	0.184	0.425
Fe^T	0.371	0.364	0.307	0.250	0.267	0.163	0.142	0.140	0.124	0.136	0.128	0.141	0.135	0.188	1.14	0.146	0.155	0.157	0.143	2.216	2.156	1.646
Mn	0.000	0.000	0.004	0.000	0.000	0.007	0.007	0.007	0.006	0.007	0.007	0.006	0.006	0.007	0.004	0.004	0.007	0.003	0.006	0.008	0.010	0.010
Mg	0.815	0.814	0.793	0.798	0.807	0.726	0.654	0.666	0.684	0.706	0.611	0.627	0.586	0.687	0.684	0.643	0.762	0.708	0.711	2.815	2.821	2.962
Ca	0.000	0.000	0.000	0.000	0.000	0.000	0.000	0.000	0.002	0.002	0.002	0.000	0.000	0.002	0.000	0.000	0.002	0.002	0.000	0.000	0.015	-
Na	0.111	0.101	0.119	0.128	0.127	0.147	0.236	0.274	0.247	0.223	0.326	0.300	0.308	0.156	0.281	0.144	0.191	0.201	0.213	0.101	0.071	0.114
K	1.859	1.888	1.805	1.856	1.830	1.670	1.697	1.791	1.644	1.673	1.582	1.611	1.617	1.720	1.664	1.722	1.547	1.690	1.691	1.864	1.905	1.876

i - inclusion in garnet c - core r - rim s - symplectite after phengite

TABLE 4.04 EMP analyses of zoisites from eclogites

	D77						D123
	EAB	EAC	EAD	EAF	EAG	EAH	
SiO_2	38.94	38.91	38.74	38.83	38.93	38.81	39.17
TiO_2	0.06	0.02	0.04	0.02	0.04	0.04	0.06
Al_2O_3	30.76	30.69	30.87	30.35	30.23	30.05	32.38
Fe_2O_3	2.14	2.28	1.84	2.34	2.28	1.88	1.91
MnO	0.03	0.03	0.03	0.02	0.00	0.02	0.02
MgO	0.02	0.03	0.02	0.02	0.03	0.08	0.00
CaO	24.57	23.79	23.25	22.89	24.08	23.55	24.35
Si	3.023	3.038	3.045	3.063	3.048	3.067	2.986
Al	2.810	2.820	2.856	2.819	2.786	2.795	2.896
Ti	0.004	0.001	0.002	0.001	0.002	0.002	0.004
Cr	-	-	-	-	-	-	-
Fe^{3+}	0.125	0.134	0.109	0.139	0.134	0.112	0.110
Mn	0.002	0.002	0.003	0.001	0.000	0.001	0.001
Mg	0.002	0.004	0.002	0.002	0.003	0.009	-
Ca	2.039	1.986	1.953	1.931	2.015	1.990	1.989
SUM	8.006	7.984	7.971	7.957	7.990	7.977	8.001

TABLE 4.05 EMP analyses of garnets from eclogites

	79/38b				D116					D69		79/9a									79/16	D77										
Sample	GLV	GLW	GLT	GMA	GAG	GAH	GAI	GAJ	GAU	GFI	GFJ	GAA	GAB	GAE	GAG	GAI	GAF	GAN	GAC	GAD	GAU	GFR	GFS	GFT	GFU	GFV	GFY	GFX	GFZ	GGA	GGC	GFW	GGT	GGS	GGR	GGQ
	III	IIc	IIIr	IIa	III	IIc	IIIr	IIIr	IIIr	Ic	IIIr	Ic	III	IIIr	Ic	IIIr	III	IIIr	III	III	III	Ic	III	IIIr	IIIr	IIIr	Ic	IIIr	IIIr	IIIr	IIIr	IIIr	Ir	III	IIIr
SiO_2	38.23	38.15	37.96	38.06	38.27	39.41	38.26	38.16	38.29	38.77	38.56	37.66	38.17	38.58	38.35	38.55	38.69	38.30	39.93	38.26	37.82	38.49	39.31	39.81	39.92	39.58	38.50	39.60	39.84	39.94	39.60	39.91	39.60	36.30	38.66	39.87
TiO_2	0.00	0.00	0.00	0.00	0.02	0.16	0.02	0.02	0.07	0.05	0.05	0.00	0.00	0.00	0.00	0.00	0.00	0.00	0.00	0.00	0.00	0.07	0.02	0.02	0.02	0.00	0.04	0.02	0.02	0.00	0.00	0.00	0.02	0.04	0.05	0.00
Al_2O_3	21.34	21.13	21.12	21.03	21.28	20.75	21.17	21.42	21.16	21.63	21.74	21.11	21.39	21.55	21.42	21.50	21.59	21.48	19.97	21.44	20.51	21.78	22.28	22.46	22.64	22.39	21.75	22.57	22.53	22.55	22.51	22.60	22.55	22.09	21.68	22.48
Cr_2O_3	0.00	0.00	0.00	0.00	0.02	0.02	0.00	0.02	0.02	0.00	0.00	0.00	0.00	0.00	0.00	0.00	0.00	0.00	0.00	0.00	0.00	0.00	0.00	0.00	0.00	0.00	0.00	0.00	0.00	0.00	0.00	0.00	0.00	0.00	0.00	0.00
Fe_2O_3	1.83	1.78	1.19	1.96	0.79	0.00	0.80	0.98	0.31	0.45	0.12	3.19	1.95	1.76	2.14	1.60	1.28	1.75	0.70	2.35	3.00	0.34	0.03	0.00	0.00	0.29	0.062	0.00	0.00	0.00	0.00	0.00	0.18	0.33	0.64	0.25
FeO	28.17	28.20	28.96	26.19	28.21	27.90	28.33	28.96	27.34	25.78	27.68	24.02	24.61	24.62	23.65	24.99	25.27	24.04	24.21	24.43	24.47	25.47	22.75	21.78	21.20	22.13	26.38	21.84	21.24	21.33	21.83	21.72	21.84	21.40	25.69	21.35
MnO	0.57	0.49	0.57	0.45	0.54	0.59	0.59	0.54	0.53	0.63	0.73	3.31	0.96	0.40	1.11	0.63	0.40	0.56	0.60	0.57	0.57	0.45	0.28	0.33	0.31	0.37	0.22	0.00	0.36	0.34	0.39	0.39	0.42	0.48	0.34	0.42
MgO	5.58	5.98	5.53	4.99	5.28	4.80	5.40	5.56	4.87	5.14	5.15	3.29	4.52	5.58	5.12	5.92	6.05	5.87	7.00	5.18	5.00	4.01	7.68	9.04	9.41	8.41	4.20	8.92	9.52	9.41	8.97	9.50	9.12	7.33	4.74	9.37
CaO	5.48	4.89	4.68	7.78	5.94	6.31	5.63	4.86	7.25	8.64	6.78	9.21	9.37	8.71	9.33	7.74	7.65	8.37	8.16	8.98	8.79	10.16	8.04	7.11	7.12	7.68	9.35	7.24	7.05	7.14	7.12	6.58	6.91	9.43	9.20	7.18
TOTAL	101.20	100.62	100.01	100.47	100.35	99.94	100.20	100.53	99.84	100.99	100.81	101.79	100.96	101.21	101.12	100.93	100.94	100.38	100.57	101.22	100.16	100.76	100.39	100.55	100.62	100.85	101.06	100.19	100.56	100.71	100.42	100.70	100.62	100.39	101.00	100.93
Si	5.939	5.952	5.972	5.948	5.988	6.161	5.995	5.965	6.014	5.996	5.994	5.873	5.928	5.942	5.925	5.951	5.964	5.936	6.147	5.911	5.928	5.978	5.994	6.011	6.005	5.987	5.971	5.998	6.000	6.008	5.993	6.006	5.982	5.992	5.980	5.994
Ti	0.000	0.000	0.000	0.000	0.002	0.019	0.002	0.002	0.008	0.006	0.006	0.000	0.000	0.000	0.000	0.000	0.000	0.000	0.000	0.000	0.000	0.008	0.002	0.002	0.002	0.000	0.005	0.002	0.002	0.000	0.000	0.000	0.002	0.005	0.006	0.000
Al	3.908	3.886	3.916	3.874	3.924	3.824	3.910	3.947	3.917	3.944	3.986	3.880	3.916	3.912	3.901	3.912	3.923	3.924	3.624	3.904	3.790	3.987	4.004	3.997	4.014	3.992	3.976	4.029	4.000	3.998	4.015	4.009	4.011	3.970	3.953	3.983
Cr	0.000	0.000	0.000	0.000	0.002	0.002	0.000	0.002	0.002	-	-	0.000	0.000	0.000	0.000	0.000	0.000	0.000	0.000	0.000	0.000	0.000	0.000	0.000	0.000	0.000	0.000	0.000	0.000	0.000	0.000	0.000	0.000	0.000	0.000	0.000
Fe^{3+}	0.214	0.209	0.141	0.231	0.093	0.000	0.094	0.116	0.036	0.052	0.014	0.375	0.228	0.204	0.249	0.186	0.149	0.204	0.081	0.273	0.354	0.039	0.004	0.000	0.000	0.034	0.072	0.000	0.000	0.000	0.000	0.000	0.021	0.037	0.075	0.029
Fe^{2+}	3.660	3.680	3.810	3.423	3.692	3.648	3.713	3.787	3.591	3.334	2.598	3.132	3.196	3.171	3.056	3.226	3.258	3.117	3.117	3.157	3.208	3.308	2.901	2.750	2.667	2.799	3.422	2.767	2.675	2.683	2.763	2.734	2.759	2.728	3.324	2.684
Mn	0.075	0.065	0.076	0.060	0.072	0.078	0.078	0.072	0.071	0.066	0.078	0.437	0.126	0.052	0.145	0.082	0.052	0.074	0.078	0.075	0.076	0.059	0.036	0.042	0.090	0.047	0.029	0.000	0.046	0.043	0.050	0.050	0.054	0.062	0.045	0.053
Mg	1.292	1.391	1.296	1.162	1.231	1.118	1.261	1.295	1.140	1.184	1.192	0.765	1.046	1.281	1.179	1.362	1.390	1.356	1.606	1.193	1.168	0.928	1.745	2.034	2.110	1.986	0.971	2.014	2.137	2.110	2.023	2.131	2.053	1.666	1.093	2.099
Ca	0.912	0.818	0.789	1.303	0.996	1.067	0.945	0.814	1.220	1.416	1.128	1.539	1.559	1. 37	1.545	1.280	1.264	1.390	1.346	1.487	1.476	1.691	1.314	1.150	1.148	1.245	1.554	1.175	1.138	1.151	1.155	1.061	1.118	1.541	1.525	1.157

TABLE 4.05 (Cont'd)

Sample	D83a GAB	D83a GAC	D181 GBH	D181 GBA	D181 GBS	D181 GBR	D181 GDO
	Ir	IIIr	Ic	IIIr	IIa	IIa	IIIr
SiO_2	38.62	36.69	38.77	38.86	38.75	37.63	39.00
TiO_2	0.07	0.09	0.05	0.04	0.07	0.12	0.00
Al_2O_3	21.50	21.69	21.70	21.79	21.63	21.01	21.77
Cr_2O_3	0.00	0.03	0.02	0.02	0.02	0.02	0.00
Fe_2O_3	0.58	0.98	1.37	1.02	0.84	1.65	0.70
FeO	23.60	25.23	21.60	21.70	21.30	23.66	22.95
MnO	0.74	0.70	0.48	0.50	0.84	3.56	0.48
MgO	5.01	7.04	7.46	7.11	6.27	2.75	7.86
CaO	10.21	6.13	8.60	9.07	10.20	10.10	7.17
TOTAL	100.24	100.59	100.06	100.11	99.92	100.50	99.93
Si	5.992	5.961	6.951	5.964	5.976	5.934	5.989
Ti	0.008	0.010	0.006	0.005	0.008	0.014	0.000
Al	3.932	3.939	3.926	3.942	3.932	3.905	3.941
Cr	0.000	0.004	0.002	0.002	0.002	0.002	0.000
Fe^{3+}	0.068	0.114	0.159	0.118	0.097	0.196	0.080
Fe^{2+}	3.062	3.252	2.773	2.786	2.748	3.12	2.948
Mn	0.097	0.091	0.062	0.065	0.110	0.476	0.062
Mg	1.158	1.617	1.706	1.626	1.441	0.646	1.799
Ca	1.682	1.012	1.414	1.492	1.686	1.707	1.180

Sample	D123 GGY	D123 GFU	D123 GIF	D123 GIQ	D123 GKQ	D123 GVO	D123 GGK	D123 GJR	D123 GJR
	Ic	Ic	Ic	Ic	Ic	IIi	IIIc	IIIr	IIIr
SiO_2	38.40	38.43	39.01	38.34	38.26	37.83	39.36	39.66	39.66
TiO_2	0.00	0.00	0.00	0.00	0.00	0.05	0.04	0.00	0.00
Al_2O_3	21.47	21.76	21.99	21.66	21.57	21.53	22.24	22.38	22.38
Cr_2O_3	0.00	0.00	0.00	0.00	0.00	0.00	0.02	0.00	0.00
Fe_2O_3	1.69	0.01	0.01	0.01	0.00	1.76	0.00	0.00	0.00
FeO	25.67	26.00	23.90	27.14	26.49	25.32	22.98	21.72	21.72
MnO	0.43	0.79	0.20	0.62	0.77	0.29	0.12	0.11	0.11
MgO	4.28	4.13	6.22	3.63	4.11	4.48	8.23	9.10	9.10
CaO	8.42	9.47	9.06	8.94	9.12	9.12	7.90	7.42	7.42
TOTAL	100.36	100.59	100.39	100.39	100.32	100.38	100.89	100.39	100.39
Si	6.012	5.986	6.000	6.006	5.988	5.909	5.972	5.998	5.998
Ti	-	-	-	-	-	0.006	0.004	-	-
Al	3.962	3.994	3.986	4.000	3.978	3.964	3.978	3.990	3.990
Cr	-	-	-	-	-	0.000	0.002	-	-
Fe^{3+}	0.200	0.002	0.000	0.000	0.000	0.207	0.000	0.000	0.000
Fe^{2+}	3.362	3.388	3.074	3.556	3.466	3.307	2.916	2.748	2.748
Mn	0.058	0.104	0.026	0.082	0.102	0.038	0.016	0.014	0.014
Mg	0.900	0.960	1.426	0.896	0.958	1.043	1.862	2.052	2.052
Ca	1.412	1.582	1.492	1.500	1.530	1.526	1.284	1.202	1.202

Sample	D205 GIQ	D205 GGF	D205 GGI	D205 GGE	D205 GGH	D205 GDM	D205 GOO	D205 GDQ	D205 GEX	D205 GFS	D205 GAA	D205 GNN	D205 GOR
	Ic	IIi	IIIr	Ii	IIIr	Ic	IIi	IIi	IIi	IIi	IIIr	IIIr	IIIr
SiO_2	37.90	38.39	38.36	37.96	39.04	37.78	38.29	38.41	38.29	38.11	38.71	38.25	38.76
TiO_2	0.00	0.00	0.00	0.00	0.00	0.00	0.00	0.00	0.00	0.00	0.00	0.00	0.00
Al_2O_3	20.47	21.39	21.17	21.40	21.83	20.77	21.37	21.60	21.19	21.09	21.43	21.73	21.57
Cr_2O_3	0.00	0.00	0.00	0.00	0.00	0.00	0.00	0.00	0.00	0.00	0.00	0.00	0.00
Fe_2O_3	2.16	1.35	1.41	1.91	0.82	1.22	1.72	1.37	1.33	1.82	1.20	1.81	1.16
FeO	24.79	25.84	24.01	26.99	24.12	27.61	24.80	25.62	26.76	28.13	25.05	23.72	24.87
MnO	1.00	0.15	0.23	0.28	0.17	2.67	0.63	0.15	0.14	0.23	0.29	0.25	0.02
MgO	4.23	5.43	6.82	4.58	7.31	2.52	5.16	5.35	5.06	4.32	6.54	6.98	6.66
CaO	9.35	7.99	7.39	7.77	7.31	8.09	8.70	8.29	7.70	7.42	7.25	7.28	7.48
TOTAL	99.90	100.53	99.39	100.89	100.59	100.66	100.67	100.79	100.47	101.12	100.47	100.02	100.53
Si	5.971	5.963	5.974	5.921	5.982	5.987	5.944	5.949	5.973	5.952	5.979	5.914	5.973
Ti	0.000	0.000	0.000	0.000	0.000	0.000	0.000	0.000	0.000	0.000	0.000	0.000	0.000
Al	3.801	3.916	3.886	3.934	3.943	3.880	3.910	3.943	3.896	3.882	3.902	3.960	3.918
Cr	0.000	0.000	0.000	0.000	0.000	0.000	0.000	0.000	0.000	0.000	0.000	0.000	0.000
Fe^{3+}	0.256	0.157	0.165	0.224	0.094	0.145	0.201	0.159	0.157	0.214	0.140	0.211	0.135
Fe^{2+}	3.266	3.357	3.128	3.520	3.090	3.660	3.220	3.319	3.491	3.674	3.236	3.067	3.206
Mn	0.133	0.020	0.030	0.037	0.022	0.358	0.083	0.020	0.019	0.030	0.038	0.033	0.003
Mg	0.993	1.257	1.583	1.065	1.669	0.595	1.194	1.235	1.176	1.005	1.506	1.608	1.530
Ca	1.578	1.330	1.233	1.299	1.200	1.374	1.447	1.376	1.287	1.242	1.200	o.206	1.235

Sample	D206 GLL	D206 GEG	D206 GEI	D206 GLN	D206 GLO	D206 GLP	D206 GLQ	D206 GLM
	Ic	IIi	IIi	IIi	IIi	IIi	IIi	IIIr
SiO_2	37.79	38.48	38.64	37.84	37.78	37.96	37.67	38.41
TiO_2	0.00	0.04	0.02	0.00	0.00	0.00	0.00	0.00
Al_2O_3	20.37	21.27	21.39	21.09	20.60	20.64	20.76	21.34
Cr_2O_3	0.00	-	-	0.00	0.00	0.00	0.00	0.00
Fe_2O_3	1.17	0.00	0.00	2.10	0.00	0.00	1.72	1.22
FeO	27.26	27.78	27.95	26.78	28.56	29.43	27.88	27.45
MnO	2.92	0.09	0.14	0.23	1.83	0.34	0.55	0.25
MgO	2.21	3.80	4.29	4.68	3.08	2.83	3.02	5.07
CaO	8.61	9.02	8.28	7.72	8.34	9.28	8.76	7.17
TOTAL	100.33	100.48	100.71	100.44	100.19	100.48	100.36	100.91
Si	6.018	6.026	6.026	5.929	6.006	6.014	5.961	5.973
Ti	0.000	0.004	0.002	0.000	0.000	0.000	0.000	0.000
Al	3.824	3.924	3.930	3.895	3.860	3.864	3.872	3.911
Cr	0.000	-	-	0.000	0.000	0.000	0.000	0.000
Fe^{3+}	0.140	0.000	0.000	0.247	0.000	0.000	0.020	0.143
Fe^{2+}	3.631	3.638	3.646	3.509	3.800	3.900	3.690	3.570
Mn	0.394	0.012	0.018	0.031	0.246	0.044	0.074	0.033
Mg	0.525	0.886	0.996	1.093	0.730	0.668	0.712	1.175
Ca	1.469	1.512	1.322	1.296	1.420	1.574	1.486	1.195

Sample	D206 GIS	D206 GVR	D206 GXT	D206 GXU	D206 GYX	D206 GYY	D206 GZX	D206 GZY
	IIIr	IIIr	IIIr	IIIr	IIIr	IIIr	IIIr	IIIr
SiO_2	38.07	38.36	38.30	38.51	38.47	38.37	38.59	38.02
TiO_2	0.00	0.02	0.04	0.40	0.02	0.05	0.04	0.05
Al_2O_3	21.26	21.32	21.24	21.24	21.46	21.17	21.43	21.19
Cr_2O_3	0.00	0.05	-	-	-	-	-	-
Fe_2O_3	1.86	0.00	0.00	0.00	0.00	0.00	1.20	0.00
FeO	27.53	27.75	27.75	27.41	29.06	27.27	26.49	28.06
MnO	0.28	0.26	0.31	0.15	0.35	0.09	0.23	0.39
MgO	5.19	4.96	4.16	4.64	4.91	4.02	5.03	4.05
CaO	6.60	7.26	8.51	7.83	6.38	9.08	7.57	7.50
TOTAL	100.80	100.08	100.31	100.21	100.65	100.05	100.58	99.26
Si	5.937	6.008	6.006	6.018	6.008	6.024	6.014	6.024
Ti	0.000	0.002	0.004	0.046	0.002	0.006	0.048	0.006
Al	3.908	3.936	3.928	3.912	3.948	3.916	3.936	3.956
Cr	0.000	0.004	-	-	-	-	-	-
Fe^{3+}	0.219	0.000	0.000	0.000	0.000	0.000	0.140	0.000
Fe^{2+}	3.591	3.636	3.640	3.586	3.796	3.582	3.452	3.720
Mn	0.037	0.034	0.040	0.024	0.046	0.012	0.030	0.050
Mg	1.206	1.158	0.972	1.080	1.142	0.940	1.096	0.956
Ca	1.103	1.234	1.430	1.310	1.168	1.528	1.262	1.272

TABLE 4.06 EMP analyses of pyroxenes in coronites

	D170																		D194					D187			6-5.5									
Sample	PAE	PAF	PAB	PAD	PAA	PAB	PDP	PDQ	HAA	HAB	HAD	HAA	HAB	HAC	HAD	HAE	HAS	HAT	PAV	PAW	PAX	PAY	PAZ	JAG	JAH	INB	PAA	PAD	PAF	PAG	PAH	PAI	PAJ	PAL	PAM	PAN	IAA	IAB
	C-ig	R-ig	C-ig	R-ig	C-ig	R-ig	s	s	C-ig	C-ig	R-ig	R-ig	C-ig	R-ig	R-ig	R-ig	s	s	tr	tr	tr	tr	tr	pl	pl	I-pl	C-ma	C-ma	C-ma	C-ma	C-ma	C-ma	C-ma	R-ma	C-ma	C-ma	I-pl	I-pl
SiO_2	49.20	49.57	49.49	48.91	49.22	49.56	50.12	50.46	52.51	52.36	52.58	52.37	52.28	53.12	51.99	52.82	52.27	52.25	50.38	50.86	53.16	51.61	52.91	60.23	59.21	56.03	59.03	56.24	55.82	56.41	56.13	55.87	56.33	56.02	56.38	56.28	56.60	55.93
TiO_2	1.02	0.91	1.05	1.02	0.92	0.83	0.48	0.41	0.14	0.25	0.07	0.11	0.25	0.09	0.13	0.13	0.05	0.05	0.48	1.09	0.37	1.68	0.63	0.00	0.00	0.00	0.06	0.07	0.06	0.06	0.04	0.06	0.06	0.04	0.06	0.06	0.00	0.00
Al_2O_3	6.51	6.11	6.42	6.31	6.20	6.62	4.77	4.37	4.26	4.26	4.04	4.00	4.18	3.92	4.34	4.12	3.89	4.12	6.45	6.02	5.26	4.58	4.44	24.54	23.93	23.75	10.60	10.39	8.83	11.09	11.31	10.72	11.26	10.63	11.56	10.09	13.33	13.34
Cr_2O_3	0.02	0.05	0.02	0.03	0.03	0.02	0.02	0.02	0.00	0.00	0.02	0.00	0.02	0.02	0.02	0.02	0.02	0.03	0.05	0.03	0.02	0.05	0.02	0.00	0.00	0.00	0.00	0.05	0.02	0.00	0.02	0.02	0.02	0.05	0.02	0.05	0.00	0.00
Fe_2O_3	1.19	1.67	1.76	1.64	1.75	1.65	1.68	1.65	0.00	0.00	0.00	0.00	0.00	0.00	0.00	0.00	0.00	0.00	8.03	7.03	4.94	4.73	3.71	0.00	0.00	0.25	3.28	2.51	3.07	0.98	2.02	1.98	3.08	2.76	1.92	2.74	0.70	2.60
FeO	5.44	4.95	5.27	5.12	6.14	5.78	5.40	5.49	17.48	16.93	18.81	17.01	16.70	17.41	18.82	17.11	17.31	17.22	0.57	1.16	1.59	2.38	2.15	1.06	0.90	1.30	1.44	1.72	1.71	1.45	0.63	2.21	1.25	1.45	1.82	1.42	1.85	1.94
MnO	0.21	0.17	0.17	0.19	0.22	0.17	0.17	0.19	0.41	0.39	0.30	0.36	0.32	0.33	0.38	0.32	0.36	0.35	0.05	0.05	0.06	0.05	0.02	0.00	0.00	0.00	0.02	0.02	0.02	0.02	0.02	0.02	0.02	0.02	0.02	0.03	0.00	0.00
MgO	13.13	12.79	13.10	12.93	13.35	12.98	13.95	14.15	25.34	25.20	24.42	25.45	25.00	25.88	24.53	25.26	25.35	25.27	12.86	13.24	12.57	13.17	12.93	0.26	0.41	0.69	8.69	8.78	9.74	9.23	9.07	8.64	8.18	8.73	8.31	9.27	7.87	7.27
CaO	21.50	22.33	22.64	22.25	20.97	22.42	23.19	23.00	0.64	1.37	0.38	0.48	1.33	0.50	0.56	0.33	0.34	0.33	17.33	16.42	18.07	18.49	19.72	0.98	1.14	1.54	13.41	13.67	15.02	14.09	13.85	13.20	12.81	13.25	12.52	14.40	11.84	10.53
Na_2O	0.68	0.77	0.69	0.65	0.69	0.65	0.66	0.65	0.02	0.00	0.00	0.00	0.00	0.00	0.00	0.00	0.00	0.02	3.22	3.44	3.60	2.94	2.88	14.48	14.33	14.25	7.10	6.99	6.14	6.80	7.03	6.97	7.57	7.12	7.50	6.67	7.90	8.30
TOTAL	98.90	99.32	100.61	99.05	99.53	100.09	100.44	100.40	100.79	100.76	100.62	99.84	100.11	101.30	100.79	100.11	99.65	99.70	99.42	99.34	99.64	99.68	99.41	101.55	99.92	100.82	100.63	100.44	100.43	100.13	100.11	99.69	100.59	100.08	100.11	101.01	100.09	99.91
Si	1.836	1.844	1.823	1.827	1.833	1.837	1.853	1.866	1.896	1.892	1.910	1.905	1.980	1.906	1.890	1.913	1.906	1.903	1.850	1.865	1.936	1.893	1.938	2.005	2.005	1.991	1.977	1.987	1.984	1.987	1.977	1.987	1.982	1.984	1.989	1.980	1.984	1.972
Ti	0.029	0.025	0.029	0.029	0.026	0.023	0.013	0.011	0.004	0.007	0.002	0.003	0.007	0.002	0.003	0.003	0.001	0.001	0.013	0.030	0.010	0.046	0.017	0.000	0.000	0.000	0.002	0.002	0.002	0.002	0.001	0.002	0.002	0.001	0.002	0.002	0.000	0.000
Al	0.286	0.268	0.279	0.278	0.272	0.263	0.208	0.190	0.181	0.181	0.173	0.612	0.179	0.765	0.186	0.176	0.167	0.987	0.279	0.260	0.266	0.198	0.192	0.963	0.955	0.944	0.441	0.433	0.370	0.461	0.470	0.449	0.462	0.444	0.481	0.418	0.551	0.554
Cr	0.001	0.001	0.001	0.001	0.001	0.001	0.001	0.001	0.000	0.000	0.001	0.000	0.001	0.001	0.001	0.001	0.000	0.001	0.001	0.001	0.001	0.001	0.001	0.000	0.000	0.000	0.000	0.001	0.001	0.000	0.001	0.001	0.001	0.001	0.001	0.001	0.000	0.000
Fe^{3+}	0.033	0.047	0.049	0.046	0.049	0.046	0.047	0.046	0.000	0.000	0.000	0.000	0.000	0.000	0.000	0.000	0.000	0.000	0.222	0.194	0.135	0.131	0.102	0.000	0.000	0.006	0.087	0.067	0.082	0.026	0.053	0.053	0.081	0.074	0.051	0.073	0.018	0.069
Fe^{2+}	0.170	0.154	0.162	0.160	0.191	0.179	0.167	0.170	0.527	0.511	0.571	0.517	0.506	0.521	0.571	0.517	0.528	0.525	0.018	0.036	0.049	0.073	0.066	0.030	0.025	0.037	0.043	0.051	0.051	0.043	0.018	0.066	0.037	0.043	0.054	0.042	0.034	0.057
Mn	0.007	0.005	0.005	0.006	0.007	0.005	0.005	0.006	0.012	0.012	0.009	0.001	0.010	0.010	0.012	0.010	0.012	0.011	0.002	0.002	0.002	0.002	0.001	0.000	0.000	0.000	0.001	0.001	0.001	0.001	0.001	0.001	0.001	0.001	0.001	0.001	0.000	0.000
Mg	0.730	0.709	0.719	0.720	0.740	0.717	0.769	0.780	1.363	1.356	1.321	1.379	1.352	1.383	1.328	1.363	1.378	1.373	0.704	0.723	0.687	0.720	0.706	0.013	0.021	0.035	0.457	0.462	0.516	0.485 0.532	0.476 0.523	0.458 0.503	0.429 0.483	0.461 0.503	0.473 0.475	0.496 0.543	0.411 0.445	0.382 0.398
Ca	0.860	0.890	0.893	0.891	0.836	0.890	0.919	0.911	0.025	0.053	0.015	0.019	0.052	0.019	0.022	0.013	0.013	0.013	0.682	0.645	0.705	0.727	0.774	0.035	0.041	0.056	0.507	0.518	0.572	0.159	0.110	0.161	0.159	0.110	0.159	0.159	0.000	0.000
Ca-Ti-Ts	2.862	2.546	2.934	2.880	2.587	2.333	1.375	1.172	-	-	-	-	-	-	-	-	-	-	1.326	3.006	1.013	4.64	1.74	0.000	0.000	0.000	0.116	0.186	0.160	0.934	2.070	0.951	1.435	1.390	0.801	1.713	1.610	2.790
Ca-Ts	10.699	10.487	10.223	10.585	10.579	10.077	6.317	5.783	-	-	-	-	-	-	-	-	-	-	12.343	7.520	4.368	1.42	2.77	0.000	0.000	0.93	1.95	0.918	1.312	43.869	42.62	42.721	43.512	41.38	46.14	38.092	51.85	49.86
Al	1.512	0.728	0.000	0.000	0.000	0.000	0.000	0.000	-	-	-	-	-	-	-	-	-	-	0.582	4.966	11.818	7.70	10.17	96.026	95.555	92.54	39.88	41.063	34.041	2.586	5.34	5.293	8.147	7.37	5.10	7.260	1.84	6.89
Acs	3.348	4.678	4.913	4.643	4.914	4.652	4.815	4.732	-	-	-	-	-	-	-	-	-	-	22.194	13.397	13.543	13.07	10.22	0.000	0.000	0.640	8.70	6.685	8.209	52.100	49.52	49.198	46.649	48.79	46.36	52.404	42.86	36.99
Wo-Hd	72.399	75.985	76.990	76.057	70.839	77.389	88.967	86.755	-	-	-	-	-	-	-	-	-	-	54.523	53.982	65.135	66.62	72.88	3.591	4.201	0.000	48.60	50.649	55.72	-								

TABLE 4.06 (Cont'd)

	D192																			D132										D208		
Sample	PBO	PBF	PBG	PBC	PBE	DCB	DDC	DDE	DCJ	PAZ	PBA	PBB	DCN	DCO	DCR	JAK	DDN	DDO	DDS	PAL	PAM	PAN	PAO	PAS	JAE	JAF	JAA	JAB	JAI	PBH	PBI	PBJ
	C-ma	C-ma	C-ma	C-ma	C-ma	R-ma	C-ma	C-ma	C-ma	pl	pl	pl	pl	pl	pl	I-pl	I-pl	I-pl	I-pl	R-ma	C-ma	C-ma	R-ma	C-ma	pl	pl	I-pl	I-pl	I-pl	v	v-s	v-s
SiO_2	56.13	55.97	56.28	56.64	56.28	56.34	56.85	56.38	56.54	56.32	56.69	56.35	57.05	56.46	56.64	56.13	57.14	56.69	56.10	56.24	56.68	56.35	56.25	56.33	56.29	56.19	55.96	55.83	56.18	56.34	54.51	53.75
TiO_2	0.00	0.00	0.00	0.00	0.00	0.07	0.07	0.07	0.20	0.00	0.00	0.00	0.04	0.07	0.07	0.00	0.04	0.04	0.09	0.00	0.00	0.00	0.00	0.00	0.00	0.00	0.00	0.00	0.00	0.00	0.00	0.00
Al_2O_3	8.67	9.82	10.15	11.48	9.80	8.38	10.74	9.86	10.96	11.41	11.79	10.73	11.90	10.80	10.77	12.30	12.46	10.97	9.15	10.49	11.19	10.76	10.98	9.92	11.52	11.06	13.20	13.07	12.94	10.25	6.84	4.32
Cr_2O_3	0.14	0.11	0.16	0.07	0.09	0.10	0.16	0.18	0.53	0.04	0.02	0.04	0.02	0.04	0.07	0.00	0.00	0.02	0.03	0.00	0.02	0.02	0.02	0.02	0.00	0.00	0.02	0.00	0.02	0.00	0.02	0.00
Fe_2O_3	2.63	2.33	1.96	0.60	2.05	2.17	0.93	1.99	0.95	2.18	1.29	1.47	0.77	1.00	1.16	0.75	0.57	1.22	3.03	1.40	0.71	1.44	1.90	1.58	0.21	1.60	1.61	0.80	0.43	2.59	1.88	0.85
FeO	2.89	2.31	2.21	2.19	2.93	3.58	3.02	2.74	2.38	2.29	2.64	2.84	2.50	3.03	3.69	2.41	3.10	3.68	3.26	2.08	2.31	2.11	1.74	1.94	2.62	2.60	3.30	3.17	3.58	2.07	2.59	3.76
MnO	0.05	0.03	0.03	0.02	0.05	0.06	0.03	0.03	0.02	0.03	0.03	0.05	0.02	0.02	0.03	0.03	0.06	0.02	0.06	0.02	0.00	0.02	0.03	0.08	0.02	0.03	0.05	0.03	0.05	0.06	0.05	0.10
MgO	9.10	8.63	8.69	8.65	8.43	9.22	8.45	8.71	8.07	7.96	7.63	8.21	8.12	8.30	8.14	7.73	7.75	8.32	9.00	8.98	8.68	8.91	8.82	9.46	8.65	8.87	7.18	7.37	7.69	8.76	11.45	13.11
CaO	14.74	13.83	13.97	13.26	13.76	14.91	13.33	13.63	13.04	12.79	12.67	13.51	12.95	13.45	13.21	12.04	12.28	13.03	14.26	14.11	13.54	14.03	13.91	14.78	13.29	13.61	10.85	11.31	11.43	13.50	18.77	20.77
Na_2O	6.27	6.79	6.83	7.14	6.79	5.97	6.95	6.81	7.24	7.43	7.61	7.02	7.47	6.97	7.01	7.64	7.69	7.03	6.37	6.70	7.04	6.77	6.89	6.37	6.95	6.87	7.95	7.75	7.59	6.98	3.98	2.25
TOTAL	100.62	99.82	100.28	100.05	100.19	100.81	100.54	100.41	99.93	100.45	100.37	100.22	100.85	100.14	100.79	99.05	101.09	101.02	101.34	100.02	100.17	100.41	100.54	100.48	99.55	100.29	99.12	99.33	99.91	100.51	100.01	99.12
Si	1.997	1.996	1.994	1.997	2.002	2.004	2.004	1.998	2.002	1.987	1.998	1.997	1.997	2.000	1.999	1.996	1.995	1.995	1.985	1.992	1.998	1.988	1.982	1.990	1.995	1.984	1.989	1.983	1.985	1.991	1.965	1.971
Ti	0.000	0.000	0.000	0.000	0.000	0.002	0.002	0.002	0.005	0.000	0.000	0.000	0.001	0.002	0.002	0.000	0.001	0.001	0.002	0.000	0.000	0.000	0.000	0.000	0.000	0.000	0.000	0.000	0.000	0.000	0.000	0.000
Al	0.364	0.413	0.424	0.477	0.411	0.351	0.446	0.412	0.457	0.475	0.490	0.448	0.497	0.451	0.448	0.516	0.513	0.455	0.382	0.438	0.465	0.448	0.456	0.413	0.481	0.460	0.553	0.547	0.539	0.427	0.291	0.195
Cr	0.004	0.003	0.004	0.002	0.003	0.003	0.004	0.005	0.015	0.001	0.001	0.001	0.001	0.001	0.002	0.000	0.000	0.001	0.001	0.000	0.001	0.001	0.001	0.001	0.000	0.000	0.001	0.000	0.001	0.000	0.001	0.000
Fe^{3+}	0.071	0.063	0.052	0.016	0.055	0.058	0.025	0.053	0.025	0.058	0.034	0.039	0.020	0.027	0.031	0.020	0.015	0.032	0.081	0.037	0.019	0.038	0.050	0.042	0.006	0.043	0.016	0.022	0.011	0.069	0.051	0.024
Fe^{2+}	0.086	0.069	0.065	0.065	0.087	0.106	0.089	0.081	0.070	0.068	0.078	0.084	0.073	0.090	0.109	0.072	0.090	0.108	0.096	0.062	0.068	0.062	0.051	0.057	0.078	0.061	0.098	0.094	0.106	0.060	0.078	0.115
Mn	0.002	0.001	0.001	0.001	0.002	0.002	0.001	0.001	0.001	0.001	0.001	0.002	0.001	0.001	0.001	0.001	0.002	0.001	0.002	0.001	0.000	0.001	0.001	0.002	0.001	0.001	0.002	0.001	0.001	0.002	0.002	0.003
Mg	0.483	0.459	0.459	0.454	0.447	0.489	0.444	0.460	0.426	0.419	0.401	0.434	0.424	0.438	0.428	0.410	0.403	0.436	0.474	0.474	0.456	0.469	0.463	0.498	0.457	0.467	0.380	0.390	0.405	0.461	0.615	0.716
Ca	0.562	0.528	0.530	0.501	0.542	0.568	0.503	0.518	0.495	0.484	0.478	0.513	0.486	0.510	0.500	0.459	0.459	0.491	0.541	0.536	0.512	0.530	0.525	0.560	0.505	0.515	0.413	0.430	0.433	0.511	0.725	0.816
Ca-Ti-Ts	0.00	0.00	0.00	0.00	0.00	0.000	0.000	0.075	0.000	0.00	0.00	0.000	0.105	0.005	0.053	0.000	0.105	0.106	0.239	0.00	0.00	0.000	0.000	0.000	0.000	0.000	0.000	0.000	0.000	0.00	0.00	0.000
Ca-Ts	0.28	0.45	0.57	0.34	0.00	0.000	0.000	0.000	0.000	1.26	0.23	0.308	0.108	0.000	0.000	0.410	0.254	0.304	1.064	0.76	0.15	1.158	1.810	0.959	0.47	1.628	1.099	1.747	1.547	0.872	3.48	2.946
Jd	35.81	40.37	41.27	47.03	41.6	35.349	44.929	41.114	46.174	44.93	48.52	44.204	48.669	45.205	44.786	50.730	50.569	44.680	35.546	42.29	46.20	42.438	41.980	39.398	47.20	42.768	53.104	51.211	50.785	40.96	22.12	13.461
Acm	7.05	6.26	5.22	1.58	5.50	5.841	2.496	5.310	2.551	5.79	3.43	3.921	2.017	2.685	3.085	2.020	1.501	3.230	8.062	3.74	1.88	3.827	5.035	4.189	0.57	4.259	1.630	2.150	1.146	6.88	5.09	2.353
Di-Hd	55.92	52.39	52.48	49.75	52.53	56.987	50.506	51.669	49.403	43.10	47.61	50.992	48.335	51.001	49.868	45.460	44.590	48.720	52.750	52.80	51.00	51.890	50.705	55.000	50.01	49.857	40.224	41.287	41.716	50.25	69.04	78.645

C - core
R - rim
I - inclusion
ig - igneous
s - symplectic
tr - transitional
pl - plagioclase site
ma - mafic site

TABLE 4.07 EMP analyses of garnets in coronites

	D187				6-5.5						D192																D132							
Sample	GBN	GBO	GBP	GBQ	GAA	GAF	GBG	GAK	GAH	GAL	DGM	DGN	DGO	DGP	DGQ	DGR	DGS	DGU	DGV	DGW	DGX	DGY	DGZ	DHA	DHB	DHD	DHF	DHG	GAH	GAH	GAO	GAP	GAQ	GAR	GAS	GAT
	out	out	out	out	out	out	out	in	in		r	r	c	c	c	r	c	c	r	r	r	c	c	r	c	r	c	c	rd	rd	cd	cd	rd	rd	r	c
SiO_2	38.40	38.59	38.56	38.54	39.53	39.10	38.92	38.94	39.25	39.11	38.6	38.6	38.0	38.9	38.5	38.4	38.4	38.5	38.6	38.5	38.4	38.9	38.3	38.6	38.4	38.4	38.4	38.5	39.09	39.33	39.45	39.03	38.96	39.31	39.14	39.19
TiO_2	0.04	0.09	0.04	0.00	0.04	0.05	0.04	0.02	0.04	0.04	0.09	0.02	0.05	0.02	0.02	0.00	0.04	0.05	0.05	0.03	0.07	0.02	0.04	0.00	0.02	0.02	0.02	0.14	0.00	0.00	0.00	0.00	0.00	0.00	0.00	0.00
Al_2O_3	22.09	21.57	21.71	21.51	22.07	21.79	21.77	21.74	21.95	21.86	21.4	21.5	21.2	21.7	21.6	21.6	21.4	21.6	21.5	21.6	21.5	21.8	21.4	21.6	21.4	21.6	21.5	21.6	22.09	22.47	21.74	21.88	21.96	21.94	21.91	21.72
Cr_2O_3	0.02	0.02	0.02	0.02	0.00	0.03	0.03	0.02	0.00	0.02	0.02	0.02	0.00	0.00	0.00	0.00	0.02	0.06	0.10	0.08	0.03	0.02	0.02	0.03	0.00	0.00	0.00	0.03	0.00	0.00	0.00	0.02	0.02	0.00	0.00	0.02
Fe_2O_3	0.02	1.02	1.65	1.49	1.26	1.76	1.48	1.30	0.87	0.99	0.63	0.65	1.03	0.47	1.12	1.19	0.84	0.92	0.52	0.71	0.67	0.63	0.71	0.75	0.82	1.63	0.99	0.72	1.54	0.00	1.14	1.48	1.36	0.99	1.26	1.23
FeO	25.32	24.45	23.70	24.82	21.24	20.62	22.75	22.11	22.66	23.02	26.23	26.11	25.07	25.08	25.90	25.83	26.46	26.37	28.13	27.66	26.99	24.63	27.40	27.83	29.16	27.84	28.21	26.35	21.33	22.27	20.79	20.48	21.16	21.80	21.85	20.08
MnO	0.45	0.42	0.42	0.43	0.26	0.26	0.33	0.37	0.33	0.47	0.80	0.76	0.65	0.33	0.31	0.56	0.68	0.79	0.83	0.82	0.92	0.40	0.80	0.76	1.02	0.19	0.91	0.76	0.36	0.39	0.40	0.39	0.42	0.40	0.37	0.36
MgO	4.67	4.92	5.43	4.82	9.22	8.22	6.76	7.51	9.09	7.78	5.12	5.19	3.84	6.15	4.35	5.52	4.38	5.09	5.49	5.45	4.74	6.70	5.31	5.52	4.58	5.84	5.31	4.91	8.72	8.86	8.19	7.94	8.48	8.92	9.04	7.41
CaO	9.25	9.81	9.57	9.55	7.31	8.79	8.93	8.36	6.07	7.37	7.88	7.86	10.09	7.92	9.47	7.35	8.65	7.65	5.78	6.16	7.57	7.48	6.39	6.06	5.97	5.88	5.72	8.06	7.42	6.23	8.74	9.09	7.72	6.95	6.61	10.31
TOTAL	100.26	100.90	101.17	101.18	100.94	100.63	101.01	100.37	100.26	100.66	100.7	100.6	99.8	100.5	101.2	100.3	100.8	100.9	100.9	100.9	100.7	100.5	100.4	101.1	101.3	101.2	101.0	101.0	100.55	99.55	100.63	100.31	100.08	100.31	100.18	100.32
Si	5.969	5.964	5.931	5.954	5.962	5.941	5.948	5.960	5.976	5.971	5.992	5.990	5.969	5.999	5.959	5.969	5.977	5.966	5.994	5.971	5.981	5.982	5.978	5.980	5.981	5.934	5.970	5.965	5.935	6.004	5.990	5.949	5.946	5.977	5.961	5.976
Ti	0.005	0.010	0.005	0.000	0.005	0.006	0.005	0.002	0.005	0.005	0.010	0.03	0.06	0.03	0.03	0.00	0.06	0.06	0.04	0.08	0.03	0.03	0.05	0.00	0.03	0.03	0.03	0.17	0.000	0.000	0.000	0.000	0.000	0.000	0.000	0.000
Al	4.047	3.929	3.936	3.917	3.923	3.902	3.922	3.922	3.939	3.933	3.917	3.933	3.926	3.944	3.942	3.958	3.927	3.946	3.935	3.949	3.947	3.952	3.938	3.945	3.930	3.935	3.940	3 946	3.953	4.043	3.891	3.931	3.950	3.932	3.933	3.904
Cr	0.002	0.002	0.002	0.002	0.000	0.004	0.004	0.002	0.000	0.002	0.03	0.03	0.00	0.00	0.00	0.00	0.03	0.07	0.12	0.10	0.04	0.03	0.03	0.04	0.00	0.00	0.00	0.04	0.000	0.000	0.000	0.002	0.002	0.000	0.000	0.002
Fe^{3+}	0.002	0.119	0.190	0.173	0.143	0.202	0.170	0.150	0.114	0.100	0.074	0.076	0.122	0.054	0.130	0.138	0.098	0.107	0.061	0.083	0.079	0.073	0.091	0.087	0.096	0.189	0.116	0.084	0.176	0.000	0.130	0.170	0.156	0.113	0.114	0.141
Fe^{2+}	3.292	3.162	3.059	3.207	2.680	2.621	2.908	2.830	2.885	2.939	3.405	3.389	3.294	3.234	3.352	3.341	3.444	3.418	3.653	3.588	3.515	3.167	3.577	3.606	3.798	3.597	3.667	3.415	2.709	2.843	2.663	2.610	2.700	2.772	2.783	2.561
Mn	0.059	0.055	0.055	0.056	0.073	0.033	0.043	0.048	0.043	0.061	0.105	0.100	0.087	0.044	0.041	0.074	0.090	0.103	0.106	0.108	0.109	0.052	0.106	0.100	0.135	0.025	0.120	0.100	0.046	0.050	0.051	0.050	0.054	0.052	0.048	0.047
Mg	1.082	1.133	1.245	1.110	2.072	1.861	1.540	1.713	2.063	1.770	1.185	1.200	0.899	1.413	1.004	1.279	1.016	1.175	1.271	1.260	1.100	1.536	1.235	1.274	1.063	1.344	1.230	1.134	1.973	2.016	1.853	1.804	1.929	2.021	2.052	1.684
Ca	1.541	1.625	1.577	1.581	1.181	1.431	1.462	1.371	0.990	1.206	1.310	1.307	1.698	1.308	1.571	1.224	1.442	1.270	0.962	1.023	1.263	1.233	1.068	1.006	0.997	0.974	0.953	1.336	1.207	1.019	1.422	1.484	1.262	1.132	1.079	1.685

ot - outer corona in - inner corona r - rim c - core d discrete grain

TABLE 4.08 EMP analyses of zoisites from coronites

	D187		D132
	IND	INE	PAH
	m	m	m
SiO_2	39.81	38.74	37.94
TiO_2	0.00	0.04	-
Al_2O_3	31.72	32.20	30.55
Fe_2O_3	0.07	0.86	2.07
MnO	-	-	0.03
MgO	0.03	0.02	0.61
CaO	23.07	23.59	24.41
Si	3.102	3.015	2.976
Al	2.910	2.950	2.802
Ti	0.000	0.002	-
Cr	-	-	-
Fe^{3+}	0.004	0.050	0.122
Mn	-	-	0.002
Mg	0.004	0.002	0.071
Ca	1.922	1.963	2.052
SUM	7.941	7.983	8.050

m = matrix phase

TABLE 4.09 EMP analyses of paragonites in coronites

	D187				D132					6.55		
	MAD	MAF	MAH	MAG	MAB	MAC	MAD	MAE	MAF	MAA	MAB	MAC
	i	m	m	m	2^o	2^o	2^o	2^o	2^o	2^o	2^o	2^o
SiO_2	46.00	45.64	45.49	45.30	46.75	46.62	46.64	46.82	46.39	46.33	45.68	45.30
TiO_2	-	-	-	-	0.06	0.07	0.06	0.06	0.04	-	-	-
Al_2O_3	39.61	39.30	39.06	39.47	39.17	39.29	39.21	39.51	39.28	38.91	38.71	38.48
FeO^T	0.57	0.32	0.13	0.20	0.33	0.28	0.33	0.66	0.36	0.17	0.19	0.20
MnO	-	-	-	-	0.02	0.02	0.02	0.00	0.00	-	-	-
MgO	0.08	0.07	0.07	0.07	0.10	0.15	0.12	0.12	0.08	0.13	0.13	0.25
CaO	0.39	0.42	0.40	0.35	0.49	0.33	0.32	0.48	0.42	0.36	0.42	0.39
Na_2O	6.44	7.17	7.26	7.36	7.12	7.02	6.87	7.08	7.05	7.07	7.01	7.13
K_2O	0.36	0.41	0.48	0.57	0.79	1.15	1.02	0.82	0.65	0.82	0.91	0.86
Si	5.974	5.952	5.960	5.917	6.011	5.996	6.011	5.985	5.993	6.015	5.986	5.970
Al^{IV}	2.026	2.048	2.040	2.083	1.989	2.005	1.989	2.015	2.007	1.985	2.013	2.030
Al^{VI}	4.029	3.986	3.984	3.987	3.939	9.943	3.959	3.930	3.966	3.962	3. 58	3.939
Ti	-	-	-	-	0.006	0.007	0.006	0.006	0.004	-	-	-
Fe^T	0.062	0.035	0.014	0.022	0.035	0.030	0.035	0.070	0.039	0.018	0.021	0.022
Mn	-	-	-	-	0.002	0.002	0.002	0.000	0.000	-	-	-
Mg	0.016	0.014	0.014	0.014	0.019	0.029	0.023	0.023	0.015	0.025	0.025	0.049
Ca	0.054	0.059	0.056	0.049	0.067	0.045	0.044	0.066	0.058	0.050	0.059	0.055
Na	1.617	1.808	1.839	1.859	1.770	1.746	1.712	1.750	1.761	1.775	1.777	1.817
K	0.059	0.068	0.080	0.095	0.129	0.188	0.167	0.133	0.107	0.136	0.152	0.144
SUM	13.837	13.968	13.988	14.025	13.969	13.991	13.949	13.978	13.951	13.967	13.992	14.026

i = inclusion m = matrix 2^o = secondary

TABLE 4.10 EMP analyses of plagioclase and spinel in coronites

	D192		D208			D170					
	DDP	DDQ	FAA	FAC	FAD	SAA	SAB	SAC	SAD	SAH	SAI
	i	i	s	s	s	1^o	s	s	s	s	s
SiO_2	68.10	68.90	67.10	66.85	65.54	0.67	0.18	0.23	0.08	0.29	0.05
TiO_2	-	-	-	-	-	0.02	0.00	0.02	0.00	0.02	0.00
Al_2O_3	19.80	19.70	19.11	19.97	20.78	59.71	62.74	61.29	62.14	62.76	63.22
Cr_2O_3	-	-	-	-	-	0.60	0.05	0.02	0.02	0.00	0.00
Fe_2O_3	1.10	0.40	0.51	0.18	0.14	2.97	1.93	2.69	2.38	0.86	1.22
FeO	-	-	-	-	-	25.06	22.56	22.64	21.17	22.63	21.88
MnO	-	-	-	-	-	0.12	0.09	0.08	0.11	0.11	0.09
MgO	-	-	-	-	-	11.01	12.84	12.50	13.34	12.68	13.04
CaO	0.85	0.43	1.78	1.52	2.27	0.06	0.00	0.00	0.00	0.00	0.00
Na_2O	11.20	11.50	11.09	10.99	10.38	-	-	-	-	-	-
K_2O	0.01	0.01	0.02	0.04	0.02	-	-	-	-	-	-
TOTAL	101.06	100.94	99.61	99.55	99.13	100.22	100.39	99.47	99.24	99.32	99.50
Si	2.958	2.984	2.963	2.947	2.906	0.018	0.005	0.006	0.002	0.008	0.001
Ti	-	-	-	-	-	0.000	0.000	0.000	0.000	0.000	0.000
Al	1.014	1.006	0.993	1.036	1.085	1.895	1.950	1.932	1.947	1.966	1.972
Cr	-	-	-	-	-	0.013	0.001	0.000	0.000	0.000	0.000
Fe^{3+}	0.034	0.013	0.017	0.006	0.005	0.060	0.038	0.054	0.048	0.017	0.024
Fe^{2+}	-	-	-	-	-	0.564	0.498	0.506	0.471	0.503	0.484
Mn	-	-	-	-	-	0.003	0.002	0.002	0.002	0.002	0.002
Ca	0.040	0.020	0.084	0.072	0.108	0.002	0.000	0.000	0.000	0.000	0.000
Na	0.943	0.966	0.947	0.937	0.890	-	-	-	-	-	-
K	0.001	0.001	0.001	0.002	0.001	-	-	-	-	-	-
TOTAL	4.990	4.989	5.006	5.001	4.995	2.997	3.000	3.000	2.999	2.999	2.999

i = inclusion in garnet s = symplectic 1^o = primary igneous

TABLE 4.11 EMP analyses of pyroxenes from charnockites, websterites and a low-K gneiss

	D99										
	PBD	PCH	PCL	PCM	PCO	HAA	HAJ	HAK	HAD	HAI	HAO
	l	p	p	r	l	l	l	c	c	r	r
SiO_2	52.78	51.62	51.45	51.39	52.65	52.15	52.10	51.25	51.58	51.49	51.44
TiO_2	0.00	0.37	0.40	0.33	0.29	0.11	0.00	0.00	0.14	0.16	0.16
Al_2O_3	1.94	1.85	2.02	1.91	2.32	1.04	0.93	1.04	1.00	0.98	1.21
Cr_2O_3	0.00	0.00	0.00	0.00	0.00	0.03	0.00	0.00	0.05	0.02	0.02
Fe_2O_3	0.76	0.95	1.03	0.78	0.01	-	-	-	-	-	-
FeO	9.65	12.27	11.81	13.78	11.32	27.37	26.61	28.08	28.94	29.33	29.13
MnO	0.25	0.44	0.33	0.41	0.25	0.73	0.64	0.71	0.71	0.74	0.07
MgO	12.64	12.29	11.49	12.63	12.12	18.58	18.75	17.66	17.92	17.91	17.49
CaO	20.76	20.53	21.46	18.24	20.70	0.82	1.24	0.57	0.75	0.53	0.68
Na_2O	0.88	0.37	0.40	0.36	0.76	0.00	0.00	0.00	0.00	0.00	0.00
TOTAL	99.67	100.70	100.39	99.84	100.42	100.85	100.30	99.31	101.09	101.18	100.85
Si	1.978	1.942	1.943	1.950	1.968	1.976	1.980	1.980	1.966	1.963	1.966
Ti	0.000	0.010	0.011	0.009	0.008	0.003	0.000	0.000	0.040	0.005	0.005
Al	0.086	0.082	0.090	0.085	0.102	0.046	0.031	0.047	0.044	0.044	0.054
Cr	0.000	0.000	0.000	0.000	0.000	0.001	0.000	0.000	0.002	0.001	0.001
Fe^{3+}	0.022	0.027	0.029	0.022	0.000	-	-	-	-	-	-
Fe^{2+}	0.303	0.386	0.373	0.437	0.354	0.866	0.844	0.906	0.921	0.938	0.929
Mn	0.008	0.014	0.011	0.013	0.008	0.023	0.020	0.023	0.023	0.024	0.022
Mg	0.706	0.689	0.647	0.714	0.675	1.048	1.061	1.016	1.017	1.017	0.996
Ca	0.834	0.828	0.868	0.742	0.829	0.033	0.050	0.023	0.031	0.022	0.028
Na	0.064	0.027	0.029	0.026	0.055	0.000	0.000	0.000	0.000	0.000	0.000

	D134										
	PAJ	PAK	PAL	PAM	PAO	PAP	PAQ	PAR	PAS	PAT	HAA	HAB	HAC	HAD
	c	r	r	r	r	r	d	c	d	c	c	r	r	r
SiO_2	51.16	53.18	51.36	53.10	51.32	51.71	53.83	51.48	52.77	53.20	51.11	51.40	51.72	51.93
TiO_2	0.66	0.31	0.61	0.06	0.64	0.59	0.06	0.59	0.24	0.18	0.16	0.12	0.28	0.21
Al_2O_3	2.82	2.48	2.77	1.00	3.01	2.59	0.84	2.88	1.53	2.19	1.40	1.14	1.54	1.63
Cr_2O_3	0.03	0.02	0.00	0.03	0.02	0.03	0.02	0.05	0.03	0.00	0.00	0.00	0.00	0.00
Fe_2O_3	1.68	2.27	3.40	2.29	2.55	3.24	1.75	2.22	2.22	3.23	-	-	-	-
FeO	9.69	6.23	7.18	7.83	7.27	7.96	6.79	10.17	7.47	6.96	28.99	28.04	26.85	23.80
MnO	0.32	0.14	0.21	0.06	0.16	0.08	0.22	0.32	0.10	0.06	0.43	0.34	0.56	0.53
MgO	12.82	12.34	11.93	12.36	12.21	11.17	13.28	13.10	12.44	11.92	17.59	17.99	18.12	19.82
CaO	20.03	21.31	21.55	22.05	21.65	20.67	22.57	18.03	22.19	20.88	0.53	0.79	1.28	1.13
Na_2O	0.70	1.77	1.32	1.16	1.01	1.71	1.04	1.11	1.11	1.89	0.07	0.05	0.29	0.23
TOTAL	99.91	100.05	100.33	99.94	99.84	99.75	100.41	99.95	100.10	100.50	100.31	99.91	100.73	99.31
Si	1.942	1.993	1.928	1.968	1.970	1.961	1.972	1.963	1.968					
Ti	0.017	0.002	0.017	0.007	0.005	0.004	0.003	0.008	0.006					
Al	0.115	0.037	0.127	0.067	0.097	0.063	0.051	0.068	0.072					
Cr	0.001	0.001	0.001	0.001	0.000	0.000	0.000	0.000	0.000					
Fe^{3+}	0.092	0.049	0.063	0.062	0.090	-	-	-	-					
Fe^{2+}	0.250	0.210	0.319	0.237	0.215	0.929	0.898	0.851	0.753					
Mn	0.003	0.007	0.010	0.003	0.002	0.014	0.011	0.018	0.017					
Mg	0.625	0.733	0.731	0.691	0.688	1.005	1.028	1.024	1.119					
Ca	0.832	0.895	0.724	0.887	0.829	0.022	0.032	0.052	0.046					
Na	0.125	0.075	0.081	0.080	0.136	0.005	0.004	0.021	0.017					

	79/B													
	PAA	PAB	PAC	PAD	PAE	PAG	PAF	HAA	HAB	HAC	HAD	PAZ	PBC	PBD
	r	r	c	c	d	d	r	c	r	c	r	c	r	r
SiO_2	53.18	53.72	53.60	53.78	54.54	54.12	54.41	54.16	54.79	54.22	54.51	55.08	54.67	54.91
TiO_2	0.11	0.07	0.07	0.07	0.02	0.50	0.39	0.07	0.02	0.07	0.07	0.02	0.02	0.02
Al_2O_3	2.35	1.90	1.83	1.35	0.74	0.68	0.51	1.36	0.08	0.17	0.07	0.02	0.02	0.02
Cr_2O_3	0.26	0.18	0.25	0.21	0.09	0.26	0.18	0.12	-	-	-	0.89	0.67	1.21
Fe_2O_3	0.78	0.88	0.91	0.86	0.32	1.27	-	-	17.41	16.95	17.53	2.17	2.21	1.77
FeO	4.44	4.14	3.85	3.81	3.99	3.39	17.71	16.93	0.49	0.39	0.47	0.08	0.03	0.05
MnO	0.19	0.13	0.13	0.11	0.14	0.10	0.47	0.43	26.51	26.23	26.80	16.55	16.66	16.67
MgO	16.03	16.75	16.27	16.06	16.14	15.65	26.69	26.69	0.86	0.72	0.16	24.58	24.56	24.77
CaO	21.48	21.38	22.09	23.43	23.83	23.57	0.30	0.55	0.02	0.00	0.00	0.57	0.43	0.52
Na_2O	0.64	0.60	0.62	0.42	0.39	0.71	0.00	0.00						
TOTAL	99.46	99.75	99.62	100.11	100.20	100.25	100.67	100.33	100.73	100.53	100.61	100.63	99.86	100.54
Si	1.954	1.964	1.964	1.968	1.992	1.979	1.969	1.960						
Ti	0.003	0.002	0.002	0.002	0.001	0.014	0.011	0.002	1.980	1.957	1.969	1.993	1.993	1.988
Al	0.102	0.082	0.079	0.058	0.032	0.029	0.021	0.057	0.000	0.002	0.002	0.001	0.001	0.001
Cr	0.008	0.005	0.007	0.006	0.003	0.008	0.005	0.003	0.020	0.074	0.031	0.029	0.025	0.026
Fe^{3+}	0.021	0.024	0.025	0.024	0.009	0.035	-	-	0.002	0.005	0.002	0.001	0.001	0.001
Fe^{2+}	0.136	0.127	0.118	0.117	0.122	0.104	0.535	0.511	-	-	-	0.024	0.018	0.033
Mn	0.006	0.004	0.004	0.003	0.004	0.003	0.014	0.013	0.525	0.511	0.529	0.066	0.067	0.054
Mg	0.878	0.913	0.889	0.876	0.878	0.853	1.439	1.438	0.015	0.012	0.014	0.002	0.001	0.002
Ca	0.846	0.837	0.867	0.918	0.932	0.923	0.012	0.021	1.427	1.411	1.442	0.892	0.905	0.900
Na	0.046	0.043	0.044	0.030	0.028	0.050	0.000	0.000	0.033	0.022	0.006	0.953	0.959	0.961
									0.001	0.000	0.000	0.040	0.030	0.037

	D45													
	PBF	PBG	PBH	PBI	PBK	PAY	HAA	HAB	HAI	HAH	HAJ	PAV	PAW	
	gr	r	r	r	c	r	c	r	r	c	r	r	r	
SiO_2	54.85	54.83	54.76	53.84	52.86	55.93	56.13	55.84	54.63	54.95	56.55	56.31	56.68	
TiO_2	0.02	0.02	0.02	0.09	0.17	0.02	0.02	0.04	0.02	0.07	0.02	0.00	0.00	
Al_2O_3	0.04	0.02	0.02	0.11	0.16	0.02	0.03	0.05	0.03	0.07	0.03	0.00	0.00	
Cr_2O_3	1.68	0.85	1.22	1.51	1.40	-	-	-	-	-	-	1.76	3.13	
Fe_2O_3	1.45	2.21	1.88	1.97	2.11	11.34	12.10	11.58	9.81	12.18	10.55	3.40	2.24	
FeO	0.06	0.08	0.06	0.05	0.06	0.14	0.14	0.13	0.11	0.10	0.10	0.03	0.02	
MnO	16.75	16.67	16.64	16.82	16.72	30.61	30.70	31.08	31.80	29.72	31.50	7.08	7.59	
MgO	24.41	24.26	24.58	23.19	22.77	0.20	0.25	0.17	0.16	0.41	0.24	11.40	12.20	
CaO	0.54	0.52	0.63	0.61	0.03	0.00	0.00	0.00	0.00	0.00	0.00	7.91	7.84	
Na_2O														
TOTAL	100.18	100.36	100.06	100.18	99.35	100.61	100.27	99.17	100.30	100.06		99.78	101.03	
Si	1.992	1.987	1.956	1.919	1.983	1.973	1.965	1.931	1.940	1.983		2.000	1.991	
Ti	0.001	0.000	0.000	0.001	0.000	0.000	0.001	0.000	0.002	0.000		0.000	0.000	
Al	0.002	0.001	0.001	0.001	0.002	0.000	0.001	0.000	0.002	0.001		0.498	0.469	
Cr	0.048	0.023	0.033	0.041	0.038	-	-	-	-	-		0.000	0.000	
Fe^{3+}	0.039	0.060	0.057	0.060	0.064	0.336	0.355	0.340	0.289	0.359	0.309	0.047	0.083	
Fe^{2+}	0.002	0.002	0.002	0.002	0.004	0.004	0.004	0.004	0.003	0.003	0.003	0.101	0.066	
Mn	0.001	0.001	0.001	0.001	0.001	0.003	0.003	0.003	0.003	0.003	0.003	0.001	0.001	
Mg	0.892	0.900	0.902	0.900	0.911	0.904	1.167	1.607	1.629	1.674	1.563	1.646	0.375	0.397
Ca	0.953	0.959	0.961	0.945	0.944	0.959	0.903	0.895	0.907	0.909	0.906	0.909	0.434	0.459
	0.040	0.030	0.037	0.047	0.038	0.037	0.040	0.043	0.002	0.009	0.000	0.000	0.000	0.000
													0.545	0.534

l - exsolution lamella p - poikilitic inclusion in opx gr - secondary granular pyroxene cl - clear (unpigmented) pyroxene

c - core r - rim

TABLE 4.12 EMP analyses of olivines in websterite and metaperidotites

	79/8	D163					D203		DF4			
	OAA	OLA	OLB	OLC	OLD	OLE	OLG	OLH	OLI	OLJ	OLK	OLL
		a	a	a	n	n	$2^{o}t$	$2^{o}an$		i-en	i-an	$2^{o}t$
SiO_2	36.83	39.21	39.17	38.99	39.28	39.00	35.92	36.19	38.22	38.11	37.91	37.61
FeO	32.44	19.71	19.76	19.92	19.80	19.54	37.76	35.81	26.61	26.82	26.03	27.67
MnO	0.82	0.49	0.49	0.55	0.47	0.50	1.13	0.98	0.61	0.70	0.64	0.68
MgO	29.76	41.53	41.03	40.75	41.59	41.29	26.14	28.19	36.09	35.59	35.69	34.74
NiO	0.09	0.09	0.05	0.09	0.09	0.09	0.08	0.11	0.14	0.11	0.12	0.09
CaO	0.40	0.00	0.04	0.04	0.01	0.08	0.01	0.01	0.00	0.00	0.06	0.00
TOTAL	100.36	101.03	100.34	100.34	101.24	100.50	101.07	101.35	101.69	101.38	100.47	100.81
Si	1.006	0.997	1.001	1.000	0.997	0.997	1.002	0.996	0.998	1.000	1.000	0.998
Fe^{2+}	0.741	0.419	0.422	0.427	0.420	0.418	0.890	0.824	0.581	0.588	0.574	0.614
Mn	0.019	0.010	0.010	0.012	0.010	0.011	0.027	0.023	0.013	0.015	0.014	0.015
Mg	1.213	1.575	1.563	1.558	1.574	1.574	1.087	1.157	1.405	1.392	1.405	1.374
Ca	0.012	0.000	0.001	0.001	0.000	0.002	0.004	0.001	0.000	0.000	0.015	0.000
TOTAL	2.994	3.003	2.999	3.000	3.003	3.003	2.998	3.003	3.002	2.999	2.990	3.025.

a = augen n = neoblast $2^{o}t$ = with talc after enstatite $2^{o}an$ = with anthophyllite after enstatite
i-an = inclusion in anthophyllite i-en = inclusion in enstatite

TABLE 4.13 EMP analyses of plagioclase in psammitic gneiss

	D178
	FAH
SiO_2	68.69
Al_2O_3	19.48
Fe_2O_3	0.14
CaO	0.35
Na_2O	11.70
K_2O	0.07
TOTAL	100.43
Si	2.992
Al	0.999
Fe^{3+}	0.005
Mg	-
Ca	0.016
Na	0.986
K	0.004
TOTAL	5.001

TABLE 4.14 EMP analyses of garnets from websterites and gneisses

	79/8					D45								D178						D24	
	GAA	GAC	GAE	GAF	GAG	GAX	GAY	GAZ	GBA	GBB	GBC	GBD	GBE	GAT	GAW	GAX	GAF	GAI	GAN	GDE	GDF
	r-cp	c	c-am	r-op	r-cp	C	r-sp	c-ch	c-ch	r-op	r-ch	r-cp	r-cp	r-ph	r-bi	c	r-ph	c-at	r-at	r	r
SiO_2	38.74	38.94	38.51	38.78	38.58	39.85	39.63	39.88	39.52	40.13	39.64	39.89	40.28	37.67	37.48	37.46	37.69	37.40	37.59	38.67	38.63
TiO_2	0.00	0.00	0.00	0.00	0.00	0.04	0.05	0.00	0.00	0.00	0.00	0.00	0.00	0.09	0.07	0.07	0.05	0.04	0.04	0.11	0.02
Al_2O_3	20.72	21.36	21.28	21.36	20.98	22.31	22.07	22.07	21.99	22.18	22.18	22.11	21.61	21.00	21.03	21.02	21.07	20.91	20.87	21.24	21.64
Cr_2O_3	0.86	0.52	0.47	0.42	0.61	0.03	0.03	0.00	0.00	0.00	0.00	0.00	0.00	0.02	0.03	0.03	0.02	0.02	0.00	0.02	0.02
Fe_2O_3	2.16	1.59	2.38	2.08	2.23	2.23	2.38	2.18	2.34	1.39	2.21	2.53	1.54	0.89	1.19	1.65	1.30	1.72	1.94	1.39	1.49
FeO	21.29	22.43	22.05	21.54	21.52	17.89	15.98	17.31	16.51	17.67	16.51	17.04	16.68	26.34	26.98	25.62	26.94	26.73	25.92	24.76	23.84
MnO	1.61	1.61	1.66	2.15	1.94	0.69	0.64	0.67	0.61	0.66	0.66	0.73	0.66	1.45	1.09	1.17	1.26	0.97	1.43	0.77	0.74
MgO	7.63	8.34	8.12	8.09	8.08	12.20	9.71	12.28	9.98	12.56	11.81	12.39	12.88	1.06	1.74	1.47	1.74	1.78	1.21	6.53	6.10
CaO	7.65	3.96	6.12	6.43	6.44	5.74	10.54	6.10	9.63	5.67	7.16	6.12	6.14	12.04	10.69	12.04	10.77	10.83	12.04	7.15	8.39
TOTAL	100.67	100.75	100.60	100.85	100.37	100.98	101.03	100.49	100.58	100.26	100.17	100.80	99.78	100.56	100.38	100.54	100.84	100.39	101.00	100.64	100.87
Si	5.948	5.953	5.909	5.930	5.933	5.917	5.917	5.940	5.925	5.976	5.923	5.924	6.013	5.973	5.951	5.93(	5.954	5.936	5.936	5.972	5.947
Ti	0.000	0.000	0.000	0.000	0.000	0.004	0.006	0.000	0.000	0.000	0.000	0.000	0.000	0.011	0.008	0.00(	0.006	0.005	0.005	0.013	0.002
Al	3.750	3.849	3.849	3.850	3.803	3.904	3.884	3.875	3.886	3.893	3.906	3.870	3.802	3.925	3.936	3.92(	3.923	3.912	3.888	3.886	3.927
Cr	0.104	0.063	0.057	0.051	0.024	0.004	0.004	0.000	0.000	0.000	0.000	0.000	0.000	0.003	0.004	0.00(	0.002	0.003	0.000	0.002	0.002
Fe^{3+}	0.250	0.183	0.275	0.239	0.258	0.249	0.268	0.244	0.264	0.156	0.249	0.282	0.173	0.106	0.142	0.19(	0.155	0.205	0.230	0.161	0.173
Fe^{2+}	2.734	2.868	2.830	2.754	2.767	2.222	1.995	2.156	2.071	2.200	2.063	2.116	2.082	3.493	3.582	3.39(	3.558	3.547	3.426	3.198	3.069
Mn	0.209	0.208	0.216	0.278	0.253	0.087	0.081	0.085	0.077	0.083	0.084	0.092	0.083	0.195	0.147	0.15(	0.169	0.130	0.191	0.101	0.096
Mg	1.746	1.900	1.857	1.844	1.852	2.700	2.161	2.726	2.230	2.787	2.630	2.742	2.865	0.250	0.412	0.34(	0.410	0.421	0.285	1.503	1.399
Ca	1.259	0.976	1.006	1.054	1.061	0.913	1.686	0.974	1.547	0.905	1.146	0.974	0.982	2.045	1.819	2.04(	1.823	1.842	2.039	1.183	1.384

TABLE 4.15 EMP analyses of amphiboles in websterites and a peridotite

		79/8						D45						D203
	Sample	AAA	AAD	AAF	AAG	AAH	AAI	AAD	AAE	AAG	AAH	AAI	AAI	AAF
		r-sp	i-gt	r-ch	r-cp	r-ch	r-ch	r-gt	c-gt	c-op	c-cp	r	r-cp	anth
	SiO_2	52.91	52.80	43.18	54.83	52.71	46.61	48.96	46.49	49.37	51.51	47.32	45.95	56.44
	TiO_2	0.09	0.07	0.24	0.06	0.09	0.20	0.13	0.18	0.15	0.09	0.09	0.74	0.02
	Al_2O_3	4.28	4.60	12.63	3.04	4.28	9.94	8.76	10.35	7.45	6.33	10.27	9.55	0.00
	Fe_2O_3	0.34	0.70	3.05	3.09	0.99	1.87	1.35	1.95	0.68	1.78	2.36	3.97	0.79
	FeO	5.93	6.91	6.64	2.57	5.39	6.53	4.76	4.98	5.39	2.89	4.21	4.75	15.21
	MnO	0.14	0.25	0.24	0.18	0.18	0.14	0.06	0.02	0.06	0.02	0.03	0.05	0.52
	MgO	19.91	19.46	15.64	20.55	19.94	17.32	18.93	17.72	19.25	20.38	18.36	17.77	24.12
	CaO	12.43	11.75	11.78	12.60	12.51	12.18	12.35	12.67	11.80	13.07	12.55	12.27	0.31
	Na_2O	0.90	0.70	2.23	0.70	0.88	1.99	1.49	1.87	1.55	1.16	1.94	1.72	0.02
	K_2O	0.30	0.32	0.61	0.14	0.26	0.57	0.42	0.65	0.29	0.06	0.16	0.56	-
T	Si	7.467	7.449	6.340	7.609	7.439	6.706	6.941	6.681	7.040	7.213	6.924	6.607	7.953
	Al^{IV}	0.533	0.551	1.660	0.391	0.561	1.294	1.059	1.319	0.960	0.787	1.276	1.393	0.047
C	Al^{VI}	0.178	0.213	0.523	0.105	0.150	0.390	0.403	0.431	0.375	0.256	0.442	0.223	-
	Fe^{3+}	0.036	0.074	0.336	0.322	0.105	0.202	0.144	0.210	0.073	0.187	0.252	0.429	0.037
	Ti	0.009	0.007	0.026	0.006	0.009	0.022	0.014	0.019	0.016	0.009	0.010	0.080	0.002
	Mg	4.185	4.089	3.420	4.248	4.192	3.712	3.997	3.793	4.089	4.251	3.886	3.806	4.961
	Fe^{2+}	0.591	0.616	0.693	0.297	0.544	0.674	0.442	0.546	0.448	0.296	0.410	0.462	-
	Mn	-	-	-	0.021	-	-	-	-	-	-	-	-	-
B	Fe^{2+}	0.108	0.198	0.121	-	0.091	0.109	0.121	0.051	0.194	0.411	0.090	0.108	1.790
	Mn	0.017	0.030	0.030	-	0.021	0.017	0.007	0.002	0.007	0.002	0.003	0.006	0.062
	Ca	1.875	1.772	1.849	1.869	1.887	1.873	1.872	1.946	1.789	1.956	1.906	1.886	0.047
	Na	-	-	-	0.131	-	-	-	-	-	-	-	-	-
A	Na	0.246	0.191	0.633	0.057	0.240	0.554	0.408	0.520	0.427	0.314	0.533	0.478	0.005
	K	0.054	0.057	0.114	0.025	0.047	0.104	0.076	0.119	0.053	0.011	0.029	0.102	-
	Method	15eNK	15eNK	15eNK	13eCNK	15eNK	15eNK	15eNK	15eNK	15eNK	15eNK	15eNK	15eNK	15eNK

TABLE 4.16 EMP analyses of micas, chlorites and talc from charnokites, websterites, gneisses

	D134		79/8				D45					D178																	D24	
Sample	HAO	MAP	MAA	CAA	CAB	CAC	CAA	CAC	CAD	CAG	CAH	MAA	MAB	MAE	MAF	MAG	MAH	MAK	MAL	MAM	MAN	MAQ	MAS	MAT	MAU	MAC	MAD	MAO	MAP	MAR	MBC	MBB
	bi	bi	phl	ch	ch	ch	ch	ch	ch	ch	ch	c-ph	r-ph	c-ph	2^o-ph	2^o-ph	r-ph	r-ph	r-ph	c-ph	c-ph	r-ph	2^o-ph	c-ph	r-ph	bi	bi	bi	bi	bi	r-ph	r-pa
SiO_2	35.78	35.90	36.12	29.44	29.40	30.40	27.18	29.50	36.03	29.87	29.96	47.82	47.22	47.30	46.39	46.46	46.71	46.36	46.42	47.09	47.61	46.29	46.25	46.91	46.59	35.78	36.05	35.25	34.55	34.54	48.03	47.21
TiO_2	3.65	3.64	0.42	-	-	-	0.02	0.00	0.02	0.00	0.00	0.63	0.55	0.54	0.64	0.57	0.64	0.68	0.72	0.53	0.46	0.64	0.75	0.57	0.67	2.35	1.99	2.00	2.18	2.00	0.26	0.04
Al_2O_3	13.28	13.11	15.99	17.71	18.06	17.16	18.20	19.78	16.53	18.69	18.66	27.09	26.52	27.43	27.48	27.17	27.10	27.65	27.08	26.91	27.01	27.65	27.14	27.00	27.35	16.14	15.41	16.34	16.40	16.50	27.90	38.14
Cr_2O_3	-	-	-	0.82	0.62	0.73	0.10	0.02	0.03	0.10	0.09	-	-	-	-	-	-	-	-	-	-	-	-	-	-	-	-	-	-	-	-	-
FeO^T	19.62	20.29	8.40	8.63	8.75	8.72	13.22	5.41	5.57	4.79	4.90	4.63	4.55	3.68	4.72	4.87	4.86	5.20	5.45	4.86	4.66	4.97	5.73	4.89	5.12	20.20	20.19	21.77	22.33	22.82	2.15	0.39
MnO	0.09	0.09	0.06	0.03	0.03	0.03	0.00	0.02	0.03	0.02	0.00	0.05	0.05	0.05	0.06	0.03	0.03	0.05	0.05	0.08	0.08	0.03	0.05	0.03	0.05	0.44	0.42	0.45	0.34	0.57	0.02	0.00
MgO	11.81	11.22	22.25	28.18	28.41	28.18	28.42	30.66	26.65	31.00	30.87	2.33	2.42	2.21	2.05	2.18	2.23	1.95	2.06	2.35	2.40	1.88	2.14	2.17	2.03	9.72	10.18	8.52	8.13	7.49	3.08	0.17
NiO	-	-	-	0.08	0.06	0.09	-	-	-	-	-	-	-	-	-	-	-	-	-	-	-	-	-	-	-	-	-	-	-	-	-	-
CaO	0.03	0.01	0.06	-	-	-	-	-	-	-	-	0.00	0.01	0.01	0.01	0.01	0.00	0.01	0.04	0.03	0.03	0.00	0.00	0.00	0.00	0.03	0.06	0.20	0.06	0.83	0.00	0.10
Na_2O	0.15	0.15	0.27	-	-	-	-	-	-	-	-	0.29	0.31	0.47	0.03	0.28	0.34	0.31	0.33	0.38	0.47	0.28	0.22	0.31	0.31	0.08	0.08	0.07	0.29	0.09	0.73	6.77
K_2O	9.44	9.56	7.05	-	-	-	-	-	-	-	-	10.82	10.63	10.46	10.91	10.73	10.79	10.78	10.64	10.47	10.24	10.80	10.62	10.73	10.73	9.92	9.46	9.66	9.58	8.87	10.05	1.12
Si	5.594	5.626	5.438	5.872	5.833	6.023	5.435	5.703	6.925	5.847	5.864	6.618	6.633	6.612	6.519	6.544	6.552	6.495	6.524	6.591	6.233	6.506	6.500	6.581	6.532	5.554	5.631	5.538	5.476	5.485	6.645	6.079
Al^{IV}	2.406	2.374	2.562	2.128	2.166	1.977	2.564	2.270	1.075	2.153	2.154	1.382	1.367	1.388	1.481	1.456	1.448	1.505	1.476	1.409	1.377	1.492	1.500	1.419	1.467	2.446	2.368	2.462	2.524	2.514	1.365	1.902
Al^{VI}	0.038	0.045	0.272	2.029	2.052	2.026	1.720	2.253	2.665	2.153	2.164	3.031	3.018	3.126	3.065	3.048	3.027	3.055	3.004	3.025	3.046	3.084	2.990	3.040	3.047	0.503	0.465	0.560	0.535	0.570	3.171	3.861
Ti	0.428	0.428	0.047	-	-	-	0.003	0.000	0.003	0.000	0.000	0.065	0.058	0.057	0.067	0.060	0.067	0.071	0.076	0.056	0.048	0.067	0.079	0.060	0.067	0.274	0.233	0.236	0.259	0.238	0.027	0.004
Cr	-	-	-	0.129	0.097	0.114	0.016	0.003	0.004	0.015	0.014	-	-	-	-	-	-	-	-	-	-	-	-	-	-	-	-	-	-	-	-	-
Fe^T	2.561	2.654	1.056	1.437	1.449	1.442	2.207	0.877	0.894	0.783	0.801	0.535	0.534	0.429	0.554	0.572	0.569	0.608	0.639	0.568	0.541	0.583	0.334	0.573	0.297	2.618	2.633	2. 855	2.954	3.026	0.248	0.042
Mn	0.012	0.012	0.008	0.005	0.005	0.005	0.000	0.003	0.005	0.003	0.000	0.006	0.006	0.006	0.007	0.004	0.004	0.006	0.006	0.009	0.009	0.003	0.006	0.003	0.006	0.057	0.055	0.059	0.045	0.076	-0.002	0.000
Mg	2.750	2.619	4.990	9.371	8.396	8.317	8.465	8.870	7.629	9.038	9.000	0.480	0.506	0.460	0.429	0.457	0.486	0.407	0.431	0.490	0.497	0.394	0.448	0.453	0.424	2.247	2.639	1.994	1.919	1.772	0.634	0.033
Ni	-	-	-	0.013	0.010	0.014	-	-	-	-	-	-	-	-	-	-	-	-	-	-	-	-	-	-	-	-	-	-	-	-	-	-
Ca	0.005	0.002	0.010	-	-	-	-	-	-	-	-	0.000	0.001	0.001	0.001	0.001	0.000	0.001	0.006	0.004	0.004	0.000	0.000	0.000	0.000	0.005	0.010	0.033	0.010	0.141	0.000	0.151
Na	0.045	0.045	0.079	-	-	-	-	-	-	-	-	0.078	0.084	0.127	0.081	0.076	0.092	0.084	0.090	0.103	0.126	0.076	0.100	0.084	0.084	0.240	0.024	0.021	0.089	0.028	0.208	1.686
K	1.879	1.908	1.351	-	-	-	-	-	-	-	-	1.907	1.901	1.862	1.952	1.924	1.927	1.923	1.904	1.866	1.814	1.933	1.900	1.917	1.916	1.961	1.882	1.932	1.933	1.794	1.768	0.184

bi = biotite ch = chlorite ph = phengite phl = phlogopite pa = paragonite ta = talc C = core R = rim
2^o = secondary

TABLE 4.17 EMP analyses of Fe-Ti oxides and spinels from charnockites, websterites and peridotites

	D99		D134	79/8							D45			D163			D203	DF4	
Sample	OLA	OLB	OAA	SPC	SPE	SPD	SPG	SPH	SPB	SPF	OAF	OAK	SAA	OAC	OAD	OAG	OAI	QAJ	OAK
	il	hm	il	il	il	il	hm	mt	mt	mt	mt	mt	sp*	mt	mt	mt	mt	il	mt
SiO_2	1.90	0.02	0.39	0.61	0.96	1.20	0.84	0.93	0.16	0.61	0.36	0.43	0.00	0.30	0.41	0.57	0.14	0.09	0.05
TiO_2	47.25	0.10	44.48	51.64	50.74	40.35	2.81	3.03	4.23	4.22	17.71	1.15	0.00	0.63	0.40	1.42	1.24	49.83	1.75
Al_2O_3	1.15	0.32	0.15	0.32	0.49	4.07	2.29	2.31	2.24	1.81	0.52	0.57	63.17	0.09	0.05	0.09	0.16	0.02	0.14
V_2O_5	2.24	0.00	0.90	0.00	0.00	0.27	0.00	0.00	0.56	0.52	0.09	0.09	0.00	0.03	0.04	0.26	0.19	0.02	0.37
Cr_2O_3	0.00	1.02	0.04	0.00	0.00	1.63	4.45	7.17	7.04	4.46	0.56	0.17	0.07	0.02	0.06	0.25	0.71	0.09	2.43
Fe_2O_3	2.38	97.85	12.59	1.79	2.82	12.97	82.91	50.89	49.86	52.50	33.46	64.67	1.24	66.61	66.86	63.82	65.15	5.31	62.94
FeO	43.46	0.66	40.04	42.05	40.95	35.99	5.82	32.65	34.26	34.65	45.03	31.21	17.55	30.87	30.78	32.18	31.65	39.31	32.34
MnO	0.50	0.04	0.16	0.64	1.37	0.48	0.23	0.34	0.34	0.30	0.11	0.06	0.00	0.15	0.13	0.11	0.13	1.31	0.18
MgO	1.09	0.05	0.44	2.52	2.56	2.81	0.63	1.44	0.51	0.72	1.86	0.83	15.46	0.55	0.50	0.31	0.33	2.42	0.21
CaO	0.45	0.00	0.00	0.16	0.17	0.00	0.00	0.00	0.00	0.00	0.00	0.00	0.00	0.00	0.00	0.00	0.00	0.00	0.00
TOTAL	100.59	100.06	99.19	99.73	10.06	99.77	99.98	98.76	99.20	99.79	99.70	99.18	97.49	99.05	99.23	99.01	99.68	98.40	100.41
Si	0.047	0.001	0.010	0.015	0.024	0.030	0.022	0.035	0.006	0.023	0.013	0.016	0.000	0.012	0.016	0.022	0.005	0.002	0.002
Al	0.033	0.010	0.004	0.009	0.014	0.118	0.071	0.103	0.100	0.080	0.026	0.026	1.973	0.004	0.002	0.004	0.007	0.001	0.006
Fe^{3+}	0.044	1.954	0.241	0.033	0.052	0.240	1.630	1.443	1.417	1.484	0.938	1.866	0.025	1.936	1.940	1.853	1.882	0.101	1.804
Ti	0.872	0.002	0.851	0.962	0.941	0.746	0.055	0.086	0.120	0.119	0.496	0.033	0.000	0.018	0.012	0.041	0.036	0.946	0.050
V	0.036	0.000	0.015	0.000	0.000	0.004	0.000	0.000	0.014	0.013	0.002	0.002	0.000	0.001	0.001	0.007	0.005	0.000	0.009
Cr	0.000	0.021	0.001	0.000	0.092	0.032	0.000	0.214	0.210	0.132	0.016	0.005	0.001	0.001	0.002	0.008	0.022	0.002	0.073
Fe^{2+}	0.895	0.015	0.852	0.871	0.844	0.740	0.127	1.029	1.082	1.089	1.403	1.001	0.389	0.991	0.993	1.038	1.016	0.830	1.030
Mg	0.040	0.002	0.017	0.093	0.094	0.103	0.023	0.081	0.029	0.040	0.103	0.047	0.611	0.032	0.029	0.018	0.019	0.091	0.012
Mn	0.010	0.001	0.003	0.013	0.029	0.010	0.005	0.011	0.011	0.010	0.003	0.002	0.000	0.005	0.004	0.004	0.004	0.028	0.006
Ca	0.012	0.000	0.000	0.004	0.004	0.000	0.000	0.000	0.000	0.000	0.000	0.000	0.000	0.000	0.000	0.000	0.000	0.000	0.000
TOTAL	1.989	2.006	1.994	2.002	2.002	2.023	1.927	2.999	2.989	2.990	2.999	2.999	2.999	2.998	2.999	2.995	2.996	2.000	2.994

il - ilmenite hm - haematite mt - magnetite sp - spinel * poor quality analysis included for reference.

TABLE 4.18 EMP analyses of epidotes in gneisses

	D178			D24
Sample	EAB	EAC	EAD	EAF
	r	r	c	r
SiO_2	38.31	38.04	38.77	38.62
TiO_2	0.11	0.11	0.15	0.06
Al_2O_3	26.72	25.08	26.69	28.04
Cr_2O_3	0.02	0.00	0.02	0.05
Fe_2O_3	8.57	11.19	8.77	6.98
MnO	0.06	0.03	0.03	0.03
MgO	0.03	0.05	0.05	0.14
CaO	22.42	22.57	22.50	22.69
Si	3.036	3.021	3.048	3.031
Al	2.493	2.345	2.470	2.590
Ti	0.006	0.007	0.009	0.003
Cr	0.001	0.000	0.001	0.003
Fe^{3+}	0.511	0.669	0.519	0.412
Mn	0.004	0.002	0.002	0.002
Mg	0.003	0.006	0.006	0.016
Ca	1.899	1.916	1.891	1.904
TOTAL	7.955	7.965	7.947	7.962

r = rim c = core

Table 4.19

Fold Phase	Layering/Foliation	Metamorphism	Remarks
	S_o		Sedimentary bedding
			Igneous layering
			Migmatite banding
		M_1	Granulite facies
?	?UPLIFT AND EROSION?		RODINGITISATION?
?	?	M_2	Amphibolite facies
F_1, F_2	S_1	M_3	Eclogite facies
F_3		M_4	Retrogression to amphibolite facies
F_4		-	Late open folds

TABLE 4.20 Results of geothermometry calculations

Sample	79/9a						79/16	79/38b				D69	D97.1	D116						D123							D181	
Probe	GAB	GAD	GAC	GAF	GAI	GAH	GAU	GLT	GLU	GLV	GMA	GFJ	GAC	GAG	GAH	GAI	GAJ	GAU	GAU	GIF	GJR	GFU	GGY	GKQ	GIQ	GGK	GBA	GBS
Spots	PAA	PAA	PAB	PAD	PAF	PAI	PAX	PBI	PBJ	PBK	MAC	PCS	PAK	PAA	PAB	PAC	PAD	PAF	MAK	ADK	ADL	ADQ	ADN	ADU	ADV	ADG	PAP	MAY
Cores/rims/inclusions	I	I	I	I	R	R	R	R	I	I	R	R	R	I	I	R	R	R	R	R	R	I	I	I	I	R	R	R
Lithology	E/M	E/M	E/M	E/M	E/M	E/M	E	E	E	E	E	E	E	E	E	E	E	E	E	E	E	E	E	E	E	E	E	E
Ellis & Green (1979):																												
K_D gt/cpx	14.75	12.80	13.24	13.56	14.02	12.66	12.50	11.72	15.31	11.41		14.59	11.76	12.78	13.72	14.68	10.05	14.24									11.83	
X_{Ca} gt	0.269	0.255	0.222	0.242	0.218	0.237	0.252	0.150	0.135	0.155		0.190	0.172	0.172	0.162	0.159	0.138	0.205									0.253	
T°C	606	625	595	604	581	614	627	556	509	577		954	583	566	548	545	590	569									639	
Graham & Powell (1984):																												
K_D gt/hbl																				8.65	3.85	7.63	9.53	9.82	9.62	6.25		
X_{Ca} gt																				0.249	0.200	0.267	0.241	0.257	0.254	0.212		
T°C																				534	666	569	511	517	519	567		
Green & Hellman (1982):																												
K_D gt/ph											6.48								9.51								7.73	
T°C											679								662								652	
Kretz (1982) exchange:																												
K_D																												
T°C																												
Kretz (1982) transfer:																												
(Ca)																												
T°C																												
Lindsley (1983):																												
T°C - cpx																												
T°C - opx																												
P estimate (Kb)	16	16	16	16	16	16	16	16	16	16	16	16	16	16	16	16	16	16	16	-	-	-	-	-	-	-	16	16

TABLE 4.20 (Cont'd)

Sample	D205								D206																			D132
Probe	GGI	GGF	GGH	GAA	GDO	GDQ	GMH	GDR	GLM	GEG	GEI	GIS	GLN	GLO	GLP	GLQ	GVR	GXT	GXU	GYX	GYY	GZX	GZY	GEO		GAH
Spots	PAP	PAJ	PAL	PAA	PAC	PAG	PBL	AAB	PBH	PBZ	PCB	AAW	AAM	AAH	AAH	AAI	AAW	ABC	ABE	ABG	ABI	ABK	ABM	ACS		JAF
Cores/rims/inclusions	R	I	R	R	I	I	R	R	R	I	I	R	I	I	I	I	R	R	R	R	R	R	R	I		R
Lithology	E	E	E	E	E	E	E	E	GA	GA	GA	GA	GA	GA	GA	GA	GA	GA	GA	GA	GA	GA	GA	GA		C
Ellis & Green (1979):																												
K_D gt/cpx	12.3	14.06	10.51	12.71	14.64	13.91	11.37		14.18	14.82	13.02																	10.53
X_{Ca} gt	0.207	0.224	0.201	0.202	0.247	0.232	0.205		0.201	0.251	0.230																	0.205
T°C	599	584	627	589	593	592	613		567	593	603																	629
Graham & Powell (1984):																												
K_D gt/hbl								4.26				5.08	8.18	8.58	9.61	11.15	5.36	5.49	7.58	8.04	10.13	7.33	7.60	9 85		
X_{Ca} gt								0.207				0.161	0.261	0.239	0.257	0.252	0.205	0.237	0.219	0.178	0.253	0.210	0.214	0 277		
T°C								645				568	552	528	521	493	592	613	529	495	509	535	531	528		
Green & Hellman (1982):																												
K_D gt/ph																												
T°C																												
Kretz (1982) exchange:																												
K_D																												
T°C																												
Kretz (1982) transfer:																												
(Ca)																												
T°C																												
Lindsley (1983):																												
T°C - cpx																												
T°C - opx																												
P estimate (Kb)	16	16	16	16	16	16	16	-	16	16	16	-	-	-	-	-	-	-	-	-	-	-	-	-		16

TABLE 4.20 (Cont'd)

Sample	D192						6-5.5				D24	D178			D99			D134				D170			
Probe	DGZ	DGK	DGF	DGX	DGM	DGH	GAK	GAL	GAM	GAA	GDF	GAF	GATR	GAF	PBO	PCH	PCN	GAM	GAY	PAL	PAJ	PDP	PDQ	PAE	PAB
Spots	DOS	PBB	DCM	DCR	DOC	DDN	PAA	PAL	PAN	IAA	PAN	MAK	MAL	MAK	HAJ	HAI	HAO	PAM	PAP	MAB	MAA	MAT	MAS	MAB	MAD
Cores/rims/inclusions/exn.lam	I	R	R	R	R	I	R	R	R	I	R	R	R	R	EL	I	R	R	R	R	C	S	S	C	R
Lithology	C	C	C	C	C	C	C	C	C	C	LKG	PG	PG	PG	CH	CH	CH	CH	CH	CH	CH	T	T	T	T
Ellis & Green (1979):																									
K_D gt/cpx	14.33	14.47	18.48	11.58	14.11	14.00	17.77	17.81	16.27	9.80	13.24							17.13	14.69						
X_{Ca} gt	0.182	0.162	0.212	0.162	0.174	0.168	0.232	0.204	0.173	0.199	0.237							0.361	0.355						
T°C	552	537	528	579	550	557	548	529	524	640	605							639	665						
Graham & Powell (1984):																									
K_D gt/hbl																									
X_{Ca} gt																									
T°C														10.61											
Green & Hellman (1982):														639											
K_D gt/ph												6.05	8.92												
T°C												578	658		1.85	1.65	1.78			2.59	2.18	1.76	1.71	1.61	1.72
Kretz (1982) exchange:															734	851	772			503	607	782	784	880	805
(Ca)															0.45	0.44	0.45			0.49	0.44	0.50	0.49	0.49	0.50
T°C															777	847	790			392	856	356	475	485	251
Lindsley (1983):																									
T°C - cpx															810	770	825			690	890	680	680	1040	900
T°C - opx															840	600	660			690	850	710	710	1000	650
P estimate (Kb)	16	16	16	16	16	16	16	16	16	16	16	16	16	16	10	10	10	16	16	10	10	10	10	10	10

TABLE 4.20 (cont'd)

Sample	79/8					D45					
Probe	GAA	GAB	GAG	PAD	GBD	GBE	GAX	PAZ	PBK	PBG	Abbreviations:
Spots	PAA	PAB	PAE	HAC	PBI	PBJ	AAD	HAA	HAH	HAI	E - eclogite
Spot Location	R	R	R	C	R	R	R	C	C	R	C - coronite
Lithology	W	W	W	W	W	W	W	W	W	W	W - websterite
Ellis & Green (1979):											LKG - low-K gneiss
$K_D^{gt/cpx}$	10.07	10.28	10.98		11.74	11.51					PG - psammite
X_{Ca}^{gt}	0.219	0.221	0.177		0.167	0.166					Gr - charnockitic
T^oC	649	646	600		579	582					GA - garnet amphibole
Graham & Powell (1984):											T - troctolite
$K_D^{gt/hbl}$							5.84				El - exsolution lamella
X_{Ca}^{gt}							0.157				I - inclusion
T^oC							583				C - core
Green & Hellman (1982):											R - rim
$K_D^{gt/ph}$											S - symplectite
T^oC											
Kretz (1982) exchange:											
K_D				2.71				2.99	3.24	2.33	
T^oC				479				434	399	564	
Kretz (1982) transfer:											
(Ca)				0.48				0.50	0.48	0.49	
T^oC				628				252	690	434	
Lindsley (1983):											
T^oC - cpx				700				650	990	540	
T^oC - opx				800				500	650	650	
P estimate (Rb)	16	16	16	10	16	16	-	10	10	10	

FIGURES

CHAPTER 5

FIGURE 5.01 Distribution of temperature estimates for eclogites based on garnet-clinopyroxene thermometry (Ellis and Green, 1979). Data from this work and Griffin et al (in press), quoted at 15 kbars. Ticked line is Fjordane Complex/Jostedal Complex boundary, with ticks pointing into Jostedal Complex. Stippled areas are Lower Palaeozoic schists, mangerite nappes and Devonian clastics.

Figure 5·01

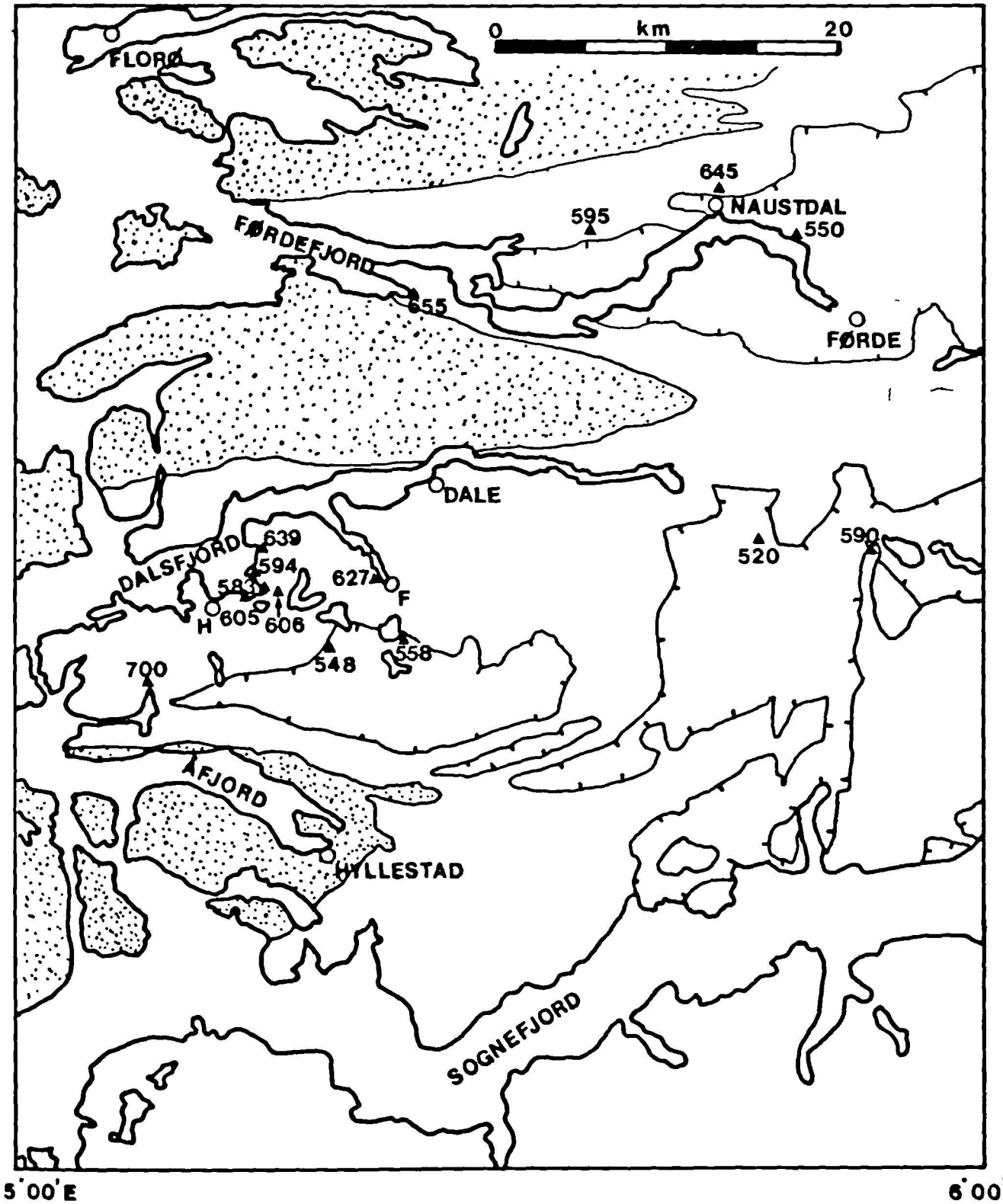
0 km 20
FLORØ
645
NAUSTDAL
595
550
FØRDEFJORD
655
FØRDE
DALE
639
DALSFJORD
594
627
F
583
H
605
606
548
558
520
590
700
FJORD
HYLLESTAD
SOGNEFJORD
5°00'E
6°00'E

FIGURES 5.02 Distribution of temperature estimates based on garnet-clinopyroxene thermometry (Ellis and Green, 1979) for eclogites after Griffin et al (in press). Heavy dashed lines are approximate isotherms, grossly simplified in the Sunnfjord area (extreme south-west of map). Temperatures calculated at 15 kbars, but note that pressure estimates increase sympathetically with temperature with a maximum of 20 kbars in coast Möre og Romsdal. See figure 1.03 for place-names.

Figure 5·02

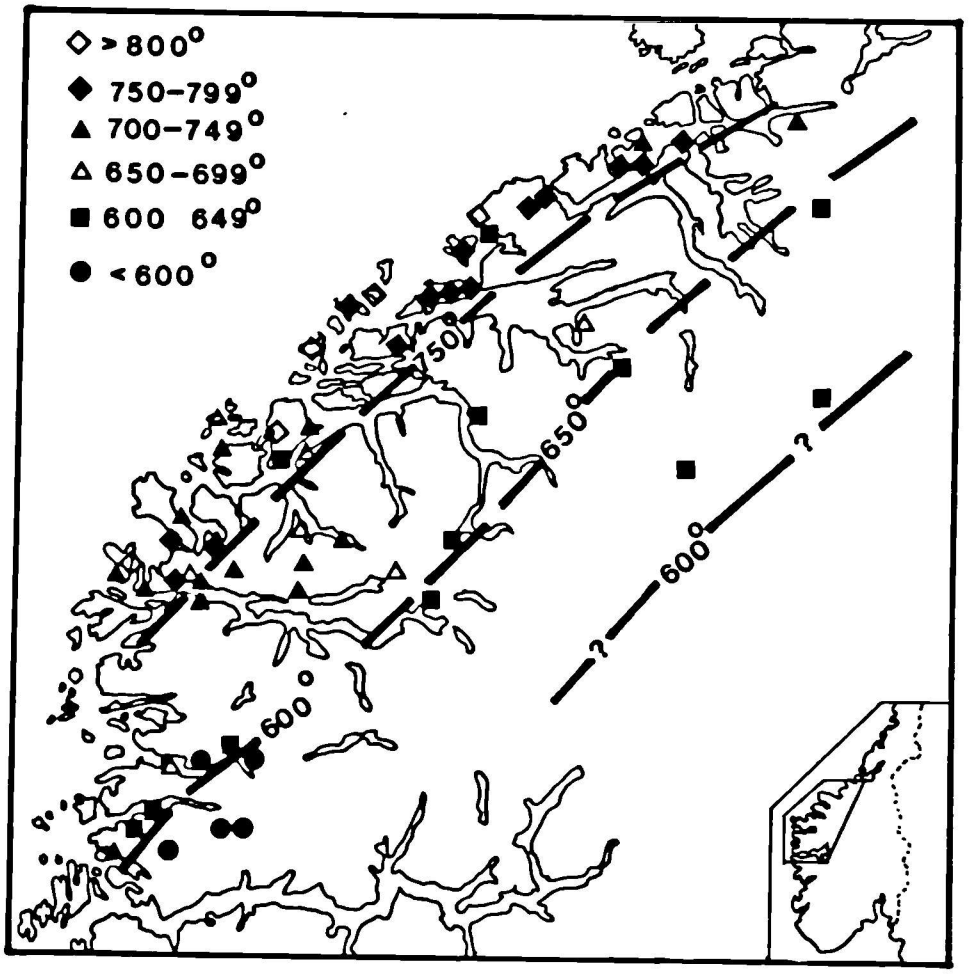

FIGURE 5.03 Thermal responses of continental crust thickened by overthrusting.

A. Section through crust (stippled) and lower lithosphere during continental subduction illustrating the 2-dimensional perturbation of the steady-state temperature distribution. Isotherms constructed for subduction at 6 cm per year for 2.8 Ma, after Bird et al (1975). Thick solid line is base of lithosphere.

B. 1 - schematic steady-state isotherm prior to overthrusting at time T_o.
   2 - geotherm immediately after overthrusting (thick line) at time t_1 with evolution of successive geotherms during thermal relaxation to a new steady-state geotherm for the thickened crust at time t_n. From Carswell + Cuthbert (in press).

C. P-T paths during thickening and erosion-controlled uplift of continental crust. Thick line is for a simple crustal doubling (note T_{max} is greater than T at P_{max}). Dashed line is for recovery during subdsuction of "old" oceanic lithosphere below the thickened crust for 20 Ma (after Rubie, 1984).

D. Schematic P-T paths illustrating the "metamorphic field gradient" and zones of different types of mineralogical evidence, a - inclusion suites, b - "peak" metamorphic conditions, c-retrogressive assemblages. From Spear et al (1984).

E. Contrasted P-T paths (1 = "prograde", 2 = "retrograde") for points A and B in B1 and B2 above.

Figure 5·03

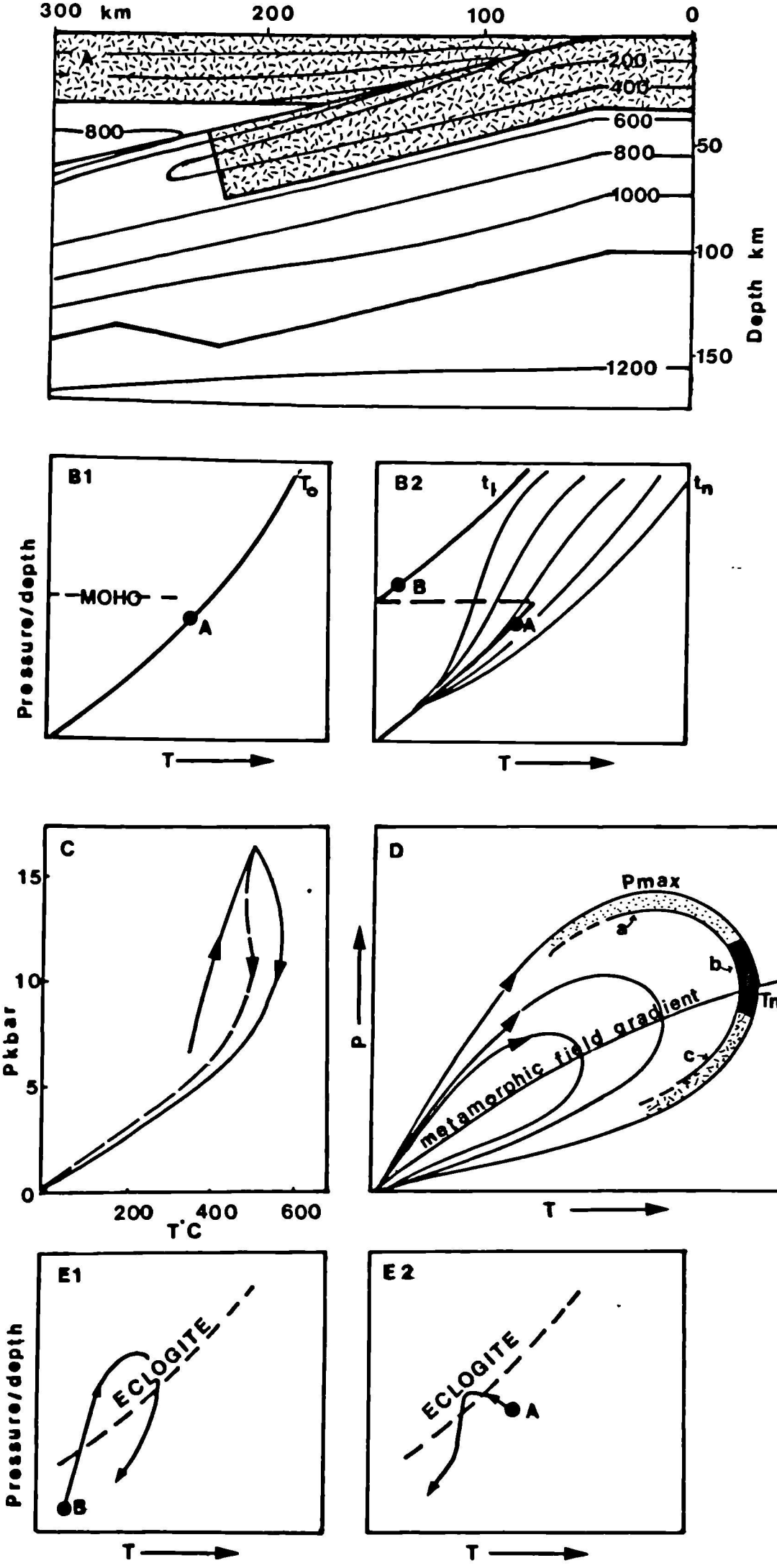
300 km
200
100
0
A
200
400
600
800
800
1000
1200
50
100
150
Depth km
B1
T_o
MOHO
A
Pressure/depth
T
B2
t_1
t_n
B
A
T
C
15
10
5
0
Pkbar
200
400
600
T°C
D
Pmax
a_1
b_1
Tmax
c_1
metamorphic field gradient
P
T
E1
ECLOGITE
B
Pressure/depth
T
E2
ECLOGITE
A
T

Appendix 3

Locations of Specimens, field sketches and photographs

Locations of all specimens, field sketches and photographs are tabulated below. Location coordinates are given as Norwegian national grid system references for grid zone designation 32V. Letters KN, LN, KP and LP refer to the 100,000 meter square identification. References give the location to the nearest ten meters.

A3.1 Specimen Locations

Specimen	Grid Ref	Bulk-rock Analysis	Probe Analysis	Lithology
79/2	KP98680313			Eclog/amphib
79/4	KP98680313	X		Grey gneiss
79/6	KP98820316		X	Honriblendite
79/8	KP98730315	X		Websterite
79/9A	KP98730315		X	Eclogite
79/11	KP98730315	X		Garnetite
79/12	KP98690301	X		Grey gneiss
79/15	LP04190400			Massive green gneiss
79/16	LP04190400		X	Eclogite
79/18	LP03660458	X		Websterite
79/19	LP02170630			Paragneiss
79/21	LP01690680			Paragneiss
79/22	KP99640751			Paragneiss
79/26	KP97680714	X		Metagabbro
79/28	KP99380329			Massive green gneiss
79/29	KP99100321			Grey geneiss
79/32	KP98240308			Breccia
79/33A	KP97980330	X		Grey gneiss
79/34A	KP97920357	X		Eclogite
79/34D	KP97920357			Harzburgite
79/37	LP05650000	X		Grey gneiss
79/38A	LN04729901	X		Amphibolite
79/38B	LN04729901	X	X	Eclogite
79/41A	KP97400162	X		Fe-Ti ore
79/41B	KP97400162	X		Fe-Ti ore
79/41C	KP97400162	X		Fe-Ti-ore
79/43A	KP99530338			Grey gneiss
79/43B	KP99530338	X		Massive green gneiss
79/44A	LP05550070	X		Pink gneiss
79/44B	LP05550070			Pink gneiss
79/45	LP05550070	X		Pink gneiss

Specimen	Grid Ref	Bulk-rock Analysis	Probe Analysis	Lithology
79/46	LN06109855	X		Pink gneiss
D1	LP04910391	X		Retrogr.eclog
D5	LP05040423	X		Coronite
D6	LP05040423	X		Coronite
D7	LP05040423	X		Coronite
D9	LP05040423	X		Dunite
D10	LP05040423	X		Dunite
D12	LP05300380	X		Eclogite
D13	LP04870349			Websterite
D14	LP04870349			Websterite
D15	LP04400314			Amphibolite
D22	KP98060268	X		Websterite
D23	KP97630270	X		Low-K gneiss
D24	KP97480268	X	X	Low-K gneiss
D25	KP97290251	X		Websterite
D26	KP96130301	X		Grey gneiss
D27	KP95980308	X		Hornblendite
D28	KP95980308	X		Websterite
D30	KP96490290	X		Grey gneiss
D32	KP97900361	X		Eclogite
D33	KP97900361	X		Retrogr. eclog
D35	KP97510374	X		Coronite
D36	KP97510374	X		Coronite
D37	KP97050390	X		Eclogite
D37A	KP95880271	X		Coronite
D37B	KP95880271	X		Coronite
D38	KP94310328	X		Eclogite
D39	KP96870223	X		Coronite
D40	KP99300245	X		Websterite
D41	KP97450156	X		Retrogr. eclog
D42	KP97570172	X		Eclogite
D43	KP97570172	X		Dunite
D44	LP00410304	X		Grey gneiss
D45	KP99960313	X	X	Websterite
D46	KP99960313	X		Eclogite
D49	KP98780355	X		Coronite
D56	KP97670675			Metagabbro
D57	KP97090734	X		Metagabbro
D60	KP96870591	X		Eclogite
D62	KP98730348	X		Retrogr. eclog
D66	KP98210313	X		Websterite
D68	LP00260079	X		Meta-diorite
D69	LP00890033	X	X	Eclogite
D71	KP99980012	X		Meta-diorite
D77	LP02650166	X	X	Eclogite
D78	KP98090319	X		Grey gneiss
D79	KP98090319	X		Grey gneiss
D80	KP98090319	X		Eclogite
D81	KP98090319	X		Eclogite
D82	KP98090319	X		Eclogite

Specimen	Grid Ref	Bulk-rock Analysis	Probe Analysis	Lithology
D83	KP98090319	X		Eclogite
D83A	KP98090319		X	Eclogite
D84	KP97890365	X		Harzburgite
D86	KP97510374	X		Coronite
D90	KP96360084	X		Eclog/amphib
D91	KP96360084	X		Eclog/amphib
D94	KP98070301	X		Websterite
D95	LP00700184	X		Retrogr eclog
D96	KP97310170	X		Anorth troct
D97	LP04990274	X		Grey gneiss
D99	LP05050271	X	X	Charno-enderbite
D101	LP04420267	X		Retrogr. eclog
D102	LP04290165	X		Eclogite
D103	LP04460214	X		Amphibolite
D104	LP04940171	X		Eclogite
D105	LP04940171	X		Amphibolite
D108	LP05320242	X		Amphibolite
D110	LP01970384	X		Massive green gneiss
D111	LP02300375	X		Dunite
D112	LP02760405	X		Massive green gneiss
D113	LP05620115	X		Massive green gneiss
D114	LP05620115	X		Massive green gneiss
D115	LP05620115	X		Massive green gneiss
D116	LP05780088	X	X	Eclogite
D117	LP05570076	X		Grey gneiss
D118	LP0394065	X		Eclog/amphib
D119	LP03910469	X		Amphibolite
D120	LP03700439	X		Massive green gneiss
D121	LP02640315	X		Low-K gneiss
D123	LP02600286	X	X	Eclogite
D124	LP04620369	X		Websterite
D127	KP99650100	X		Coronite
D128	KP99880111	X		Dunite
D129	LP01150290	X		Eclogite
D130	LP01400360	X		Dunite
D131	KP95940252	X		Coronite
D132	KP95850260	X	X	Coronite
D133	KP95760265	X		Coronite
D134	KP97930341	X	X	Metabasalt
D135	KP97930341			Metabasalt
D138	LP05100401			Zoisitite
D140	LP05190401	X		Zoisitite
D141	LP05190401	X		Dunite
D142	KP98630125	X		Coronite
D143	KP98610095	X		Anorth. troct
D144	LP04690439	X		Harzburgite
D145	LP04690439	X		Harzburgite
D146	LP04690439			Dunite
D148	LP05410356	X		Garnetite
D149	LP05410356	X		Dunite

Specimen	Grid Ref	Bulk-rock Analysis	Probe Analysis	Lithology
D152	KP97400162			Metabasite
D153	KP97400162			Metabasite
D155	KP97400162	X		Metabasite
D156	KP97230166	X		Coronite
D163	LP05300380	X	X	Harzburgite
D168	LP05200325			Low-K gneiss
D170	KP98610095		X	Anorth troct
D171	KP98860103			Coronite
D174	KP98210313	X		Garnet-mica rock
D175	KP97980303			Eclogite
D176	KP97980303			Eclogite
D177	KP97980303			Eclog/amphib
D178	KP96760600		X	Paragneiss
D179	KP96760600		X	Paragneiss
D181	KP96880596		X	Backvein
D184	KP99530338	X		Massive green gneiss
D187	KP97510374		X	Coronite
D192	KP97510374		X	Coronite
D194	KP97510374		X	Coronite
D203	KP97839362		X	Harzburgite
D205	KP97920357		X	Eclogite
D206	KP97920357	X	X	Eclog/amphib
D208	KP97510374		X	Omph vein
DF4	KP97830362	X	X	Harzburgite
DG-1	LP05050267	X		Grey gneiss
DG-2	LP05050267	X		Grey gneiss
DG-5	LP05050267	X		Grey gneiss
DG-7	LP05050267	X		Grey gneiss
6-55	KP97510374		X	Coronite

A3.2 Field Sketches and Photographs.

Figure	Grid Ref	Photomicrograph Specimen No
2.01	LP02170630	
2.02	LP02170630	79/19
2.03	LP01690680	79/21
2.04	KP98690760	
2.05	KP96760600	
2.06	KP96880596	D181
2.07	LP01400360	
2.08	KP98610095	
2.09	KP98610095	D143
2.10	KP98610095	D143
2.11	KP98630125	
2.12	KP98630125	
2.13	KP96360084	

Figure	Grid Ref	Photomicrograph Specimen No
2.14	KP95850260	D132
2.15	KP95760265	D133
2.16	KP97900361	D32
2.17	KP98730348	D62
2.18	KP97920357	D206
2.19	KP97920357	D205
2.20	KP97830362	D203
2.21	KP97830362	
2.22	KP97510374	
2.23	KP97510374	
2.24	KP97510374	
2.25	KP97510374	D187
2.26	KP97510374	D194
2.27	KP97400162	79/41B
2.28	LP03940465	
2.29	LP05190401	
2.31	KP98110317	
2.32	KP98110317	
2.33	KP05010281	
2.34	LP05050271	D99
2.35	LP00410304	D44
2.36	KP98680313	79/4
2.37	KP98090319	
2.38	KP98090319	
2.39	KP98090319	
2.40	KP97930341	D134
2.41	LP04910275	
2.42	LP04910275	
2.43	KP97900330	
2.44	LP04400314	
2.45	LP02600286	D123
2.46	LP02650166	D77
2.47	KP97980303	D175
2.48	LP04190400	79/15
2.49	KP99530338	D184
2.50	KP98240308	
2.52	KP98730315	
2.53	KP98830317	
2.54	KP99960313	D45
2.55	LN04729901	79/38B
2.56	LP05780088	D116
2.57	KP98630125	
2.58	KP98550458	
2.59	LP01150290	
2.60	LP01590413	
2.61	KP98240308	
2.62	KP98830317	
2.63	LP05570066	
2.64	KP96760600	
2.66	KP96760600	D178
2.67	KP96870223	D39

Figure	Grid Ref	Photomicrograph Specimen No
2.68	KP96760600	D179
2.69	KP05300380	D163
2.70	LP05550070	79/44B
4.05	KP97920357	D206

J. metamorphic Geol. 1983, **1**, 63–90

A tectonic model for the metamorphic evolution of the Basal Gneiss Complex, Western South Norway

S. J. CUTHBERT, M. A. HARVEY & D. A. CARSWELL, *Department of Geology, University of Sheffield, Mappin Street, Sheffield S1 3JD, UK*

Abstract. A review of currently available information relevant to the Basal Gneiss Complex (BGC) of Western South Norway, combined with the authors' own observations, leads to the following conclusions.

1. Most of the BGC consists of Proterozoic crystalline rocks and probably subordinate Lower Palaeozoic cover.
2. The last major deformation of these rocks was during the Caledonian orogeny and involved large-scale thrusting, recumbent folding and doming. The structural development of the BGC is closely tied in with that of the Caledonian allochthon.
3. The whole eclogite-bearing part of the BGC has suffered a high pressure metamorphism with conditions of between 550°C, 12.5 kbar (Sunnfjord) and about 750°C, 20 kbar (Møre og Romsdal) at the metamorphic climax.
4. This metamorphism was of Caledonian age, probably rather early in the Caledonian tectonic history of the BGC and is considered to have been a rather transient event.

By setting these conclusions in a framework provided by geophysical evidence for the deep structure of the crust in southern Norway we have constructed a geotectonic model to explain the recorded metamorphic history of the BGC. It is suggested that considerable crustal thickening was caused by imbrication of the Baltic plate margin during continental collision with the Greenland plate. This resulted in high pressure metamorphism in the resulting nappe stack. Progradation of the suture caused underthrusting of the Baltic foreland below the eclogite-bearing terrain causing it to emerge at the Earth's surface, aided by tectonic stripping and erosion.

Application of isostacy equations to the model shows that eclogites can be formed by *in-situ* metamorphism in crustal rocks and reappear at the land surface above a normal thickness of crust in a single orogenic episode of approximately 65–70 Ma duration.

0263–4929/83/0300–0063 $02.00

Key-words: Caledonides; eclogites; geothermobarometry; isostacy; tectonics

INTRODUCTION

The Basal Gneiss Complex (*BGC*) of Western South Norway forms the deepest exposed structural level of the Scandinavian Caledonides (Fig. 1), being the largest of a number of basement windows in the extensive area of Caledonian nappes in Norway and Sweden (Holtedal & Dons, 1960; Roberts, Thon, Gee & Stephens, 1981).

It seems likely that this gneiss region has had a complex structural and metamorphic history, containing as it does elements resulting from Proterozoic (Svecofennian and Sveconorwegian–Grenvillian) and Caledonian orogenic events.

A particular feature of this basement window is the common occurrence of lithologies with relict high-pressure mineral assemblages, the most obvious being eclogites and garnetiferous peridotites. The gneissic hosts to these relics are commonly metamorphosed in the almandine–amphibolite or epidote–amphibolite facies. However, both low-pressure and high-pressure granulitic parageneses have been increasingly recognized in recent years (see, for instance, Griffin & Mørk, 1981).

The origin and age of these high-pressure relics are still highly controversial. Garnet peridotites and eclogites have been interpreted as solid intrusions from deeper crustal levels or from the mantle (O'Hara & Mercy, 1963; Carswell, 1968b; Lappin & Smith, 1978; Gebauer, Lappin, Gruenefelder, Koestler & Wyttenbach, 1982) or to have been metamorphosed *in-situ* in their host gneisses from low pressure protoliths (Bryhni, Krogh & Griffin, 1977; Griffin & Qvale, 1981; Griffin, Austrheim, Grastad, Bryhni, Krill, Mørk, Qvale & Tørudbakken, 1981). Geochronological results have been variously interpreted as showing a Proterozoic age for the 'main metamorphism' of eclogite-bearing gneisses (Råheim, 1977, 1979, 1981), a Caledonian 'eclogite forming event' (Griffin & Brueckner, 1980, 1982) and tectonic

GEOLOGICAL MAP OF THE HELLEVIK – FLEKKE AREA, SUNNFJORD, SOUTHWEST NORWAY

SJ CUTHBERT 1985

Enclosure 1

VEVRING COMPLEX OR HOLSEN GROUP

VEVRING COMPLEX

- paragneiss, granitic gneiss — VARDEHEIA UNIT
- phengite eclogite, chlor. harzburgite, acid intrusive metabasites, dunite — FLEKKE UNIT
- low-K gneiss, eclogite, pyroxenite — GJØRLANGER UNIT
- thrust ?
- BASAL GNEISS (JOSTEDAL COMPLEX)

DALSFJORD

GJØRLANGERFJORD

Straumsnes
Åsnesvika
Åsnes Skifabrikk
Andalsvik
Eikerol
EIKEROLHEIA
ÅRSTEINHEIA (444m)
VARDEHEIA (459m)
Elde
Flekkefjord
Haugland
Balsarvik
Solvik
Gjørlanger
Storetj
Tyssekvam
HÅHEIA (455m)
Leirpol
Solhiem
Flekke
DAURAMAISNIPA
Trollefoss
Renestraumsvn
Renestraum
Hellevik
AUREVÅGEN
Sordalsvn
Sørdal
Eiketj.
Steindalstj.
SAURDALSFJELL (312m)
Instetj.
Svartetj.
Fjelltj.
Lonedalsvn
KLIBBERN (400m)
Tyssedalsvatnet
Jyttevatnet
Botnatj.
Breidvatnet
Kuseltj.
Hovlandsvatnet
(607)
(57)

60°20'N
5°25'E
0 km 2

-(57)- road
Fe – Ti ore mine (disused)
A augen gneiss
An anorthositic troctolite
C charnockitic rock
Co coronitic meta-troctolite
D basic dyke
E eclogite
GA garnet amphibolite
Gr granitic rock
MG metagabbro/norite

LITHOLOGICAL BOUNDARIES
observed
gradational or inferred
conjectural or poorly defined
▲M postulated base of Sunnfjord Nappe, m-mylonite

STRUCTURAL ELEMENTS
foliation surface (S_1)
lineation (axis of minor fold or crenulation in S_1)

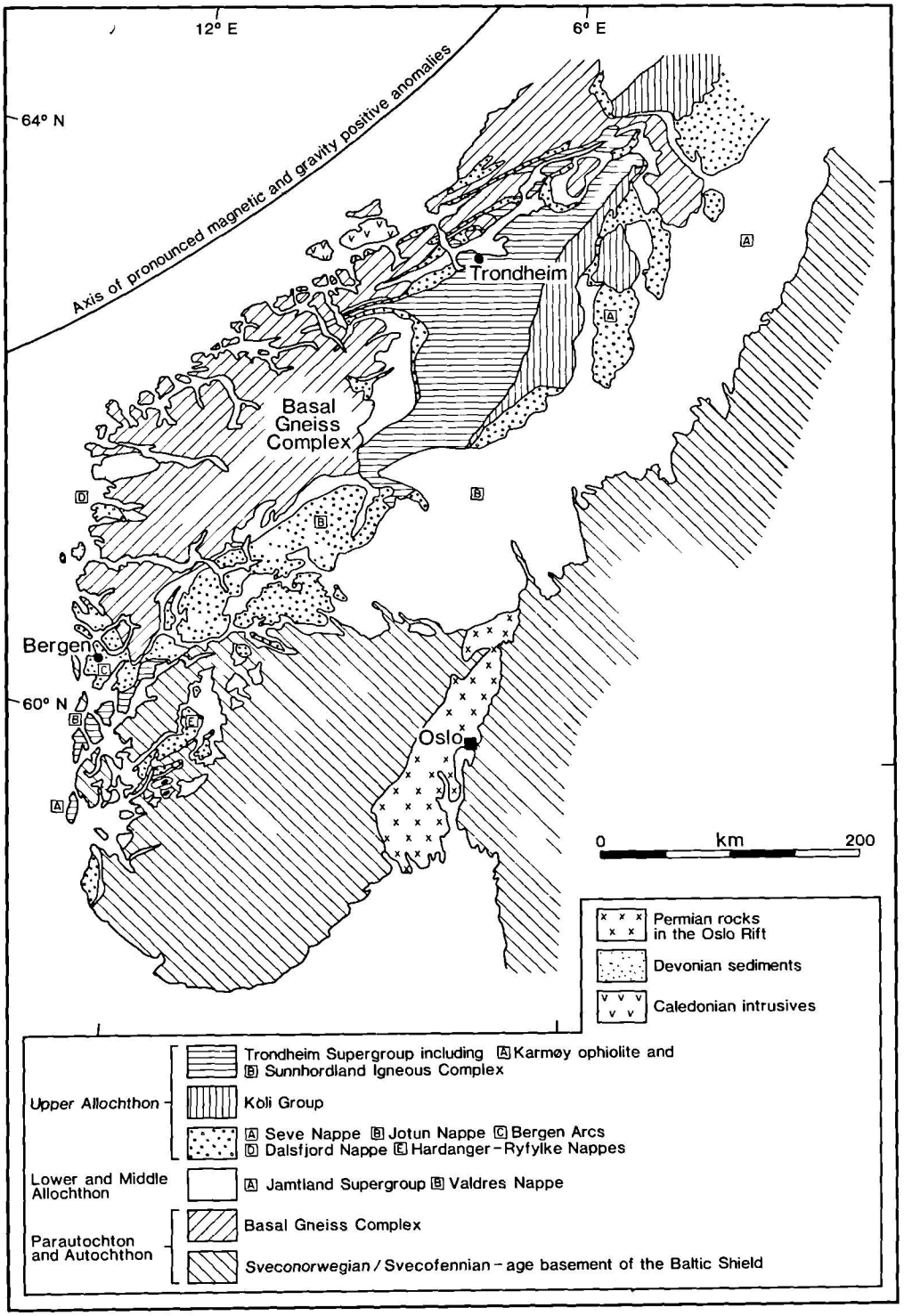

Fig. 1. Map showing the main tectonostratigraphic units of southern Scandinavia (after Roberts *et al.*, 1981).

juxtaposition of units with widely differing provenances (Mearns & Lappin, 1982 a,b,c).

The BGC is surrounded by outcrops of overlying allochtonous nappes which include units of postulated ophiolites, island-arc sequences, continental sediments and deep-seated continental crust. Some of these units also contain eclogites and garnet peridotites (Gee, 1975, 1978; Gee, Guezou, Roberts & Wolff, 1982; Guezou, 1981; Stephens & Gee, 1981; Andresen & Faerseth, 1982; van Roermund, 1981). Locations for place names are given in Fig. 2.

The aim of this paper is to develop a tectonic model which fits the petrological features of the high pressure parageneses in the BGC whilst attempting to be consistent with geochronological, tectonostratigraphic and geophysical data currently available for this part of the Caledonide belt. We hope that presentation of this model as a working hypothesis will stimulate future research, which will doubtless lead to its refinement.

THE GEOLOGICAL SETTING OF THE BASAL GNEISS COMPLEX

The history of the development of interpretation of geological relationships within the BGC and between the BGC and its cover has been characterized by an increasing awareness of the effect of the Caledonian orogeny (for reviews see Bryhni & Grimstad, 1970, pp. 106–109 and Carswell, 1973a).

Recent work by Gee (1980) has shown that the autochthonous Proterozoic crystalline basement at the thrust front of the Central Scandinavian Caledonides in Sweden has a characteristic cover sequence of late Precambrian and Lower Palaeozoic sediments including quartzites, greywackes, locally limestones and green or red shales and a radiogenic black shale. These form the Jämtland Supergroup. The sole thrust of the Caledonian allochthon and parautochthon rides in the black shales which have acted as a plane of

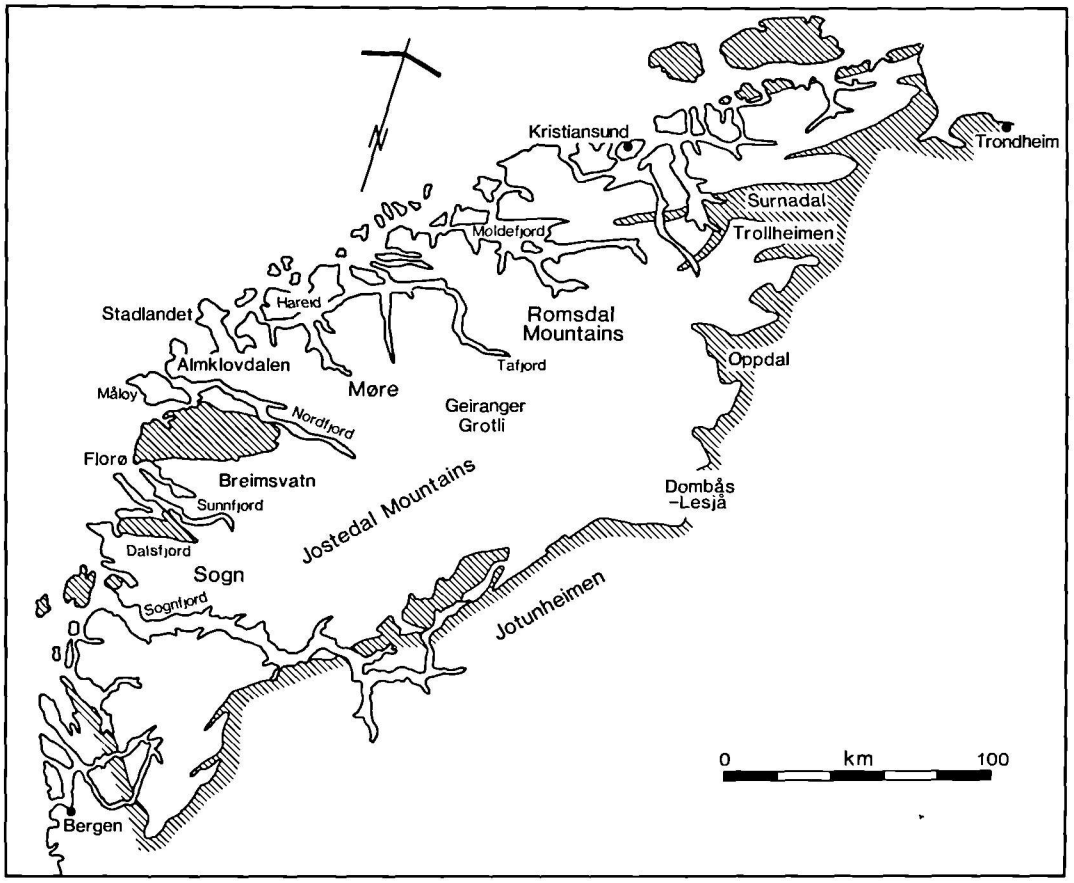

Fig. 2. Map of western south Norway showing the positions of localities mentioned in the text. Basal Gneiss Complex unshaded, higher tectonostratigraphic units shaded.

décollement (Gee, 1978, 1980). This horizon can be traced westwards below the parautochthon and allochthon within the Jämtland basement window, the Grong-Olden culmination, the Tømmerås window and the Trollheimen antiform, the last of which lies on the eastern margin of the BGC (Fig. 1).

Near the Swedish–Norwegian border the detachment surface passes into an imbricated basement, where the basement-cover sequence is repeated parautochthonously. Gee (1980), therefore, suggests that the allochthon has an origin far to the W of its present position, possibly as much as 1000 km. Imbrication of the basement in the windows implies basement shortening of at least 70 km. The metamorphic grade of the black shale increases westwards, as does the pervasive foliation in the basement associated with Caledonian thrusting.

The tectonostratigraphy of the allochthon, parautochthon and autochthon in central Scandinavia is summarized in Fig. 1. The major elements of this sequence have now been recognized in the Trollheimen antiform (Gee, 1980). They can be found further S in Oppdal (Krill, 1980; Gee, 1980) and the Dombås-Lesja area (Guezou, 1978) and to the N and W in the Surnadal and Kristiansund areas (Krill, 1981a; Hernes, 1955; Raheim, 1972). Further to the W in the BGC strong deformation and metamorphism makes correlation more difficult. However, broadly similar sequences with a heterogeneous 'cover' sequence over a more homogeneous 'basement' are seen at Grotli (Strand, 1969; Bryhni, 1977), Tafjord (Bryhni, 1977; Brueckner, 1977), Breimsvatn (Bryhni, 1977; Bryhni & Grimstad, 1970) and possibly Sunnfjord (Skjerlie, 1969; Skjerlie & Pringle, 1978). In most of these areas it has been demonstrated that units with differing origins have been tectonically juxtaposed prior to recumbent isoclinal folding and doming. Most of these units W of Surnadal contain eclogites and garnetiferous ultrabasites. These and other high pressure metamorphic relics will be discussed in more detail below.

The eastern margin of the BGC exhibits 'Stockwerk'-type tectonics in its relationship to the low-grade rocks of the overlying Trondheim Supergroup. Recent work by Krill (1980, 1981a) in the Oppdal-Surnadal area shows that Pennine-style Caledonian F_1 recumbent folds formed in the 'infrastructure', folding a series of thrust-juxtaposed units. These folds do not involve the 'superstructure' (the Støren unit of the Trondheim Supergroup). Younger, upright folds involve both the infrastructure and the superstructure and become tighter downwards from the base of the Støren unit. Metamorphic grade increases westwards (downwards) in the superstructure, as it does in the infrastructure. Eclogites appear within 20 km of the base of the infrastructure except at Surnadal where they appear within 5 km, apparently by prograde metamorphism via amphibolites. Rb-Sr studies of metabasic dykes in the Saetra nappe and late granitic intrusions (see below) suggest that both the folding and metamorphism is Caledonian (Krill, 1981b).

It would therefore appear that the main Caledonian deformation and metamorphism occured *in-situ* beneath the superstructure apparently formed by the allochthon. Whether the present superstructure is the same as that which originally formed the overburden to the BGC during the early period of metamorphism, or whether it has tectonically replaced an earlier overburden seems equivocal at present (Krill, 1980).

The history of the nappe-pile overlying the BGC and the basement to the E has been summarized by Gee (1975, 1978) and Gee *et al.* (1982). They suggest that the early development of the nappes follows obduction of ophiolites onto the Baltic continental margin in the early Ordovician. Then final closure of the Iapetus ocean resulted in the Greenland continental margin overthrusting that of the Baltic plate during the Middle and Upper Silurian. The resulting compressional regime led to considerable basement shortening and imbrication of basement and cover. Subsequent basement uplift then resulted in translation and stretching of the nappes towards the present Caledonian front in the east.

The Seva nappe of Jämtland, Central Scandinavian Caledonides, also contains eclogite and garnet-peridotite bodies. Roermund (1981) has found that the eclogites are comparable to those in the BGC and restoration of the Seve to its possible pre-translation position reveals that the regional P–T variation seen in eclogites from this nappe complex matches that of western Norway (van Roermund, 1981; Bryhni *et al.*, 1977; Krogh, 1977a; Griffin & Mørk, 1981). As Seve lithostratigraphic units are recognized in the eastern BGC (Table 1) and can be traced into eclogite-bearing terrains (Krill, 1981a) it seems sensible to conclude that the allochthonous Seve nappe now seen in Sweden was originally rooted in the BGC, or at least had a common early metamorphic history with it.

Bordering the BGC to the S and SW is the huge Jotun nappe which consists of Precambrian anor-

Table 1. Summary of the metamorphic evolution of the coronitic metadolerites, after Griffin & Råheim (1973) and Griffin & Bryhni (1977). The development of corona types is shown for reactions between (A) igneous plagioclase and olivine; (B) igneous plagioclase and clinopyroxene; and (C) igneous plagioclase and orthopyroxene. Each column represents the order of corona shells observed at each stage in the metamorphic evolutionary sequence, with short solid lines separating successive shells. Numbers indicate the reactions responsible for each stage of corona formation, as outlined at the bottom of the table. Plag = plagioclase; Ol = Mg-rich olivine; Cpx = clinopyroxene; Opx = orthopyroxene; Sp = spinel; Gnt = garnet; Omph = omphacite; Qtz = quartz; Rt = rutile

Decreasing T, increasing P →								Decreasing P, T constant?
(A)								
	→	Plag / Cpx *I* + Sp / Opx / Ol	→	Plag / Cpx I + Sp	→	Plag	→	Plag / Gnt / Plag II / low Na Cpx / high Na ± Opx, Ol
Plag Ol	(1)		(2) (3) (4)	Gnt / Cpx II / Opx / Ol	(2) (3) (4) (5) (8) (9)	Gnt / Omph ± Opx ± Ol	(10) (11) (12)	
(B)								
		→	Plag	→ (6) (7)	Plag	→	Plag / Gnt / Plag II / low Na Cpx / High Na
Plag Igneous Cpx		(6) (7)	Gnt / Omph / Cpx II + Rt	(8) (9)	Gnt / Omph + Rt	(10) (11) (12)	
(C)								
		→	Plag	→ (4) (5)	Plag	→	Plag / Gnt ± Qtz / Plag II / low Na Cpx / high Na ± Cpx
Plag Igneous Opx		(4) (5)	Gnt / low Al Opx	(7) (8) (9)	Gnt ± Qtz / Omph / Opx	(10) (11) (12)	

Reactions:
(1) Ol + plag → Al-Opx + Al-CpxI + Sp. (2) Al-px's + Sp + plag → Gnt + low Al-Cpx II + low Al-Opx. (3) $6MgSiO_3 + CaAl_2Si_2O_8 + MgAl_2O_4 \rightarrow CaMgSi_2O_6 + 2Mg_3Al_2Si_3O_{12}$. (4) $4MgSiO_3 + CaAl_2Si_2O_8 \rightarrow CaMgSi_2O_6 + Mg_3Al_2Si_3O_{12} + SiO_2$. (5) $MgAl_2SiO_6 + 2MgSiO_3 \rightarrow Mg_3Al_2Si_3O_{12}$. (6) $CaMgSi_2O_6 + MgAl_2SiO_6 \rightarrow CaMg_2Al_2Si_3O_{12}$. (7) $NaAlSi_3O_8 + CaAl_2SiO_6 \rightarrow NaAlSi_2O_6 + CaAl_2Si_2O_8$. (8) $CaAl_2Si_2O_8 + CaMgSi_2O_6 \rightarrow Ca_2MgAl_2Si_3O_{12} + SiO_2$. (9) $NaAlSi_3O_8 \rightarrow NaAlSi_2O_6 + SiO_2$. (10) $CaMg_2Al_2Si_3O_{12} \rightarrow MgAl_2SiO_6 + CaMgSi_2O_6$. (11) $Ca_2MgAl_2Si_3O_{12} + SiO_2 \rightarrow CaMgSi_2O_6 + CaAl_2Si_2O_8$. (12) $NaAlSi_2O_6 + SiO_2 \rightarrow NaAlSi_3O_8$.

thosites, ultramafites, pyroxene granulites, etc., with a peripheral group of amphibolite-facies gabbroic and granitic rocks (Battey & McRitchie, 1973). It lies in a large, synclinal depression known as the 'Faltungsgraben'. Gravity studies of the nappe have shown it to be a wedge-shaped prism with a deep, dense root and a thickness of 10–15 km (Smithson, Ramberg & Grønlie, 1974). It is structurally overlain by the Trondheim nappe and underlain by Eocambrian (Sparagmitic) to

Cambro-Silurian sediments. In the S (Valdres area) the autochthonous Proterozoic basement has an autochthonous veneer of Middle Cambrian shale. This is overlain by two imbricate duplex sheets of sediments, roofed by the Valdres nappe composed of Eocambrian–Ordovician sediments, on an allochthonous gneissic basement. The Valdres nappe is in turn overlain by the Jotun nappe whose southward movement here is well established (Hossack, 1978; Hossack, Nickelson & Garton, 1981), and has caused considerable telescoping of the cover sequence. From this it has often been assumed that the Jotun nappe is a large, far-travelled thrust nappe. The existence of smaller, Jotun-like thrust sheets on the W coast of Norway (e.g. the Dalsfjord nappe) has led to the suggestion that these outcrops represent the trailing edge of the Jotun nappe and that the BGC is a tectonic window within it (Skjerlie, 1969; Hossack, 1982).

However, structural evidence from the northern margin of the Jotun nappe against the BGC may suggest that it has moved to the NW here (Battey & McRitchie, 1973; Banham, Gibbs & Hopper, 1979). This has led to the alternative suggestion that the Jotun nappe has had a local derivation, whereby it has risen directly from the root of the Faltungsgraben as an 'Ivrea-type flake' (Battey & McRitchie, 1973; Smithson *et al.*, 1974; Banham *et al.*, 1979). Underlying the northern margin of the Jotun nappe is a sequence of parautochthonous sediments and metavolcanics, locally with pillow-lavas and serpentinites (Banham *et al.*, 1979; Elliot & Cowan, 1966) and a postulated 'exotic olistostrome melange' (Gibbs, 1982). Two explanations for this are: either the northern Jotun nappe front represents a Caledonian suture zone (Banham *et al.*, 1979) or the opposing senses of motion of the nappe margins and underlying tectonostratigraphy are the result of the compressive telescoping of a rifted marginal basin, the nappe representing the root of the central graben high (Gibbs, 1982).

Along the SW extension of the Faltungsgraben lie the nappes of the Hardangervidda area and those of the Bergen arcs. Andresen & Faerseth (1982) have summarized the relationships here, which show close similarities to the Jotunheim and, to some extent, the Trondheim areas. Lying above the foreland Proterozoic basement and its cover (Vidda Group) is the Hardangervidda-Ryfylke nappe complex, whose lower unit (Hosmasjø/Nupsfonn allochton) correlates with the nappes of the Valdres area and whose upper units, the Dyrskard, Kvitenut and Revsegg units, are correlated with the Jotun nappe and perhaps, in part, the Røros schists at Surnadal. Overlying this is the Sunnhordland nappe complex, consisting of ophiolites and island-arc volcanics, possible continental rift volcanics and intrusives, allochthonous basement and later sediments associated with uplift of this sequence.

In their synthesis of this area, Andresen & Faerseth (1982) suggest that the ophiolites were obducted onto an Andean-type Baltic margin prior to the Ashgillian. Following intrusion by granodiorites this sequence was thrust over the Proterozoic basement (Dyrskard-Kvitenut-Revsegg allochthon) and the whole stack was then translated over the autochthonous basement and the Vidda Group.

Similar rocks to those of the Jotun-Hardanger areas occur in the Bergen arcs (Sturt, Skarpenes, Ohanian & Pringle, 1975; Sturt & Thon, 1976; Andresen & Faerseth, 1982). However, here the eugeoclinal rocks (Major and Minor Arcs) correspond to the Sunnhordland Nappe Complex and presumably the Trondheim nappe, but form the lowest tectonic unit above the basement gneisses and are overlain by allochthonous Proterozoic crystalline rocks (Ulrikkens Gneiss Complex, Anorthosite Complex). The Anorthosite Complex contains eclogites of postulated Caledonian, or possibly Sveconorwegian age (Austrheim & Råheim, 1981; Austrheim, 1981; Austrheim & Griffin, 1982) and may be correlated with the Jotun nappe. However, as it has had a different structural history it may represent a higher structural level than that observed in the Jotun nappe (Andresen & Faerseth, 1982). The Bergen Arcs are also commonly thought to comprise far-travelled nappes with a source off the present W coast of Norway (Sturt *et al.*, 1975; Austrheim, 1981).

A similar sequence to that in the northern Jotunheimen is found in the Dalsfjord area, Sunnfjord, where a sheet of mangerites (the Dalsfjord nappe) has been thrust over metagreywackes (Askvoll Group) and in turn overthrust by a eugeoclinal ophiolite/island arc sequence (Stavfjord anticline) prior to emplacement of the thrust stack onto the Baltic margin (now the BGC) (Skjerlie, 1969, 1974; Furnes, Skjerlie & Tysseland, 1976).

Suggested correlations of the Hardanger, Bergen and Dalsfjord nappe sequences with the Jotun nappe mitigate against its local origin and favour its evolution as a far-travelled sheet. In this case its huge thickness must have greatly contributed to the load over the eclogite-bearing BGC. However, resolution of the problems of interpretation of the structures and lithologies of

northern Jotunheimen will be necessary before a local origin can be discounted. If such an origin should be ultimately proven some very large scale mechanism must be invoked to explain the upward travel of such a large, dense mass and its super-position over less dense crustal material.

In summary, the BGC appears to consist of an intensely imbricated and interfolded mass of crystalline pre-Caledonian basement and autochthonous and allochthonous cover, the major part of which bears common relics of high pressure assemblages. It forms a window within overlying nappes of basement, cover and oceanic rocks of considerable overall thickness. Representatives of most of these allochthonous units can be found within the BGC. Three stages in the development of the orogen appear to have occurred. The first involved obduction of oceanic crust and island-arcs in the early-middle Ordovician, the second involved stacking and recumbent folding of imbricate sheets of basement, cover and obducted rocks during the early-middle Silurian continental collision and the third involved 'basement' uplift, uprooting of the nappes and their translation on a dècollement plane towards the Swedish and S Norwegian foreland. Following this, in the early-middle Devonian, late orogenic intermontane basins formed controlled by either hinged normal faults or strike-slip faults (Bryhni, 1981).

GEOCHRONOLOGY

From the foregoing it is apparent that the Caledonian history of the BGC is bracketed by two ages; the upper age of the rocks formed prior to the development of the allochthon, corre sponding to the Llandoverian of the Köli Supergroup (Gee, 1975, 1978) and the early-middle Devonian age of the late-orogenic, unmetamorphosed sediments found in fault-bounded basins on the W coast of Norway. These sediments overlie eclogite-bearing gneisses and must therefore mark the end of a period of very considerable uplift, especially if a Caledonian age and crustal *in-situ* metamorphic origin for the eclogites is accepted (see below).

Viewing the ages obtained from whole-rock Rb-Sr isochron studies of gneisses in the BGC (e.g. Brueckner, 1972, 1979) it is noticeable that they bear a close similarity to those seen in the Svecofennian and Sveconorwegian provinces in the foreland of southern Norway and Sweden, although perhaps the age distribution in the BGC is more complex. However, mineral ages are markedly different. Mineral ages in the Baltic foreland unaffected by the Caledonian orogeny are usually similar to the whole-rock ages (Brueckner, 1972) but in the BGC Rb-Sr mineral ages generally show late Caledonian provenance, clustering tightly between 380 Ma, and 405 Ma. This is perhaps not surprising in view of the position of the BGC in relation to the rest of the Caledonide belt, but considerable controversy revolves around the interpretation of these ages.

One school of thought is that the Proterozoic whole-rock Rb-Sr ages represent a metamorphic event, usually at amphibolite facies, and that the Caledonian Rb-Sr mineral ages are a result of post-orogenic cooling related to uplift or of a relatively unimportant thermal event resetting the isotopic system (Råheim, 1977, 1979; Pigeon & Råheim 1972; Skjerlie & Pringle, 1978; Solheim, 1980; Mearns & Lappin, 1982 a,b,c). That implies that most, if not all the major metamorphism in the BGC occurred in the Sveconorwegian or Svecofennian and the Caledonian effect is minimal. The pervasive nature of the amphibolite-facies metamorphism, allied with independent evidence for a Caledonian eclogite-forming event has led Mearns & Lappin (1982 a,c) and Gebauer *et al.* (1982) to suggest that the eclogites were tectonically introduced into the gneisses from deeper lithospheric levels during the Caledonian orogeny. Mearns & Lappin (1982c) from a study of granulite-facies 'mangerites' in the Selje area, Stadlandet, further suggest the influence of a 700 Ma granulite-facies event which seriously disturbed the Rb-Sr system by Rb loss after intrusion at 1520 Ma. However, Lappin, Pidgeon & van Breemen (1979) have shown that the composition of these rocks has not changed significantly since intrusion except for some K-metasomatism. Furthermore, there are no other records of an important 700 Ma granulite-facies event. This age comes from a plagioclase–garnet whole-rock Sm-Nd isochron for a basic dyke and may either be a mixed age or a relict igneous age.

Research workers who consider whole-rock Rb-Sr isochrons to record a metamorphic event clearly recognize that the low initial ratios of these isochrons puts severe constraints on the time which elapsed between magmatic crystallization of the rock suite and metamorphism. In fact the time period may easily lie within the error envelope of the isochron age. Upper intersection U-Pb ages from discordant zircons are often close to Rb-Sr whole rock ages and are taken to indicate the time of magmatic crystallization (Pigeon & Råheim, 1972; Lappin *et al.*, 1979). Lower inter-

section ages are usually around 400 Ma suggesting a pervasive Caledonian event.

The other school of thought considers that whole rock Rb-Sr isochrons represent magmatic crystallization ages and that subsequent events have only caused minor disturbance to the isotopic system (Brueckner, 1972, 1979; Carswell & Harvey, 1983; Harvey, unpublished data; Krill & Griffin, 1981). The significance of the Caledonian mineral ages is less certain. Brueckner (op. cit.) gives two possibilities; that the metamorphism was Proterozoic but a slight re-heating event reset the mineral ages ('limited Caledonization') or that the most severe recrystallization was Caledonian ('severe Caledonization'). With respect to the latter, Brueckner (1979) points out that the youngest good whole-rock ages for the gneisses are 960 Ma (granodiorite near Geiranger) and 975 Ma (Hestbrepiggan granite). Both of these rock suites have a pervasive tectonic fabric which must have been imposed during either the late Sveconorwegian or the Caledonian. In addition to this we note that the evidence of Gee (1980) and Krill (1980) in favour of a Caledonian age for the main deformation in the BGC strongly supports a 'severe Caledonization'. Also, Krill (1981a) reports a 745 Ma whole rock Rb-Sr date for a pretectonic dyke in the Saetra unit near Oppdal and a 345 Ma Rb-Sr mineral isochron age from a granitic intrusion cutting a regionally mapped thrust surface in the same area, bracketing tte tectonic events within the Caledonian orogeny.

A recent study of coexisting green (Caledonian) and brown (Sveconorwegian) biotites from near the Caledonian front in SW Norway (Verschure, Andressen, Boelrijk, Hebden, Maier, Priem & Verdurmen, 1980) shows that resetting of biotite Rb-Sr and K-Ar ages at temperatures of up to 400 C may require complete recrystallization. This brings into question the validity of models requiring a limited Caledonian heating event. Krill & Griffin (1981) comparing interpretations of whole rock Rb-Sr ages from the BGC with those in the Alps suggest that such ages can record magmatic events despite very strong tectonism and metamorphism. They reject the likelihood of large-scale homogenization of isotope systems during orogenesis.

Whilst it is not intended to review the distribution of whole-rock ages within the BGC, it is significant that all reliable ages for gneisses are either Svecofennian or Sveconorwegian, dominantly the former. Good evidence for Caledonian protolith ages comes from Gee's (1980) correlation of Cambrian sediments into the Trollheimen area. Other evidence comes from the common lithological comparison of metaquartzites and arkoses with the Eocambrian Sparagmites of southern Norway.

We, therefore, prefer the interpretation that whilst the main crust-forming events for lithologies in the BGC were Proterozoic, the tectonic and metamorphic events responsible for the present state of this area were dominantly Caledonian.

Outside the BGC in S Norway granulite-facies assemblages are common in Proterozoic gneisses. Also, relict granulite-facies parageneses are sometimes found within amphibolite-facies gneisses of the BGC (Lappin *et al.* 1979; Krogh, 1980a, Mearns, 1982; Cuthbert, unpublished data). In view of the Proterozoic provenances of the BGC gneisses, it seems reasonable to expect to encounter relics of such older parageneses. Bryhni, Fitch & Miller (1971) carried out $^{39}Ar/^{40}Ar$ age spectrum analysis on a clinopyroxene from an augen-gneiss in the Fjordane complex, Gloppen. The most retentive argon gave an age of 1550 Ma, which may record the age of its crystallization, under granulite-facies conditions.

However, eclogite-facies relics are also found in the gneisses, as eclogites, garnet peridotites and isolated gneissic domains containing omphacitic pyroxene or diopside–plagioclase symplectites. These also show the influence of pervasive later amphibolitization. At Flekke, Sunnfjord, low-pressure granulites are preserved (Opx + Cpx + plag + K-feldspar + quartz) with garnet coronas forming on orthopyroxene aggregates (Cuthbert & Carswell, 1982). This is taken to indicate a superimposed higher pressure (and lower temperature) event, correlated with similar textural development in partially eclogitized metabasites. Identical relationships are seen at Flatraket, Stadlandet (Cuthbert, unpublished data) and in the Bergen Arcs (Austrheim & Griffin, 1982). In all these areas subsequent pervasive amphibolite-facies recrystallization has occurred. Hence there is evidence here that a high pressure event postdates the Proterozoic granulites and predates the amphibolite-facies metamorphism. Resolution of the complex polymetamorphic history of the BGC undoubtedly requires very careful petrographic observations before any *a-priori* assumptions can be made about the relative (or absolute) ages of the mineral parageneses.

Recent evidence has begun to throw light on the age of eclogite formation. Krogh, Myson & Davis (1973) reported a U-Pb zircon age of 401 ± 20 Ma from the Ulsteinvik eclogite, Hareidland. The zircons contained inclusions of eclogite-facies

minerals but no secondary minerals, hence the age was taken as a minimum age for formation of the eclogite. However, this age is not entirely unambiguous in that it only provides an upper limit for this event and there is evidence for some older, inherited zircon in the rock.

Griffin & Brueckner (1980) have presented five two-point Sm-Nd mineral isochrons using garnets and clinopyroxenes from eclogites. Ages in the range 407–477 Ma were obtained, in close agreement with the results of Krogh *et al.* (1973) and slightly older than, but overlapping with, Rb-Sr mineral ages from the gneisses. Sm-Nd and Rb-Sr isotope systematics suggest that at least some of the eclogite protoliths had a long crustal history prior to the Caledonian orogeny. Further work (Griffin & Brueckner, 1982) has demonstrated the difficulty of obtaining meaningful Sm-Nd ages from eclogites with equilibrium temperatures below about 700 C due to disequilibrium distribution of REE between garnet and pyroxene. Samples with zoned garnets tend to give much older ages. A five-point Rb-Sr mineral isochron from the Verpeneset eclogite, Nordfjord, gave an age of 398 ± 1 Ma with an initial ratio of 0.7034, suggesting that the protolith is probably Palaeozoic and thus the metamorphism Caledonian.

Mearns & Lappin (1982b) have reported Sm-Nd garnet–clinopyroxene whole-rock isochron ages for garnet lherzolites and associated garnet pyroxenites as well as for an 'external' or 'country-rock' eclogite and a garnet whole-rock age from a grey gneiss. The eclogite gave an age of 408 ± 8 Ma, the gneiss 414 ± 31 Ma, suggesting recrystallization or 'thermal resetting' of Proterozoic material during the Caledonian orogeny. The ultramafites gave much older ages and a low εNd (1029 ± 34 Ma, $\varepsilon\text{Nd} = -1.6$; 1316 ± 138 Ma, $\varepsilon\text{Nd} = -1.4$) suggesting crystallization soon after formation of the whole-rock in the mantle and that these rocks have apparently not been disturbed by any Caledonian metamorphic events.

Gebauer *et al.* (1982) have also reported Caledonian ages for eclogites from U-Pb zircon discordia, which suggest protolith formation in the Svecofennian and Sveconorwegian and eclogite metamorphism at about 400 Ma.

Krill (1981) has produced a Rb-Sr whole rock isochron for an intermediate gneiss which is interbanded with eclogite-bearing mica schists of the Blaho unit W of Oppdal, giving an age of 583 ± 69 Ma. This further supports a Caledonian age for the eclogite metamorphism.

Some indication of the severity of the Caledonian thermal event is given by Devonian mineral ages from pegmatites which cut eclogites, indicating temperatures high enough to cause anatexis well into the waning stages of the orogeny (Griffin & Mørk, 1981).

Together these various data strongly indicate that the major crust-forming events for the lithologies in the BGC were Proterozoic, dominantly in the Svecofennian but with significant contributions from the Sveconorwegian and Caledonian events. It is quite possible that much of this crustal (and mantle?) material suffered high-grade amphibolite and/or granulite facies metamorphism prior to the early Palaeozoic, but a growing body of evidence supports a major tectonometamorphic event in the BGC during the Caledonian orogeny, commencing at least as early as 420 Ma. The significance of the eclogite mineral ages depends upon prejudicial interpretation of the origins of these controversial rocks (*cf.* Bryhni *et al.*, 1977; Lappin & Smith, 1978; Smith, 1980; Carswell & Gibb, 1980; Griffin *et al.*, 1981), but it is possible that this orogenic event involved depression of very large masses of continental crust to great depths prior to their exhumation and exposure at the land surface by the early to middle Devonian.

METAMORPHIC EVOLUTION OF THE BASAL GNEISS COMPLEX

Much of the research carried out in the BGC has centred around two rather exotic and enigmatic rock-types, the eclogites and the garnetiferous peridotites. This is especially true of work during the last 20 years; a result of the surge of interest in the nature of the upper mantle. The fact that these eclogite-facies assemblages occur in a terrain apparently consisting largely of amphibolite-facies assemblages has caused discussion of an intensity which is out of all proportion to their rather insignificant volume. This metamorphic contrast has led to the eclogites being described as 'foreign inclusions' (e.g. Lappin, 1966) and evolutionary models involving tectonic transport of eclogites and peridotites from sub-crustal depths to high lithospheric levels have been developed to explain their presence (Lappin & Smith, 1978; O'Hara, 1976; Smith, 1980).

There is, however, a growing body of evidence (outlined below) to suggest that in many cases eclogites and even garnet peridotites have been formed by metamorphism *in-situ* within their country rocks. Conclusive proof of this has profound tectonic consequences as it implies that large masses of buoyant continental crust have

been subjected to unusually large confining pressures.

Occurrence of eclogite-facies rocks

Eclogites occur in both the Jostedal and Fjordane complexes of Bryhni (1966), but are more common in the latter unit. They are also reported from the Vikvatn sequence in the Tafjord area, but not in the basal Fetvatn gneisses (Brueckner, 1977). They occur in the Frei group of the Kristiansund area (Råheim, 1972; Griffin & Råheim, 1973; Krogh, 1980b) and in Surnadal (Tørudbakken, 1981). Hence the eclogites occur in most, if not all, of the lithologic units of the BGC, to within 25 km of its border with the overlying allochthon in the E. However, eclogites are apparently absent in the BGC to the S of Sognfjord.

In the more heterogeneous rock sequences (e.g. the Fjordane complex) eclogites are frequently associated with anorthosites (Eskola, 1921; Brueckner, 1977; Bryhni, 1966; Brastad, 1983; Griffin & Mørk, 1981) as well as obvious supracrustal rocks (Bryhni, 1966; Carswell & Harvey, 1983; Harvey, unpublished data). Garnet peridotites appear to be confined to these heterogeneous gneisses (Bryhni, 1966; Carswell, 1973a; Brueckner, 1977) but are generally absent to the S of Nordfjord, where hydrous peridotites are more normally present. The close association of some peridotites to what are apparently layered basic bodies and to anorthosites has often been noted (Schmitt, 1964; Eskola, 1921; Brueckner, 1977; Bryhni, 1966; Brastad, 1982). Some authors have noted the common occurrence of garnet peridotites in steeply inclined shear belts (Bryhni, 1966; Lappin, 1966) but Brueckner (1977) considers this to be due to their 'stratigraphic' position on the limbs of large-scale folds.

Lappin (1966) suggested that eclogites share most of the structural history of the surrounding gneisses at Selje, Stadlandet, and Almklovdalen, but that anorthosites and garnet peridotites were introduced at successively later stages. However, Medaris (1980) has found that all the structural elements in the gneisses at Almklovdalen are shared by the peridotites. Similar relationships occur in peridotites at Rødskaret, Gurksøy (Griffin and Mørk, 1981). At Kalskaret, Tafjord, peridotites, anorthosites, eclogites and gneisses have all undergone the same structural history (Brueckner, 1977). At Bjørkedalen, eclogites show gradational contacts towards anorthosites and close association with peridotites, all of which have at least two fold episodes in common with the gneisses (Brastad, 1982, 1983). In all these examples the earliest obvious pervasive foliation is associated with amphibolite facies assemblages which postdate the eclogite-facies parageneses. Hence the eclogites and garnet peridotites can be described as relics whose mineral facies would appear to have converged with that of the gneisses during deformation associated with amphibolite-facies metamorphism.

Foreign versus in-situ metamorphism

Early arguments in favour of the foreign tectonic origin of eclogites and peridotites stemmed from the apparent difference in metamorphic grade between these rocks and their host gneisses, the commonly sheared margins of the bodies and, in the case of the peridotites, the lack of a thermal metamorphic aureole around them (O'Hara & Mercy, 1963; Lappin, 1966; Carswell, 1968a). Later evidence in favour of this hypothesis came from geothermometric/geobarometric studies. Lappin & Smith (1978) derived temperatures of 700–800°C and pressures of 30–45 kbar for primary assemblages in orthopyroxene-eclogites from Stadlandet, using the

$$K_D \overset{\text{Gt–Cpx}}{Fe^{2+}/Mg^{2+}}$$

method of Råheim & Green (1975), the two-pyroxene solvus of Wood & Banno (1973) and the solubility of alumina in orthopyroxene and garnet (Wood & Banno, 1973). Reconstruction of the composition of an early high-Al orthopyroxene, now containing exsolution lamellae of garnet, and an early clinopyroxene with lamellae of orthopyroxene allowed estimates of pre-exsolution conditions at 1200–1370°C, and 30–40 kbar. Similar results were obtained by Carswell (1973b) for an exsolved orthopyroxene lens within a garnet-peridotite. In both cases it was postulated that the rocks formed in the upper mantle prior to tectonic intercalation into the crustal rocks.

More recent arguments in favour of the foreign origin of the eclogites and garnet-peridotites have centred around the radiometric age differences between these rocks and their host gneisses, the arguments for and against which are outlined above. The emphasis of interpretation for the eclogites has now shifted from an origin in the upper mantle to one in subducted or deeply obducted oceanic crust (O'Hara, 1976; Gebauer *et al.*, 1982; Mearns & Lappin, 1982a; Smith, 1981). Smith (1980, 1981) has expanded upon this idea, suggesting that the diversity of lithologies and mineral facies found within the BGC is a result of

production of a 'gigantic tectonic mèlange' during Caledonian orogenesis which shuffled rocks from a range of lithospheric levels with little mineralogical or isotopic re-equilibration. While this idea may provide a crude description of the tectonostratigraphy of the BGC, it is considered that the information presented in this synthesis shows that Smith's (1980) model breaks down under detailed scrutiny.

Much of the geological evidence in favour of the foreign origin hypothesis is equivocal. The sheared margins often seen on bodies of eclogite in the gneisses can be more simply explained by differential movement of the eclogite during boudinage of a continuous metabasic sheet within the less competant gneisses. At Flemsøy, Sunnmøre, bodies of corona-bearing metadolerite are frequently boudinaged. Sheared margins are frequently transformed to eclogite and field evidence suggests that bodies of eclogite in the country-rock have been torn from the dolerite margins during deformation. These are indeed 'foreign inclusions', but movements of no more than a few metres are required to explain their present position (Mørk, 1982).

The lack of a thermal metamorphic aureole around the peridotites is perhaps not surprising in view of their complex structural history, during which deformation would surely have obliterated the evidence for any such aureole and has certainly frequently disrupted any observed backwall metasomatic reaction zones. Geochemical evidence (Carswell, Krogh & Griffin, 1983) from some of the more iron-rich garnetiferous peridotites such as in the Eiksunddal eclogite complex (Schmitt, 1964) suggest that these were probably of low pressure igneous origin, originally having been olivine gabbro–peridotite cumulates.

Unequivocal geological evidence in favour of a foreign origin for the eclogite-facies inclusions in the gneisses is difficult to envisage. As the most feasible mechanism for tectonic emplacement might be introduction along large crustal dislocations, one might expect to find eclogites strongly associated with major lithological boundaries. This has not been demonstrated as yet, to our knowledge, although such a situation may be complicated by polyphase folding following emplacement. However the observation that peridotites are sometimes associated with shear zones (Bryhni, 1966; Lappin, 1966) is interesting in the light of continuing assertions that these rocks were indeed foreign to the continental crust prior to the eclogite-forming metamorphism (Carswell & Gibb, 1980; Medaris, 1980).

Geological evidence in favour of crustal eclogite-facies metamorphism can perhaps be divided into two types. The first is the preservation of features demonstrating that the rock was indigenous to its surrounding crustal rocks prior to eclogite-facies metamorphism. The second is the preservation of features within the rock showing that its protolith had a low-pressure origin. If evidence for only the latter exists it is difficult to deny a foreign origin, as deep level obduction (Lappin, 1977; Lappin & Smith, 1978; Smith, 1980, 1981) of eclogitic oceanic crust may explain its present position. If the surrounding crustal rocks have co-facial high-pressure parageneses then *in-situ* metamorphism is likely to have occurred, but this says little about the pre-metamorphic tectonic history of the eclogite. In view of the known tectonostratigraphy of the BGC it is not unlikely that fragments of oceanic crust formed part of the early nappe pile (*c.f.* Krill, 1980, 1981).

Evidence for the crustal derivation of eclogites has been reviewed by Bryhni *et al.* (1977), Krogh (1977a) and Griffin *et al.* (1981) and in several contributions in Griffin & Mørk (1981). Perhaps the most obvious indigenous crustal eclogites are the sills and dykes of metadolerites and metabasalts which preserve relics and eclogitic pseudomorphs of low-pressure igneous phases. These are known from the Surnadal synform (Tørudbakken, 1981; Tørubakken & Råheim, 1981), the Molde peninsula (Harvey, unpublished data; Carswell & Harvey, 1983), Kristiansund (Raheim, 1972; Griffin & Råheim, 1973), Sunnmøre (Mørk, 1982; Gjelsvik, 1952), Flatraket, Stadlandet (Lappin, 1966), Måløy (Bryhni *et al.* 1977) and Dalsfjord, Sunnfjord (Cuthbert & Carswell, 1982; Cuthbert, unpublished data). Original igneous margins are preserved at Midøy, Moldefjord (Griffin & Carswell, 1983), at Flatraket and Maløy, where the dykes intrude granulite facies mangerites (Bryhni *et al.*, 1977) and at Dalsfjord (Cuthbert & Carswell, 1982; Cuthbert, unpublished data). Where the margins of these bodies are sheared but not hydrated, granoblastic aggregates of garnet and omphacite occur which are often indistinguishable from the eclogite pods found elsewhere in the gneisses.

Within these metadolerites the original igneous assemblage appears to have been plagioclase + clinopyroxene ± olivine ± orthopyroxene ± oxides. The common coexistence of plagioclase and olivine indicates crystallization at pressures certainly less than 10 kbar (Mysen & Heier, 1972) and temperatures greater than 1100°C. A sequence of corona-forming reactions has pro-

gressively transformed this assemblage to essentially bimineralic eclogite. These reactions are summarized in Table 1, and discussed further below.

Layering is a common feature of both eclogites and garnet peridotites. At Ulsteinvik and Eiksunddal eclogite mineralogical layering has been demonstrated to mimic original igneous layering, sometimes rhythmic in character (Schmitt, 1964; Mysen & Heier, 1972; Carswell *et al.*, 1983). Other types of layering in eclogites may be a result of eclogitization of sediments, or interbanded sediments and igneous rocks. A number of occurrences of eclogite along western Nordfjord expose interbanded pyroxene-rich or quartz-rich layers (Bryhni, 1966; Bryhni & Griffin, 1971; Bryhni, 1981) and in the Moldefjord area marble lenses occur within a large area of retrograded eclogite. The marbles contain silica-rich layers and grade into eclogites (Hernes, 1954; Carswell & Harvey, 1983; Harvey, unpublished data). Carswell & Harvey (1983) consider these rocks to have been submarine basic volcanics interbedded with limestones.

High-pressure assemblages in the gneisses

It has been recognized for some time that high-pressure parageneses are occasionally preserved in the gneisses.

Pelitic gneisses adjacent to the Ulsteinvik eclogite, Hareidlandet, contain the assemblage garnet + omphacite + biotite + plagioclase + quartz, the omphacite now being represented by a diopside–plagioclase symplectite. Gneissic meta-xenoliths in this eclogite have the assemblages garnet + orthopyroxene + plagioclase + quartz and garnet + kyanite + clinopyroxene + plagioclase + quartz. Garnets in these xenoliths contain inclusions of omphacitic pyroxene (Mysen & Heier, 1972; Griffin & Mørk, 1981). These assemblages suggest metamorphism under the same conditions as the eclogite (800°C, and 18 kbar–Griffin *et al.*, 1981).

Syenitic gneisses from Tafjord also locally contain symplectic clinopyroxenes (Brueckner, 1977), as do some augen gneisses in the Moldefjord area (Carswell, 1981; Carswell & Harvey, 1983). In the latter case the symplectites are rimmed by rather grossular-rich garnet coronas, suggesting equilibration at >9 kbar at 700–800°C (*cf.* Green and Mysen, 1972).

In the intermediate augen-gneisses (mangerites) at Flatraket, Stadlandet, and Måløy, the assemblage garnet $\pm$ clinopyroxene + plagioclase + K-feldspar + quartz $\pm$ kyanite is found, garnet–clinopyroxene pairs giving the same equilibration temperatures as the adjacent eclogites (Krogh, 1977b, using

$$K_D \overset{\text{Gt–Cpx}}{Fe^{2+}/Mg^{2+}}$$

as for Ellis & Green, 1979).

Krogh (1980a,b) has demonstrated co-facial eclogites and gneisses from two areas; Førde, Sunnfjord and Kristiansund. At Førde, rather low-temperature eclogites record conditions of 630 ± 35°C, 15.0 ± 2.5 kbar (Naustdal) and 540 ± 35°C, 12.5 ± 2.5 kbar (Kvineset). In the gneisses garnet-omphacite pairs give similar temperatures (Ellis & Green, 1979). The assemblages annite + K-feldspar + magnetite + quartz, ferropargasite + garnet + plagioclase + clinopyroxene + magnetite + quartz, garnet + acmitic clinopyroxene + plagioclase + magnetite and garnet + phengite + annite + quartz which occur in the gneisses are also compatible with the conditions deduced for the eclogites. At Kristiansund, three garnet granulite samples contain garnet + clinopyroxene + quartz + epidote $\pm$ plagioclase $\pm$ amphibole $\pm$ rutile, the garnets containing inclusions of clinopyroxene, quartz and rutile or clinopyroxene, quartz, biotite and white mica. Using garnet–clinopyroxene pairs, jadeite content of omphacite, garnet + clinopyroxene + plagioclase + quartz in the absence of orthopyroxene and $CaAl_2Si_2O_6$-rich clinopyroxene + quartz, conditions for the granulites are estimated at 18.5 $\pm$ 3.0 kbar and 750 ± 50°C (see Fig. 4).

On Midøy, Moldefjord, anatectic backveins of gneiss in eclogites preserve the assemblage Ca-rich garnet + kyanite + plagioclase + quartz $\pm$ K-feldspar $\pm$ omphacite. Geobarometry on this assemblage (method of Ghent, 1976) gives a pressure of 19–21 kbar at 750°C. This pressure is the same as that deduced for many eclogites in this area. Hence, in this case, both geological and mineral-chemical data suggest an *in-situ* metamorphic origin for the eclogite (Griffin & Mørk, 1981; Griffin & Carswell, 1983). The assemblage garnet + plagioclase + kyanite + quartz is being discovered widely in the BGC and gives metamorphic conditions compatible with those for adjacent eclogites (Griffin, pers. comm., 1982).

Similar anatectic backveins are known from the Førde area (Krogh, 1980a) and the Dalsfjord area (Cuthbert, unpublished data) in Sunnfjord, where they contain garnet + (diopside + plagioclase symplectite) or omphacite + phengite + quartz and are gradational into garnet + omphacite + phengite eclogites.

Hence it is becoming apparent that high-

pressure assemblages are not uncommon in the gneisses. Indeed, they may prove to be as common as the more obvious eclogites and garnet peridotites. However, in common with the latter, these assemblages are often retrograded to hydrous amphibolite-facies assemblages.

Orthopyroxene eclogites and garnet peridotites

In a recent review of orthopyroxene-bearing eclogites in the BGC, Carswell *et al.* (1983) have derived metamorphic equilibration pressures considerably lower than those obtained earlier by Lappin & Smith (1978). Eclogites within gneisses ('external eclogites') have values of 700–740°C, and 17–18 kbar, whilst 'eclogites' (garnet websterites) forming layers within garnet peridotite gave 710 C, and 20 kbar. Hence conditions deduced for these rock types appear to be mutually compatible and also match conditions for more aluminous eclogites and high-pressure granulites in the NW coastal areas of the BGC.

Considerable disequilibrium among orthopyroxene, clinopyroxene and garnet exists in these rocks and may have been the cause of previous anomolously high pressure estimates. Furthermore Carswell *et al.* (1983) suggest that the pyroxenes with exsolution features were probably never in equilibrium with garnet, invalidating the high pressure and temperature values derived from the reconstructed mineral analyses (Carswell, 1973a; Lappin & Smith, 1978).

An upper mantle origin for some of the peridotites is still postulated (Carswell, 1968a, b, 1973b; Carswell & Gibb, 1980; Carswell *et al.*, 1983; Medaris, 1980, 1982) on the basis of bulk-rock geochemistry, mineralogical comparisons with nodules from kimberlites and geothermobarometry. Until recently there has been a tacit assumption that they represented primary sub-continental mantle, but recent evidence has complicated the issue. Griffin & Qvale (1981, see also Griffin & Mørk, 1981) have favourably compared the composition of an eclogite body within the Almklovdalen peridotite at Raudkleivane with that of ferroan basaltic amphibolite dykes in Caledonian alpine-type serpentinites from the Bergen area. The Raudkleivane eclogite contains garnets with strong prograde zoning (see below) and amphibolite facies mineral relics and it is inferred that this peridotite has evolved by prograde ('crustal') metamorphism of a serpentinized peridotite.

Carswell *et al.* (1983) have reported the presence of early spinel relics with garnet coronas in geochemically similar peridotites to that at Almklovdalen, providing further evidence of prograde metamorphism. This raises the possibility that some of the garnet peridotites may have been derived from sub-oceanic mantle. Some features of garnetiferous peridotites like those at Kalskaret, Tafjord (Carswell, 1968a) are similar to those described in some ophiolites containing primary high P–T mantle assemblages (Spray, 1982). These are thought to be fragments of lithosphere from incipient rifts or marginal basins where large scale mantle diapirism has taken place. This similarly deserves further investigation, particularly in view of the contention of Gebauer *et al.* (1982) that some eclogites had basaltic protoliths originating in back-arc basins.

The uniformity of P–T estimates for eclogites and garnet peridotites indicates that, whatever their origin, they have been metamorphosed under very high confining pressure. Carswell & Gibb (1980) have suggested that the peridotites gained their present mineralogical constitution *after* emplacement into their present host rocks during high P/T metamorphism operative on a regional scale.

Prograde and retrograde metamorphism and P/T trajectories

Evidence for a low-pressure pre-eclogite facies metamorphism is commonly preserved in eclogites in the BGC, in the form of corona structures and compositional zoning in minerals, usually in garnets.

Table 1 shows the sequence of corona-forming reactions, as described by Griffin & Bryhni (1977), Griffin & Raheim (1973) and Griffin & Heier (1973). Early reactions consume the solidus phases, producing low-pressure granulite assemblages (e.g. aluminous pyroxenes + spinel + plagioclase) then high-pressure granulites (garnet + low Al pyroxenes + plagioclase) before final consumption of plagioclase to produce omphacitic pyroxene and almandine-pyrope-grossular garnet. Griffin & Raheim (1973) considered that these reactions were a continuous sequence occurring during cooling and compression from solidus conditions. However, studies in the anorthosites of the Bergen Arcs show that although this may have been the case for the granulite-facies coronas, the eclogite event was superimposed at a later, separate stage (Austrheim & Griffin, 1982). Also at Dalsfjord, Sunnfjord, low-temperature breakdown of plagioclase predates the eclogite-facies corona assemblage, implying considerable cooling prior to eclogitization (Cuthbert & Carswell, 1982; Cuthbert, unpublished data). Late

stage breakdown of omphacite and garnet produce secondary plagioclase coronas, which Griffin and Råheim (1973) have interpreted as being a result of strong decompression.

Although the coronites provide striking examples of eclogitization of low-pressure protoliths, the likelihood of temporal breaks in their evolution and strong overstepping of the stability fields of the minerals involved (*cf.* Griffin & Råheim, 1973) makes construction of P/T trajectories for their evolution difficult.

Chemical zoning in garnets is common in the eclogites and, locally, the gneisses southwards from Nordfjord. Relict mineral suites (including amphibole, zoisite, white mica, feldspars and pyroxenes) are often preserved within garnets. Thus these rocks provide a useful window for examination of the pre-eclogitic history of the BGC.

Two early studies (Bryhni & Griffin, 1971; Råheim & Green, 1975) discussed the interpretation of compositional zonation in garnets. The factors affecting zoning patterns include rates of intergrain and volume diffusion (controlled by temperature, fluids, deformation and cooling rate), fractionation due to removal of components from the reacting system into earlier grains, distribution coefficients (K_D) for continuous exchange reactions and availability of new components during mineral breakdown resulting from discontinuous reactions. The latter two are P/T dependent. The good correlation between mineral compositional variation and zonal changes in inclusion suites (e.g. Bryhni *et al.*, 1977; Krogh, 1980a, and unpublished data) suggests a strong P/T effect and therefore confirms the usefulness of these features in the deduction of P/T histories.

Figure 3 shows zoning profiles from three eclogite garnets, from Gjørlanger by Dalsfjord, Sunnfjord (Cuthbert, unpublished data), Verpeneset, Nordfjord (Bryhni & Griffin, 1971; Krogh, unpublished data) and Langvatnet, Molde peninsula (Harvey, unpublished data). The examples from Gjørlanger and Verpeneset both contain relict amphibolite-facies assemblages in garnet cores and eclogite-facies assemblages nearer the rims. The amphibolite–eclogite transition is marked by a strong rimward increase in pyrope content and a decrease in spessartine and almandine. In the Verpeneset example amphibole compositions show a systematic variation from the core, with a marked change at the eclogite transition. Similar patterns are found in eclogites from the Naustdal area, Sunnfjord (Krogh, 1980a) but the rim zone assemblages and the eclogite matrices are characterized by the presence of glaucophanitic amphibole. Although these patterns can be partly explained by chemical fractionation, the evidence for prograde metamorphism is particularly convincing here.

Suggested P/T paths for the Sunnfjord eclogites and gneisses (after Krogh, 1980a) and the Verpeneset and Romsdalshorn eclogites are shown in Fig. 4. Maximum conditions for the Sunnfjord area are 510–630°C, and 12–15 kbar (Krogh, 1980a; Cuthbert & Carswell, 1982; Cuthbert, unpublished data) and for the Verpeneset eclogite are 740°C, and 17–19 kbar.

In contrast to the above, the Langvatnet eclogite garnets show rather flat profile (Fig. 3) and narrow, retrogressive rims (decreasing $Mg^{2+}/(Mg^{2+}+Fe^{2+})$; Mn and Ca show similar profiles). The garnets sometimes contain inclusions of rutile, omphacite and quartz, with no obvious zonal arrangement. Similar profiles are reported for an eclogite garnet from Reset, outer Romsdal (Krogh, unpublished data) and appear to be common in eclogites where

$$K_{D\,Fe^{2+}/Mg^{2+}}^{Gt\text{–}Cpx}$$

is less than 6.0, corresponding to temperatures above about 725°C. This may be a result of more effective volume diffusion in garnets at these high temperatures, wiping out any prograde zoning. The narrow, retrograde rims may thus represent late growth or restricted re-equilibration due to limited intergrain diffusion below this threshold temperature. The matrix omphacites have lower jadeite contents than the inclusions, possibly reflecting a significant drop in pressure at a late stage. This is the opposite to the situation found in prograde eclogite garnets at Naustdal (Krogh, 1980a) and Verpeneset (Krogh, unpublished data).

Secondary, retrogressive features of eclogites include breakdown of omphacite to diopside–plagioclase or amphibole–plagioclase symplectites, breakdown of garnet + quartz to produce enstatite + plagioclase, and reaction of garnet + clinopyroxene to produce amphibole + plagioclase ± enstatite symplectites. Phengites in eclogites and gneisses breakdown to biotite + phengite or biotite + K-feldspar + kyanite. Glaucophane and barroisite may be replaced by amphiboles more similar to those in garnet cores. Prograde garnets (e.g. Fig. 3c) show narrow retrograde rims in some cases. Latest stage alteration involves the formation of chlorite and epidote after garnet (Krogh, 1977a, and un-

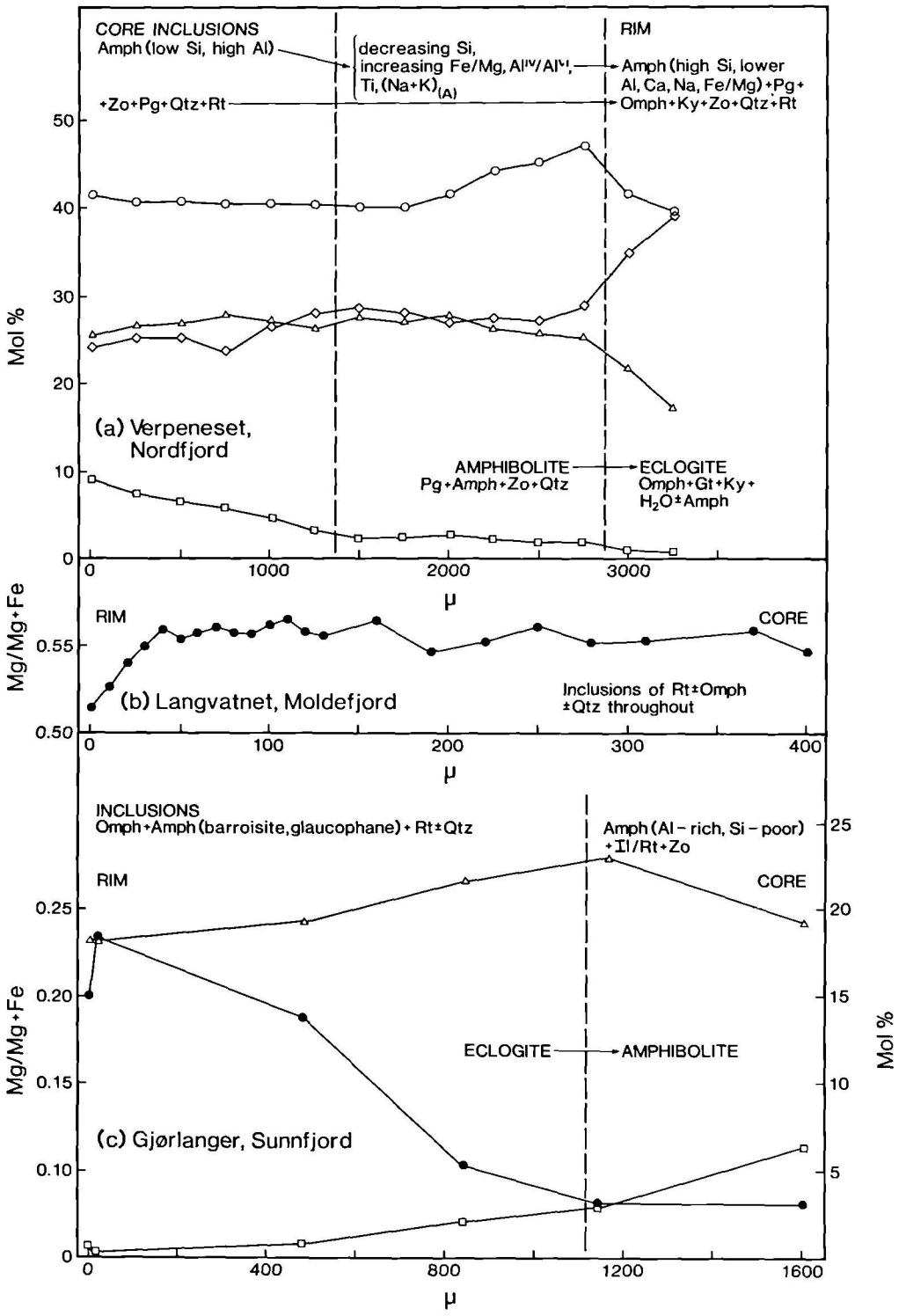

Fig. 3. Compositional zoning profiles and mineral inclusion suites for garnets from Verpeneset, Nordfjord (Krogh, unpublished data), Langvatnet, Moldefjord (Harvey, unpublished data) and Gjørlanger, Sunnfjord (Cuthbert, unpublished data). Open circles—almandine component; triangles—grossular component; diamonds—pyrope component; squares—spessartine component; closed circles—$Mg^{2+}/(Mg^{2+}/Fe^{2+})$. Amph = amphibole; Zo = zoisite; Pg = paragonite; Qtz = quartz; Rt = rutile; Omp = omphacite; Ky = kyanite; and Il = ilmenite.

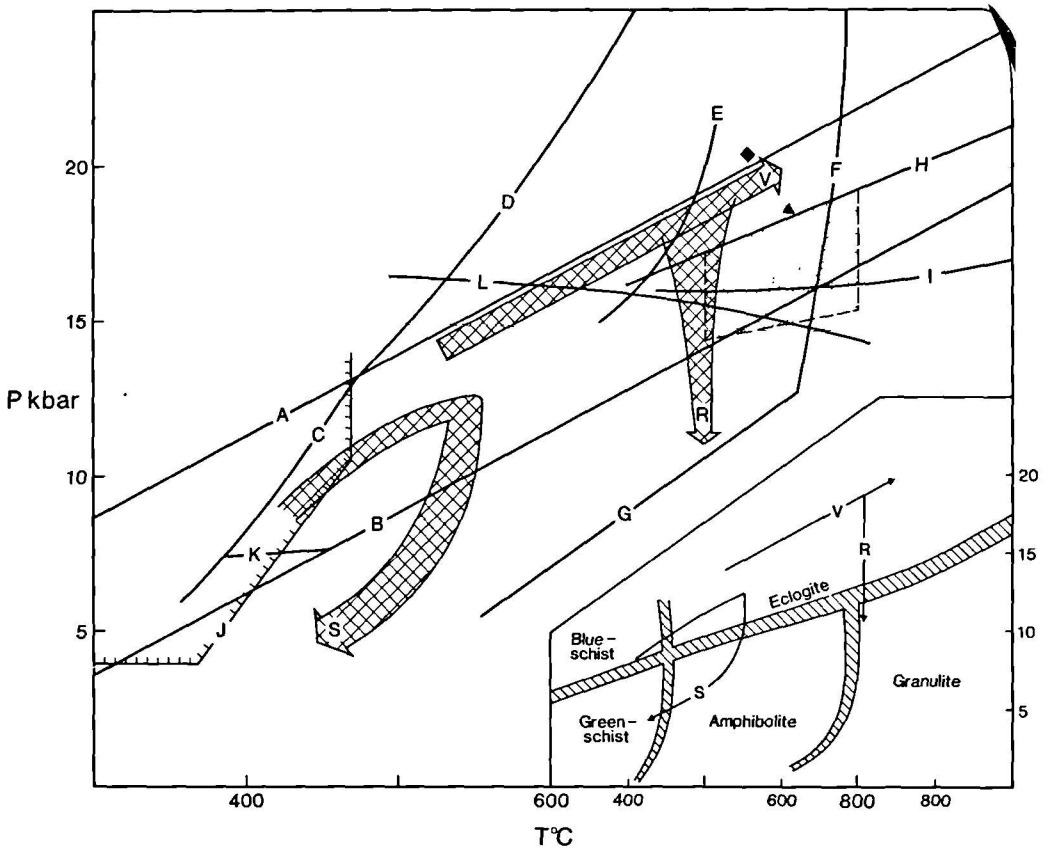

Fig. 4. Petrogenetic grid showing P/T trajectories for eclogites from Sunnfjord (s) (after Krogh, 1980a). Verpeneset (V) and Romsdalshorn (R), Møreog Romsdal (Krogh, unpublished data). A—Ab = Jd + Qtz (Holland, 1979, 1980), B—lower stability of $DiJd_{40}$ + Qtz (Holland, 1979, 1980), C—Lws + Ab = Zo + Pg + Qtz + vapour (Holland, 1979), D—Lws + Jd = Zo + Pg + Qtz + vapour (Holland, 1979), E—wet eclogite solidus (Lambert & Wyllie, 1972), F—Zo + Ky + Qtz = liq. + vapour (Boettcher, 1970), G—Zo + Ky + Qtz = An + vap (Boettcher, 1970), H—plagioclase out in high-Al basalt andesite (extrapolated from Stern, Hung & Wyllie, 1975), I—special iherzolite–garnet lherzolitetransition (O'Hara, Richardson & Wilson, 1971), J—maximum stability field for glaucophane, ticks point towards stability field (Maresch, 1977), K—Marg + Ab = Pg + Zo + Qtz (Franz & Althaus, 1977), L—Pg = $DiJd_{40}$ + Ky + vapour (Holland, 1979). Stippled area—P/T conditions deduced for granulites near Kristiansund (Krogh, 1980b). Triangle—best estimate of P/T for orthopyroxene eclogites in the BGC (Carswell *et al.*, 1983). Diamond—best estimate of P/T for garnet lherzolites in the BGC (Carswell & Gibb, 1980). Inset—P/T trajectories plotted against generalized metamorphic facies boundaries.

published data; Lappin & Smith, 1978; Griffin & Carswell, 1983). These features are thought to be a result of strong decompression with little change in temperature, imparting a rather hairpin-shaped profile to P/T trajectories (Fig. 4) (Krogh, 1977a, 1980a; Griffin *et al.*, 1981). Similar profiles are reported from other orogenic belts containing eclogites implying, perhaps, a common tectonic process for their metamorphic evolution (e.g. Ernst & dal Piaz, 1978; Ernst, 1977, 1981; Maresch & Abraham, 1981).

Regional temperature and pressure variation

It will be apparent from what has been said above that a range of P/T conditions occurs not only within individual eclogites, but also between them. Bryhni *et al.* (1977); Krogh (1977a); Griffin & Mørk (1981) and Griffin *et al.* (1981) have plotted

$$K_D^{Gt\text{–}Cpx}{}_{Fe^{2+}/Mg^{2+}}$$

values for rim compositions and estimated temperature on a map of the BGC and find a systematic increase in K_D and T towards the NW coast. The lowest temperatures are recorded in Sunnford, where 'type C' glaucophane-bearing eclogites outcrop. The highest temperatures are recorded between Stadlandet and Kristiansund. Pressures also increase in the same sense for the eclogites and continuing research suggests a similar pattern is recorded in garnet + plagioclase + kyanite + quartz assemblages in the gneisses (Griffin, pers. comm.).

This regional pattern is thought to be a result of crustal 'subduction' during continental collision (Krogh, 1977a), now thought to be of Caledonian age, as discussed above. The variation is consistent with the findings of Krill (1981b) who reported decreasing

$$K_D \begin{matrix} \text{Gt–Biot} \\ Fe^{2+}/Mg^{2+} \end{matrix}$$

values (*cf.* Ferry & Spear, 1978) westwards from the eastern margin of the BGC and westward change of metabasites from amphibolites to eclogites.

The superimposition of this regional variation of temperature and pressure on the structurally complex BGC puts strong constraints on tectonic models for the origin of the eclogite-facies assemblages. First, it implies superimposition of high-pressure metamorphism on existing major structures. Second, it considerably reduces the credibility of foreign origin hypotheses unless some special mechanism can be explained for the variation which is consistent with regional geological relationships. Further resolution of this matter urgently requires extensive fieldwork to map out the major tectonic units, and detailed petrographic and geothermobarometric studies across large amplitude structures to ascertain the relative age of eclogite metamorphism with respect to deformation episodes.

In order for the regional variaton to have remained intact the BGC must have emerged as a fairly rigid, coherent body. The pressure variation implies that the uplift hinged somewhere in the SE, possibly near to Jotunheimen. Some disturbance of the iso-K_D lines seems to have occurred in Sunnfjord, perhaps due to late movement at the base of the Sunnfjord nappe (Griffin & Mørk, 1981; Cuthbert, unpublished data).

Summary of metamorphic evolution

High-pressure assemblages seem to have formed early in the observed tectonic history of the BGC, probably early in the formation of the present tectonostratigraphy. This metamorphism has affected all the lithologies and any 'foreign' fragments (oceanic crust, and upper oceanic, back-arc or sub-continental mantle) have equlibrated essentially in their present position relative to their host gneisses. A P/T history is recorded in which low-pressure protoliths suffered a rapid compression with some heating, followed by a rapid decompression which may have been nearly adiabatic or isothermal. Disequilibrium on all scales, including preservation of pre-Caledonian parageneses, prograde Caledonian parageneses and mineral zoning and only partial retrogression implies that the high-pressure event was rather short-lived. The regional P/T variation implies superimposition of an increasing overburden towards the W, up to about 65 km in thickness. The preservation of blueschist-type parageneses in Sunnfjord implies short-lived depression of rather cold (upper?) continental crust to considerable depths (up to 45 km).

GEOPHYSICS

The aim of this section is twofold. The first part will discuss evidence for the deep structure of the BGC and adjacent areas. The second part will explore the isostatic constraints on the evolution of the eclogite bearing terrain and attempt to throw some light on the possible thermal evolution of the BGC.

Deep structure

It is now generally accepted that the Caledonian orogenic belt has formed as a result of the collision of the Baltic–European continental plate with the Greenland–American continental plate following closure of the Iapetus ocean (e.g. Dewey, 1969, 1982; Phillips, Stillman & Murphy, 1976). The presence of ophiolite fragments in thrusted nappes in the Scandinavian Caledonides suggests that a geosuture exists close to the present coast of western Norway, marking the line of continental collision (Gale & Roberts, 1974; Gee, 1975, 1978; Furnes *et al.*, 1976; Andresen & Faerseth, 1982).

A comprehensive geophysical survey off the Norwegian coast (Talwani & Eldholm, 1972) has revealed the presence of a marked belt of high gravity and magnetic anomalies parallel to the coast between Trondheim and Stadlandet, trending towards Shetland and the N coast of Scotland. These are attributed to intrabasement density contrasts of pre-Permian age and have been related to dense Lewisian mafic granulites, as seen

in NW Scotland (Talwani & Eldholm, 1972; Watts, 1971). Gee (1975) suggests that these anomalies mark a dramatic change in the nature of the basement crust and may mark the junction between the ancient, Lewisian-type crust of Greenland and Scotland and the granitic, Gothogrenvillian-type crust of the Baltic shield. In this case the line may well represent a geosuture. However, the close proximity of these anomalies to the ophiolites on the W coast of Norway, and in particular to that on Shetland (Mcquillan & Brooks, 1967; Pritchard, 1981) may suggest that they represent an ophiolite-lined suture. Interpretation of the significance of these anomalies is complicated by their proximity to the Great Glen transform fault. Very large strike-slip movements on this fault may put the Lewisian rocks in close proximity to present northern Norway (Kent & Opdyke, 1979) perhaps invalidating these hypotheses. However, smaller movements (< 500 km) constrained by the geometry of the Barrovian metamorphic zones of Scotland, may only slightly affect the continuity of the anomalies as they lie essentially parallel to the fault.

The presence of a geosuture so close to the BGC may mean that the leading edge of the Greenland Plate may have over-ridden the BGC and therefore could provide at least part of the great overburden required to satisfy the geobarometric estimates. Such a hypothesis can only be very simplistic in view of the complex nature of the plate-margin collisions (Dewey, 1982). The presence of eclogites and garnet peridotites on the corresponding east coast of Greenland (Smith & Cheeney, 1981) suggests depression of the Greenland margin to great depths implying also either that this part of the E Greenland Caledonides represents part of the same structural entity as the BGC and the suture lies further west still, or that both margins have been depressed below some intervening structure, perhaps a microcontinent, an Andean-type orogen or just a telescoped continental margin similar to that envisaged here for the BGC but thrust in an opposing direction. Thus, although at present we may be able to pin-point the primary geosuture (if such a structure exists), we still cannot precisely reconstruct the nature of the upper collided plate. Seismic reflection studies akin to the COCORPS or BIRPS experiments may help to resolve this problem in the future.

Seismic refraction and reflection studies in S Norway give some clues to the deep structure of the BGC. A recent COCORP reflection profile has revealed the presence of a crustal low velocity layer (LVL) at approximately 12–14 km below the present land surface in the Møre area (Mykkeltveit, Husebye & Oftedahl, 1980). This LVL has been best defined over a length of about 50 km, and seems to be about 4 km thick with a westward dip of $< 2°$ (Fig. 5E). It cannot be explained by heat flow anomalies and Mykkeltveit *et al.* (1980) suggested that the LVL results from incorporation of oceanic crust and sediments during overthrusting of the BGC over the Baltic margin. Such a model has many faults, on the basis of the information outlined in this paper, not the least of which is that it precludes the development of Caledonian eclogites in the BGC.

Seismic refraction studies carried out by workers at the Seismological Observatory at Bergen show similar results to those of Mykkeltveit *et al.* (1980). Sellevoll & Warrick (1971) discussed the results of two traverses across S Norway, from Fedje (Bergen Arcs) to Grimstad (S coast) and Florå (W coast, BGC) to Åsnes (near Swedish border in Proterozoic foreland). They constructed a model in which the crust outside the Caledonides has a 6.00 km/sec P-wave velocity for the upper crustal layer, underlain by a 6.51 km/sec layer below about 18 km, with the Moho reflector at about 33 km. An interesting observation is that within the area corresponding to the BGC and the Bergen Arcs an additional upper high-velocity layer (6.32 km/sec) is present. It was suggested that this is underlain by a low velocity layer with a base at about 14–17 km. The velocity of the LVL was taken as that of the surface layer at Grimstad (6.00 km/sec). Also Kanestrøm (1977) has described a detailed refraction study in the Møre area to the W of that by Mykkeltveit *et al.* (1980) and found evidence for a LVL (5.00 km/sec) 7 km thick with its top at 9 km. The upper layer velocity was 6.20 km/sec, also higher than that in the foreland.

From these studies another interpretation for the velocity reversal may be suggested in which the LVL results from the superposition of a high velocity layer over crust of normal velocity distribution. This does not entirely discount the presence of supracrustal material in the LVL. The anomolously high upper layer velocity is interesting in that it coincides with the outcrop of an eclogite-bearing terrain where dense high-pressure parageneses may still be common, despite retrogression.

In recent years seismic mapping of velocity changes and reversals has made significant contributions to our knowledge of orogenic belts, indicating the superposition of large masses of crystalline continental crust over each other and over supracrustal layers in, for example, the

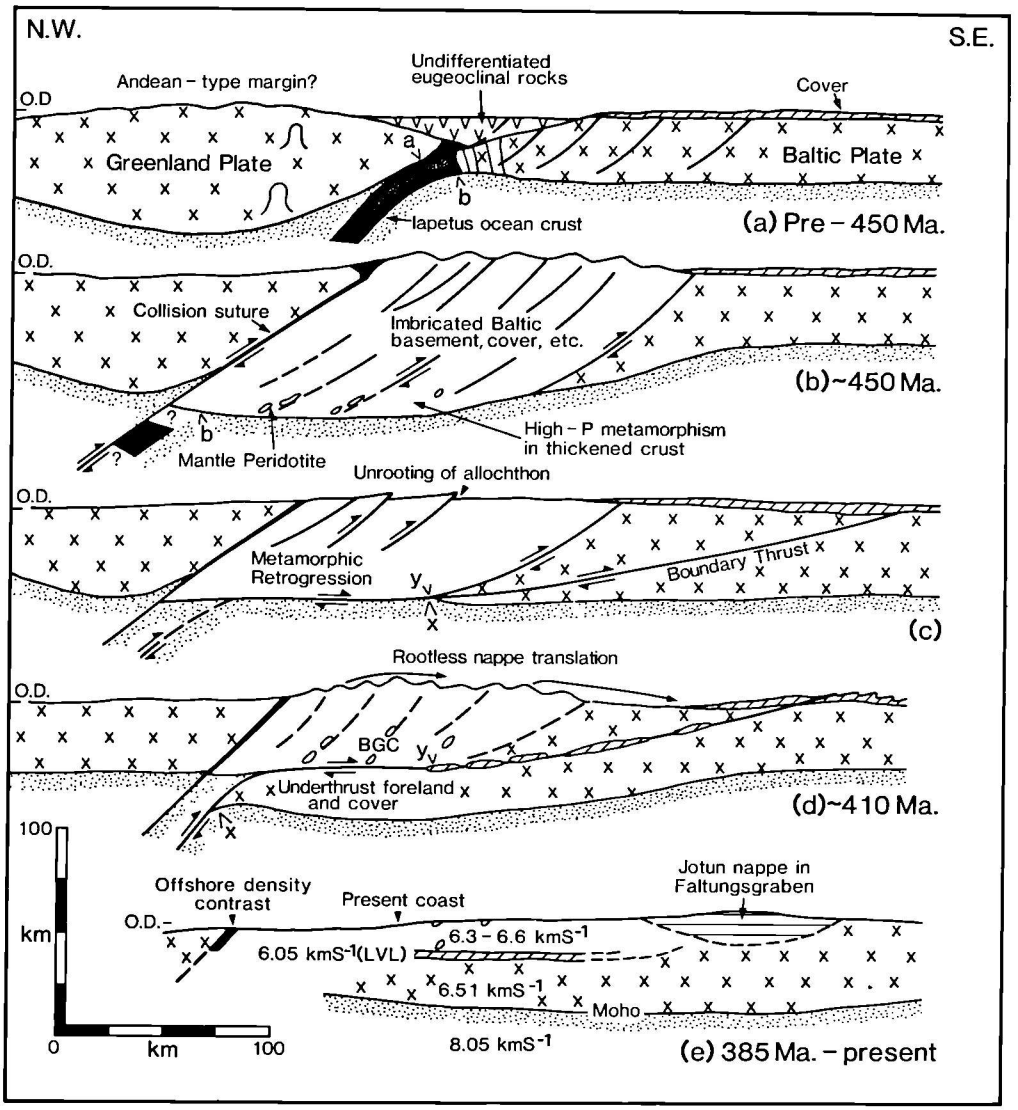

Fig. 5. Evolutionary model for the Basal Gneiss Complex, as described in the text. For details see Table 2.

Appalachians (Cook, Albaugh, Brown, Kaujman, Oliver & Hatcher, 1979), the Alps (Hsü, 1979) and the Scottish Caledonides (Soper & Barber, 1982). The latter two examples suggest crustal-scale imbrication. A major problem in developing a tectonic model for the BGC is to find a viable mechanism by which crust which has been buried to depths of up to 70 km can be restored to the Earth's surface and still have a crust of near-normal thickness beneath it. We suggest that following the early phase of collision, in which the eclogitic parageneses formed in a tectonically thickened and overthrust continental margin, a phase of suture progradation (Roeder, 1979) caused underthrusting of continental crust (and supracrustal cover?) below the eclogite-bearing terrain, hence providing the isostatic impetus for its uplift.

Isostasy and thermal history

Bird, Toksöz & Sleep (1975) have made a theoretical study of the mechanical and thermal effects of continent–continental collision. They found that when subduction of continental crust follows that of the oceanic slab, the greater thickness of the

continental lithosphere tends to resist bending, so that downwarping tends to occur at some distance in front of the original suture zone. Furthermore, the buoyancy of the continental crust introduces large deviatoric stresses on the downgoing slab. A combination of these factors causes a large, low angle thrust to form in the underthrust plate, making it easier for the continental crust to continue underthrusting. This results in suture progradation. Should the contact between the dense oceanic crust and the continental crust be disrupted by this shearing, the oceanic slab will become detached and sink, perhaps removing the driving force for continental underthrusting. In this case crustal doubling will cease and isostatic compensation, aided by surface erosion, will act to restore the crust to a more normal thickness. Bird *et al.* (1975) and Toksöz & Bird (1977) have applied this model to the Zagros mountains and the Himalayas.

Dewey (1982) shows that during continental convergence crustal imbrication will tend to occur by reversal of listric normal faults formed during the early phases of basin development. The form taken by this 'tectonic telescoping' will vary between thin-skinned flaking and whole-crust imbrication, depending on the previous thermal history of the margin. Where the cold, 'elastic lid' is of crustal depth, faulting may take in slivers of upper mantle material during thrusting.

A combination of the latter two mechanisms would tend to produce a prism of imbricated crust, possibly of great thickness, between the primary geosuture and a low angle prograde suture, a situation apparently developing at present in the Zagros mountains and the Himalayas (Bird *et al.*, 1975; Powell & Conaghan, 1973; Barazangi & Ni, 1982; Shackelton, 1981) and one which may be directly analogous to the S Norwegian Caledonides.

The thermal effect of this geotectonic scenario will depend on a number of factors, including the rate of underthrusting (and, therefore, frictional heat production), the rate of surface erosion, the effect of density changes due to metamorphic reactions with high ΔV, the effect of radiogenic self-heating and the previous thermal history of the continental margins (England & Richardson, 1977; Bird *et al.*, 1975; Toksöz & Bird, 1977; Richardson & England, 1979; Draper & Bone, 1981). The existence of blueschist mineralogy in parts of the BGC suggests downward transport of fairly cold crustal material. Its preservation suggests high initial uplift rates and rapid exhumation, which may require tectonic stripping in addition to erosion (Draper & Bone, 1981). However, the P–T conditions for garnet peridotites and eclogites in the Molde-Kristiansund area ($\sim 750°C$, and 20 kbar) lie along the Precambrian shield geotherm (Carswell & Gibb, 1980) and may indicate some thermal relaxation to a more stable geotherm prior to uplift here, in an area which may be closer to the mantle heat flux source.

Most recent thermal models of overthrust orogenic belts (England & Richardson, 1977; Richardson & England, 1979; Thompson, 1981) result in a P–T path where some heating follows the metamorphic pressure peak. Although this may be the case in the north-western part of the BGC, where retrograde garnet zoning is prevalent, it does not appear to be the case further S where very little change in T or even some cooling has occurred during decompression. Rubie (1982) has produced a model for the history of the Alpine Sezia-Lanzo zone in which a temperature rise during uplift is prevented by continuing subduction of cold oceanic crust beneath the emerging crustal slab. Bird *et al.* (1975) show that significant heat transfer and self-heating do not occur in an underthrust continental slab until about 30 Ma after collision. Hence preservation of low-T parageneses in the overlying thickened crust may be a result of the blanketing effect of the under thrust slab.

An alternative to this model might be that the recorded P–T trajectory is a result of interruption of thermal relaxation by very rapid uplift. It is interesting that the known volume of late orogenic Devonian sediments does not balance the removal of up to 65 km of crust by erosion. The known volume includes that found in seismic studies of the Norwegian Sea and Northern North Sea where basin accumulations of up to 6 km occur (Talwani & Eldholm, 1972). This discrepancy may be accounted for by considerable tectonic stripping, which would be the result of the unrooting and eastward translation of the nappe pile, as envisaged by Gee (1975, 1978, 1980). Very rapid unloading would have resulted from this.

Griffin *et al.* (1981) and Griffin & Mørk (1981) have noted the close similarity between the apparent regional P–T variation in the BGC and that occurring at present at the top of the underthrust continental slab in the Zagros mountains (Bird *et al.*, 1975). This may support the ideas outlined above, but far better resolution of this variation will be necessary before this similarity can be seen as anything but fortuitous. Indeed, it seems likely that in a tectonic window such as the BGC any observed P–T variation may be a result

of erosion to different crustal levels, a situation which may prove very useful for resolution of the thermal structure of the crust if its detailed tectonic structure is ever resolved. Moreover, the possibility that the P–T variation is diachronous cannot be ruled out as yet.

In order to test the feasibility of the collision–underthrusting–recovery scenario outlined above we have applied the isostacy equations of Ahnert (1970) as used by England & Richardson (1977) to a geotectonic model embodying the geological, geochronological, petrological and geophysical features outlined above. The equations relate crust and mantle densities, surface height and erosion as follows:

$$H = H_0 - Fe$$

(2b of England & Richardson, 1977)

and

$$E = E_{max}(1 - \exp(-t/\lambda))$$

(4b of England & Richardson, 1977)

where H_0 is the surface height at time $t = 0$, H is the surface height at time t, $F = (1 - \rho c/\rho m)$, ρc and ρm being the densities of eroded material and the mantle respectively. E is the amount eroded after time t, E_{max} the amount eroded after infinite time and λ the erosional time constant. The values for these parameters were set by observing the follwing constraints.

1. Maximum estimated pressures from mineral geobarometry are about 20 kbar, indicating burial depths of about 65 km for rocks now at the present land surface. Hence $E_{max} = 65$ km.
2. Ahnert (1970) suggests that erosion rates seen in large mid-latitude drainage basins indicate erosional time constants as small as 55 km. This may be a maximum value if exhumation is enhanced by tectonic stripping, depending on the rate of nappe translation. A value of $\lambda = 55$ km is taken here.
3. Radiometric ages on eclogite minerals cluster around 420–400 Ma, with some as early as 447 Ma. If these are taken to be fairly early closure ages then maximum crustal depth for the BGC was reached at least as early as 420 Ma. A lower bracket for commencement of final continental collision is set by the lowest Silurian age for part of the Köli supergroup (at least 450 Ma). We have set the maximum crustal depth achieved during collision at about 450 Ma for the purposes of this calculation.
4. The end of orogenesis (i.e. uplift) was achieved by the time of deposition of the Devonian clastics in middle Devonian times, and we use an age of about 385 Ma here.
5. The total custal thickness achieved during collision is equal to E_{max} plus the depth to the present LVL, taken at ~ 14 km. This level is assumed to have been the Moho. Hence the crustal thickness at that time was about 80 km. The distance from the LVL to the present Moho is rather variable due to the coastwards rise in Moho level away from the Jotun nappes (Sellevol & Warrick, 1971; Ramberg & Grønlie, 1969; Kanestrøm, 1973), but is generally about 25 km. For the purposes of the calculation it is assumed that this amount was added to the base of the imbricate prism at some time after primary collision (the 'secondary underthrusting event').
6. The present crustal thickness is about 40 km (maximum) with a surface elevation of about 1.5 km. The crustal thickness at time $t = 0$ is arbitrarily set at 35 km, although it may have been somewhat thinner due to marginal extension during opening of Iapetus.

Manipulation of these figures led, by trial and error, to a three stage scheme in which crustal protoliths could be depressed to 65 km and returned to the surface within 73 Ma (Table 2). This is slightly longer than the period indicated by the time constraints. It was found necessary to divide the secondary underthrusting event into two periods with a small thickening phase after the main one. Division of these main events into a number of smaller increments would probably further reduce the time needed. It is clear that a single stage thickening event would not have returned the eclogites to the surface in the time available, indicating the importance of the secondary underthrusting to provide the buoyancy impetus for their exhumation. Any delayed recovery due to the development of an 'eclogite anchor' (Richardson & England, 1979) would also result in a poor fit with the time constraints. Maximum surface heights were broadly compatible with those of the Himalayan belt at the present time.

AN EVOLUTIONARY MODEL FOR THE BASAL GNEISS COMPLEX

The model present here is intended to relate the main geological and geophysical features of the South Norwegian Caledonides to the metamorphic evolution of the BGC as indicated by studies of relict high pressure assemblages. We make no detailed attempt to explain the pre-collisional history of this part of the orogen. For reviews of this see Gee (1975, 1978), Gee *et al.* (1981), Stevens & Gee (1981) and Andresen & Faerseth (1982).

Table 2. Calculated crustal thickening and erosion scheme for the evolution of the Basal Gneiss Complex during the Caledonian orogeny using equations 2b and 4b of England & Richardson (1977)

Time Interval t (Ma)	Crustal Thickness (km)	Surface Height H (km)	Crust Eroded E (km)	Event	Fig.	Age
	32	0			5A	Pre-450 Ma
			−48	Continental collision, crustal thickening by imbrication		
33	80	8.75		Partial thermal recovery, high P/T metamorphism	5B	~450 Ma
			+28.2	Isostatic recovery and erosion, retrogressive metamorphism	5C	
	51.8	3.6				
			−25	Second suture develops with underthrusting of Baltic foreland	5D	
	76.8	8.2				
15			+15.5	Isostatic recovery, tectonic stripping and erosion, continuing retrogressive metamorphism	5D	~410 Ma
	61.2	5.3				
			− 2.5	Further crustal thickening, final eastward translation of allochthon		
	63.7	5.8				
25			+23.7	Isostatic recovery and erosion		
	40	1.5				
				Deposition of Devonian molasse	5E	~385 Ma

Figure 5 presents a series of sections showing the main features of the evolutionary model, which are also summarized in Table 2.

In developing the model the following assumptions were made.

1. The eclogites and garnet peridotites equilibrated *in-situ* within their present host gneisses. Hence the whole BGC has suffered eclogite facies metamorphism.
2. The major structures in the BGC are of Caledonian age.
3. The eclogite facies metamorphism was of Caledonian age.
4. The LVL represents a structural discontinuity in the crust.

All these assumptions are still matters of intense debate, but we believe that the information outlined in this paper strongly supports them as correct assumptions. The model is described below.

Following closure of the Iapetus ocean and obduction of ophiolites and eunimatic island-arc sequences in the early Ordovician (A in Fig. 5), the Greenland and Baltic margins collided. The Baltic margin underthrust that of Greenland and was tectonically telescoped, possibly along pre-existing faults, leading to the development of a stack of thrust sheets consisting largely of Proterozoic crystalline basement and cover, including some early Palaeozoic cover rocks. Caledonian ophiolites were also incorporated in the thrust stack and in the suture zone. Incorporation of ultrabasic fragments probably occurred at this stage, either due to thrusts transecting the upper sub-continental mantle or due to incorporation of basal oceanic or marginal basin lithosphere. The thrust stack included not only rocks now present in the BGC, but also those in the allochthon.

The considerable horizontal shortening resulting from this collision caused great crustal thickening (up to 80 km) so that pressures large enough to form eclogite facies assemblages prevailed. Initially compression was much more rapid than warming, so that low-temperature amphibolites and low-T glaucophane eclogites formed. Ultimately thermal relaxation due to conduction of mantle heat flux and radiogenic self-heating would have occurred, but this seems to have affected only those rocks which have attained the greatest depths (i.e. those which record the highest pressures) as they record the highest temperatures and show no prograde garnet zoning. However, the widespread disequilibrium shown in the BGC by mineral zoning, carona formation and relict granulite and igneous assemblages, as well as the preservation of low-T eclogites, implies that in large volumes of this early nappe pile, thermal relaxation was every limited and hence this high pressure event was only transient. Our isostatic calculations indicate a period of 33 Ma for this event, which is consistent with the thermal modelling of Bird *et al.*

(1975), and the time available between the deposition of the Köli supergroup and eclogite mineral (closure?) ages. Andréasson & Gorbatschev (1980) describe the metamorphism of the nappes in the Trondheim-Østersund area and suggest that common inverted metamorphic gradients are a result of incomplete thermal equilibration during early nappe thrusting. They also note evidence for early high-P metamorphism in some of the nappes as well as a westward increase in metamorphic grade. These features are consistent with the model. Andréasson & Gorbatschev (1980) suggested that the high-P event may have only lasted 15 Ma.

The overburden for the high-P metamorphism was probably largely provided by the great thickness of the nappe pile. The value of 65 km for the overburden may be an overestimate if there was a large amount of dense oceanic crust in the thrust stack.

At this stage the strong positive buoyancy of the thickened prism of nappes caused strong uplift, aided by surface erosion upon its emergence above sea level. This would have had two effects. Firstly, the decompression would have caused retrogression of the high-pressure mineral assemblages, observed as symplectitization of omphacitic pyroxene and phengitic mica, followed by development of amphibolite-facies assemblages. The completeness of retrogression was probably aided by deformation—relict mineral assemblages are most commonly observed in the least deformed rocks. Geothermometry indicates that very little change in temperature occurred during decompression. This may have been a consequence of the low rate of thermal conduction relative to uplift, as a result of which the uplift was essentially adiabatic. Thus the lack of extra thermal energy to drive reactions across kinetic barriers may have resulted in the common preservation of high pressure relics (Lappin & Smith, 1978). Griffin & Mørk (1981) note that many retrogressive assemblages record pressures equivalent to 8–10 km. This may be a result of either a slowing down of the rate of uplift or a major deformational event.

The second effect of the uplift would have been to cause gravitational instability in the higher parts of the nappe pile. This could have caused the commencement of translation of the allochthon away from its root zone in the nappe pile and towards the foreland. We speculate that the stretching involved in this translation may have been responsible for the pervasive amphibolite-facies foliation in the gneisses and the common boudinage seen in the eclogites. Recumbent isoclinal folding occurred at or slightly before this stage. Some eclogite-bearing units were involved in the nappe translation now seen in the Seve nappe in Sweden (Roermund, 1981).

At some time during this uplift period a major low-angle crustal fracture formed in the Baltic foreland (suture progradation). The foreland was then underthrust along this fracture below the eclogite-bearing base of the BGC. The thrust surface is now seen as the LVL, either as a result of emplacement of normal density upper crust below eclogite-bearning gneisses, or due to the incorporation of some supracrustal sedimentary cover into this fracture system. The former alternative implies that little or no mineralogical equilibration to higher pressure parageneses took place at the top of the underthrust slab.

The surface expression of this thrust may be where the basal décollement to the allochthon in central Sweden passes into the basement in the Grong-Olden culmination. This 'boundary thrust' would be analogous to the Main Boundary Thrust of the southern Himalayas (Powell & Conaghan, 1973; Shackleton, 1981; Baraganzi & Ni, 1982). The geometry of the boundary thrust further SW depends upon interpretation of the Jotun nappe. If it is accepted that the nappe has travelled from a source in the NW then its outcrop may simply cover the boundary thrust. If, however, this Nappe has had a local, deep rooted source, its emplacement may have been a direct consequence of this suture progradation, either as a result of the detachment of an 'Ivrea-type flake' (Battey & McRitchie, 1973; Smithson & Ramberg, 1974; Banham *et al.*, 1979) or telescoping an ensialic marginal basin (Gibbs, 1982). In either case the formation of the duplex thrust system in the Valdres area may be at least partly a result of off-scraping of the supracrustal sediments against the upper end of the boundary thrust as the foreland moved north-westwards below the hanging wall.

This phase of crustal doubling provided further impetus for uplift and nappe translation, with the unrooted allochthon being replaced by higher units from the NW. In Sunnfjord, a break of about 3.5–6.0 kbar is indicated by the different parageneses in the eclogite-bearing basement and the overlying Cambro-Silurian schists (Griffin & Mørk, 1981), but retrogressive assemblages in the gneisses may be broadly consistent with the conditions indicated by the schists, indicating that their final juxtapositioning occurred after uplift of at least 25 km. Hence the final uplift stage was probably only accompained by surface erosion and not tectonic stripping. The effect of adiabatic

upward transport of rather warm crust to these higher levels may well have had a strong thermal effect on the overlying allochthon, but this does not seem to be well documented, although Andréasson & Gorbatschev (1980) mention a 'thermal pulse' succeeding nappe translation.

Final emergence of the BGC in the early middle Devonian produced the present geometry of this part of the orogen, with the development of molasse-filled intermontaine basins controlled by late faulting. Guezou (pers. comm., 1981), associates this with late transverse movement near the primary suture due to oblique collision. The appearance of the BGC as a culmination within the surrounding allochthon may be associated with frequently observed late dome structures (e.g. Løset, 1977). If the regional P–T variation observed by Krogh (1977a) and Griffin *et al.* (1981) survives detailed scrutiny, it would appear that after imbrication and inter-folding of the lithologies forming the BGC it acted as a coherent body during uplift, except for minor movements as may be observed in the Sunnfjord area.

Elucidation of the history of the BGC has great importance in geodynamic modelling of the Caledonides as it is likely that its uplift provided the driving force for final translation of the allochthon into its present position. Studies of high-pressure relics such as eclogites, garnet peridotites and high-pressure granulites play an important part in this modelling.

ACKNOWLEDGEMENTS

This paper has grown considerably since its original conception and has benefited from critical comments by D. G. Gee and anonymous referees, as well as discussions with N. J. Soper, J. -C. Guezou, I. Bryhni and many others. S. J. Cuthbert and M. A. Harvey acknowledge studentships from the Natural Environment Research Council and D. A. Carswell, financial support from the University of Sheffield.

REFERENCES

Ahnert, F., 1970. Functional relationship between denudation, relief and uplift in large mid-latitude drainage basins. *Am. J. Sci.*, **268**, 243–63.

Andréasson, P. G. & Gorbatschev, R., 1980. Metamorphism in extensive nappe terrains: a study of the Central Scandinavian Caledonides. *Geol. För. Stockholm Förh.*, **102**, 335–57.

Andresen, A. & Faerseth, R., 1982. An evolutionary model for the south-west Norwegian Caledonides. *Am. J. Sci.*, **282**, 756–82.

Austrheim, H., 1981. Bergen Arcs. In: *Excursions in the Scandinavian Caledonides. U.C.S. Excursion No. B1: Eclogites and Basal Gneisses in West Norway.* (eds. W. L. Griffin & M. B. E. Mørk), pp. 74–82. Uppsala Caledonide Symposium.

Austrheim, E. & Griffin, W. L., 1982. Shear deformation and eclogite formation within granulite-facies anorthosites of the Bergen Arcs, western Norway. *Abstr. First Int. Eclogite Conf., Clermont Ferrand, Terra Cognita*, **2**, 315.

Austrheim, H. & Råheim, A., 1981. Age relationships within the high grade metamorphic rocks of the Bergen Arcs, western Norway. *Abstr. Uppsala Caledonide Symp. Terra Cognita*, **1**, 33.

Banham, P. H., Gibbs, A. D. & Hopper, F. W. M., 1979. Geological evidence in favour of a Jotunheimen Caledonian suture. *Nature*, **277**, 289–91.

Barazangi, M. & Ni, J., 1982. Velocities and propagation characteristics of Pn and Sn beneath the Himalayan arc and Tibetan plateau: Possible evidence for underthrusting of Indian continental lithosphere beneath Tibet. *Geology*, **10**, 179–85.

Battey, M. H. & McRitchie, W. D., 1973. A geological traverse across the pyroxene-granulites of Jotenheimen in the Norwegian Caledonides. *Nor. Geol. Tidsskr.*, **53**, 237–65.

Bird, P., Toksoz, M. N. & Sleep, N. H., 1975. Thermal and mechanical models of continent-continent convergence zones. *J. Geophys. Res.*, **80**, 4405–16.

Boettcher, A. L., 1970. The system $CaO-Al_2O_3-SiO_2-H_2O$ at high pressures and temperatures. *J. Petrol.*, **11**, 337–79.

Brastad, K., 1982. Eclogites within the Bjørkedalen peridotite, western Norway. *Abstr. First Int. Eclogite Conf., Clermont Ferrand. Terra Cognita*, **2**, 327.

Brastad, K., 1983. Relations between anorthosites, eclogites and ultramafics in Bjørkedalen, west Norway. *Proc. Uppsala Caledonides Symp.* (In press).

Brueckner, H. K., 1972. Interpretation of Rb-Sr ages from the Precambrian and Palaeozoic rocks of southern Norway. *Am. J. Sci.*, **272**, 334–58.

Brueckner, H. K., 1977. A structural, stratigraphic and petrologic study of anorthosites, eclogites and ultramafic rocks and their country rocks, Tafjord area, western south Norway. *Nor. Geol. Unders.*, **332**, 1–53.

Brueckner, H. K., 1979. Precambrian ages from Geiranger-Tafjord-Grotli area of the Basal Gneiss Region, west Norway. *Nor. Geol. Tidsskr.*, **59**, 141–53.

Bryhni, I., 1966. Reconnaissance studies of gneisses, ultrabasites, eclogites and anorthosites in outer Nordfjord, western Norway. *Nor. Geol. Unders.*, **241**, 1–68.

Bryhni, I., 1977. The gneiss region west and northwest of Jotunheimen. In: *The Norwegian Geotraverse Project. A Norwegian Contribution to the International Upper Mantle Project and the International Geodynamics Project.* (ed. K. S. Heier), pp. 227–246.

Bryhni, I., 1981. Nordfjord-Sognfjord Devonian Basins. In: *Excursion in the Scandinavian Caledonides, U.C.S. Excursion No. B1: Eclogites and Basal Gneisses in west Norway.* (eds. W. L. Griffin & M. B. E. Mørk), pp. 58–63. Uppsala Caledonide Symposium.

Bryhni, I., Fitch, F. J. & Miller, J. A., 1971. $^{40}Ar/^{39}Ar$ dates from recycled precambrian rocks in the gneiss

region of the Norwegian Caledonides. *Nor. Geol. Tidsskr.*, **51**, 391–406.

Bryhni, I. & Griffin, W. L., 1971. Zoning in eclogite garnets from Nordfjord, west Norway. *Contrib. Mineral. Petrol.*, **32**, 112 25.

Bryhni, I. & Grimstad, E., 1970. Supracrustal and infracrustal rocks in the gneiss region of the Caledonides west of Breimsvatn. *Nor. Geol. Unders.*, **266**, 105 40.

Bryhni, M., Kroph, E. & Griffin, W. L., 1977. Crustal derivation of Norwegian eclogites: A review. *N. Jb. Mineral. Abh.*, **130**, 49–68.

Carswell, D. A., 1968a. Picritic magma—residual dunite relationships in garnet peridotite at Kalskaret near Tafjord, southern Norway. *Contrib. Mineral. Petrol.*, **19**, 97 124.

Carswell, D. A., 1968b. Possible primary upper mantle peridotite in Norwegian basal gneiss. *Lithos*, **1**, 322 355.

Carswell, D. A., 1973a. The age and status of the basal gneiss complex of north-west southern Norway. *Nor. Geol. Tidsskr.*, **53**, 65–78.

Carswell, D. A., 1973b. Garnet pyroxenite lens within Ugelvik layered garnet peridotite. *Earth Planet. Sci. Lett.*, **20**, 347–52.

Carswell, D. A. & Gibb, F. G. F., 1980. The equilibration conditions and petro-genesis of European crustal garnet lherzolites. *Lithos*, **13**, 19–29.

Carswell, D. A. & Harvey, M. A., 1983. The intrusive history and tectono-metamorphic evolution of the Basal Gneiss Complex in the Moldefjord area, west Norway. *Proc. Uppsala Caledonide Symp.* (In press).

Carswell, D. A., Krogh, E. J. & Griffin, W. L., 1983. Norwegian orthopyroxene eclogites: Calculated equilibration conditions and petrogenetic implications. *Proc. Uppsala Caledonide Symp.* (In press).

Cook, F. A., Albaugh, D. S., Brown, L. D., Kaufman, S., Oliver, J. E. & Hatcher, Jr., R. D., 1979. Thin-skinned tectonics in the crystalline southern Appalachians, COCORP seismic profiling of the Blue-Ridge and Piedmont. *Geology*, **7**, 563–7.

Cuthbert, S. J. & Carswell, D. A., 1982. Petrology and tectonic setting of eclogites and related rocks from the Dalsfjord area, Sunnfjord, west Norway. *Abstr. First Int. Eclogite Conf., Clermont Ferrand. Terra Cognita*, **2**, 315.

Dewey, J. F., 1969. Evolution of the Appalachian/Caledonian orogen. *Nature*, **222**, 124–9.

Dewey, J. F., 1982. Plate tectonics and the evolution of the British Isles. *J. geol. Soc. London*, **139**, 371–412.

Draper, G. & Bone, R., 1981. Denudation rates, thermal evolution and preservation of blueschist terrains. *J. Geol.*, **89**, 601–13.

Elliot, R. B. & Cowan, D. R., 1966. The petrochemistry of the amphibolites of the Holleindalen Greenstone Group, Jotunheimen, Norway. *Nor. Geol. Tidsskr.*, **46**, 309–25.

Ellis, D. J. & Green, D. H., 1979. An experimental study of the effect of Ca upon Garnet-Clinopyroxene Fe-Mg exchange equilibria. *Contrib. Mineral. Petrol.*, **71**, 13–22.

England, P. C. & Richardson, S. W., 1977. The influence of erosion upon the mineral facies of rocks from different metamorphic environments. *J. geol. Soc. Lond.*, **134**, 201–13.

Ernst, W. G., 1977. Tectonics and prograde versus retrograde P-T trajectories of high pressure metamorphic belts; In: High pressure-low temperature metamorphism of the Oceanic and Continental Crust in the Western Alps. *Rendiconti Societa Italiana di Mineralogia e Petrologia*, **33**, 221–252.

Ernst, W. G., 1981. Petrogenesis of eclogites and peridotites from the western and Ligurian Alps. *Am. Mineral.*, **66**, 443–72.

Ernst, W. G. & dal Piaz, G. V., 1978. Mineral parageneses of eclogitic rocks and related mafic schists of the Piedmont ophiolite nappe, Breuil-St. Jacques area, Italian western Alps. *Am. Mineral.*, **63**, 621–40.

Eskola, P., 1921. On the eclogites of Norway. *Skr. Norske Vidensk-Akad. i Oslo, Mat-naturv., kl.*, **8**, 1–118.

Ferry, J. M. & Spear, F. S., 1978. Experimental calibration of partitioning of Fe and Mg between biotite and garnet. *Contrib. Mineral. Petrol.*, **66**, 113–7.

Franz, G. & Althaus, E., 1977. The stability relations of the paragenesis paragonite-zoisite-quartz. *N. Jb. Miner. Abh.*, **130**, 159–67.

Furnes, H., Skjerlie, F. J. & Tysseland, M., 1976. Plate tectonic model based on greenstone geochemistry in the late Precambrian-Lower Palaeozoic sequence in the Solund-Stavfjorden areas, west Norway. *Nor. Geol. Tidsskr.*, **56**, 161–86.

Gale, H. G. & Roberts, D., 1974. Trace-element geochemistry of Norwegian lower Palaeozoic basic volcanics and its tectonic implications. *Earth Planet. Sci. Lett.*, **22**, 380–90.

Gebauer, D., Lappin, M. A., Gruenefelder, M., Koestler, A. & Wyttenbach, A., 1982. Age and origin of some Norwegian eclogites: a U-Pb zircon and REE study. *Abstr. First Int. Eclogite Conf., Clermont Ferrand. Terra Cognita*, **2**, 323.

Gee, D. G., 1975. A geotraverse through the Scandinavian Caledonies—Ostersund to Trondheim. *Sver. Geol. Unders. Ser. C.*, **417**, 1–66.

Gee, D. G., 1978. Nappe displacement in the Scandinavian Caledonides. *Tectonophysics*, **47**, 393–419.

Gee, D. G., 1980. Basement-cover relationships in the central Scandinavian Caledonides. *Geol. För. Stockholm. Förh.*, **102**, 455–74.

Gee, D. G., Guezou, J. C., Roberts, D. & Wolff, J. C., 1982. The central-southern segment of the Scandinavian Caledonides. *Abstr. Uppsala Caledonide Symp. Terra Cognita*, **1**, 45.

Gent, E. D., 1976. Plagioclase–garnet–Al_2SiO_5–quartz, a potential geobarometer–geothermometer. *Am. Mineral.*, **61**, 710–14.

Gibbs, A. D., 1982. Northerly transport and exotic olistostrome in northern Jotunheim: Possible implications. *Abstr. Scandinavian Caledonides Research Seminar, Bedford College, London.* Convenor: P. Banham.

Gjelsvik, T., 1952. Metamorphosed dolerites in the gneiss area of Sunnmøre on the west coast of southern Norway. *Nor. Geol. Tidsskr.*, **30**, 31–134.

Green, D. H. & Mysen, B. A., 1972. Genetic relationship between eclogite and hornblende + plagioclase pegmatite in W. Norway. *Lithos*, **5**, 147–161.

Griffin, W. L., 1972. Formation of eclogites and the

coronas in anorthosites, Bergen Arcs, Norway. *Geol. Soc. Am. Memoir*, **135**, 37–63.

Griffin, W. L., Austrheim, H., Grastad, K., Bryhni, I., Krill, A., Mørk, M. B. E., Qvale, H. & Tørudbakken, B., 1981. High pressure metamorphism in the Scandinavian Caledonides. *Abstr. Uppsala Caledonide Symp. Terra Cognita*, **1**, 48.

Griffin, W. L. & Brueckner, H. K., 1980. Caledonian Sm-Nd ages and a crustal origin for Norwegian eclogites. *Nature*, **285**, 319–21.

Griffin, W. L. & Brueckner, H. K., 1982. Rb-Sr and Sm-Nd studies of Norwegian eclogites *Abstr. First Int. Eclogite Conf., Clermont Ferrand. Terra Cognita*, **2**, 324.

Griffin, W. L. & Bryhni, I., 1977. Corona reactions and the eclogite problem. In: *The Norwegian Geotraverse Project. A Norwegian Contribution to the International Upper Mantle Project and the International Geodynamics Project* (ed. K. S. Heier), pp. 247–264.

Griffin, W. L. & Carswell, D. A., 1983. Geochronological setting of in-situ eclogite metamorphism in western Norway. *Proc. Uppsala Caledonide Symp.* (in press).

Griffin, W. L. & Heier, K. S., 1973. Petrological implications of some corona structures. *Lithos*, **6**, 315–35.

Griffin, W. L. & Mørk, M. B. E., 1981. Introduction. In: *Excursion in the Scandinavian Caledonides Excursion No. B1: Eclogites and Basal Gneisses in West Norway* (eds. W. L. Griffin & M. B. E. Mørk), pp. 2–12, Uppsala Caledonide Symposium.

Griffin, W. L. & Qvale, H., 1981. Superferric eclogites and the crustal origin of garnet peridotite. *Abstr. Uppsala Caledonide Symp. Terra Cognita*, **1**, 48.

Griffin, W. L. & Råheim, A., 1973. Convergent metamorphism of eclogites and dolerites, Kristiansund area, Norway. *Lithos*, **6**, 21–40.

Guezou, J.-C., 1978. Geology and structure of the Dombås-Lesja area, southern Trondheim region, south central Norway. *Nor. Geol. Unders.*, **340**, 1–34.

Guezou, J.-C., 1981. A geodynamic model for the central and southern parts of the Scandinavian Caledonides. *Abstr. Uppsala Caledonide Symp. Terra Cognita*, **1**, 49.

Hernes, I., 1954. Eclogite-amphibolite on the Molde peninsula, southern Norway. *Nor. Geol. Tidsskr.*, **33**, 163–84.

Hernes, I., 1955. Geologisk oversikt over Molde-Kristiansundsområdet. *Det. kyl. Norske Vidensk. Selsk. Skifter*, **5**, 1–17.

Holland, T. J. B., 1979. Experimental determination of the reaction paragonite = jadeite + kayanite + H_2O, and internally consistent thermodynamic data for part of the system Na_2O–Al_2O_3–SiO_2–H_2O, with applications to eclogites and blueschists. *Contrib. Mineral. Petrol.*, **68**, 293–301.

Holland, J. T. B., 1980. The reaction albite = jadeite + quartz determined experimentally in the range 600–1200°C. *Am. Mineral.*, **65**, 129–34.

Holtedahl, O. & Dons, R. F., 1960. Geologiske kart over Norge, Bergrunnskart 1:1000,000. *Nor. Geol. Unders.* **208**.

Hossack, J. R., 1978. The correction of stratigraphic sections for tectonic finite strain the Bygdin area, Norway. *J. geol. Soc. London*, **135**, 229–41.

Hossack, J. R., 1982. A geological section from the foreland across the Valdres and Jotunheim areas to the west coast of Norway. *Abstr. Scandinavian Caledonides Research Seminar, Bedford College, London*, Convenor: P. Banham.

Hossack, J. R., Nickelsen, R. P. & Garton, M., 1981. The geological section from the foreland up to the Jotun sheet in the Veldres area, south Norway. *Abstr. Uppsala Caledonide Symp. Terra Cognita*, **1**, 52.

Hsü, K. F., 1979. Thin skinned plate tectonics during Neo-Alpine orogenesis. *Am. J. Sci.*, **279**, 353–66.

Kanestrøm, R., 1973. A crust-mantle model for the NORSAR area. *Pure Appl. Geophys.*, **105**, 729–40.

Kanestrøm, R., 1977. Seismic investigations of the crust and Moho in southern Norway. In: *The Norwegian Geotraverse Project. A Norwegian Contribution to the International Upper Mantle Project and the International Geodynamics Project.* (ed. K. S. Heier), pp. 143–9.

Kent, D. V. & Opdyke, N. D., 1979. The early Carboniferous palaeomagnetic field of North America and its bearing on the tectonics of the Northern Appalachians. *Earth Planet. Sci. Lett.*, **44**, 365–72.

Krill, A. G., 1980. Tectonics of the Oppdal area, central Norway. *Geol. För. Stockholm Förh.*, **102**, 523–30.

Krill, A. G., 1981a. Rb-Sr study of metamorphosed dolerite dykes and psammite: 'Precambrian' *vs.* 'Caledonian' orogenesis in the western gneiss region of Norway. *Abstr. Uppsala Caledonide Symp., Terra Cognita*, **1**, 56.

Krill, A. G., 1981b. 'Stockwerk' tectonic relationships between the Trondheim synclinorium and the Western Gneiss Region of Norway. *Abstr. Uppsala Caledonide Symp., Terra Cognita*, **1**, 56.

Krill, A. G. & Griffin, W. L., 1981. Interpretation of Rb-Sr dates from the Western Gneiss Region: A cautionary note. *Nor. Geol. Tidsskr.* **61**, 83–6.

Krogh, E. J., 1977a. Evidence of Precambrian continent–continent collision in Western Norway. *Nature*, **267**, 17–9.

Krogh, E. J., 1977b. Crustal and in-situ origin of Norwegian eclogites. Reply. *Nature*, **269**, 730.

Krogh, E. J., 1980a. Geochemistry and petrology of glaucophane-bearing eclogites and associated rocks from Sunnfjord, western Norway. *Lithos*, **13**, 355–80.

Krogh, E. H., 1980b. Compatible P-T conditions for eclogites and surrounding gneisses in the Kristiansund area, western Norway. *Contrib. Mineral. Petrol.*, **75**, 387–93.

Krogh, T. E., Mysen, B. O. & Davis, G. L., 1973. A Palaeozoic age for the primary minerals of a Norwegian eclogite. *Carnegie Inst. Wash. Yearb.*, **73**, 575–6.

Lambert, I. B. & Wyllie, P. J., 1972. Melting of gabbro 'quartz eclogite' with excess water to 35 kilobars, with geological applications. *J. Geol.*, **80**, 693–708.

Lappin, M. A., 1966. The field relationships of basic and ultrabasic masses in the Basal Gneiss Complex of Stadlandet and Almklovdalen, Nordfjord, S. W. Norway. *Nor. Geol. Tidsskr.*, **46**, 439–95.

Lappin, M. A., 1977. Crustal and in-situ origin of Norwegian eclogites. *Nature*, **269**, 730.

Lappin, M. A., Pidgeon, R. T. & van Breemen, O., 1977. Geochronology of basal genisses and mangerite syenites of Stadlandet, west Norway. *Nor. Geol. Tidsskr.*, **59**, 161–81.

Lappin, M. A. & Smith, D. C., 1978. Mantle equilibrated orthopyroxene eclogite pods from the Basal Gneisses in the Selje district, western Norway. *J. Petrol.*, **19**, 530–84.

Løset, F., 1977. Three fold phases in the northern part of Trollheimen in the Norwegian Caledonides. *Nor. Geol. Tidsskr.*, **57**, 121–31.

Lund, G. E., 1979. Crustal structure along the Blue Road Profile in northern Scandinavia. *Geol. För. Stockholm Förh.*, **101**, 191–204.

Maresch, W. V., 1977. Experimental studies on glaucophane: An analysis of present knowledge. *Tectonophysics*, **43**, 109–25.

Maresch, W. V. & Abraham, K., 1981. Petrography, mineralogy and metamorphic evolution of an eclogite from the island of Margarita, Venezuela. *J. Petrol.*, **22**, 337–62.

Mearns, E. W. & Lappin, M. A., 1982a. The origin and age of 'external eclogites' and gneisses from the Selje district of the western gneiss region, Norway. *Abstr. First Int. Eclogite Conf., Clermont Ferrand. Terra Cognita*, **2**, 324.

Mearns, E. W. & Lappin, M. A., 1982b. A Sm-Nd isotopic study of 'internal' and 'external' eclogites, garnet lherzolites and grey gneiss from Almklovdalen, western Norway. *Abstr. First Int. Eclogite Conf., Clermont ferrand. Terra Cognita*, **2**, 324.

Mearns, E. W. & Lappin, M. A., 1982c. Poster Contribution. *First Int. Eclogite Conf., Clermont Ferrand.*

Medaris, Jr. L. G., 1980. Petrogenesis of the Lien peridotite and associated eclogites, Almklovdalen, western Norway. *Lithos*, **13**, 339–53.

Medaris, Jr. L. G., 1982. A review of garnet peridotites within gneiss in western Norway. *Abstr. First Int. Eclogite Conf., Clermont Ferrand. Terra Cognita*, **2**, 303.

Mørk, M. B. E., 1982. A gabbro-eclogite transition of Flemsøy, Sunnmøre, western Norway. *Abstr. First Int. Eclogite Conf., Cleremont Ferrand. Terra Cognita*, **2**, 316.

Mykkeltveit, S., Husebye, E. S., Oftedahl, C., 1980. Subduction of the Iapetus Ocean crust beneath the Møre Gneiss Region, Southern Norway. *Nature*, **288**, 473–5.

Mysen, B. O. & Heier, K. S., 1972. Petrogenesis of eclogites in high grade metamorphic gneisses exemplified by the Hareidland eclogite, western Norway. *Contrib. Mineral. Petrol.*, **36**, 73–94.

McQuillin, R. & Brooks, M., 1967. Geophysical surveys in the Shetland Islands. *Institute of Geological Sciences, Geophysical Paper No. 2.* HMSO, London.

O'Hara, M. J., 1976. Origin of the Norwegian eclogites. *Progr. Expt. N.E.R.C.*, **3**, 252.

O'Hara, M. J. & Mercy, E. L. P. 1963. Petrology and petrogenesis of some garnetiferous peridotites. *Trans. Roy. Soc. Edin.*, **65**, 251–314.

O'Hara, M. J., Richardson, S. W. & Wilson, G., 1971. Garnet-peridotite stability and occurrence in crust and mantle. *Contrib. Mineral. Petrol.*, **32**, 48–68.

Phillips, W. E. A., Stillman, C. J. & Murphy, J., 1976. A Caledonian plate tectonic model. *J. geol. Soc. Lond.*, **132**, 579–609.

Pidgeon, R. T. & Råheim, A., 1972. Geochronological investigation of the gneisses and minor intrusive rocks from Kristiansund, west Norway. *Nor. geol. Tidsskr.*, **52**, 241–56.

Powell, C. Mc.A. & Conaghan, P. J., 1973. Plate tectonics and the Himalyas. *Earth Planet. Sci. Lett.*, **20**, 1–12.

Prichard, H. M., 1981. The Shetland Ophiolite. *Abstr. Uppsala Caledonide Symp. Terra Cognita*, **1**, 65.

Råheim, A., 1972. Petrology of high grade metamorphic rocks of the Kristiansund area. *Nor. Geol. Unders.*, **279**, 1–75.

Råheim, A., 1977. A Rb, Sr study of the rocks of the Surnadal syncline *Nor Geol. Tidsskr.*, **57**, 193–204.

Råheim, A., 1979. Structural and metamorphic break between the Trondheim basin and the surnadal synform. *Nor. Geol. Tidsskr.*, **59**, 195–8.

Råheim, A., 1981. Age relationships in the western gneiss region. *Abstr. Uppsala Caledonide Symp. Terra Cognita*, **1**, 67.

Råheim, A. & Green, D. A., 1975. P,T paths of natural eclogites during metamorphism—a record of subduction. *Lithos*, **8**, 317–28.

Ramberg, I. B. & Grønlie, G., 1969. A crustal section across the Caledonian mountain belt (Norway) based on gravity data. *Bolletino di Geofisica Teorica ed Applicata*, **11**, 219–26.

Richardson, S. W. & England, P. C., 1979. Metamorphic consequences of crustal eclogite production in overthrust orogenic zones. *Earth Planet. Sci. Lett.*, **42**, 183–90.

Roberts, D., Thon, A., Gee, D. G. & Stephens, M. B., 1981. Scandinavian Caledonides–Tectonostratigraphy map, scale 1:1,000,000. *Uppsala Caledonide Symp.*

Roeder, D., 1979. Continental collisions. *Rev. Geophys.*, **17**, 1098–1109.

Roermund, H. L. M. van, 1981. On the eclogites of the Seve Nappe central Scandinavian Caledonides. *Abstr. Uppsala Caledonides. Abstr. Uppsala Caledonide Symp. Terra Cognita*, **1**, 70.

Rubie, D. C., 1982. A kinematic model for metamorphism and deformation in the Sesia-Lanzo zone, western Alps. *Abstr. First Int. Eclogite Conf. Clermont Ferrand. Terra Cognita*, **2**, 308–9.

Schmitt, H. H., 1964. Metamorphic eclogites of the Eiksund area, Sunnmøre Norway. *Abstr. Am. Geophys. Union*, **43**, 128.

Sellevoll, M. A. & Warrick, R. E., 1971. A refraction study of the crustal structure in southern Norway. *Bull. Seismol. Soc. Am.*, **61**, 457–71.

Shackleton, R. M., 1981. Structure of southern Tibet: Report on a traverse from Lhasa to Khatmandu organised by Academia Sinica. *J. Struct. Geol.*, **3**, 97–105.

Skjerlie, F. J., 1969. The pre-Devonian rocks in the Askvoll-Gaular area and the adjacent districts, western Norway. *Nor. Geol. Unders*, **258**, 325–59.

Skjerlie, F. J., 1974. The lower Palaeozoic sequence of the Stavfjord district, Sunnfjord. *Nor. Geol. Unders*, **302**, 1–32.

Skjerlie, F. J. & Pringle, I. R., 1978. A Rb/Sr whole rock isochron date from the lowermost gneiss complex of the Gaular area, west Norway and its regional implications. *Nor. Geol. Tidsskr.*, **58**, 259–65.

Smith, D. C., 1980. A tectonic melange of foreign eclogites and ultramafites in west Norway. *Nature*, **287**, 366–7.

Smith, D. C., 1981. A reappraisal of factual and mythical evidence concerning the metamorphic and tectonic evolution of eclogite-bearing terrain in the Caledonides. *Abstr. Uppsala Caledonide Symp. Terra Cognita*, **1**, 73.

Smith, D. C. & Cheeny, R. F., 1981. A new occurrence of garnet ultrabasite in the Caledonides: A Cr-rich chromite-garnet-lherzolite from Tvaerdalen, Liverpool land, east Greenland. *Abstr. Uppsala Caledonide Symp. Terra Cognita*, **1**, 74.

Smithson, S. B., Ramberg, I. B. & Grønlie, G., 1974. Gravity interpretation of the Jotun Nappe of the Norwegian Caledonides. *Tectonophysics*, **22**, 205–22.

Solheim, S., 1980. Geochronological investigations in the Oppdal area, central Norway. *Nor. Geol. Tidsskr.*, **60**, 175–88.

Soper, N. J. & Barber, A. J., 1982. A model for the deep structure of the Moine thrust zone. *J. geol. Soc. Lond.*, **139**, 127–38.

Spray, J. G., 1982. Mafic segregations in ophiolite mantle sequences. *Nature*, **299**, 524–8.

Stephens, M. B. & Gee, D. G., 1981. A plate-tectonic model for Caledonian orogenesis in the central Scandinavian Caledonides. *Abstr. Uppsala Caledonide Symp. Terra Cognita*, **1**, 76.

Stern, C. R., Huang, W.-L, & Wyllie, P. J., 1975. Basalt-andesite-rhyolite H_2O: Crystallisation intervals with excess H_2O and H_2O-undersaturated liquidus surfaces to 35 kbars with implications for magma genesis. *Earth Planet Sci. Lett.*, **28**, 189–96.

Strand, T., 1969. Geology of the Grotli area. *Nor. Geol Tidsskr.*, **49**, 341–60.

Sturt, B. A., Skarpenes, O., Ohanian, A. T. & Pringle, I. R., 1975. Reconnaissance Rb/Sr isochron study in the Bergen Arc System and regional implications. *Nature*, **253**, 589–99.

Sturt, B. A. & Thon, A., 1974. The age of orogenic deformation in the Swedish Caledonides. *Am. J. Sci.*, **276**, 385–9 .

Talwani, M. & Eldholm, O., 1972. Continental margin off Norway: A geophysical study. *Geol. Soc. Am. Bull.*, **83**, 3575–606.

Thompson, A. B., 1981. The pressure-temperature (P,T) plane viewed by geophysicists and petrologists. *Abstr. Uppsala Caledonide Symp. Terra Cognita*, **1**, 11–20.

Toksöz, M. N. & Bird, P., 1977. Modelling of temperatures in continental convergence zones. *Tectonophysics*, **41**, 181–93.

Tørudbakken, B., 1981. Trondheim-Surnadal. In: *Excursions in the Scandinavian Caledonides U.C.S. Excursion No. B1: Eclogites and Basal Gneisses in west Norway* (eds. W. L. Griffin & M. B. E. Mørk), pp. 13–19. Uppsala Caledonide Symposium.

Tørudbakken, B. & Råheim, A., 1982. An in-situ metamorphosed eclogite near the Surnadal syncline and its implications for the metamorphic relationships in the Surnadal area. *Abstr. First Int. Eclogite Conf., Clermont Ferrand. Terra Cognita*, **2**, 79.

Verschure, R. H., Andressen, P. A. M., Boelrijk, N. A. I. M., Hebden, E. H., Maier, C., Priem, H. N. A. & Verdurmen, E. A. Th., 1980. On the thermal stability of Rb-Sr and K-Ar biotite systems: Evidence from coexisting Sveconorwegian (ca. 870 Ma) and Caledonian (ca. 400 Ma) biotites in S. W. Norway. *Contrib. Mineral. Petrol.*, **74**, 245–52.

Watts, A. B., 1971. Geophysical investigations on the continental shelf and slope north of scotland. *Scott. J. Geol.*, **7**, 189–218.

Wood, B. J. & Banno, S., 1973. Garnet-orthopyroxena and orthopyroxene-clinopyroxene relationships in simple and complex systems. *Contrib. Mineral. Petrol.*, **42**, 109–24.

Received 9 July 1982; revision accepted 10 December 1982.

Note added in proof

It has been brought to our attention that the Griffin & Mørk (1981) reference is not widely available. Readers are advised instead to refer to the major new review paper on 'High-pressure metamorphism in the Scandinavian Caledonides' by W. L. Griffin, H. Austrheim, K. Brastad, I. Bryhni, A. G. Knill, E. J. Krogh, M. B. E. Mørk, H. Qvale & T. Tørudbakken to be published shortly in: *The Caledonian Orogen—Scandinavia and Related Areas* (eds. B. A. Sturt & D. G. Gee), John Wiley.